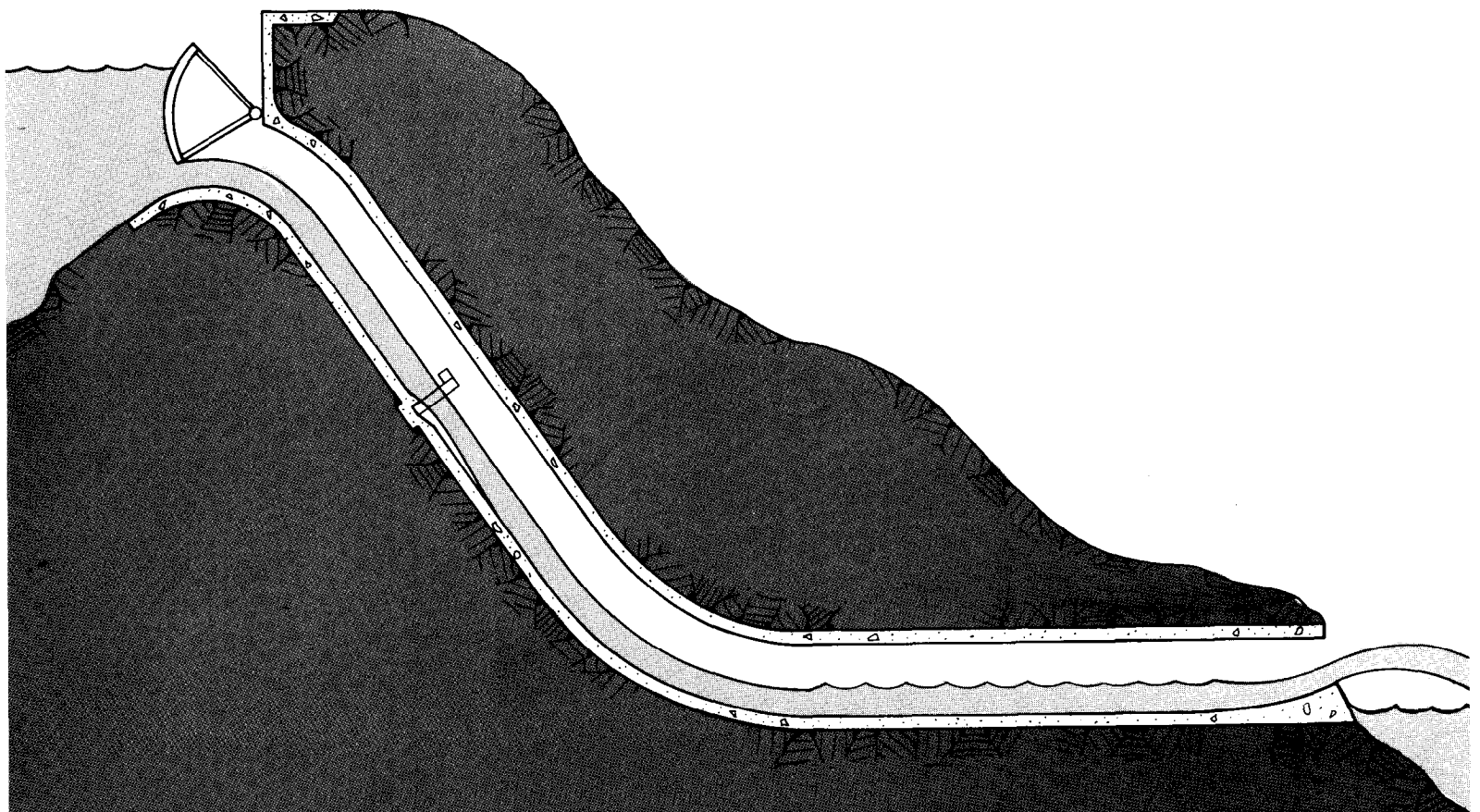


A WATER RESOURCES TECHNICAL PUBLICATION

ENGINEERING MONOGRAPH NO. 42

CAVITATION IN CHUTES AND SPILLWAYS



UNITED STATES DEPARTMENT OF THE INTERIOR
BUREAU OF RECLAMATION

TECHNICAL REPORT STANDARD TITLE PAGE

1. REPORT NO. Engineering Monograph No. 42		2. GOVERNMENT ACCESSION NO.		3. RECIPIENT'S CATALOG NO.	
4. TITLE AND SUBTITLE Cavitation in Chutes and Spillways				5. REPORT DATE April 1990	
				6. PERFORMING ORGANIZATION CODE	
7. AUTHOR(S) Henry T. Falvey				8. PERFORMING ORGANIZATION REPORT NO. Engineering Monograph No. 42	
9. PERFORMING ORGANIZATION NAME AND ADDRESS Bureau of Reclamation Denver Office PO Box 25007 Denver, Colorado 80225				10. WORK UNIT NO. D-3750	
				11. CONTRACT OR GRANT NO.	
12. SPONSORING AGENCY NAME AND ADDRESS Same				13. TYPE OF REPORT AND PERIOD COVERED	
				14. SPONSORING AGENCY CODE DIBR	
15. SUPPLEMENTARY NOTES Microfiche and/or hardcopy available at the Denver Office Editor: RNW					
16. ABSTRACT <p>The purpose of this monograph is to give the designer of hydraulic structures both an understanding of cavitation and the design tools necessary to eliminate or reduce the damaging effects of cavitation in chutes and spillways. The monograph discusses basic concepts, cavitation damage, practical methods of coping with cavitation damage, design recommendations, the influence of geometry and aeration, and Bureau of Reclamation field experience. Two executable and one source and data diskettes are (included herein) used to analyze specific structures. They will run on IBM AT compatible computers. Includes 3 disks, 93 figs., 232 refs., 5 apps., 159 equations, and 145 pp.</p>					
17. KEY WORDS AND DOCUMENT ANALYSIS a. DESCRIPTORS-- / *aerators/ *air entrainment/ *cavitation/ *computer programs/ *damage/ *design criteria/ *invert geometry/ *open channels/ *surface irregularities/ *theory/ spillways/ high velocity flow/ tunnel spillways/ erosion damage b. IDENTIFIERS-- / Blue Mesa Dam/ Flaming Gorge Dam/ Glen Canyon Dam/ Hoover Dam/ Kortes Dam/ McPhee Dam/ Yellowtail Dam c. COSATI Field/Group 1300 COWRR: 1407 SRIM:					
18. DISTRIBUTION STATEMENT Available from the National Technical Information Service, Operations Division, 5285 Port Royal Road, Springfield, Virginia 22161.				19. SECURITY CLASS (THIS REPORT) UNCLASSIFIED	
				20. SECURITY CLASS (THIS PAGE) UNCLASSIFIED	
				21. NO. OF PAGES 145	
				22. PRICE	

A WATER RESOURCES TECHNICAL PUBLICATION

ENGINEERING MONOGRAPH NO. 42

**CAVITATION IN CHUTES
AND SPILLWAYS**

by
Henry T. Falvey
Research Engineer

April 1990

Denver Office
Denver, Colorado 80225

UNITED STATES DEPARTMENT OF THE INTERIOR



BUREAU OF RECLAMATION



Mission: As the Nation's principal conservation agency, the Department of the Interior has responsibility for most of our nationally-owned public lands and natural and cultural resources. This includes fostering wise use of our land and water resources, protecting our fish and wildlife, preserving the environmental and cultural values of our national parks and historical places, and providing for the enjoyment of life through outdoor recreation. The Department assesses our energy and mineral resources and works to assure that their development is in the best interests of all our people. The Department also promotes the goals of the Take Pride in America campaign by encouraging stewardship and citizen responsibility for the public lands and promoting citizen participation in their care. The Department also has a major responsibility for American Indian reservation communities and for people who live in Island Territories under U.S. administration.

ENGINEERING MONOGRAPHS are published in limited editions for the technical staff of the Bureau of Reclamation and interested technical circles in Government and private agencies. Their purpose is to record developments, innovations, and progress in the engineering and scientific techniques and practices which are used in the planning, design, construction, and operation of water and power structures and equipment.

First Printing April 1990—1,500 copies





FRONTISPIECE.—Glen Canyon Dam. Left Spillway Tunnel Sept. 1983. The “big hole” in the spillway invert was 11 meters deep. Photo C557-400-690NA

Mission of the Bureau of Reclamation

The Bureau of Reclamation of the U.S. Department of the Interior is responsible for the development and conservation of the Nation's water resources in the Western United States.

The Bureau's original purpose "to provide for the reclamation of arid and semiarid lands in the West" today covers a wide range of interrelated functions. These include providing municipal and industrial water supplies; hydroelectric power generation; irrigation water for agriculture; water quality improvement; flood control; river navigation; river regulation and control; fish and wildlife enhancement; outdoor recreation; and research on water-related design, construction, materials, atmospheric management, and wind and solar power.

Bureau programs most frequently are the result of close cooperations with the U.S. Congress, other Federal agencies, States, local Governments, academic institutions, water-user organizations, and other concerned groups.

The research covered by this report was funded under the Bureau of Reclamation Program Related Engineering and Scientific Studies (PRESS) allocation No. DR-203 *Prevention of Cavitation to Flow Surfaces*.

When Congress authorized the reclamation of arid and semiarid lands in the West with the Reclamation Act of 1902, the Secretary of the Interior established the Reclamation Service within the United States Geological Survey. In 1907, the Reclamation Service became an independent agency within the Department of the Interior. By action of the Secretary of the Interior in 1923, the Reclamation Service became the Bureau of Reclamation. In November 1979, the name was changed to the Water and Power Resources Service by Secretarial Order, and in May 1981, the Secretary of the Interior changed the agency's name back to the Bureau of Reclamation.

Reprinting or republication of any portion of this publication should give appropriate credit to the Bureau of Reclamation—U.S. Department of the Interior.

The information contained in this report regarding commercial products or firms may not be used for advertising or promotional purposes and is not to be construed as an endorsement of any product or firm by the Bureau of Reclamation.

Preface

This monograph is not intended to be a comprehensive treatise on cavitation in hydraulic structures. Instead, only highlights of cavitation theory are presented to give the reader a sense for the basic mechanisms that must be understood before engineering problems and solutions can be discussed. Many of the basic cavitation concepts are treated in much more detail by Knapp, Daily, and Hammitt in their classic book *Cavitation* which is available through the Institute of Hydraulic Research, University of Iowa, Iowa City, Iowa.

The purpose of this monograph is to give the designer of hydraulic structures both an understanding of cavitation and the design tools necessary to eliminate or reduce the damaging effects of cavitation in hydraulic chute and spillway structures. In the monograph:

- Chapter 1 discusses highlights of cavitation theory.
- Chapter 2 presents cavitation characteristics of typical surface irregularities. (The material in the first two chapters is applicable to both open and closed conduit systems.)
- Chapter 3 is a discussion of cavitation damage.
- Chapter 4 treats the influence of geometry.
- Chapter 5 addresses aeration and aerators.
- Chapter 6 contains recommendations for designers. (This chapter should help in specifying surface tolerances and deciding when special designs such as aerators are necessary.)
- Chapter 7 concludes with selected Bureau of Reclamation field experiences.

Several appendixes are included in the monograph which describe computer programs useful in the analysis of specific geometries:

- Appendix A contains the algorithms to calculate the cavitation and damage indexes for open channel flow situations.
- Appendix B describes a program to plot the cavitation and flow characteristics.
- Appendix C contains descriptions of two programs to investigate the effect of changes in the invert geometry on the cavitation index.
- Appendix D contains a description of a computer code used to design aerators.
- Appendix E contains the description of a program to determine the damage potential of a structure using historical data.

All programs in this monograph are written in Microsoft-Fortran.¹ The plotting program is written in PLOT88² which is compatible with Microsoft-Fortran. They have been compiled to run on an IBM PC compatible computer. The programs are included on three diskettes.

The first, **Source and Data** contains the source codes and example data for the executable programs. The source codes and their respective program names are as follows:

- | | |
|--|------------|
| • Flow and cavitation properties | WS77.FOR |
| • Plot of cavitation and flow properties | PLOT77.FOR |
| • Damage index from historical data | DINDX.FOR |
| • Trajectories from aerators | TRAJ.FOR |
| • Constant cavitation number profile | ECAVNO.FOR |
| • Controlled pressure profile | CONSTP.FOR |

¹ Registered trademark of Microsoft, Inc., 16011 NE 36th Way, Box 97017, Redmond WA 98073-9717.

² Registered trademark of Plotworks, Inc., PO Box 12385, La Jolla CA 92037-0635.



Acknowledgments

Cavitation in Chutes and Spillways has been in preparation for over eight years. To acknowledge all who influenced the direction of this effort during its writing is impossible. Nevertheless, some contributors deserve special recognition. Many thanks to T. J. Rhone, who undertook the task of collating the editorial comments into a final manuscript following my retirement in July 1987. Appreciation is expressed to the following individuals who reviewed the manuscript:

Task Committee on Cavitation in Hydraulic Structures, Hydraulics Division, American Society of Civil Engineers	A. F. Babb R.E.A. Arndt F. DeFazio
Water Resources Planning Commission, Taipei, Republic of China	C. M. Wu
Sinotech, Taipei, Republic of China	T. L. Chung Y. Cheng
University of Wisconsin	J. A. Hoopes
Snowy Mountain Engineering Corporation	E. J. Lesleighter
Pacific Gas and Electric Company	W. English
Harza Engineering Company	C. Y. Wei
Bureau of Reclamation	P. H. Burgi K. W. Frizell E. W. Holroyd J. H. LaBoon B. F. Mefford T. J. Rhone R. V. Todd J. C. Wadge R. N. Walters

The careful scrutiny of the manuscript by these individuals eliminated many errors and helped to explain areas which were not too clear. The review by Professor Hoopes was especially appreciated for its detailed thoroughness.

The plotting program was revised by K. W. Frizell to make it more flexible. The method of determining the radius of curvature from three points in the water surface program was contributed by E. W. Holroyd. C. M. Wu noted the similarity of the cavitation inception data for away-from-the-flow offsets with into-the-flow offsets. Technical editing and continuity for publication was performed by R. N. Walters.

Finally, I would like to thank my mentor, D. "Mike" Colgate, who first introduced me to the subject of cavitation. We spent many happy hours discussing various details on this fascinating subject.

Should the effort here result in value, it is because, as Sir Isaac Newton said:

"If I have seen further it is by standing upon the shoulders of giants."

Letter Symbols and Quantities

SYMBOL	QUANTITY	SYMBOL	QUANTITY
A	One-half amplitude of maximum negative pressure fluctuation	d_i	Initial dimensionless flow depth for constant cavitation number profile
A_j	Cross-sectional area of jet	d_k	Critical depth
A_g	Constant for a specific gas, mass, and temperature	d_n	Dimensionless flow depth
A_n	Dimensionless pressure ratio	d_o	Ramp height or offset height
A_o	Cross-sectional area of upstream pipe	E	Eötvös number
A_r	Jet trajectory coefficient	E_d	Depth of cavitation damage
A_t	Area of cross section	E_f	Potential energy of flow
A_v	Cross-sectional area of air duct	E_o	Potential energy at reference point
a	Experimental coefficient	e	2.71828 . . .
B	Boussinesq number	F	Froude number
B_g	Bulk modulus of gas	F_o	Froude number of flow at ramp
B_j	Width at lower end of spillway	F	Cosine of invert slope
B_m	Bulk modulus of mixture	F_r	Resistance factor
B_u	Width at upper end of spillway	f	Darcy-Weisbach friction factor
B_w	Bulk modulus of water	$f(s)$	A specified function
b	Experimental coefficient	$f(N)$	A function in terms of N
C	Experimental coefficient	f_0	Value of function at point 0
C_a	Mean air concentration of developed aeration	f_1	Value of function at point 1
C_b	Borda loss coefficient	f_2	Value of function at point 2
C_c	Stabilized damage depth factor	G	Iteration function
C_f	Mean resistance coefficient	g	Gravitational constant (acceleration)
C_g	Centrifugal acceleration factor	H	Characteristic dimension, offset height, length of cylinder, etc.
C_l	Summation of loss coefficients through the air duct	H_a	Atmospheric head
C_n	Pressure factor	H_b	Reservoir elevation minus elevation at point b
C_o	Mean air concentration at beginning of aeration	H_d	Pressure head downstream of valve or orifice
C_p	Pressure coefficient	H_i	Initial head at beginning of constant cavitation number profile
$(C_p)_{min}$	Most negative value of Euler number on body	H_t	Total head upstream of valve
C_{pr}	Minimum pressure coefficient of roughness	H_f	Head loss due to friction
C_w	Air concentration at wall	H_u	Pressure head upstream of valve or orifice
C_x	Mean air concentration at distance $(L_x - L_i)$	H_v	Vapor pressure (absolute) in terms of head
C_1	Constant	ΔH	Negative pressure head pulsation at offset
C_2	Constant	h	Maximum time-average negative pressure head on the irregularity
c	Experimental coefficient	h_i	Flow depth downstream of impact point
D	Width or depth of section	h_l	Head loss from crest to first station
D_e	Diameter of pipe	h_c	Critical depth
D_i	Damage index	h_o	Flow depth at end of ramp
D_j	Diameter of jet	h_p	Pool depth
D_o	Flow depth upstream of offset	h_w	Wall pressure head
D_p	Damage potential	I_c	Cavitation damage intensity
D_s	Stabilized depth of damage	i	Damage coefficient
d	Flow depth normal to invert	K_n	Curvature normal to streamline
d_c	Flow depth at beginning of constant cavitation number profile	K_r	Cavitation index in terms of relative head
d_e	Flow depth from constant cavitation number profile	K_s	Curvature of streamline
d_f	Effective flow depth at first station	K_t	Cavitation index in terms of total head
		k	Ideal gas constant
		k_r	Constant to control the radius of curvature

SYMBOL	QUANTITY	SYMBOL	QUANTITY
k_s	Sand grain roughness or rugosity	r	Radius of bubble
L	Difference in stationing between upper and lower ends of spillway	r_c	Critical radius
L_c	Run of chamfer	S	Boundary layer shape parameter
L_i	Slope distance downstream from aerator to beginning of aeration	S_b	Coordinate distance on invert curve
L_j	Slope distance from aerator to impact point of jet	S_f	Friction slope
L_k	Length of cavitation cloud	S_1	Upstream slope
L_s	Distance over which friction loss occurs	S_2	Downstream slope
L_v	Length of vertical curve	s	Coordinate distance tangent to streamline
L_x	Slope distance downstream from aerator	s_m	Maximum value of s for a controlled pressure profile
M	Mass of one mole of a gas	T	Top width of water surface at first station
m	Mass of gas	T_c	Temperature, Celsius
N	Variable	T_k	Temperature (absolute), Kelvin
ΔN	Interval between points 0, 1, and 2	t	Time
n_m	Number of moles	t_c	Cumulative time of operation
n	Coordinate distance normal to streamline	t_o	Integration constant
P	Pressure intensity	U_a	Velocity tangent to streamline at point a
P_a	Atmospheric pressure	U_b	Velocity at the boundary
P_b	Pressure in plane of irregularity	U_i	Mean velocity of jet at impact point
P_d	Difference between minimum fluid pressure and vapor pressure	U_n	Velocity normal to streamline
P_e	Pressure in core of jet	U_o	Mean flow velocity at ramp lip
P_g	Gauge pressure	U_s	Velocity tangent to streamline
P_h	Pressure in free stream in plane of offset	u'	Root mean square value of the longitudinal velocity component
P_j	Pressure under the jet	V	Flow velocity
P_m	Pressure at roughness	V_a	Characteristic velocity
P_o	Reference pressure	V_b	Free stream velocity in plane of offset
P_p	Partial pressure of gas	V_c	Flow velocity in circular conduit
P_r	Reduced pressure (vacuum)	V_e	Velocity in core of jet
P_s	Saturation pressure	V_h	Velocity at height of offset
P_u	Pressure in free stream upstream of beginning of boundary layer	V_m	Average flow velocity
P_v	Vapor pressure of water	V_o	Reference velocity for cavitation index
P_w	Minimum pressure due to roughness	V_r	Reference velocity for damage potential
ΔP	Change in pressure	V_s	Velocity of sound
Q	Discharge	V_u	Free stream velocity upstream of beginning of boundary layer
Q_a	Air discharge in duct	V_w	Velocity at roughness
Q_e	Entrained air flow rate	V_y	Velocity at height y
Q_w	Water flow rate	v	Point velocity at flow depth
q	Unit discharge of water	v'	Root mean square value of the transverse velocity component
q_a	Unit discharge of air	W	Width of section
q_n	Dimensionless unit discharge	X	Horizontal distance from beginning of vertical curve
R_e	Reynolds number	X_b	Distance from start of boundary layer
R_h	Reynolds number based on height of offset and free stream velocity	X_i	Horizontal distance from end of ramp to jet impact location
R_x	Distance Reynolds number	X_n	Horizontal distance from end of ramp to centerline of jet at impact point
R	Radius of curvature of reference streamline	X_o	Distance downstream from aerator to beginning of aeration
R'	Radius of conduit	x	Horizontal coordinate
R_b	Radius of curvature at the boundary	Y_i	Elevation at impact point
R_g	Engineering gas constant	Y_n	Elevation of centerline of jet at impact point
R_h	Hydraulic radius	Y_o	Elevation of ramp lip
R_n	Dimensionless radius of curvature	y	Vertical coordinate
R_o	Initial radius of bubble		
R_u	Universal gas constant		

SYMBOL	QUANTITY	SYMBOL	QUANTITY
Z	Elevation	Z_i	Invert elevation of first point
Z_a	Elevation at point a	Z_r	Elevation of reservoir
Z_g	Energy gradeline elevation	Z_o	Reference elevation
α	Henry's law, coefficient	ρ_g	Density of gas
α_o	Kinetic energy coefficient	ρ_m	Density of mixture
β	Gas concentration	σ	Cavitation index
β_a	Air flow ratio	σ_b	Cavitation index based on free stream condition in plane of offset
δ	Boundary layer thickness	σ_c	Cavitation index in circular conduit
δ_d	Displacement thickness	σ_e	Cavitation index in constant cavitation number spillway
δ_m	Momentum thickness	σ_f	Cavitation index of flow
δ_o	Pressure intensity coefficient, one-half amplitude of maximum negative pressure fluctuation divided by average velocity head	σ_{fh}	Cavitation index of flow based on conditions at height of offset
ϵ	Interfacial surface tension	σ_h	Cavitation index based on conditions at height of offset
ζ	Vorticity	σ_i	Incipient cavitation index
η	Dimensionless head	σ_j	Cavitation index for a submerged jet
θ	Angle between tangent to invert and horizontal	σ_k	Cavitation index based on average velocity over height of offset
θ_d	Deflection angle of a vertical curve	σ_r	Cavitation index of a body having an isolated roughness
θ_e	Angle between the tangent to nappe at ramp and horizontal	σ_s	Cavitation index when damage begins
θ_i	Angle between downstream chute invert and horizontal	σ_u	Cavitation index based on free stream condition upstream of start of boundary layer
θ_j	Angle between centerline of jet at impact point and invert of chute	τ	Collapse time of a bubble
θ_o	Angle between ramp and horizontal	v	Volume
θ_u	Angle between upstream chute invert and horizontal	v_g	Volume of gas
θ_e'	Effective ramp angle	v_o	Original volume
θ_o'	Tangent to jet trajectory	v_w	Volume of water
μ	Dimensionless convergence ratio	Δv	Change in volume
ν	Kinematic viscosity	ϕ	Angle between ramp and invert
ξ	Dimensionless distance horizontal	ψ	Volume of air per volume of mixture
ξ_i	Initial dimensionless distance horizontal	Ω	Potential of external force
π	3.14159 . . .	ω	Angular velocity
ρ	Density of water	\propto	Varies as
ρ_a	Density of air		

Contents

Preface	<i>Page</i> v
Acknowledgments	vii
Letter Symbols and Quantities	viii
Chapter 1: Basic Concepts	
Description of Cavitation	1
Derivation of Cavitation Parameter	2
Formation of Cavitation	5
Theory	5
Empirical verification	6
Collapse Dynamics	8
Sonic Velocity of Gas Mixture	10
Bibliography	13
Chapter 2: Cavitation Characteristics of Flow Surfaces	
Categories of Surface Roughness	15
Singular Asperities	16
Into-the-flow offsets	16
Away-from-the-flow offsets	21
Holes in boundary	22
Transverse grooves	23
Grooves parallel with flow	23
Uniform roughness	23
Combination of uniform and isolated (singular) roughnesses	23
Superposition Principle	26
Bibliography	28
Chapter 3: Cavitation Damage	
Mode of Damage	29
Factors Affecting Cavitation Damage on a Surface	29
Cause of cavitation	29
Damage location	30
Cavitation intensity	31
Velocity effect	33
Air content effect	34
Surface resistance to cavitation damage	34
Exposure time effect	35
Parameters for Predicting Damage	35
Damage potential	37
Damage index	37
Design values	38
Recognition of Cavitation Damage	39
Texture	39
Symmetry	41
Origin	41
Bibliography	48
Chapter 4: Control of Cavitation Index by Geometry	
Control Methods	49
Equations of Motion	49
Velocity and Pressure at Flow Boundary	50
Geometric Relationships	52
Cavitation Parameter	52
Constant Cavitation Number Spillway	52
Controlled Pressure Spillway Profile	53

CONTENTS—Continued

	<i>Page</i>
Changing Invert Curvature—Example	54
Constant cavitation number profile	54
Controlled pressure profile	55
Changing Surface Roughness—Example	55
Bibliography	57
Chapter 5: Aerator Design	
Justification for Aerators	59
Types of Aerators	60
Location of Aerator	60
Ramp Design	60
Air Vent Design	63
Air vent configurations	63
Air flow relationships in ducts	64
Estimation of air entrainment capacity of the jet	64
Offset Design	66
Aerator Spacing	67
Design Procedure	69
Bibliography	71
Chapter 6: Design Recommendations	
Background	73
Specifications of Surface Tolerances	74
Offset	74
Slope	74
Uniformly distributed roughness	74
Flow surface tolerance: definition and specifications	74
Geometric Considerations	76
Design Procedure	77
Bibliography	78
Chapter 7: Spillways — Field Experience	
Case Studies	79
Blue Mesa Dam	79
Flaming Gorge Dam	80
Glen Canyon Dam	81
Hoover Dam	83
Kortes Dam	84
Yellowtail Dam	85
Bibliography	90
Appendixes:	
A. Cavitation Characteristics for Open Channel Flow Program	
Program Description	91
Algorithms Used in Program	91
Friction factor	91
Curvilinear flow	92
Pressure distribution on steep slopes	93
Kinetic energy correction factor	93
Critical depth	93
Cavitation computations	94
Air entrainment	94
Profile Types	94
Computational Problems	94
Starting station	94
Starting depth	94
Impossible flow conditions	96

CONTENTS—Continued

	<i>Page</i>
Cross Section Shapes	96
Trapezoidal	96
Circular	96
Egg shape	96
Horseshoe	97
Composite	97
Modified horseshoe	97
User defined circular-arc cross section	97
Input File	98
Glen Canyon Left Tunnel Spillway—Input	103
Typical Output	104
Hydraulic properties of Glen Canyon left tunnel spillway — output	104
Cavitation properties of Glen Canyon left tunnel spillway — output	105
Formatted geometry file of Glen Canyon left tunnel spillway — output	106
Plot file of Glen Canyon left tunnel spillway — output	107
Bibliography	108
B. Cavitation and Flow Characteristics Plotting Program	
Program Description	109
Communications ports	109
Model of output device	109
Program Output	110
C. Geometry Programs	
Program Description	113
Constant Cavitation Number Spillway	113
Controlled Pressure Spillway	114
Constant Cavitation Number Input	115
Constant Cavitation Number Output — Solid Body Rotation Assumption	116
Constant Cavitation Number Output — Irrotational Flow Assumption	118
Controlled Pressure Profile — Input	121
Controlled Pressure Profile — Output	122
D. Aerator Trajectory Program	
Program Description	125
Program Input	126
Program Output	127
E. Damage Index — From Historical Data Program	
Program Description	129
Program Input	130
Program Output	132
Cavitation References	135

TABLES

Table		
1-1	Properties of pure water	3
1-2	Influence of surface tension and air content on incipient cavitation index	8
2-1	Triangular and circular arc irregularity coefficients	19
2-2	Cavitation characteristics of holes in a boundary	22
3-1	Length of cavitation cavities in Glen Canyon Dam left tunnel spillway — station 760.70 (m)	30
3-2	Length of cavitation cavities in Glen Canyon Dam left tunnel spillway — station 739.38 (m)	30
3-3	Damage indexes for Glen Canyon Dam left tunnel spillway	38
3-4	Design values of damage potential and damage index	39
5-1	Location of aerator and critical discharge	61
5-2	Maximum pressure drop and air duct velocity	64
6-1	Grinding tolerances for high velocity flow	73
6-2	Flow surface tolerances	74
6-3	Specification of flow surface tolerance	76

CONTENTS—Continued

FIGURES		<i>Page</i>
<i>Number</i>		
1-1	Phase diagram for water	1
1-2	Pressure distribution on hemispherical rod	2
1-3	Definition of pressure scales	2
1-4	Reference velocity definition	3
1-5	Reference conditions for shear flow	4
1-6	Development of cavitation	5
1-7	Equilibrium conditions for vapor bubbles containing air	5
1-8	Henry's law coefficients	7
1-9	Effect of velocity on vaporous and gaseous cavitation	7
1-10	Bubble history for flow around a 1.5 caliber ogive	8
1-11	Collapse mechanisms of bubbles	9
1-12	Cavitation of baffle piers in Bonneville Dam model	12
1-13	Sonic velocity of air-water mixtures	12
2-1	Typical isolated roughness elements found in hydraulic structures	15
2-2	Incipient cavitation characteristics of offsets	16
2-3	Incipient cavitation characteristics of chamfered and elliptically rounded offsets	17
2-4	Cavitation characteristics of chamfers	18
2-5	Cavitation characteristics of isolated irregularities	20
2-6	Pressure distribution at a gate slot	21
2-7	Cavitation characteristics of a backward facing step, sudden expansions, and submerged jet	22
2-8	Cavitation damage at a "bug hole"	24
2-9	Cavitation characteristics of holes	24
2-10	Cavitation characteristics of gate slots	25
2-11	Cavitation damage in longitudinal grooves	26
3-1	Glen Canyon Dam, left tunnel spillway — station 760.70	31
3-2	Glen Canyon Dam, left tunnel spillway — station 739.38	32
3-3	Hoover Dam, Nevada tunnel spillway — Christmas-tree pattern of damage	33
3-4	Cavitation damage rate	33
3-5	Cavitation damage with respect to cavitation index	34
3-6	Comparative cavitation resistance of various materials	35
3-7	Cavitation damage rate	35
3-8	Damage experience in spillways	36
3-9	Variation in damage index with discharge and time	38
3-10	Glen Canyon Dam, left tunnel spillway	40
3-11	Glen Canyon Dam, left tunnel spillway — damage at station 760.20	41
3-12	Texture of cavitation damage in steel	42
3-13	Cavitation damage in concrete	43
3-14	Bradbury Dam, California, damage produced in 254-mm-dia. butterfly valve by sediment-laden water	44
3-15	Kortes Dam, Wyoming, freeze-thaw damage	45
3-16	Palisades Dam, symmetrical damage in outlet structure	46
3-17	Palisades Dam, outlet works—vortex caused damage downstream of slide gate ...	47
4-1	Definition sketch of intrinsic coordinate system	50
4-2	Definition sketch for integration along a streamline	51
4-3	Definition sketch for geometry	52
4-4	Glen Canyon Dam, left spillway tunnel—cavitation index for flow of 475 m ³ /s ...	54
4-5	Glen Canyon Dam, equal cavitation number spillway profile — cavitation index for flow of 475 m ³ /s	55
4-6	Glen Canyon Dam, controlled pressure spillway profiles — cavitation index for flow of 475 m ³ /s	56
4-7	Effect of rugosity on cavitation characteristics	56

CONTENTS—Continued

FIGURES		<i>Page</i>
<i>Number</i>		
5-1	Types of aerators	60
5-2	Length of jet trajectory	61
5-3	Jet trajectory coefficients	62
5-4	Air supply to aerators	63
5-5	Air vent critical pressure ratio	65
5-6	Air entrainment under nappe	66
5-7	Pool depth under nappe	66
5-8	Converging offset downstream of aerator	67
5-9	Development of self aerated flow	68
5-10	Air concentration at wall	69
6-1	Hoover Dam, Nevada, spillway — concrete surface near station 994.00	75
6-2	Lombardi crest	76
7-1	Blue Mesa Dam, tunnel spillway — aeration slot	79
7-2	Flaming Gorge Dam, tunnel spillway — aeration slot	81
7-3	Glen Canyon Dam, tunnel spillways — aeration slots	81
7-4	Glen Canyon Dam, tunnel spillways — major damage	82
7-5	Glen Canyon Dam, tunnel spillways — damage profiles	83
7-6	Hoover Dam, tunnel spillways — aeration slots	83
7-7	Hoover Dam, Arizona tunnel spillway — major damage (1942)	84
7-8	Hoover Dam, Arizona tunnel spillway — misalignment that caused major damage	85
7-9	Kortes Dam, tunnel spillway — profile	86
7-10	Kortes Dam, tunnel spillway — invert cavitation damage (left side) caused by freeze-thaw popout (right)	87
7-11	Kortes Dam, tunnel spillway — springline damage	88
7-12	Yellowtail Dam, tunnel spillway — profile	89
7-13	Yellowtail Dam, tunnel spillway — major damage downstream of elbow	89
7-14	Yellowtail Dam, tunnel spillway — damage in elbow	89
7-15	Yellowtail Dam, tunnel spillway — aeration slot	89
A-1	Piezometric pressure with curvilinear flow	92
A-2	Pressure distribution on steep slope	93
A-3	Profiles of gradually varied flow — classification	95
A-4	Trapezoidal and rectangular cross sections	96
A-5	Circular cross section	96
A-6	Egg-shape cross section	97
A-7	Horseshoe cross section	97
A-8	Composite cross section	97
A-9	Modified horseshoe cross section	97
A-10	User defined circular-arc cross section	97
B-1	Glen Canyon Dam, left spillway tunnel — comparisons of outputs	111

Basic Concepts

Chapter 1

DESCRIPTION OF CAVITATION

Cavitation is a process that usually is associated with damage to a surface or marked by intense noise. Both phenomena may occur during cavitation, but actually cavitation is neither of these. Instead, *cavitation* is defined as the formation of a bubble or void within a liquid. If the void is filled primarily with water vapor, the process is further classified as *vaporous cavitation*. If the void is filled primarily with gasses other than water vapor, the process is called *gaseous cavitation*. The distinction between these two types of cavitation are explained further in Formation of Cavitation — Theory.

An understanding of the cavitation process can be obtained by examining the process of boiling. When water is heated the temperature increases which results in increases in its vapor pressure. When the vapor pressure equals the local pressure, boiling will occur. At the boiling point, water is changed into water vapor. This change first occurs at localized points within the water and it is observed as small bubbles.

The temperature at which boiling occurs is a function of pressure. As pressure decreases, boiling will occur at lower and lower temperatures. Since the pressure is a function of elevation, boiling occurs at lower temperatures at higher elevations as noted on figure 1-1. If it were possible to go to a high enough elevation, boiling would occur at room temperature.

Although cavities are formed in water by boiling and the process occurs when the local pressure equals the water vapor pressure, a technical difference between boiling and cavitation exists. *Boiling* is the process of passing from the liquid to the vapor state by changing temperature while holding the local pressure constant. *Cavitation* is the process of passing from the liquid to the vapor state by changing the local pressure while holding the temperature constant (fig. 1-1). The local pressure reductions associated with cavitation can be caused by turbulence or vortices in flowing water.

An example of bubble formation within a liquid, which occurs by reductions in pressure, can be seen when a bottle containing a carbonated liquid is opened. Upon opening the bottle, bubbles form within the liquid and rise to the surface. While in the capped bottle, the liquid is under enough pressure to keep the carbon dioxide in solution. However, as the bottle is opened, the pressure is reduced and the liquid becomes supersaturated relative to the carbon dioxide. Therefore, the carbon dioxide begins to diffuse out of the liquid. It should be noted that this example is one of so called “gaseous cavitation” in which vapor pressure of the liquid was never reached.

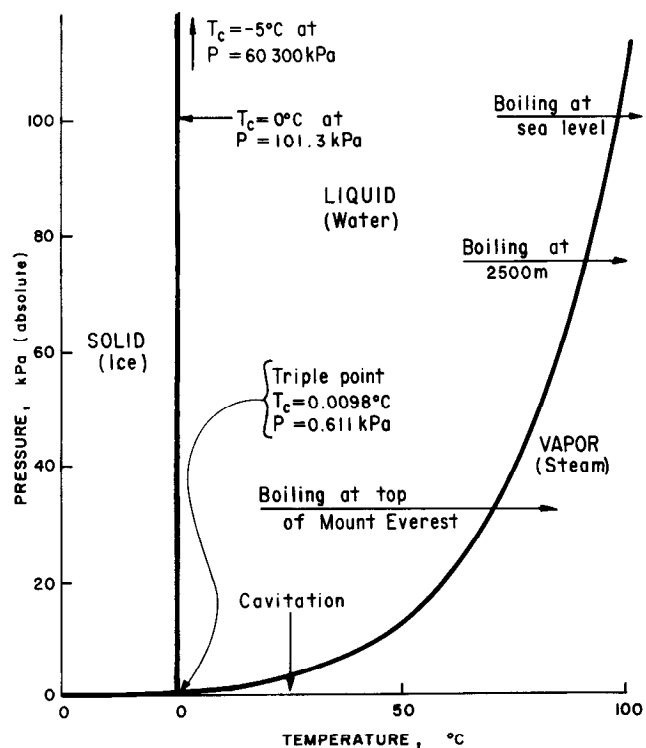


FIGURE 1-1.—Phase diagram for water.

In hydraulic structures, water contains air bubbles and various types of impurities of many different sizes. As will be seen later, microscopic air bubbles or impurities in the water are necessary to initiate cavitation. However, once started, vaporization is the most important factor in the cavitation bubble growth. The presence of air bubbles in the flow also has an effect on damage and noise produced by the cavitation.

In addition to describing cavitation by the contents of the void; that is, by vaporous or gaseous, cavitation also can be described by its occurrence. For instance, if the pressure of flowing water is decreased through increases in the flow velocity, a critical condition is reached when cavitation will just begin. This critical condition is called *incipient cavitation*. Similarly, if cavitation exists and the flow velocity is decreased or the pressure is increased, a critical condition is reached when the cavitation will disappear. This condition is called *desinent cavitation*. Incipient cavitation and desinent cavitation often do not occur at the same flow conditions. The distinction is especially important in laboratory investigations, but can usually be ignored for all practical purposes in hydraulic structures.

Finally, a set of critical flow conditions exists for which the individual cavitation bubbles suddenly transition into one large void. Conditions under which the large void occurs is called variously as *cavity flow*, *developed cavitation*, or *supercavitation*.

DERIVATION OF CAVITATION PARAMETER

The preceding section alluded to the existence of a critical combination of the flow velocity, flow pressure, and vapor pressure of the water at which cavitation will appear, disappear, or spontaneously transition into supercavitation. A parameter exists which can be used to define these various occurrences of cavitation. The parameter is known as the *cavitation index* and is derived below.

The equation for steady flow between two points in a flow stream is known as the Bernoulli equation. It can be written:

$$\frac{\rho V_o^2}{2} + P_o + Z_o \rho g = \frac{\rho V^2}{2} + P + Z \rho g \quad 1.1$$

where:

- P = pressure intensity
 - P_o = reference pressure
 - V = flow velocity
 - V_o = reference velocity
 - Z = elevation
 - Z_o = reference elevation
 - g = gravitational constant (acceleration)
 - ρ = density of water
- (The subscript o refers to upstream flow location as noted on fig. 1-2.)

In dimensionless terms, the comparable equation results in a pressure coefficient, C_p :

1.2

$$C_p = \frac{(P + Z \rho g) - (P_o + Z_o \rho g)}{\rho V_o^2 / 2} = \frac{E_f - E_o}{\rho V_o^2 / 2} = 1 - \left(\frac{V}{V_o}\right)^2$$

where:

E_f = potential energy of flow (defined by values in parentheses)

E_o = potential energy at reference point

In many cases, the gravitational terms are small relative to the pressure term or they are about equal; thus, the pressure coefficient can be written:

$$C_p = \frac{P - P_o}{\rho V_o^2 / 2} \quad 1.3$$

The pressure coefficient is also known as the pressure parameter or *Euler number*.

The value of the Euler number, at any point on a body, is a constant as long as the minimum pressure on the body is greater than the vapor pressure of water. For example, on figure 1-2, the pressure at any point on a rod—having a hemispherical end—is predictable in terms of the upstream conditions. However, if the pressure at the location that corresponds to the minimum Euler number drops to vapor pressure, then the pressure at that point will not decrease any further. The upstream conditions that correspond to the onset of cavitation can be calculated by replacing the boundary pressure in equation 1.2 with vapor pressure and setting the value of the ratio equal to the minimum Euler number. The resulting parameter is known as the *cavitation index*, σ .

$$\sigma = \frac{E_o - Z_o \rho g - P_v}{\rho V_o^2 / 2} = -(C_p)_{min} \quad 1.4$$

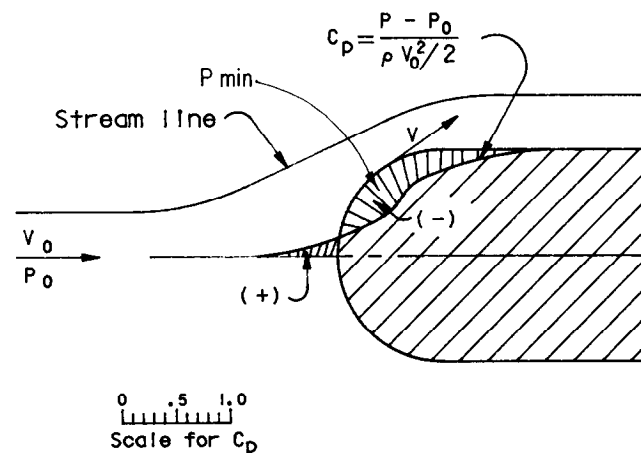


FIGURE 1-2.—Pressure distribution on hemispherical rod.

If elevations Z and Z_o are equal, the cavitation index is expressed as:

$$\sigma = \frac{P_o - P_v}{\rho V_o^2 / 2} = -(C_p)_{min} \quad 1.5$$

where P_v is the vapor pressure of water.

For smooth streamlined bodies, the most negative pressure occurs on the boundary. For these cases, the cavitation index can be estimated from pressure measurements made on the surface. However, if the body is not streamlined, the flow will separate from the body and the most negative pressures will occur within the flow. In these cases, the cavitation index will be less than the absolute value of the minimum Euler number on the body.

To avoid ambiguities, both vapor pressure and reference pressure are referenced to absolute zero pressure as shown on figure 1-3. For example, in absolute units, the reference pressure is given by:

$$P_o = P_a + P_g \quad 1.6$$

In the literature, sometimes one notes a reference to a reduced or vacuum pressure. This is done to avoid expressing the gauge pressure as a negative number when the reference pressure is less than the atmospheric pressure. When using values of the vacuum pressure, the appropriate relationship for the reference pressure, P_o , is given by:

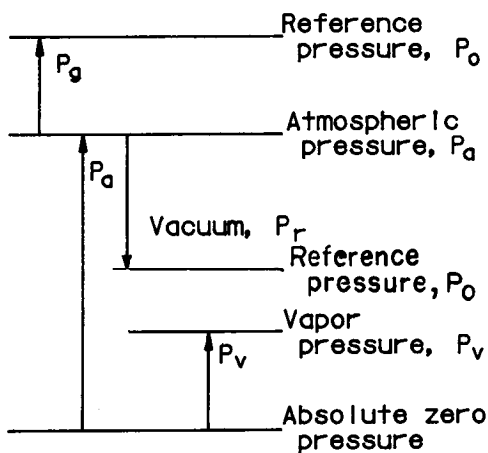
$$P_o = P_a - P_r \quad 1.7$$

where:

P_a = atmospheric pressure

P_g = gauge pressure

P_r = reduced pressure (vacuum)



Note: All arrows are defined to point in positive direction.

FIGURE 1-3.—Definition of pressure scales.

For example, the cavitation index can be calculated for the following conditions by using equations 1.5 and 1.6:

$$\begin{aligned} T_c &= 10^\circ\text{C} & V &= 30.0 \text{ m/s} \\ P_v &= 1.23 \text{ kPa} & P_g &= 9.8 \text{ kPa (1.0 m water column)} \\ P_a &= 101.0 \text{ kPa} & \rho &= 999.7 \text{ kg/m}^3 \end{aligned}$$

$$\sigma = \frac{(101.0 + 9.8 - 1.23) \times 10^3}{999.7 [(30)^2 / 2]} = 0.244$$

Table 1-1 provides values of density, vapor pressure, and viscosity of water as a function of temperature.

Table 1-1.—Properties of pure water

Temperature °C	Density kg/m ³	Vapor pressure kPa	Kinematic viscosity m ² /s × 10 ⁶
0	999.868	0.61	1.787
5	999.992	0.87	1.519
10	999.726	1.23	1.307
15	999.125	1.70	1.140
20	998.228	2.33	1.004
25	997.069	3.16	0.893
30	995.671	4.23	.801
35	994.055	5.62	.724
40	992.238	7.38	.658
45	990.233	9.58	.602
50	988.052	12.3	.553
60	983.20	19.9	.475
70	977.77	31.1	.413
80	971.80	47.3	.365
90	965.31	70.1	.326
100	958.36	101.3	.294

In practical situations, flow conditions are not as ideal as those shown on figure 1-2. For instance, for a bluff body within a boundary layer, the definition of the cavitation index depends upon the reference location as shown on figure 1-4. In this case, three different reference locations are noted; the three locations and corresponding cavitation indexes are:

1. Far upstream and outside of the effects of the boundary layer;

$$\sigma_u = \frac{P_u - P_v}{\rho V_u^2 / 2} \quad 1.8$$

2. Immediately upstream of an offset and at the maximum height of the offset;

$$\sigma_h = \frac{P_h - P_v}{\rho V_h^2 / 2} \quad 1.9$$

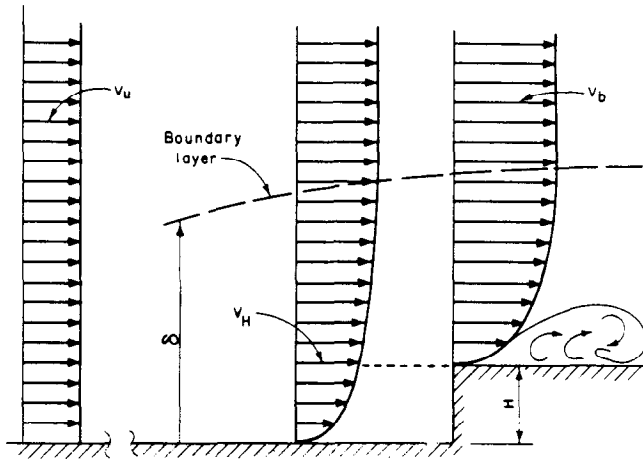


FIGURE 1-4.—Reference velocity definition.

3. Outside of the boundary layer and in the plane of the offset;

$$\sigma_b = \frac{P_h - P_v}{\rho V_b^2/2} \quad 1.10$$

where:

P_h = pressure in free stream in plane of offset

P_u = pressure in free stream upstream of beginning of boundary layer

P_v = vapor pressure of water

V_b = free stream velocity in plane of offset

V_h = velocity at height of offset

V_u = free stream velocity upstream of beginning of boundary layer

For shear flows, several forms of the cavitation parameter have been proposed. Each is based upon easily measurable reference conditions. For example, the cavitation index for a submerged jet, σ_j , shown on figure 1-5a is given by:

$$\sigma_j = \frac{P_e - P_v}{\rho V_e^2/2} \quad 1.11$$

where:

P_e = pressure in core of jet

V_e = velocity in core of jet

Other types of shear flow include discharges through gates, valves, and orifices as shown on figure 1-5b. For these, to define an appropriate reference flow and velocity is often difficult. In these cases, another form of the cavitation index, K_t , had been recommended by Ball [1].¹ It is:

$$K_t = \frac{H_d - H_v}{H_t - H_d} \quad 1.12$$

where:

H_d = pressure head downstream of valve (12 pipe diameters [1])

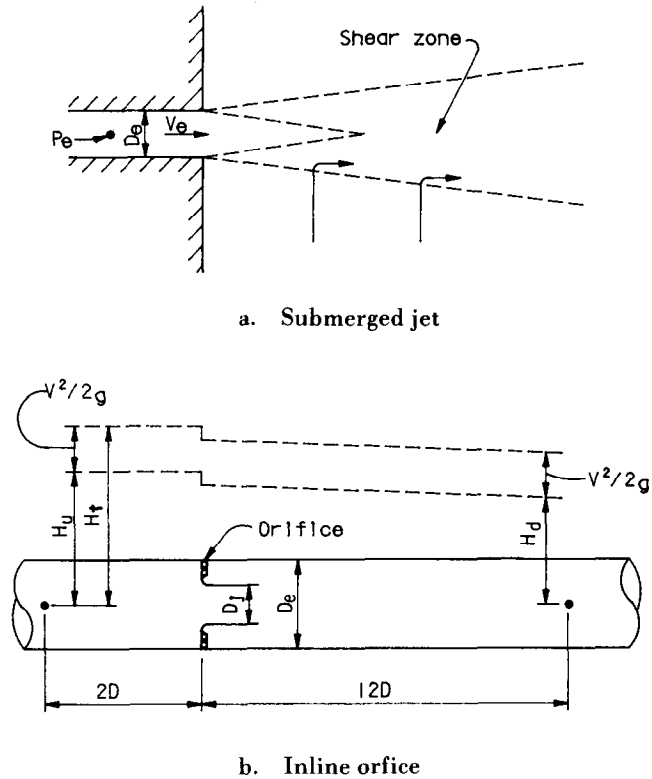


FIGURE 1-5.—Reference conditions for shear flow.

H_t = total head (pressure plus velocity) upstream of valve (2 pipe diameters [1])

H_v = vapor pressure expressed in head relative to atmospheric pressure

An alternate form of this equation is:

$$K_r = \frac{H_d - H_v}{H_u - H_d} \quad 1.13$$

where H_u equals pressure head upstream of valve.

These expressions can be shown to be related to equation 1.11 by:

$$K_t = \frac{\sigma_j + 1 - C_b - (A_j/A_o)^2}{(A_j/A_o)^2 + C_b} \quad 1.14$$

and

$$K_r = \frac{\sigma_j + 1 - C_b - (A_j/A_o)^2}{C_b} \quad 1.15$$

where:

A_o = cross-sectional area of upstream pipe

C_b = Borda loss coefficient = $(H_u - H_d) / (V_e^2/2g)$

In these equations, energy loss between the upstream section and the vena contracta has been neglected.

Although one parameter such as the cavitation index—in whatever form it is expressed—cannot

¹ Number within brackets refers to the bibliography.

describe many of the complexities of cavitation, it is an extremely useful parameter to indicate the state of cavitation in a hydraulic structure. For example, for flow past a sudden into-the-flow offset, cavitation will not occur if the cavitation index (defined by equation 1.8) is greater than about 1.8 as noted on figure 1-6. As the cavitation index decreases below 1.8, more and more cavitation bubbles form within the flow. To the naked eye, the cavitation appears to be a fuzzy white cloud. However, a flash photograph reveals that the cloud consists of individual bubbles. For even lower values of the cavitation index, the cloud suddenly forms one long supercavitating pocket.

FORMATION OF CAVITATION

Theory

Water does not spontaneously change from the liquid to the vapor state as either the temperature

is raised or the pressure is decreased. Water which has been distilled and filtered many times can sustain extremely large negative pressures without cavitating. Cavitation and boiling are both observed to begin at the location of impurities in the flow or at minute cracks on a smooth boundary. It is not known if particles of dirt serve as nuclei for the vaporization. However, Katz [2] observed that the appearance of visible cavitation in flowing water was always preceded by the occurrence of a swarm of microscopic bubbles in a small region of the flow field. The importance of bubbles—as cavitation nuclei—has been known for a long time and all of the theory, for the formation of cavitation, has been built up around the existence of microscopic bubbles in the flow.

Spherical bubble stability was studied by Daily and Johnson [3]. The force balance on a hemispherical section of a bubble shown on figure 1-7 containing water vapor and a gas is given by:

$$\pi r^2 (P_v + P_p) = 2\pi r \epsilon + \pi r^2 P_o \quad 1.16$$

or

$$P_v + P_p = \frac{2\epsilon}{r} + P_o \quad 1.17$$

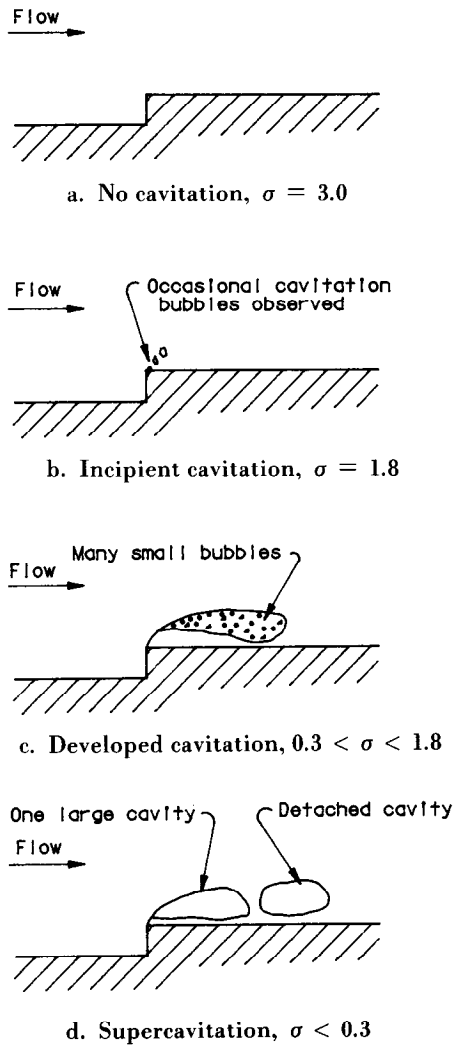


FIGURE 1-6.—Development of cavitation.

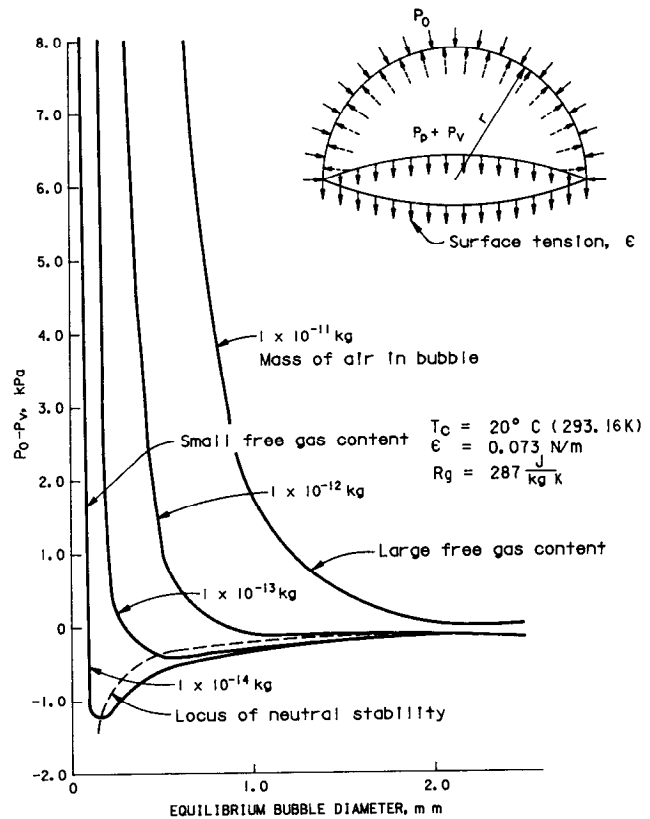


FIGURE 1-7.—Equilibrium conditions for vapor bubbles containing air.

where:

- r = radius of bubble
- P_o = reference pressure (of fluid surrounding the bubble)
- P_p = partial pressure of gas
- P_v = vapor pressure of water
- ϵ = interfacial surface tension
- π = 3.14159 . . .

Assuming gas in the bubbles obeys the perfect gas law:

$$P_p = \frac{n_m R_u T_k}{v_g} = \frac{n_m R_u T_k}{\pi r^3} = \frac{m R_g T_k}{\pi r^3} \quad 1.18$$

where:

- m = mass of gas, kg
- n_m = number of moles = m/M
- M = mass of one mole of gas, kg
- R_g = engineering gas constant², J/(kg·K) for air
- R_u = universal gas constant, J/(mole·K)
- T_k = temperature (absolute), Kelvin³
- v_g = volume of gas

Equation 1.17 becomes:

$$P_o - P_v = \frac{A_g}{r^3} - \frac{2\epsilon}{r} \quad 1.19$$

where A_g is constant for a specific of gas, mass, and temperature; i.e., $A_g = m R_g T_k / \pi$.

Equation 1.19 gives the solution of a family of curves for various quantities of air in the bubbles as shown on figure 1-7.

These curves represent the equilibrium condition for the vapor bubble containing air. The stability of the bubble can be investigated by examining the full differential equation of the bubble [4]. The equation is:

$$\pi \left[r \frac{d^2 r}{dt^2} + \frac{3}{2} \left(\frac{dr}{dt} \right)^2 \right] = - \left(P_o - P_v + \frac{2\epsilon}{r} - \frac{A_g}{r^3} \right) \quad 1.20$$

If the right side of the equation is positive, the bubble will grow. Conversely, if the right side of the equation is negative, the bubble will decrease in diameter. Thus, the right side of the equation represents a force that causes the bubble size to change. The bubble stability is determined by the algebraic sign of the right side of the equation. The condition of neutral stability—known as the locus of neutral stability—occurs when the right side of equation 1.20 is equal to zero. This curve, shown on figure 1-7, is defined by:

$$P_d = P_o - P_v = - \frac{4}{3} \left(\frac{\epsilon}{r_c} \right) \quad 1.21$$

where:

- P_d = difference between minimum fluid pressure and vapor pressure
- r_c = critical radius = $\frac{3}{2} \left(\frac{m R_g T_k}{\pi \epsilon} \right)$

This theoretical development provides insight into the mechanics of the formation of cavitation. For example, if a bubble with a small free gas content is convected into a low-pressure region, the bubble diameter will remain about constant. However, if the pressure decreases enough for the bubble dimensions to reach the critical radius, the bubble size will increase explosively (fig. 1-7). The rapid expansion is only possible through vaporization of the water with little contribution from the expansion of the gas. Therefore, the process is one of vaporous cavitation.

Conversely, if a bubble containing a large free gas content is convected into a low-pressure region, the bubble diameter will continually expand without ever reaching a critical radius. In this case, the bubble expansion is primarily due to expansion of the gas. This nonexplosive growth of the bubble in which vapor pressure is never reached is characteristic of gaseous cavitation.

Empirical Verification

A theory should not only provide insights into the mechanics of a phenomenon, but it also should be experimentally verifiable. Holl [5] initiated an empirical study of the effects of air content on cavitation by rewriting equation 1.17 in the following form:

$$\frac{P - P_v}{\rho V_o^2 / 2} = \frac{P - P_o}{\rho V_o^2 / 2} + \frac{\alpha \beta}{\rho V_o^2 / 2} - \frac{2 \epsilon / r}{\rho V_o^2 / 2} \quad 1.22$$

where:

- P = pressure (from which the bubble begins to decrease in size)
- α = Henry's law coefficient
- β = gas concentration (moles of gas per mole of solute)

In comparing equation 1.22 with equations 1.3 and 1.5, observe that:

- the first term corresponds to σ ,
- the second term corresponds to $-C_p$,
- the third term represents the effects of the gas in the bubble, and
- the fourth term represents the effects of surface tension.

In equation 1.22, the partial pressure of the gas in the bubble has been replaced by the saturation pressure of the gas. For small gas concentrations,

² The properties of dry air (molecular weight = 28.97 kg) are: engineering gas constant 287 J/(kg·K), and universal gas constant 8314 J/(mole·K).

³ Kelvin = 273.16 + °C

the saturation or partial pressure of the gas is given by Henry's law:

$$P_s = \alpha \beta \tag{1.23}$$

The value of Henry's law coefficient is a function of both the type of gas and the water temperature as noted on figure 1-8. The coefficient is expressed in terms of pressure per mole fraction. The mole fraction is defined as the number of moles of gas per mole of solute.

Holl [5] found good agreement between the onset of cavitation predicted by equation 1.22 and the inception of cavitation on a hydrofoil for air concentrations between 7 and 17 moles of air per million moles of water. One example of the tests is that of investigations on a hydrofoil shown on figure 1-9. The test velocities ranged between 12 and 23 meters per second. The observed bubble diameters were on the order of 0.25 millimeter. The points denoting areal cavitation correspond to

vaporous cavitation. The points denoting spots of cavitation were individual bubbles on the hydrofoil surface that correspond to gaseous cavitation. For this hydrofoil, the theoretical minimum Euler number is 0.8. Test data indicate a cavitation index of 0.45. The reason for the difference between these two values is unknown.

NACA 16012 HYDROFOILS

$$t_{MAX} = 0.12 C$$

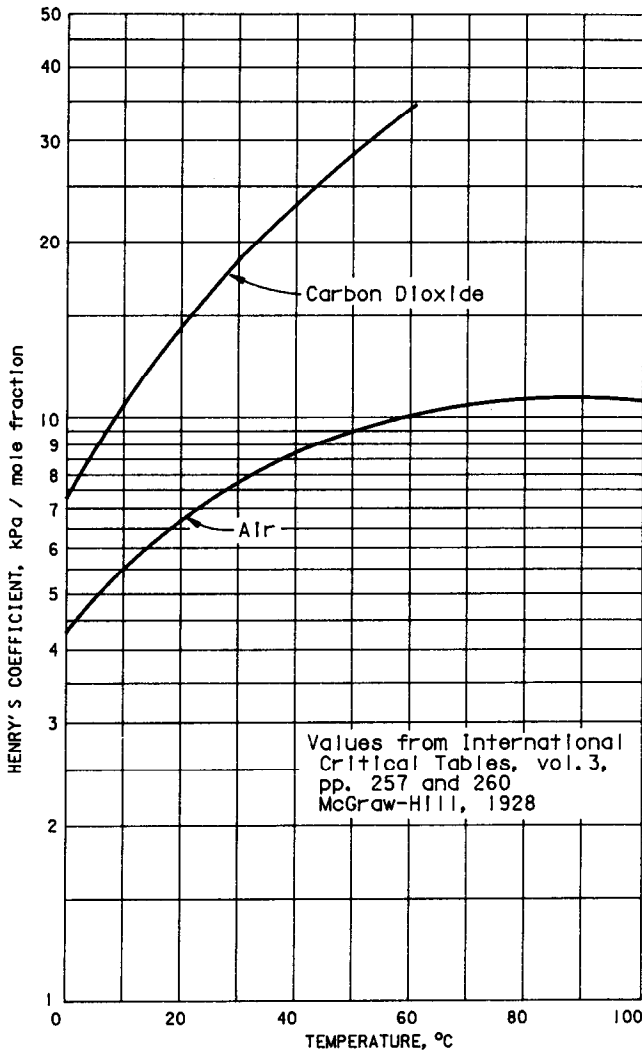
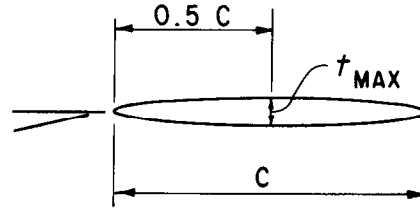
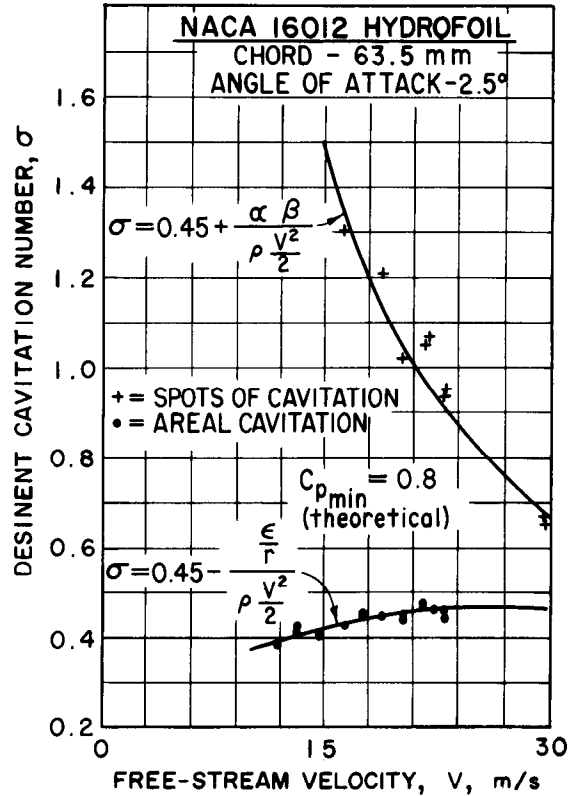


FIGURE 1-8.—Henry's law coefficients.



LEGEND

- $r = 0.0625 \text{ mm}$
- $T_c = 23.6^\circ \text{ C}$
- $\alpha = 17.3 \times 10^{-6}$
- $\beta = 7.1 \times 10^6 \text{ kPa/mole}$
- $\epsilon = 0.0740 \text{ n/m}$
- $\rho = 997.39 \text{ kg/m}$

FIGURE 1-9.—Effect of velocity on vaporous and gaseous cavitation.

The order of magnitude of the gaseous and surface tension terms in equation 1.22 and their relative importance in the experiments of Holl is estimated in table 1-2. The cavitation indices are calculated from equation 1.22 and the minimum value of the Euler number observed from the experiments. The value of the air concentration is not significant for vaporous cavitation nor is surface tension significant for gaseous cavitation.

Table 1-2.—Influence of surface tension and air content on incipient cavitation index

Temperature, °C		23.6	
Henry's coefficient, kPa/mole fraction		7.1×10^6	
Air concentration, mole fraction		17.3×10^{-6}	
Water density, kg/m ³		997.39	
Surface tension, N/m		0.0740	
Bubble radius, mm		0.0625	
Mass of gas in bubble, kg		1.1×10^{-15}	
Minimum Euler number		0.45	
Velocity, m/s		15.0	30.0
dissolved gas effects	$\frac{\alpha\beta}{\rho V_o^2/2}$	0.85	0.212
cavitation index for gaseous cavitation		1.30	0.66
surface tension effects	$\frac{2\epsilon/r}{\rho V_o^2/2}$	-0.048	-0.005
cavitation index for vaporous cavitation		0.402	0.445

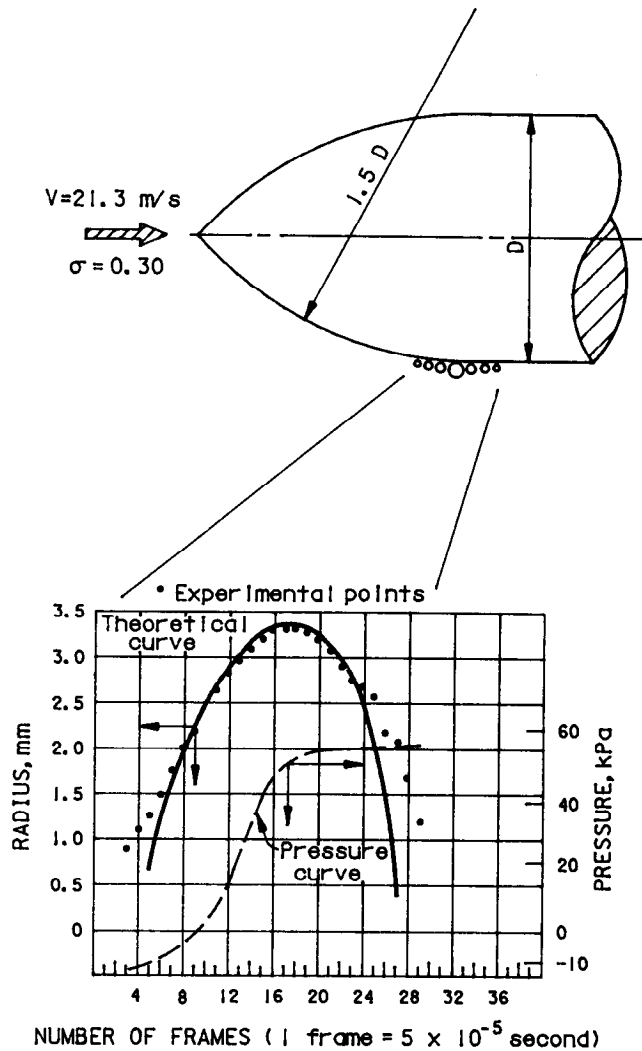
The experiment of Holl indicates that the magnitude of the flow velocity and the dissolved air concentrations have a major effect on the occurrence of cavitation. The significance is that if model studies are to predict accurately the cavitation potential of flows in the prototype, the model studies must be conducted with either high velocities or low dissolved air concentrations.

The requirement for high velocities means that Euler or Reynolds scaling may not be possible for closed conduit models. Similarly, Froude scaling may not be possible for open channel models if accurate simulation of the cavitation phenomenon is to be obtained.

The influence of air content and surface tension on the magnitude of the cavitation index are not the only factors which can be empirically verified. Plesset [6] investigated the change in size of a cavitation bubble as it passed through a pressure gradient as shown on figure 1-10. The theory, as expressed by equation 1.20, predicts reasonably well the growth and decay portions of the bubble history.

COLLAPSE DYNAMICS

In the previous section, growth and decay of bubbles was considered using a theory that assumed water to be incompressible. In addition, the vapor

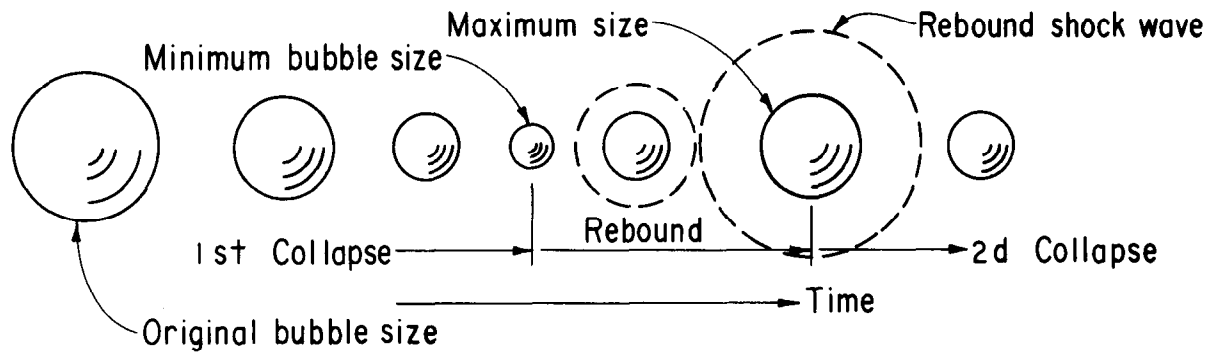


Note: One frame is approximately equivalent to 1 mm of displacement along the body of revolution. Theoretical curve: solution for a cavity of constant vapor density and temperature in an incompressible liquid with a variable pressure field.

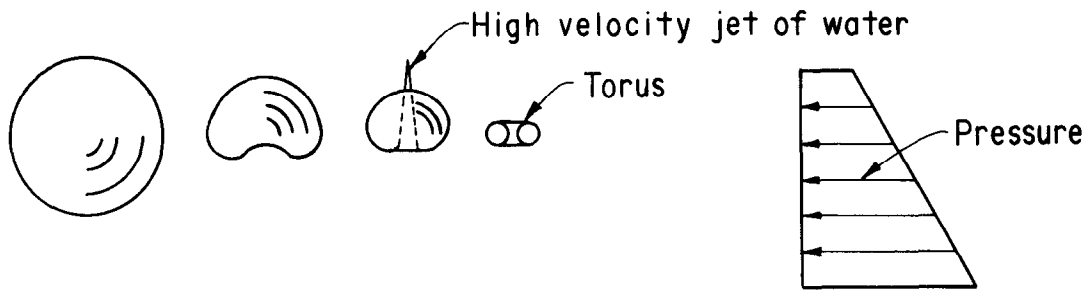
FIGURE 1-10.—Bubble history for flow around a 1.5-caliber ogive (Plesset [6]).

pressure, surface tension, and temperature were all considered to be constant. In reality, as a bubble collapses these assumptions are not valid. To simulate the collapse dynamics it is necessary to consider the compressibility of water, the compressibility of the gas in the bubble, and the enthalpy changes. These considerations result in six differential equations and four algebraic equations that must be solved simultaneously [4].

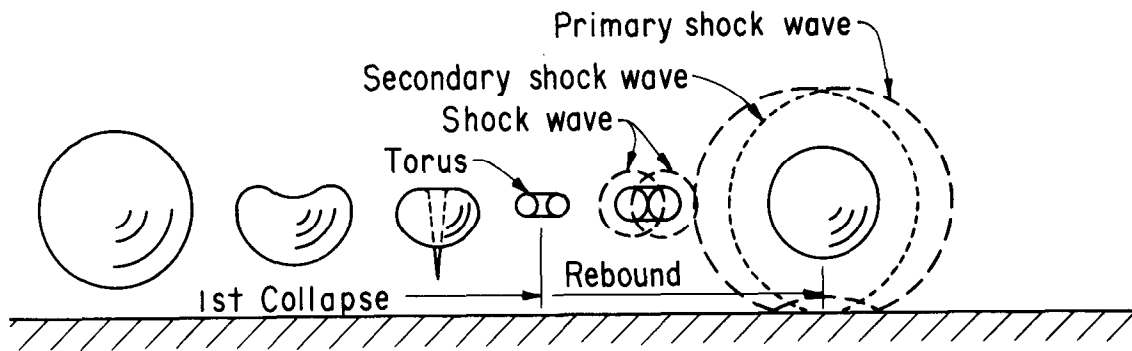
Numerical solution of the equations reveals that bubble collapse consists of phases in which the bubble diameter decreases, reaches a minimum value, and then grows or rebounds as shown on figure 1-11. The process is repeated for several cycles



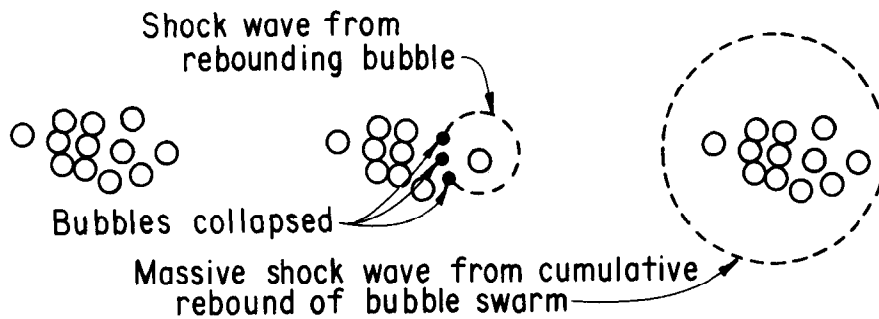
a. Collapse of an individual bubble in a quiescent fluid



b. Collapse of an individual bubble in a hydraulic gradient



c. Collapse of an individual bubble near a boundary



d. Collapse of a swarm of bubbles

FIGURE 1-11.—Collapse mechanisms of bubbles.

with the bubble diameter decreasing during each cycle until it finally becomes microscopic in size.

During the reversal or rebound phase, a shock wave forms. The shock wave velocity—as it radiates outward from the center of collapse—is equal to the speed of sound in water. Assuming that water is incompressible, Hickling and Plesset [7] found that the shock wave intensity varies inversely with the distance from the collapse center. At a distance of two times the initial bubble radius from the collapse center, the pressure intensity is about 200 times the ambient pressure at the collapse site. The following example illustrates a method of estimating the collapse pressure.

Assume a bubble diameter of 0.1 millimeter and a flow depth of 2.0 meters, then

$$\begin{aligned} \text{Water pressure} &= 2.0 \text{ m } (999 \text{ kg/m}^3) 9.8 \text{ m/s}^2 \\ &= 19\,580 \text{ Pa} \\ \text{Ambient pressure} &= \text{water pressure} + \text{barometric} \\ &\quad \text{pressure} \\ &= 19.58 \text{ kPa} + 101.3 \text{ kPa} \\ &= 120.9 \text{ kPa} \\ \text{Pressure intensity 0.1 mm from collapse center} &= 200 \times 120.9 \text{ kPa} \\ &= 24\,200 \text{ kPa} \end{aligned}$$

These computations ignore the effect of the initial bubble diameter and the water temperature on collapse pressure. Fujikawa and Akamatsu [8] show that both parameters have a significant influence. They found that the collapse pressure increased as either the initial bubble diameter or the water temperature decreases.

Theory also allows estimating the time for a bubble to collapse. The collapse time, τ , is given approximately by [4]:

$$\tau = R_o \left(\frac{\rho}{P_o} \right)^{1/2} \quad 1.24$$

where:

$$\begin{aligned} P_o &= \text{reference pressure (at collapse site)} \\ R_o &= \text{initial radius of bubble} \\ \rho &= \text{density of water} \end{aligned}$$

For a bubble having an initial diameter of 0.1 millimeter and an ambient pressure corresponding to 2.0 meters of water, the collapse time is:

$$\tau = 0.0001 \left(\frac{999}{120\,900} \right)^{1/2} = 9.1 \text{ microseconds}$$

Several factors modify the collapse mechanism of a purely spherical bubble. For instance, if the bubble collapses in the presence of a pressure gradient, the shape of the bubble does not remain symmetrical. Pressure gradients exist in flow around submerged bodies. If the bubble collapses near a boundary, the boundary restricts the flow toward the bubble which also causes an asymmetric collapse.

Both cases cause one side of the bubble to deform into a jet which penetrates the opposite side of the bubble as depicted on figure 1-11. The jet formed by the unsymmetrical collapse of a single bubble is called a *microjet*. The velocities of microjets are large. Hammitt [9] concluded that in most cases cavitation damage was due primarily to the liquid microjet impact on the surface and not to the spherical shock waves which emanate from the rebounding bubble. However, more recent photoelastic studies [8] have shown that the shock wave generates much higher pressure impulses than the jet.

If more than one bubble is present, the collapse of the first will produce shock waves that radiate to other bubbles. These shock waves will cause the sudden unsymmetrical collapse of neighboring bubbles. The jet formed by the unsymmetrical collapse of a bubble caused by shock waves is called an *ultrajet*. The velocities produced by ultrajets are on the order of one-half the sonic velocity of the liquid, Tomita and Shima [10]. Ultrajets generate higher pressure intensities than either spherical shock waves or microjets.

Unfortunately, theory does not exist to predict the magnitude of the pressures generated by the collapse of a swarm of bubbles. One can hypothesize: if one bubble in a swarm collapses, the shock wave the bubble produced during rebound will cause other bubbles in the vicinity to collapse. The process will continue in the form of a chain reaction until the remainder of the swarm effectively collapses simultaneously. It is logical that the synchronous collapse of a bubble swarm would produce a higher pressure intensity than the random collapse of individual bubbles in the swarm.

Another important factor influencing collapse of the cavitation bubble is the presence of vortices within the flow. Shear flows generate vortices that collect bubbles on their axes. Depending upon the proximity of bubbles, they may remain near each other in a swarm or they may coalesce into one filament shaped bubble as shown on figure 1-12.

Damage caused by the group of bubbles—trapped on the axis of a vortex—can be many times greater than that caused by the collapse of an individual bubble or even a swarm of bubbles. For example, an individual bubble having a 2.7-millimeter diameter can create a depression in aluminum which is about 0.2 millimeter in diameter [4]. However, cavitation occurring in the vortices of the shear layer formed by a partially opened slide gate (operating submerged) has caused depressions up to 16 millimeters long and measured pressure intensities of 1500 megapascals, Lesleighter [11].

SONIC VELOCITY OF GAS MIXTURE

The forgoing noted the sonic velocity of the fluid surrounding the collapsing bubble is a significant

parameter with respect to the pressure intensities generated by the collapse. The most important factor influencing the sonic velocity of the surrounding fluid is the presence of an undissolved gas in the liquid. In this case, the gas is air in the form of air bubbles. For this development, the bubble mixture is considered to be a uniform distribution of air bubbles in water.

In solids, disturbances produce longitudinal waves, transverse shear waves, and gravity waves. However, fluids cannot sustain a shear wave. The longitudinal waves in a liquid propagate at the speed of sound. The velocity of sound in an elastic medium is inversely proportional to the square root of the density of the material and directly proportional to the square root of the bulk modulus. The sonic velocity, V_s , is mathematically expressed as:

$$V_s = \left(\frac{B_m}{\rho_m} \right)^{1/2} \quad 1.25$$

where:

B_m = bulk modulus of mixture = $-\Delta P / (\Delta v / v_o)$
 ΔP = change in pressure
 Δv = change in volume
 v_o = original volume
 ρ_m = density of mixture

The density, ρ_m , of a homogeneous bubble mixture is given by:

$$\rho_m = \rho (1 - \psi) + \rho_g \psi \quad 1.26$$

where:

ρ = density of water
 ρ_g = density of gas
 ψ = volume of air per volume of mixture

The gas density, ρ_g , is determined from:

$$\rho_g = \frac{P}{R_g T_k} \quad 1.27$$

where:

R_g = engineering gas constant
 T_k = temperature (absolute), Kelvin

The bulk modulus, B_m , of a homogeneous mixture can be obtained from:

$$B_m = \frac{-\Delta P}{(\Delta v_w / v) + (\Delta v_g / v)} \quad 1.28$$

or

$$B_m = \frac{B_w B_g}{(1 - \psi) B_g + \psi B_w} \quad 1.29$$

where:

B_w = bulk modulus of water
 B_g = bulk modulus of gas

The bulk modulus of water varies with temperature. However, the variation is less than 4 percent from a value of 1.07 gigapascals over the temperature range 0 to 15 °C.

The bulk modulus of air for an adiabatic process is given by:

$$B_g = k P \quad 1.30$$

where:

k = ideal gas constant
 P = pressure intensity

Substitution of equations 1.26, 1.29 and 1.30 into equation 1.25 gives;

$$V_s = \left(\frac{k B_w P}{[(1 - \psi)kP + \psi B_w] [(1 - \psi)\rho + \psi \rho_g]} \right)^{1/2} \quad 1.31$$

This relationship has an unusual characteristic. At atmospheric pressure and an air concentration of only 0.1 percent, the sonic velocity of the mixture is equal to the sonic velocity in air as shown on figure 1-13. For higher air concentrations—at atmospheric pressure—the sonic velocity is less than the sonic velocity in air! At higher pressures, a larger air concentration is needed for the sonic velocity of the mixture to equal the sonic velocity of air.

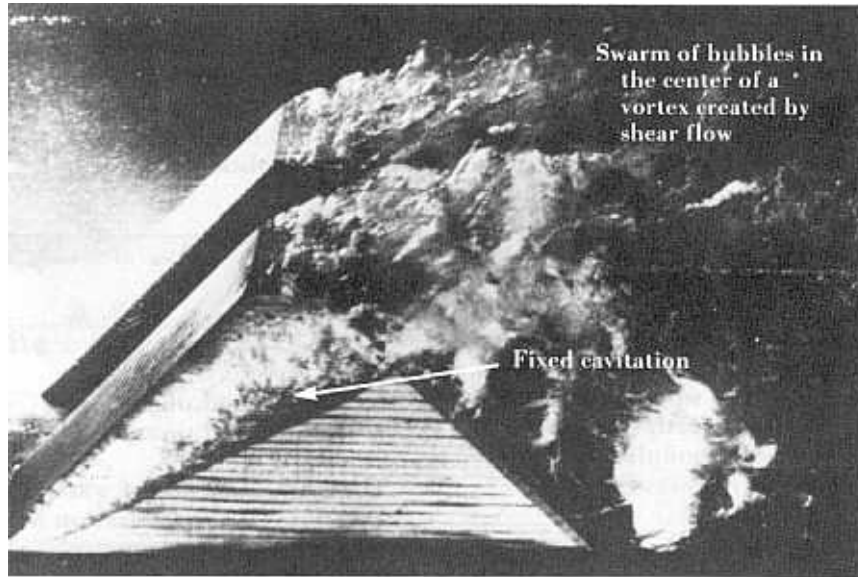


FIGURE 1-12.—Cavitation of baffle piers in Bonneville Dam model [U.S. Army Corps of Engineers].

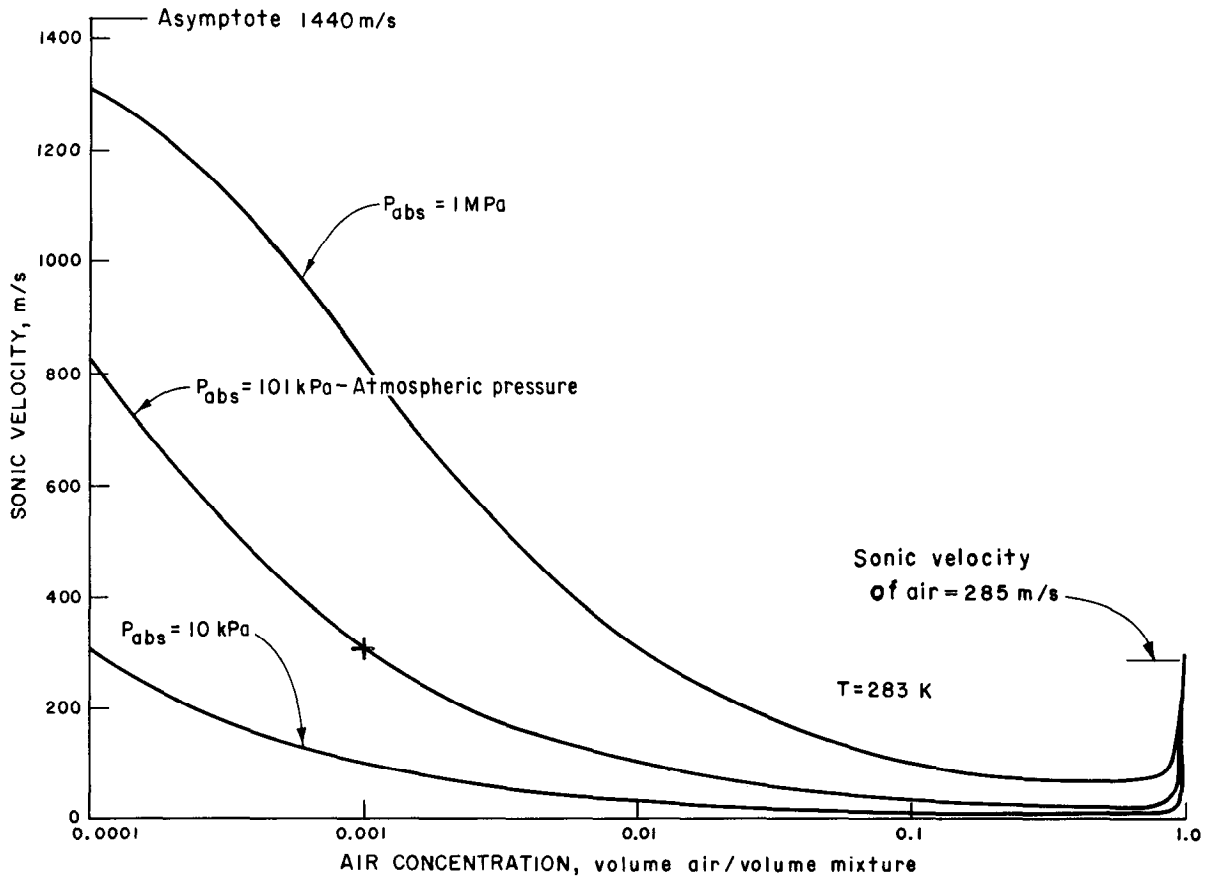


FIGURE 1-13.—Sonic velocity of air-water mixtures.

BIBLIOGRAPHY

- [1] Ball, J. W., "Cavitation Characteristics of Gate Valves and Globe Valves Used as Flow Regulators Under Heads up to About 125 ft.," *Transactions of the American Society of Mechanical Engineers*, vol. 79, No 9, August 1957.
- [2] Katz, J., "Cavitation Phenomena Within Regions of Flow Separation," *Journal of Fluid Mechanics*, vol. 140, pp. 397-436, 1984.
- [3] Daily, J. W., Johnson, V. E. Jr., "Turbulence and Boundary Layer Effects on Cavitation Inception From Gas Nuclei," *Transactions of the American Society of Mechanical Engineers*, vol. 78, pp. 1695-1706, 1956.
- [4] Knapp, R. T., Daily, J. W., Hammitt, F. G., *Cavitation*, McGraw-Hill, Inc., New York, 1970.
- [5] Holl, J. W., "An Effect of Air Content on the Occurrence of Cavitation," *Journal of Basic Engineering*, *Transactions of the American Society of Mechanical Engineers*, series D, vol. 82, pp. 941-946, December 1960.
- [6] Plesset, M. S., "The Dynamics of Cavitation Bubbles," *Journal of Applied Mechanics*, *American Society of Mechanical Engineers*, vol. 16, pp. 277-282, 1949.
- [7] Hickling, R., Plessett, M. S., "Collapse and Rebound of a Spherical Bubble in Water," *Physics of Fluids*, vol. 7, pp. 7-14, 1964.
- [8] Fujikawa, S., Akamatsu, T., "On the Mechanisms of Cavitation Bubble Collapse," *International Association for Hydraulic Research, 10th Symposium of Section for Hydraulic Machinery, Equipment and Cavitation*, Tokyo, pp. 91-102, 1980.
- [9] Hammitt, F. G., "Cavitation Erosion: The State of the Art and Predicting Capability," *Applied Mechanics Reviews*, vol. 32, No. 6, pp. 665-675, June, 1979.
- [10] Tomita, Y., Shima, A., "Mechanisms of Impulsive Pressure Generation and Damage Pit Formation by Bubble Collapse," *Journal of Fluid Mechanics*, vol. 169, pp. 535-564, 1986.
- [11] Lesleighter, E., "Cavitation in High-Head Gated Outlets — Prototype Measurements and Model Simulation," *International Association for Hydraulic Research, 20th Congress, Moscow*, vol. 3, sec. b., pp. 495-503, September 1983.

Cavitation

Chapter 2

Characteristics of Flow Surfaces

CATEGORIES OF SURFACE ROUGHNESS

Upon examining the flow surface of a hydraulic structure, the flow surface irregularities or the surface roughness can be characterized usually as belonging to one of two main categories (1) singular (isolated) roughnesses or (2) uniformly distributed roughnesses. Singular roughnesses are irregularities in a surface that are large relative to the surface irregularities from where they protrude. A uniformly distributed roughness is a surface texture that does not contain singular roughnesses. Between these two extremes is a category of moderate height singular roughnesses in combination with a uniformly distributed roughness which has not been systematically studied.

Sometimes, singular roughnesses are referred to as local asperities. Typical examples of these in hydraulic structures include:

- offset into-the-flow, fig 2-1a;
- offset away-from-the-flow, fig 2-1b, c, d;
- voids or grooves, fig 2-1e; and
- protruding joints fig 2-1g.

In all these cases, cavitation is formed by turbulence in the shear zone; the action is produced by the sudden change in flow direction at the irregularity. The location of the shear zone can be predicted from the shape of the roughness. Depending upon the shape of the roughness, cavitation bubbles will collapse either within the flow or near the flow boundary.

Figure 2-1f depicts cavitation above a distributed roughness. Cavitation occurs within the flow because of turbulence generated by the roughness of the boundary. The cavitation location is not predictable; however, cavitation always occurs within the body of the flow for distributed roughnesses.

This chapter contains compilations of cavitation characteristics for various types of roughness elements. The correlations were derived, for the most part, from tests conducted with either a singular roughness or a distributed roughness. An example is given for tests conducted with a typical concrete surface eroded by sand abrasion. This example illustrates the need for further studies of the combined effect of singular roughnesses on large scale distributed roughnesses.

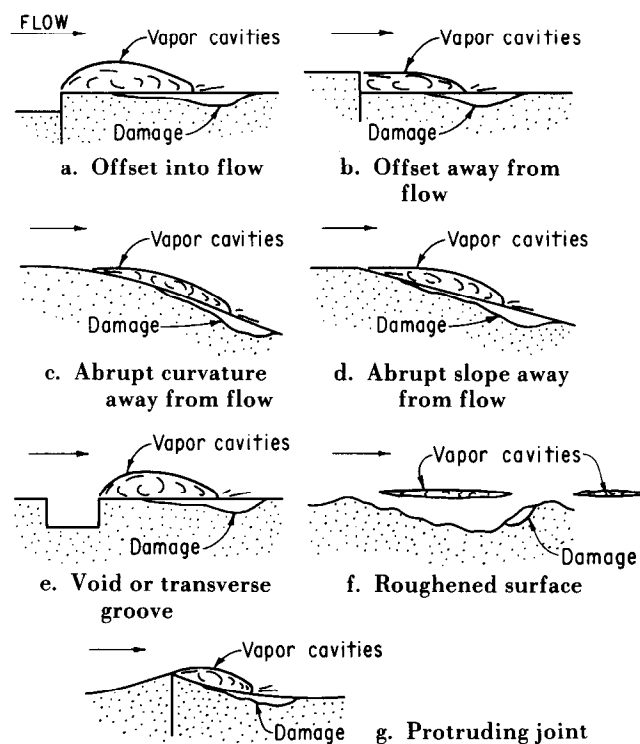


FIGURE 2-1.—Typical isolated roughness elements found in hydraulic structures.

Flow over curved boundaries that contain singular roughnesses exhibit different cavitation characteristics than flow over a flat plate having the same local asperities. Therefore, a method is given to estimate cavitation characteristics for flow over curved boundaries. This method is known as the *superposition principle*.

SINGULAR ASPERITIES

Two types of singular asperities exist: misalignments and isolated irregularities. Misalignments include both sudden and gradual changes in the alignment (figs. 2-1a, b, c, and d). The height dimension of misalignments is many times smaller than the length dimension. Isolated irregularities have approximately equal magnitudes of length and height (see fig. 2-5). For each of these specific classes of surface roughness types, cavitation indexes will be discussed in the following sections.

Into-the-Flow Offsets

The earliest studies of singular asperities concentrated on cavitation characteristics at misalignments. Investigations of into-the-flow offsets were presented as design curves by Colgate and Elder [1]

and are shown on figure 2-2. (Many of these curves were used by Ball [2]). Data were obtained in a test facility which was 102 millimeters high by 152 millimeters wide. The test section was located immediately downstream from a specially designed transition that produced an extremely thin boundary layer. For the larger offsets, the data are in error because blockage effects were not taken into account. The families of curves were corrected for blockage and expressed in a more compact form in 1977 by Colgate [3]. The condensed form was made possible by expressing the curves in terms of a cavitation index referenced to the plane of the offset, see equation 1.10. The technique permitted all the characteristics of the sudden offsets to be drawn on a single plot as shown on figure 2-3a. For chamfers having length to height ratios less than 5:1, the cavitation characteristics are a function of the offset height. A similar plot, shown on figure 2-3b, was made for rounding the leading edge of the offset to an ellipse.

Jin, et al. [4] also conducted studies of offsets and chamfers in a water tunnel. The test section was 200 by 200 millimeters and located immediately downstream of a convergent section. The boundary layer was extremely thin in this facility—as with the tests by Colgate. Jin found that the incipient cavitation index, σ_i , for chamfers could be expressed

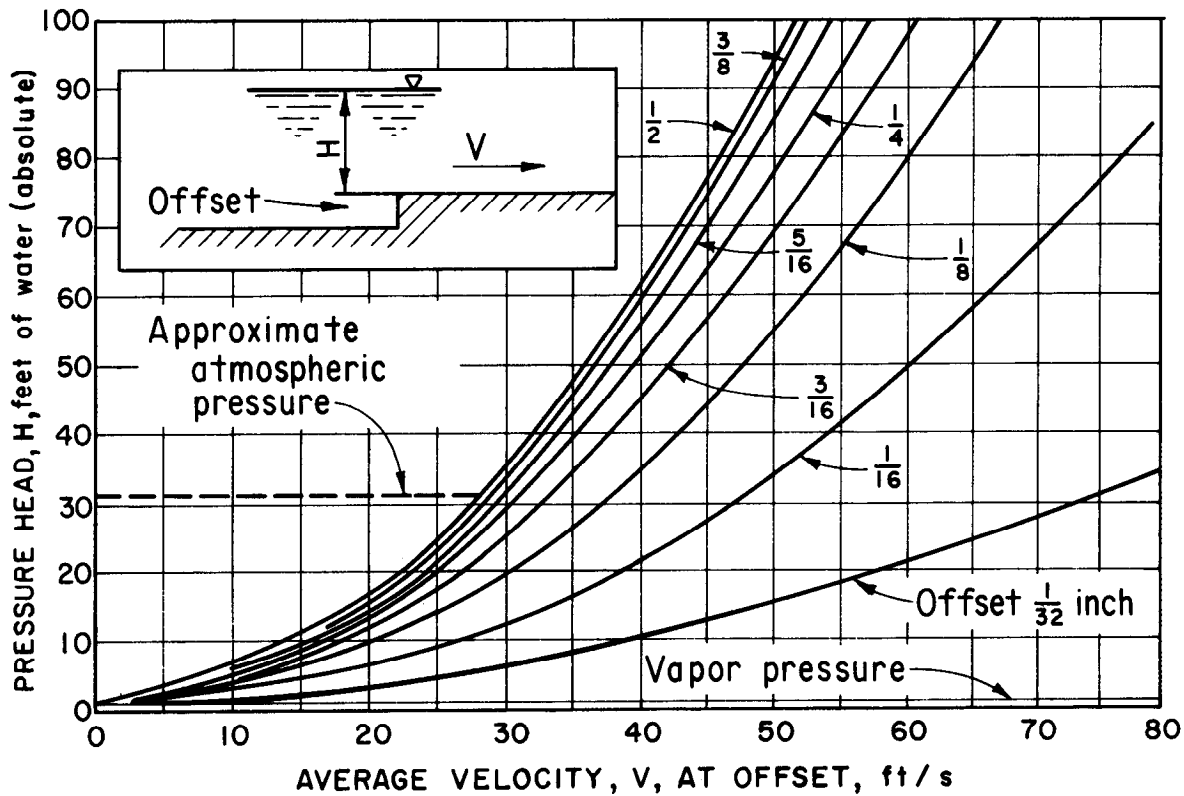


FIGURE 2-2.—Incipient cavitation characteristics of offsets (Colgate and Elder [1]).

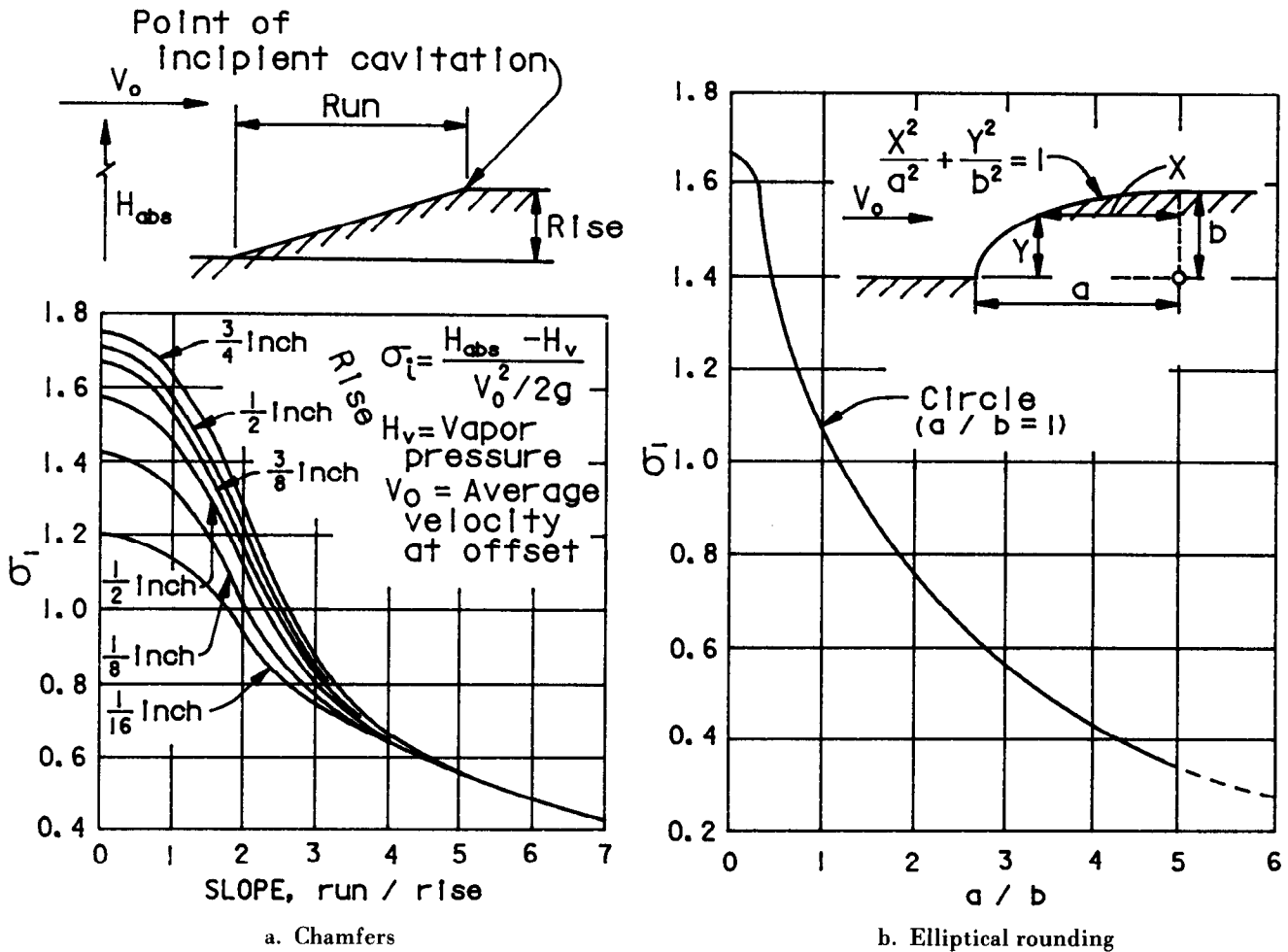


FIGURE 2-3.—Incipient cavitation characteristics of chamfered and elliptically rounded offsets.

according to the following empirical relationship for $L_c/H > 5.0$:

$$\sigma_i = 1.8 \left(\frac{L_c}{H} \right)^{-0.7} \quad 2.1$$

where:

H = height of offset

L_c = run of chamfer

σ_i = incipient cavitation index

Zharov [5] conducted experiments wherein the boundary layer thickness was 9 to 11 millimeters. Offset heights of 3, 6, 10, and 15 millimeters were tested. By using a cavitation index referenced to the height of the offset, as in equation 1.9, investigations showed the index was independent of the relative height and Reynolds number. The Reynolds numbers tested ranged from 10^3 to 10^6 .

A comparison of results, by the three investigators, shown on figure 2-4 reveals that the experiments of Colgate and Jin agree closely and actually compliment each other. For small chamfers ($L_c/H \leq 1$), Zharov's results also agree with Colgate and Jin. However, for large chamfers, the cavitation characteristics differ. One reason for the difference in

the results might be that Zharov tested with a significant boundary layer thickness.

Another method of accounting for the velocity distribution within the boundary layer was based on the frozen streamline theory of Holl [6]. He proposed that the relationship between the cavitation index without a boundary layer was related to the cavitation index with a boundary layer by:

$$\sigma_k = \sigma_u \left(\frac{V_a}{V_u} \right)^2 \quad 2.2$$

where:

V_a = characteristic velocity

V_u = reference free stream velocity

σ_k = cavitation index based on average velocity over height of offset

σ_u = cavitation index without a boundary layer

The characteristic velocity is the average velocity over the height of the offset and is defined as:

$$V_a = \left(\frac{1}{H} \int_0^H V_y^2 dy \right)^{1/2} \quad 2.3$$

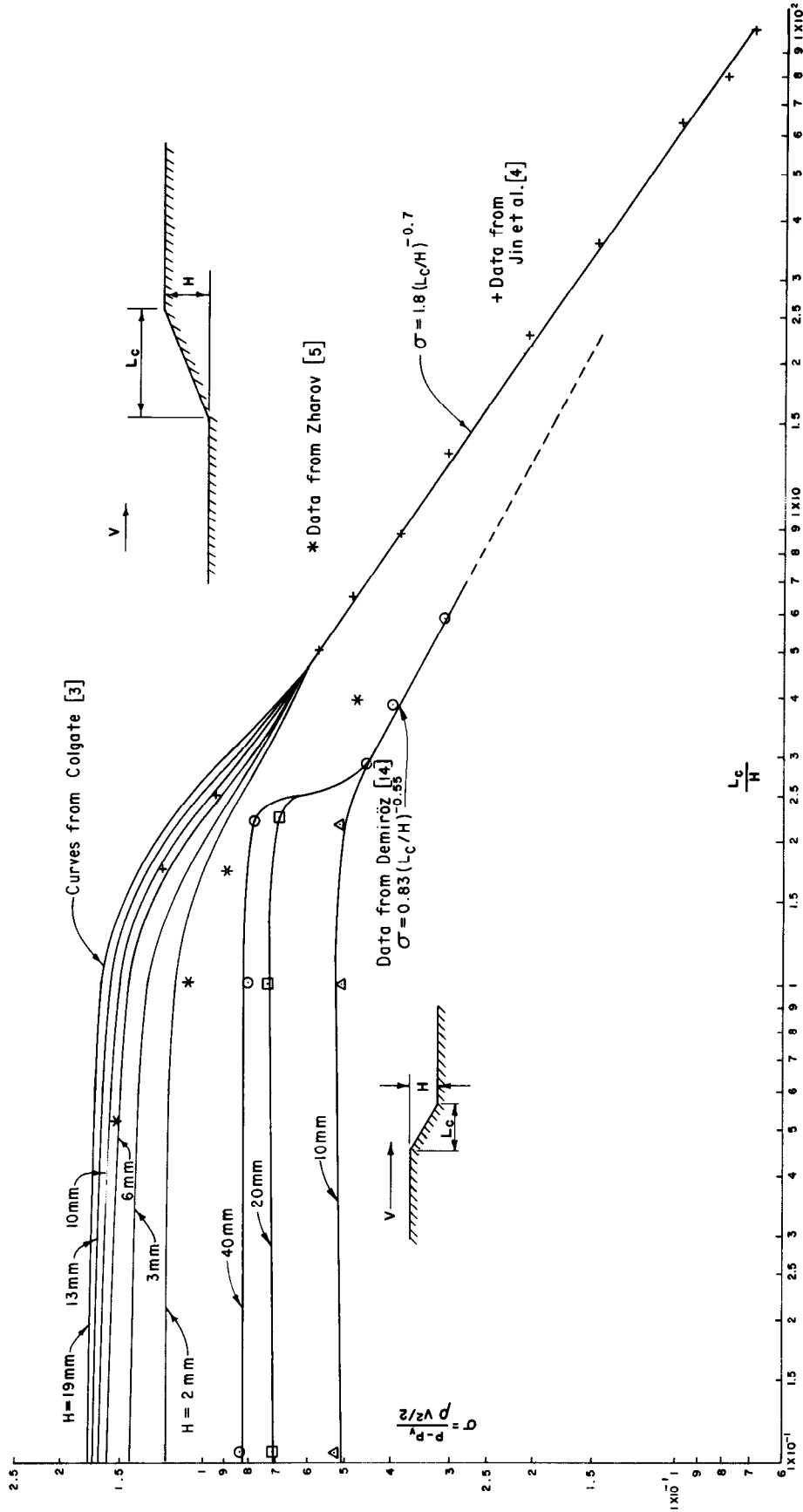


FIGURE 2-4.—Cavitation characteristics of chamfers.

where:

- H = height of offset
 V_y = velocity at height y
 V_a = characteristic velocity
 y = vertical coordinate (distance from boundary)

For the one-fifth power law distribution of velocity, equation 2.2 results in:

$$\sigma_k = 0.71 \sigma_u \left(\frac{H}{\delta} \right)^{0.4} \quad 2.4$$

where δ equals boundary layer thickness.

Clearly, equation 2.4 demonstrates that the data of Zharov should lie below that of Colgate and Jin, when all three are compared using a cavitation index that is based on a thin boundary layer.

This approach, by Holl, should permit tests both with and without a boundary layer to be referenced to a common base. For example, the cavitation index with a thin boundary layer should be able to be predicted from equation 2.4 using data taken from tests with a boundary layer. However, this approach only yielded fair results. Therefore, attempting to characterize the cavitation index only by some representative velocity within the boundary layer appears too simplistic.

Other studies of isolated asperities used a better method to account for the velocity distribution in the boundary layer, Arndt et al. [7]. They concluded that cavitation index should be a function of the relative thickness of the boundary layer, the Reynolds number of the flow, and a boundary layer shape factor. This is expressed as:

$$\sigma_i \propto f \left(\frac{H}{\delta}, R_h, S \right) \quad 2.5$$

where:

- R_h = Reynolds number based on height of offset and free stream velocity
 S = boundary layer shape parameter

The *boundary layer shape parameter*, S , is defined as the ratio of the displacement thickness to the momentum thickness:

$$S = \frac{\delta_d}{\delta_m} \quad 2.6$$

The *displacement thickness*, δ_d , is defined as:

$$\delta_d = \int_0^{\delta} \left(1 - \frac{V_y}{V_b} \right) dy \quad 2.7$$

and the *momentum thickness*, δ_m , is defined as:

$$\delta_m = \int_0^{\delta} \left(\frac{V_y}{V_b} \right) \left(1 - \frac{V_y}{V_b} \right) dy \quad 2.8$$

where V_b equals free stream velocity in the plane of the offset.

For a fully developed boundary layer over a flat smooth surface, the shape parameter, S , is approximately equal to 1.3.

To correlate the data for several types of isolated roughnesses, equation 2.5 is assumed to have the functional form:

$$\sigma_r = C \left(\frac{H}{\delta} \right)^a \left(\frac{V_b \delta}{\nu} \right)^b \left(\frac{1}{S} \right)^c \quad 2.9$$

where ν equals kinematic viscosity and a , b , c , and C are experimentally determined coefficients. It was not possible to calculate the value of the shape parameter for all the tests reported by Arndt et al. [7]. Therefore, for the majority of the tests, correlations were formed by ignoring the shape parameter term and using an equation of the form:

$$\sigma_r = C \left(\frac{H}{\delta} \right)^a \left(\frac{V_b \delta}{\nu} \right)^b \quad 2.10$$

The values of the coefficients are shown in the table on figure 2-5. The range of the relative offset heights for the two-dimensional offsets was about $0.015 < H/\delta < 3.4$.

The relative importance of the boundary layer shape parameter can be discerned in table 2-1 for a triangular and a circular arc irregularity. In these two cases, sufficient measurements were made so that the boundary shape parameter could be determined.

Table 2-1.-Triangular and circular arc irregularity coefficients

Irregularity	a	b	c	C
Triangular	0.361	0.196	-	0.152
	0.40	0.20	0.45	0.182
Circular arc	0.344	0.267	-	0.041
	0.30	0.15	0.70	0.171

The following correlations are recommended for design purposes.

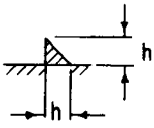
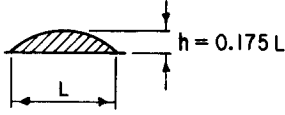
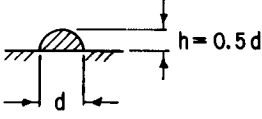
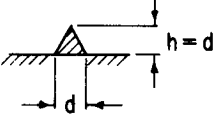
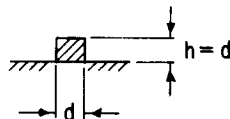
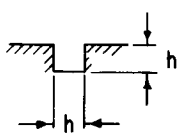
Into-the-flow misalignments:

- Elliptically rounding fig. 2-3b
 Chamfered leading edge fig. 2-4

Isolated irregularities:

- Triangles, circular arcs, etc. fig. 2-5

Since the into-the-flow misalignments do not include the effect of boundary layer, cavitation indexes will tend to be too large. If desired, part of the boundary layer effect can be approximated by using the values of the cavitation index taken from figures 2-3b and 2-4 together with equation 2.4.

Symbol	Irregularity	Flow dimensions	Data source	a	b	C	
△	Triangles	2	Holl, 1960	0.361	0.196	0.152	
○	Circular arcs	2	Holl, 1960	0.344	0.267	0.041	
▲	Hemispheres	3	Benson, 1966	0.439	0.298	0.0108	
●	Cones	3	Benson, 1966	0.632	0.451	0.00328	
■	Cylinders	3	Benson, 1966	0.737	0.550	0.00117	
□	Slots (Grooves)	2	Bohn, 1972	0.041	0.510	0.000314	

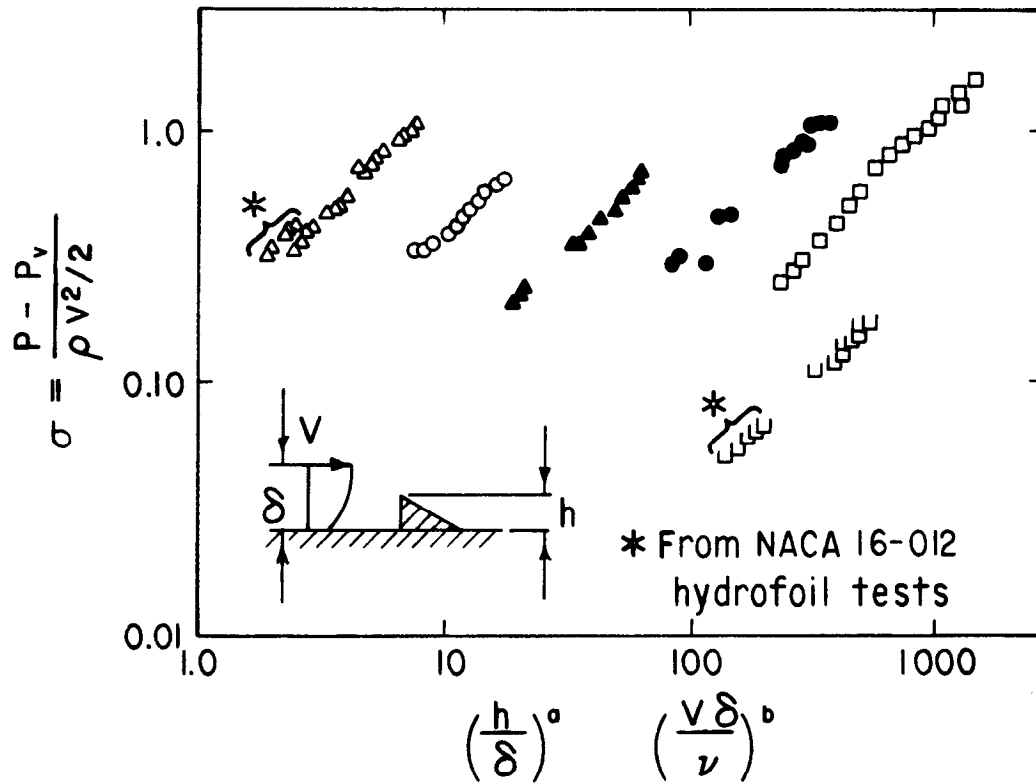


FIGURE 2-5.—Cavitation characteristics of isolated irregularities.

Away-From-the-Flow Offsets

Away-from-the-flow offsets include a wide variety of flow conditions that all have similar characteristics. These include sudden expansions, submerged jets, backward facing steps, and chamfers.

Cavitation associated with away-from-the-flow offsets usually is assumed to occur first in the core of the large shear layer eddies which form downstream from the offset. If cavitation forms, in the eddies' core, it can be shown that the incipient cavitation number must be less than or equal to 1.0, Johnson [8]. However, more recent studies have shown incipient cavitation actually begins in a three-dimensional flow structure within the region of separation and not in the eddies' core, Katz and O'Hern [9]. Therefore, incipient cavitation can occur at cavitation indexes much higher than 1.0.

Published data are somewhat difficult to compare because of different definitions for the reference

pressure. Studies by Ball [10] indicated the pressure immediately upstream of the offset is less than either the upstream or the downstream free stream pressure as shown on figure 2-6.

Nevertheless, data for two-dimensional backward facing steps (Johnson [8]), sudden expansions (Vigander [11]), and submerged jets (Appel [12]), all compare favorably and are shown on figure 2-7. The three-dimensional cavitation characteristics of sudden expansions do not fit the two-dimensional trends, Rouse and Jezdinsky [13]. This difference may be due either to the choice of the reference location or to three-dimensional expansions being less likely to cavitate than the two-dimensional flows.

Chamfers that are away-from-the-flow have cavitation characteristics similar to into-the-flow chamfers, Demiroz [14] (fig. 2.4). The data are not complete enough for an accurate comparison, but it appears that the cavitation index for the away-

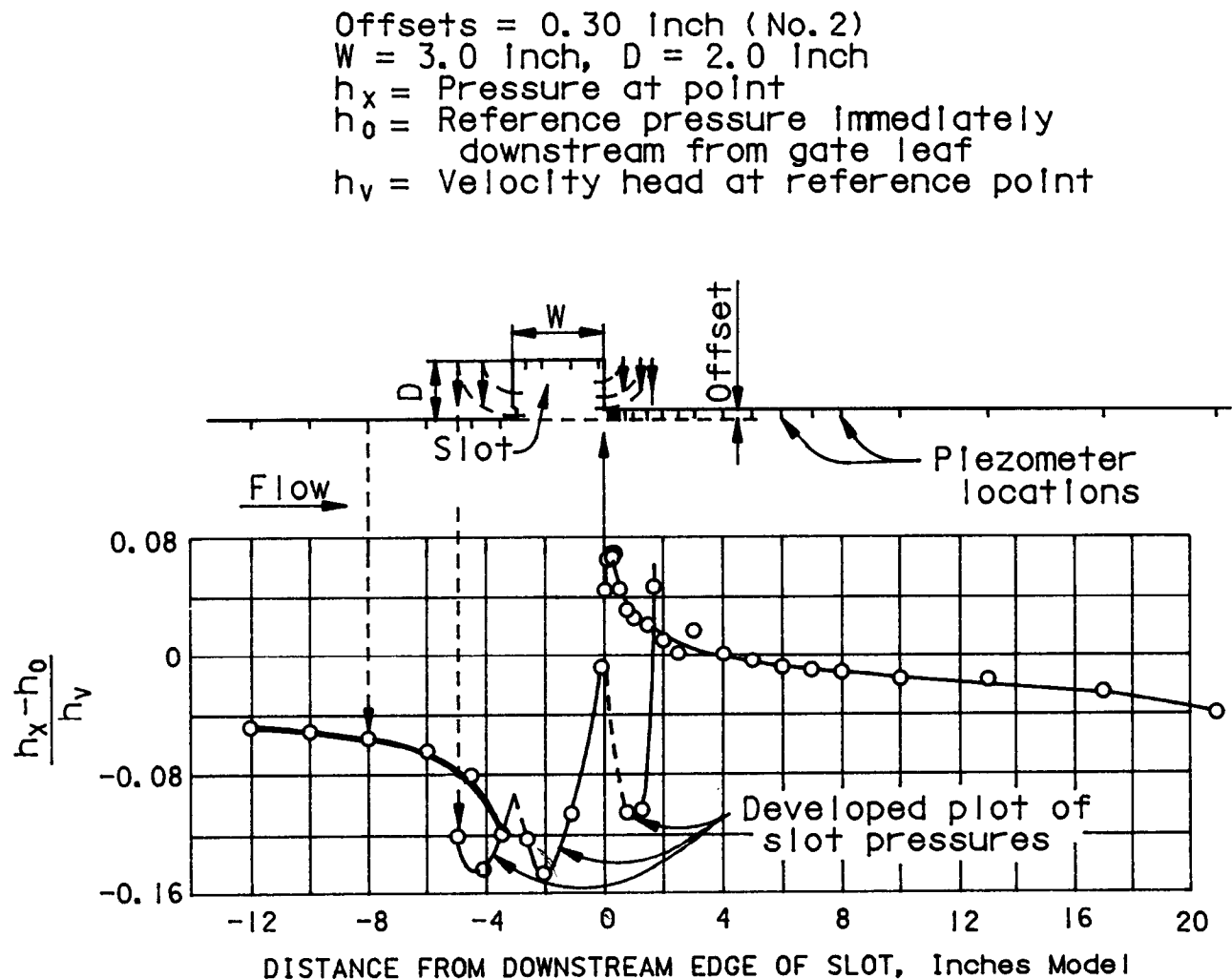


FIGURE 2-6.—Pressure distribution at a gate slot.

from-the-flow chamfers is about one-half that of the into-the-flow chamfers.

Holes in Boundary

When concrete is poorly consolidated against a form, air pockets form on the concrete surface. The pockets are referred to as "bug holes" because they appear to have been made by a bug burrowing into the surface. At high-flow velocities, these holes can be the source of cavitation damage, Ball [15] as shown on figure 2-8. In 1960, common practice was to fill all holes larger than 12 millimeters in diameter for velocities greater than 30 meters per second.

In 1984, a study of cavitation characteristics of holes in a surface was conducted, Mefford and Falvey [16]. This investigation used the same parameters that had been used by Arndt et al. [7] (fig. 2-5).

It was determined that a circular hole in the boundary is much less conducive to cavitate than a circular arc-type calcite deposit as noted on figure 2-9. In addition, a hole whose diameter is four times its depth has an incipient cavitation index which is one-sixth that of a hole whose diameter is twice its depth. This indicates, rather than filling holes, it might be better to enlarge them by making their diameter four times the depth of the hole.

Table 2-2 provides coefficients for the cavitation characteristics of holes for use in equation 2.10.

Table 2-2.—Cavitation characteristics of holes in a boundary

Depth/Diameter	a	b	C
0.25	0.488	0.788	0.000105
0.50	0.532	0.626	0.000687

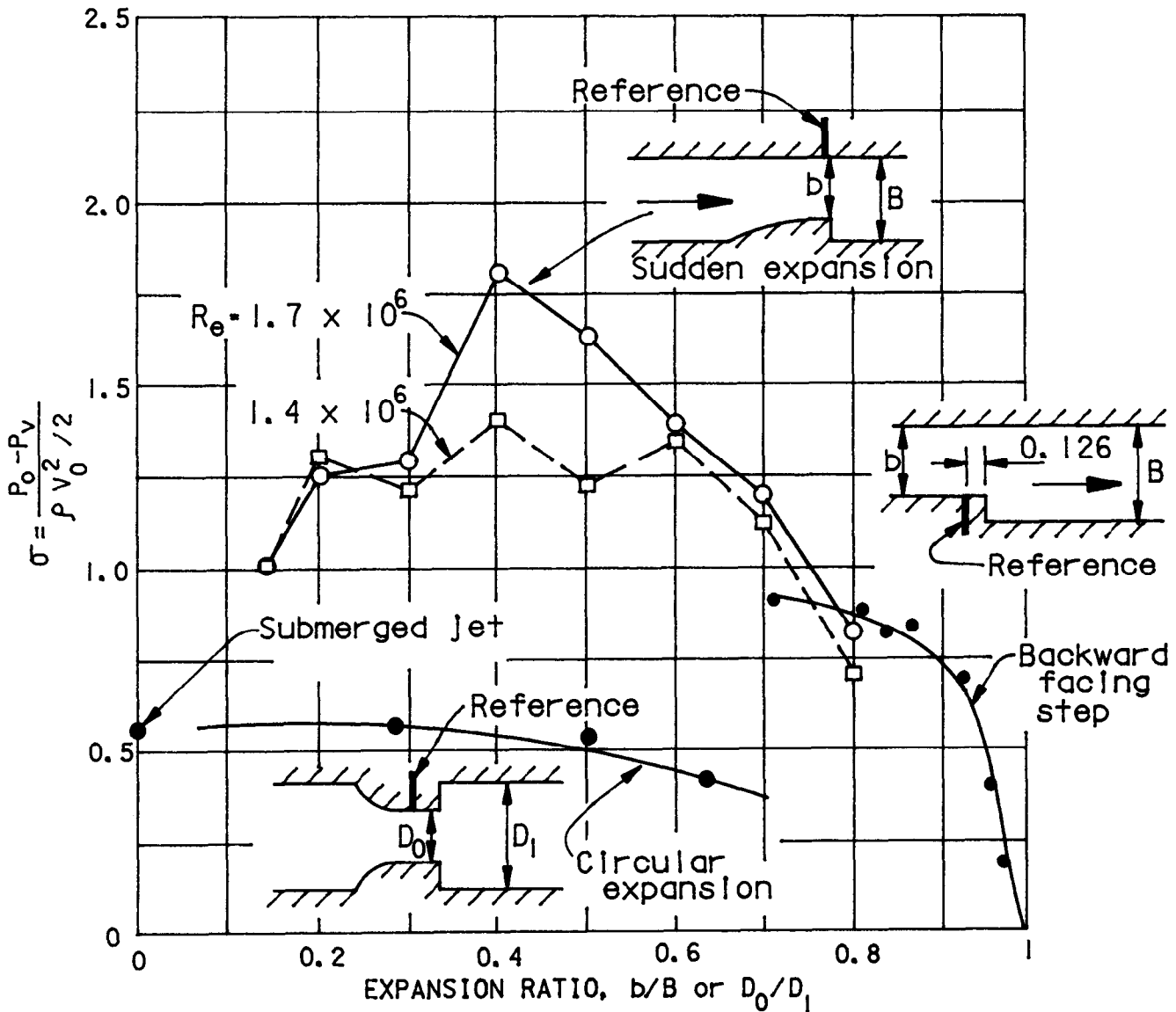


FIGURE 2-7.—Cavitation characteristics of a backward facing step, sudden expansions, and submerged jet.

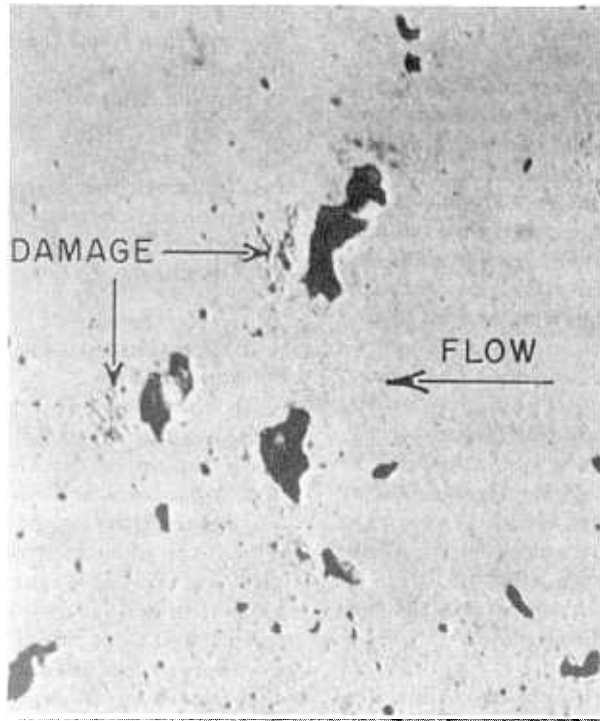


FIGURE 2-8.—Cavitation damage at a "bug hole."

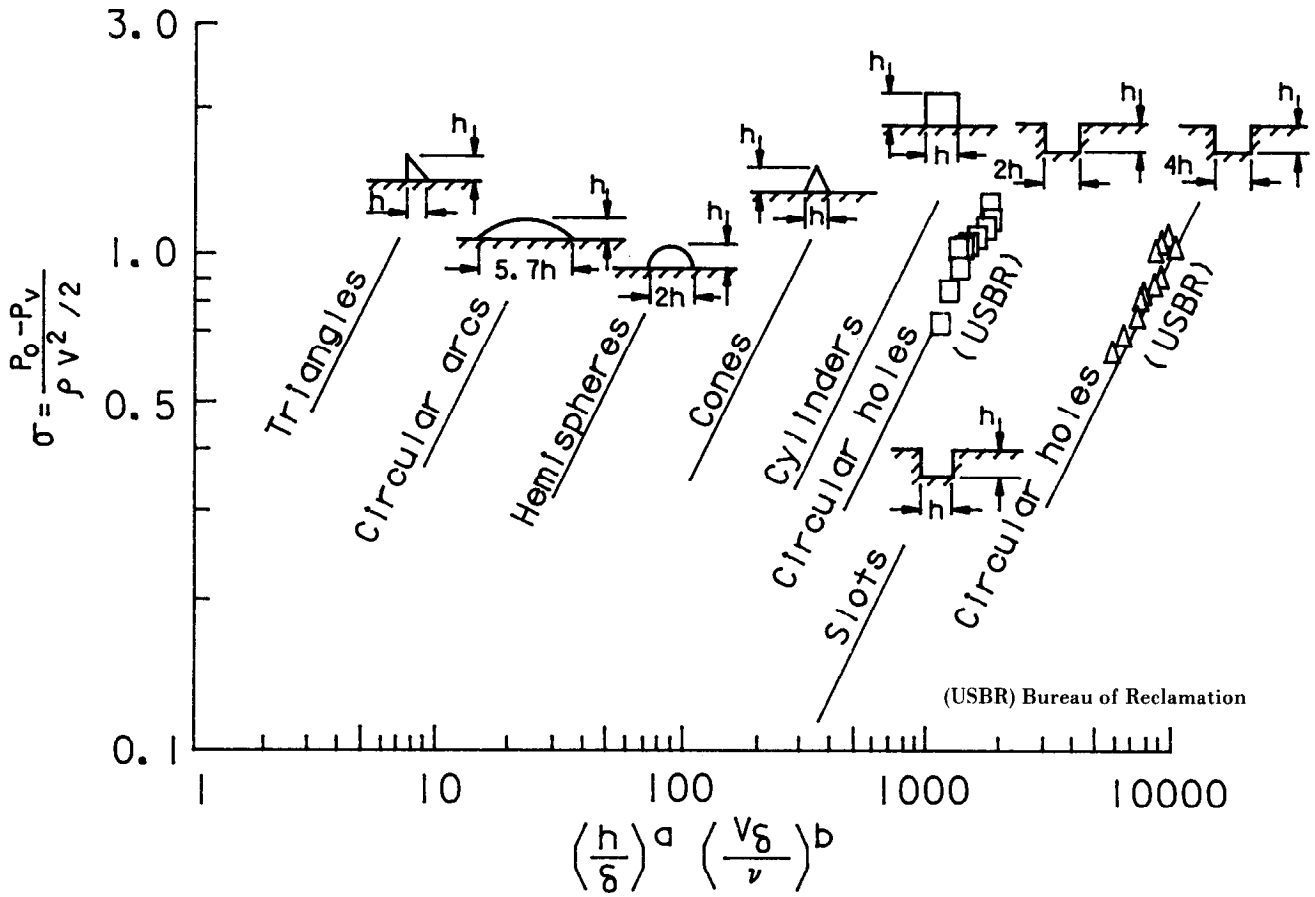


FIGURE 2-9.—Cavitation characteristics of holes.

Transverse Grooves

Transverse grooves in a boundary may be significant or they may be small. Large grooves are commonly referred to as slots. Typical examples of slots in a hydraulic structure are supports for stop logs or slide gates. Whereas, examples of grooves are transverse construction joints. Cavitation characteristics of these two extremes are different and, therefore, have been studied in different manners. With grooves, boundary layer effects are large and the presence of flow boundaries opposite the groove are insignificant. With slots, boundary layer effects are usually small but the effect of geometry on the other side of the flow channel can be large.

Characteristics of grooves have been studied by Bohn [7] and Ward [17]. Bohn's investigations were only concerned with a square groove and the results are presented on figure 2-5. Since the investigations by Ward were of a preliminary nature and did not consider the effect of the boundary layer thickness they are not included in this monograph.

Studies of slots were performed by Jin et al. [4]. Because of the experimental configuration, the boundary layer thickness was negligible. Therefore, the results cannot be compared to values given by Bohn. The investigations were not made at fixed values, of slot lengths to conduit width ratios, so the results should be used with caution.

The ratio of slot width to effective conduit width, in the tests by Jin, varied between 0.056 and 0.309. The discontinuity in the curves of the cavitation indexes between width to depth ratios of 1.5 to 2.0 might have resulted from the influence of the opposing boundary as noted on figure 2-10a. The beneficial effects of sloping the downstream corner of the slot were also studied as noted on figure 2.10b.

Grooves Parallel With Flow

Theoretically, grooves or vertical misalignments in the flow surface that are parallel with the flow direction should produce vortices which can result in cavitation. However, the cavitation potential of this type of irregularity is so small that grooves parallel with the flow have not been studied in the laboratory. In the field, damage at longitudinal grooves is rarely observed.

One of the few examples of cavitation damage in longitudinal grooves was observed in the outlet-works chute at the Bureau of Reclamation's Palisades Dam shown on figure 2-11. Flow enters the chute from four 2286- by 2743-millimeter slide gates and two 2438-millimeter hollow-jet valves, Schuster [18]. The two hollow-jet valves are centered between the two pairs of slide gates. A model study indicated that the lowest pressure in the chute, downstream from the slide gates, was negative 0.85

meter of water. This pressure was located 13.7 meters downstream from the gate frame exit on the center-line of the chute.

The location of the damage (noted on fig. 2-11) was not measured. However, from an examination of the photographs, the damage appears to be located near the minimum pressure location. The minimum pressure condition corresponds to a cavitation index of approximately 0.09 for a slide gate discharge of $156 \text{ m}^3/\text{s}$.

Uniform Roughness

In the preceding singular roughness elements, the shear layer could be located within a specified local region of the flow field. Incipient cavitation was observed within this localized shear layer. However, with flow over a uniform roughness—such as a layer of sand grains—a shear layer exists over the entire flow surface. Therefore, incipient cavitation will occur randomly over the flow surface. If the cavitation index is lowered below the incipient conditions, cavitation will appear in sheets—above the surface. The location of these sheets is influenced by the magnitude and spectrum of turbulent fluctuations within the boundary layer, as well as the number, size, and distribution of nuclei within the boundary layer.

Little information is known about the pressure spectrum over smooth and rough boundaries in a turbulent boundary layer. Assuming that the root-mean-square value of the turbulent fluctuations is the significant parameter to be used for estimating the cavitation potential of boundary layer flow, Arndt [7] developed the following relationship for incipient cavitation, σ_i :

$$\sigma_i = 16 C_f = 4 f \quad 2.11$$

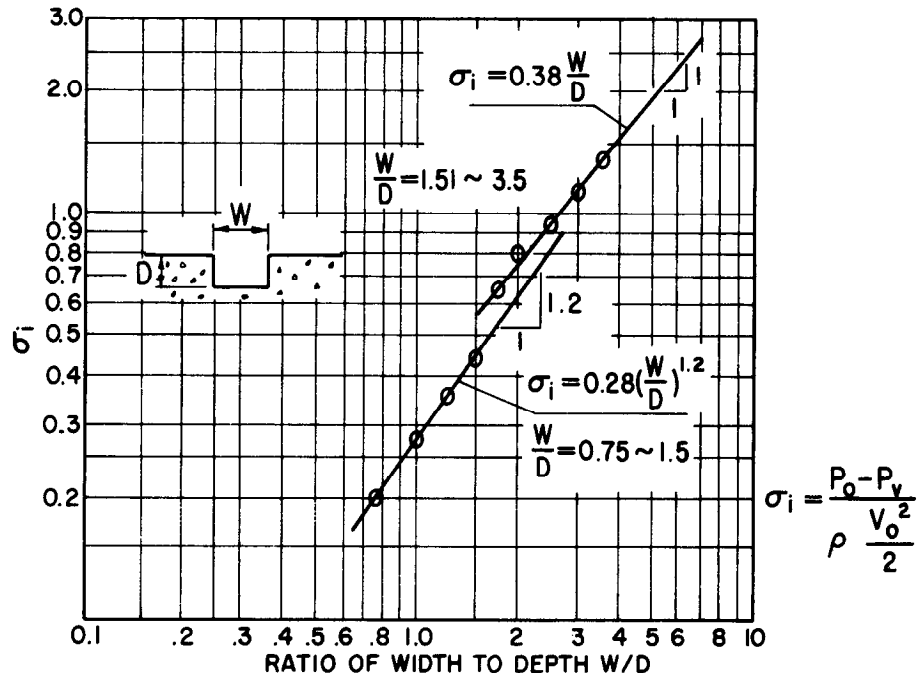
where:

- C_f = mean resistance coefficient
- f = Darcy-Weisbach friction factor

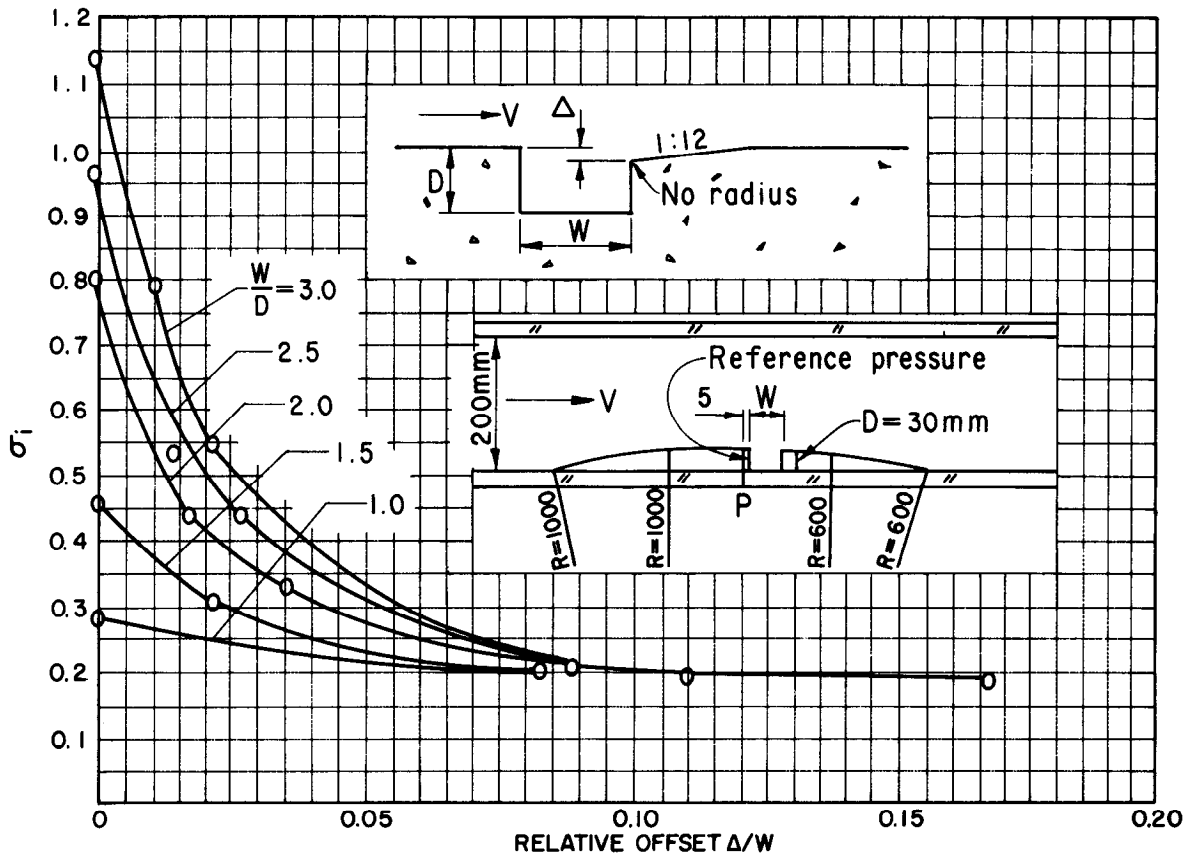
Combination of Uniform and Isolated (Singular) Roughnesses

Flow over a concrete surface which has eroded (e.g., by sediment motion) presents a special type of surface roughness. It is neither an isolated roughness nor a uniform roughness. Colgate [19] studied cavitation characteristics of flow over two plaster casts made of the eroded flow surface at the Bureau's Davis Dam. The value of the coefficient, in equation 2.11, changed from 16 to 59.9 ± 2.2 and 42.2 ± 1.5 for the two casts, respectively.

A similar study was conducted for the eroded surface in the Arizona spillway tunnel of Hoover Dam. Two casts were studied—one in a relatively smooth area near the end of the vertical bend. The



a. Rectangular slot



b. Offset downstream edge

FIGURE 2-10.—Cavitation characteristics of gate slots.

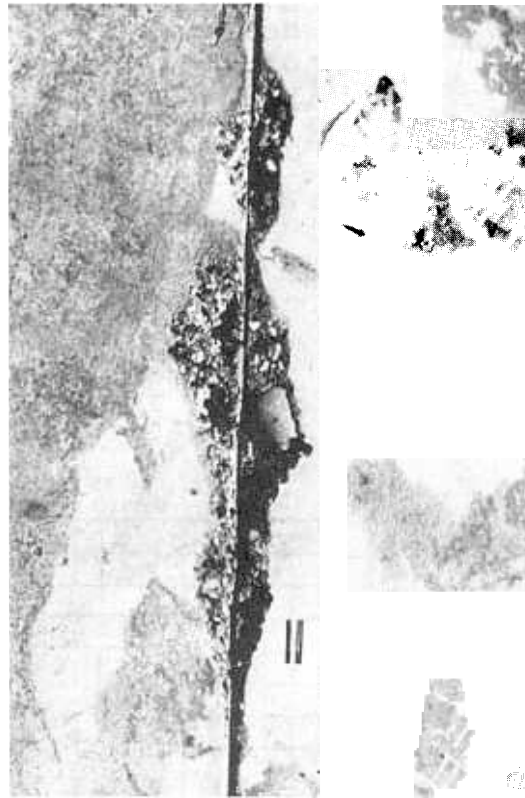
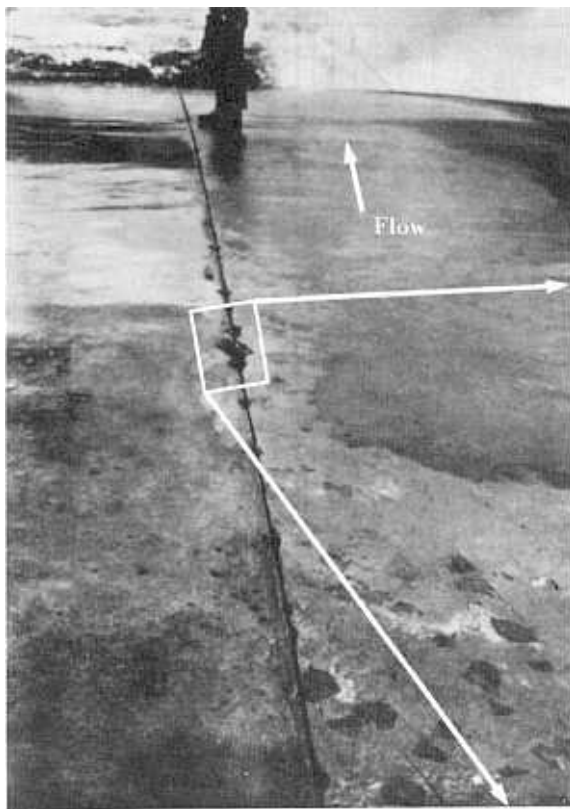


FIGURE 2-11. Cavitation damage in longitudinal grooves.

second cast was made in a rough area about 300 meters downstream of the elbow (see fig. 6-1). In this case, the value of the coefficient, in equation 2.11, changed from 16 to 60.5 ± 8.7 and 73.9 ± 9.4 for resistance coefficients of 0.017 ± 0.001 and 0.023 ± 0.004 , respectively. The latter values correspond to the rougher concrete section.

Both examples illustrate the difficulty of estimating cavitation characteristics of a surface that is neither an isolated nor a uniformly distributed roughness. The mean roughness coefficients for the eroded surfaces were about four times greater than the experiments reported by Arndt et al. [7].

Cavitation inception is dependent upon magnitude and duration of the negative pressure fluctuations. The derivation of equation 2.11 uses a root-mean-square value to characterize the pressure fluctuation magnitude. However, the pressure

fluctuations are not Gaussian—even if the turbulent fluctuations are Gaussian, Arndt and Daily [20]. Therefore, using the root-mean-square value in the derivation can be questioned. In addition, Arndt et al. [7] noted that the high frequency portion of the pressure spectrum caused by flow over a rough boundary does not scale in the same manner as that over a smooth wall. Scaling turbulent eddies over smooth and rough boundaries is in need of further research.

SUPERPOSITION PRINCIPLE

If an isolated roughness occurs on a flat surface, the correlations developed in the previous sections can be used without modification. However, if an isolated roughness occurs on the curved wall of a submerged body—such as the center pier of the

intake to a spillway—the correlations must be modified to account for the curvature of the streamlines. The method of accounting for the curvature is known as the *superposition principle*. The derivation of the principle is reproduced here following that of Cahuff and Wislicenus [21] (see also Holl [6]).

The roughness on the boundary of a curved surface can be expected to produce a local reduction in its pressure. The pressure at the roughness, P_m , expressed in terms of a pressure coefficient, C_{pr} , is given by:

$$C_{pr} = \frac{P_m - P_h}{\rho V_b^2 / 2} \quad 2.12$$

where:

- C_{pr} = pressure coefficient at roughness
- P_m = pressure at roughness
- P_h = pressure in free stream in plane of offset
- V_b = free stream velocity in plane of offset

For incipient cavitation, the pressure at the roughness will be approximately equal to the vapor pressure of water. Thus, equation 2.12 can be expressed as:

$$C_{pr} = \frac{P_m - P_w}{\rho V_w^2 / 2} \left(\frac{V_w}{V_b} \right)^2 + \frac{P_w - P_h}{\rho V_b^2 / 2} \quad 2.13$$

where:

- P_w = minimum pressure due to roughness
- V_w = velocity at roughness

By substituting the definition of the pressure coefficient (equation 1.2) and the cavitation index (equation 1.4) into equation 2.13, the cavitation index of a body having an isolated roughness, σ_r , is given by:

$$\sigma_r = \sigma (1 - C_{pr}) - C_{pr} \quad 2.14$$

where σ equals cavitation index (on a flat plate).

This latter expression is the equation of the superposition principle.

BIBLIOGRAPHY

- [1] Colgate, D., Elder, R., "Design Considerations Regarding Cavitation in Hydraulic Structures," Tenth Hydraulic Division Conference, American Society of Civil Engineers, Urbana, IL, August 16-18, 1961.
- [2] Ball, J. W., "Cavitation From Surface Irregularities in High Velocity," Proceedings of the American Society of Civil Engineers, vol. 102, No. HY9, pp. 1283-1297, September 1976.
- [3] Colgate, D., "Cavitation Damage in Hydraulic Structures," International Conference on Wear of Materials, St. Louis, MO, pp. 433-438, April 25-28, 1977.
- [4] Jin, T., Liu, C., Liu, X., "Cavitation Inception of Gate Slots," Department of Hydraulics, Water Conservancy and Hydro-Electric Power, Scientific Research Institute, Beijing, China, 1980.
- [5] Zharov, N.E., "O melodike opredeleniia kriticheskikh chisel kavitatsii obtekanii nerovnostei" (Cavitation Parameters of Flows Near Surface Irregularities), Izvestiia VNIIG im. B. E. Vedeneeva, Sb., nauchnykh trudov, vol. 126, Leningrad, pp. 43-48, 1978, (USBR translation, book No. 12,245, paper No. 6).
- [6] Holl, J. W., "The Inception of Cavitation on Isolated Surface Irregularities," *Journal of Basic Engineering*, Transactions of the American Society of Mechanical Engineers, pp. 169-183, March 1960.
- [7] Arndt, R.E.A., Holl, J. W., Bohn, J. C., Bechtel, W. T., "Influence of Surface Irregularities on Cavitation Performance," *Journal of Ship Research*, vol. 23, No. 3, pp. 157-170, September 1979.
- [8] Johnson, V. E., "Mechanics of Cavitation," *Journal of the Hydraulics Division*, Proceedings of the American Society of Civil Engineers, vol. 89, No. HY3, pp. 251-275, May 1963.
- [9] Katz, J., O'Hern T. J., "Cavitation in Large Scale Shear Flows," *Journal of Fluids Engineering*, Transactions of the American Society of Mechanical Engineers, vol. 108, pp. 373-376, September 1986
- [10] Ball, J. W., "Hydraulic Characteristics of Gate Slots," *Journal of the Hydraulics Division*, Proceedings of the American Society of Civil Engineers, vol. 85, No. HY10, pp. 81-114, October, 1959.
- [11] Vigander, S., "An Experimental Study of Wall-Pressure Fluctuations in a Cavitating Turbulent Shear Flow," Studies in Engineering Mechanics, Center for Research, Inc., University of Kansas, Lawrence KS, Report No. 21, 116 pp., May 1965.
- [12] Appel, D. W., "An Experimental Study of the Cavitation of Submerged Jets," Iowa Institute of Hydraulic Research, Progress Report for the Office of Naval Research, Contract No. ONR-500(03), 9 pp., June 1956.
- [13] Rouse, H., Jezdinsky, V., "Cavitation and Energy Dissipation in Conduit Expansions," Proceedings of the International Association for Hydraulic Research, 11th Congress, Leningrad, 1965.
- [14] Demiroz, E., Acatay, T., "Influence of Chamfers Away From Flow on Cavitation Inception," XXI Congress of the International Association for Hydraulic Research, Melbourne, Australia, seminar 2, 4 pp., 1985.
- [15] Ball, J. W., "Why Close Tolerances are Necessary Under High-Velocity Flow," Bureau of Reclamation Report No. HYD-473, October 1960.
- [16] Mefford, B. W., Falvey, H. T., "Cavitation Inception From Cylindrical Holes," Conference on Water for Resources Development, American Society of Civil Engineers, Coeur d'Alene, ID, pp. 422-426, August 1984.
- [17] Ward, T. M., "Slot Cavitation," Cavitation and Polyphase Flow Forum, American Society of Mechanical Engineers, pp. 24-26, 1973.
- [18] Schuster, J. C., "Hydraulic Model Studies of the Palisades Dam Outlet Works and Spillway, Palisades Project, Idaho, Bureau of Reclamation Report No. HYD-350, June 1956.
- [19] Colgate, D., "Cavitation Damage of Roughened Concrete Surfaces," American Society of Civil Engineers, annual convention, Pittsburg, PA, October 1956.
- [20] Arndt, R.E.A., Daily, J. W., "Cavitation in Turbulent Boundary Layers, Cavitation State of Knowledge," Fluids Engineering and Applied Mechanics Conference, American Society of Mechanical Engineers, Northwestern University, pp. 64-86, 1969.
- [21] Calehuff, G. L., Wislicenus, G. F., "ORL Investigations of Scale Effects on Hydrofoil Cavitation," Ordnance Research Laboratory, Pennsylvania State University, TM 19.4212-03, 1956.

Cavitation Damage Chapter 3

MODE OF DAMAGE

Several mechanisms are usually involved in damage of hydraulic structures. For example, when cavitation forms because of a surface irregularity, surface damage will begin at the downstream end of the cloud of collapsing cavitation bubbles. After some time, an elongated hole will form in the concrete surface. As time progresses, the hole will get larger with high velocity flow impinging on the downstream end of the hole. This flow creates high pressures within the minute cracks around individual pieces of aggregate or within temperature cracks which form during the curing process. Pressure differentials between the impact zone and the surrounding area are created which can cause aggregate, or even chunks of concrete, to be broken from the surface and swept away by the flow. This damage process can be accurately regarded as erosion; whereas, the loss of material due to cavitation is not strictly erosion. Here, erosion is defined as an abrasion, dissolution, or transport process. As erosion from high velocity flow continues, reinforcing bars can become exposed. The bars may begin to vibrate which can lead to mechanical damage of the surface (see frontispiece).

At the Bureau's Glen Canyon Dam, concrete lumps were found attached to the end of the reinforcing steel. At this stage, high velocity flow acting on the lumps rip reinforcement bars from the concrete even though the steel may be imbedded as deep as 150 millimeters. After the structure's lining has been penetrated, erosion can continue into the underlying foundation material. When damage penetrates the liner, the integrity of the structure is the first concern.

At the end of the chapter, assessment is made as to whether the severe damage was caused strictly by cavitation.

FACTORS AFFECTING CAVITATION DAMAGE ON A SURFACE

As high velocity flow passes over a surface, a potential exists for the surface to be damaged by cavitation. Various factors that determine whether or not the surface will be damaged include:

- cause of the cavitation
- location of the damage
- intensity of the cavitation
- magnitude of the flow velocity
- air content of the water
- resistance of the surface to damage
- length of time the surface is exposed

Cause of Cavitation

As demonstrated earlier, cavitation will occur whenever the local pressure in flowing water drops below vapor pressure. For instance, this can happen during the down surge of a water hammer wave when the piezometric pressure in a pipe drops below atmospheric pressure. However, the more common sources of cavitation in hydraulic structures are irregularities in the flow surface. Details of the cavitation characteristic for surface irregularities are covered in detail in chapter 2.

Shear flows also create cavitation. The submerged jet is an example of a shear flow (see fig. 1-4). The shear is generated between the high velocity jet and the relative quiescent fluid surrounding the jet. Shear flows also occur in the flow adjacent to the flow surface. Investigators are just beginning to study cavitation characteristics of shear flows next to a boundary.

Damage Location

Cavitation damage always occurs downstream from the source of the cavitation. Stinebring [1] showed for a cylinder—with its end facing into the flow—that the damage begins when the length of the cavitation cloud is equal to the diameter of the cylinder. Also, he found that the length of the cavitation cloud, L_k , was given by:

$$\frac{L_k}{H} = 2 \left(\frac{\sigma_s}{\sigma} \right)^{2.63} \quad 3.1$$

where:

H = characteristic dimension, offset height, radius of cylinder, etc.

L_k = length of cavitation cloud

σ = cavitation index of the flow

σ_s = cavitation index when damage begins, σ_s corresponds to cavitation index when $L_k/H = 1$

Stinebring also showed that maximum damage occurs near the end of the cavitation cloud. His experiments agree relatively well with observations of cavitation damage in the Glen Canyon Dam tunnel spillways.

After approximately 20 days of operation, at a discharge of about 205 m³/s, damage was observed in the left tunnel spillway downstream of a calcite deposit which formed in a shrinkage crack as shown on figure 3-1a. After 3-day operation, at an average discharge of about 425 m³/s, a second damaged area was observed downstream of the first as shown on figure 3-1b.¹

Equation 3.1 can be used to predict the distance to maximum damaged areas. Appropriate values are given in table 3-1. Note the locations were estimated relatively well for the approximations that must be made for the estimated height of the calcite deposits and their cavitation characteristics.

This analysis shows that the distance to maximum damage increases as both the discharge and the height of the surface irregularity increase. The photographic survey indicates the extent of damage; that is, the length of the damaged area also increases as the height of the irregularity increases.

Farther up—in the spillway—damage was observed, but two distinct areas of damage did not develop as shown on figures 3-2a and 3-2b. Stinebring's equation predicts a difference between the two damaged areas as shown in table 3-2. However, the difference is so small relative to the size of the damaged area that two areas of damage cannot be discerned.

¹ Estimating distance from the surveyors rod, in the photograph, is impossible because the rod is not parallel with the concrete surface. (The rod is graduated in feet.)

Table 3-1.—Length of cavitation cavities in Glen Canyon Dam left tunnel spillway — station 760.70 (m).

Dis-charge m ³ /s	Estimated height of deposit, mm	Cavitation index of deposit*	Distance to maximum damage, m [†]
205	7	0.713	0.99
425	7	0.728	1.22

* The cavitation index of the deposit is determined using the equation for a circular arc given in chapter 2 (see fig. 2-5) where ($T_c = 5^\circ\text{C}$):

$Q = 205 \text{ m}^3/\text{s}$ $V_u = 40.82 \text{ m/s}$ $\delta = 1.62 \text{ m}$

$Q = 425 \text{ m}^3/\text{s}$ $V_u = 45.37 \text{ m/s}$ $\delta = 1.64 \text{ m}$

† Cavitation indexes of the flow, at this station, are:

$\sigma = 0.141$ at $Q = 205 \text{ m}^3/\text{s}$, and

$\sigma = 0.133$ at $Q = 425 \text{ m}^3/\text{s}$.

Table 3-2.—Length of cavitation cavities in Glen Canyon Dam left tunnel spillway — station 739.38 (m)

Dis-charge m ³ /s	Estimated height of deposit, mm	Cavitation index of deposit*	Distance to maximum damage, m [†]
205	5	0.635	0.55
425	5	0.652	0.67

* The cavitation index of the deposit is determined using the equation for a circular arc given in chapter 2 (see fig. 2-5) where ($T_c = 5^\circ\text{C}$):

$Q = 205 \text{ m}^3/\text{s}$ $V_u = 40.86 \text{ m/s}$ $\delta = 1.06 \text{ m}$

$Q = 425 \text{ m}^3/\text{s}$ $V_u = 45.15 \text{ m/s}$ $\delta = 1.06 \text{ m}$

† Cavitation indexes of the flow, at this station, are:

$\sigma = 0.138$ at $Q = 205 \text{ m}^3/\text{s}$, and

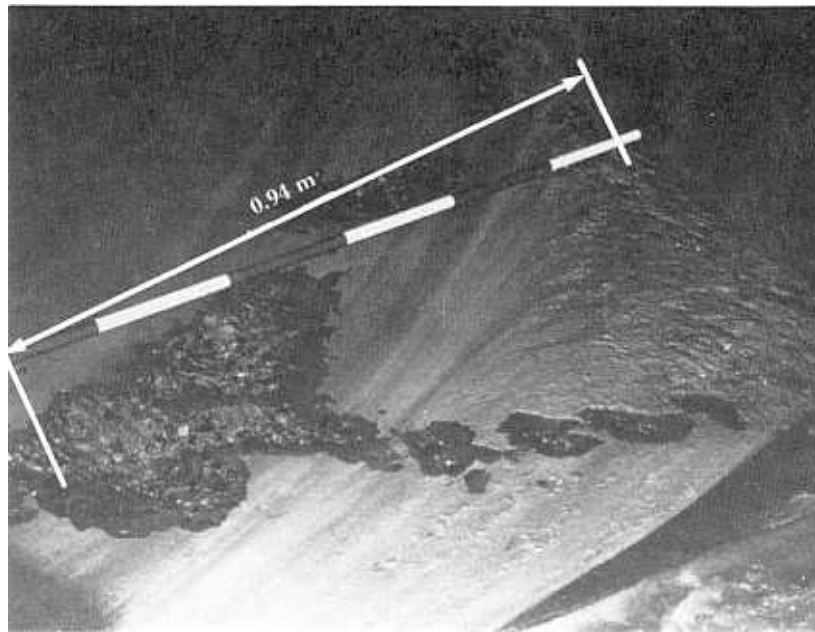
$\sigma = 0.132$ at $Q = 425 \text{ m}^3/\text{s}$.

These two observations bring into question a widely held assumption about the formation of cavitation damage. This assumption is that cavitation tends to “leapfrog”—forming a Christmas-tree shaped damage pattern as shown on figure 3-3. That is, once cavitation damage has formed, it is assumed that the damaged area becomes a source of cavitation which then creates another damage area downstream. Because the damaged area is larger than the irregularity which caused it, the process continues to produce larger and larger damage areas.

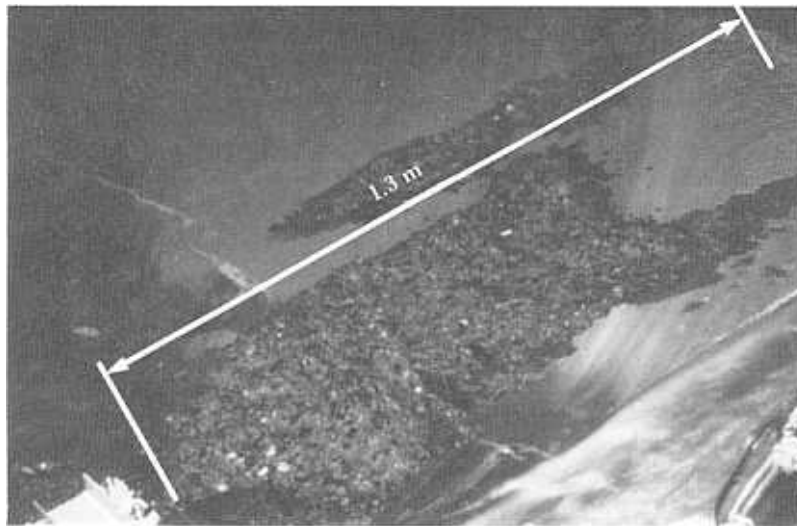
The excellent prediction of the observed damage patterns using equation 3.1 shows that only consideration of changes in discharge is sufficient to explain the leapfrog pattern in the damage observed in the Glen Canyon tunnel spillway.

The Christmas-tree pattern of damage develops only after the depth of the cavitation damage becomes large relative to the flow depth. For a large hole, the damage mechanism is undoubtedly more that of erosion—by a high velocity jet on a rough surface—than that of cavitation. The erosion of a surface by a high velocity jet in the absence of cavitation has not been systematically studied.

Cavitation Damage



a. Damage observed during a photographic survey (fall, 1981)



b. Damage observed on June 6, 1983

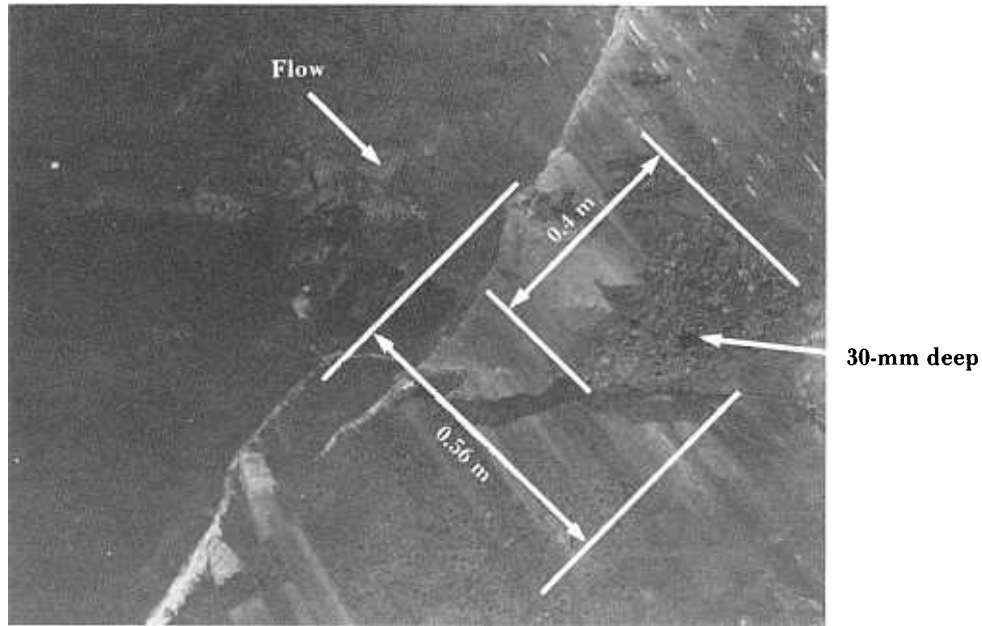
FIGURE 3- Glen Canyon Dam, left tunnel spillway — station 760.70 (m).

Cavitation Intensity

Cavitation intensity is an extremely difficult parameter to quantify. Stinebring [2] observed that as the cavitation index, σ , decreases relative to the incipient index, σ_i , the damage rate increases slowly as noted on figure 3-4. If the cavitation index is decreased further, a zone is reached where the damage rate (expressed as pits per square centimeter per second) is inversely proportional to the cavitation index. Further decreasing the index

results in a point being reached where the damage rate has a maximum value. As the index is decreased even further, the damage rate decreases. From this, it appears that the cavitation intensity increases and then decreases as the cavitation index is lowered below the value of the incipient cavitation index. The noise spectrum has a similar behavior.

Colgate [3] proposed a similarly shaped curve for the damage intensity as the cavitation index decreases (decreasing ambient pressure). Also, he indicated the maximum of the total damage curve



a. Damage observed during a photographic survey (fall, 1981)



b. Damage observed on June 6, 1983

FIGURE 3-2.—Glen Canyon Dam, left tunnel spillway — station 739.38 (m).

does not coincide with the maximum of the damage intensity curve. In addition, he showed the area of damage continues to grow larger as the cavitation index decreases as shown on figure 3-5.

Colgate's observations can be explained by the following reasoning. As damage rate increases—for decreasing values of the cavitation index—the length of the cavitation cloud increases. However, length of the cavitation cloud is sensitive to variations in velocity. Therefore, length of the damage area tends to get larger and larger as the difference between

the incipient cavitation index and the cavitation index of the flow increases. Thus, the intensity, measured in pits per square centimeter per second, may decrease while the total amount of material removed actually increases.

Damage observed in hydraulic structures occurs downstream of an irregularity at distances up to 100 times the height of the irregularity. A solution of equation 3.1, for these distance to height ratios, indicates the cavitation index of the flow must be on the order of one-sixth of the incipient cavitation

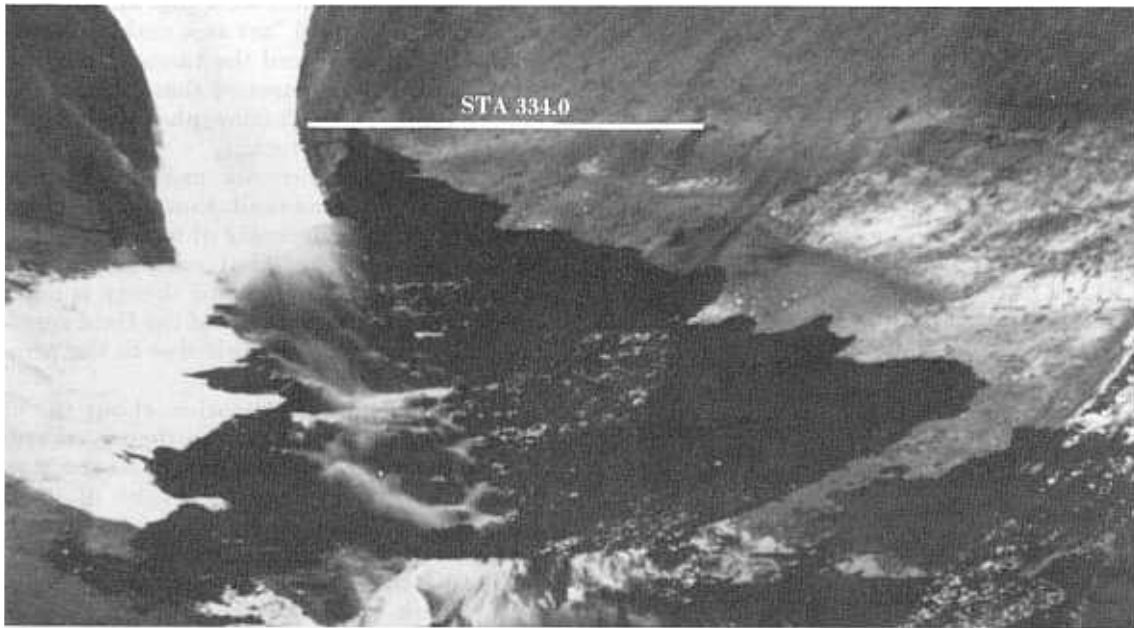


FIGURE 3-3.—Hoover Dam, Nevada tunnel spillway — Christmas-tree pattern of damage.

index. Therefore, based upon figure 3.4, damage which occurs in hydraulic structures is in the decreasing range of damage rates. Rarely are laboratory experiments made in this range because of the difficulty to create a facility that will produce damage at such low values of the cavitation index. Consequently, the only reliable data must come from field observations. Unfortunately, there is a paucity of good data!

Velocity Effect

A common assumption is that a potential for damage exists when the flow velocity exceeds some critical value. Some justification exists for this assumption. For instance, a typical value of the incipient cavitation index for abrupt changes in geometry is on the order of 2.0. If this value is substituted into equation 1.5, along with the assumption that the reference pressure is equal to the barometric pressure at sea level, the resulting velocity is equal to 10.0 m/s. Therefore, it is prudent to investigate the possibility of cavitation for velocities exceeding 10 m/s.

If a surface is exposed to cavitation, at a constant velocity, for a while material will not be lost from the surface. This period is known as the incubation phase. The surface then enters an accumulation phase wherein the rate of loss increases dramatically with time. This is followed by a steady-state phase and the rate of loss is constant. The steady-state phase may be preceded by an attenuation phase in which the rate of loss decreases. These phases are

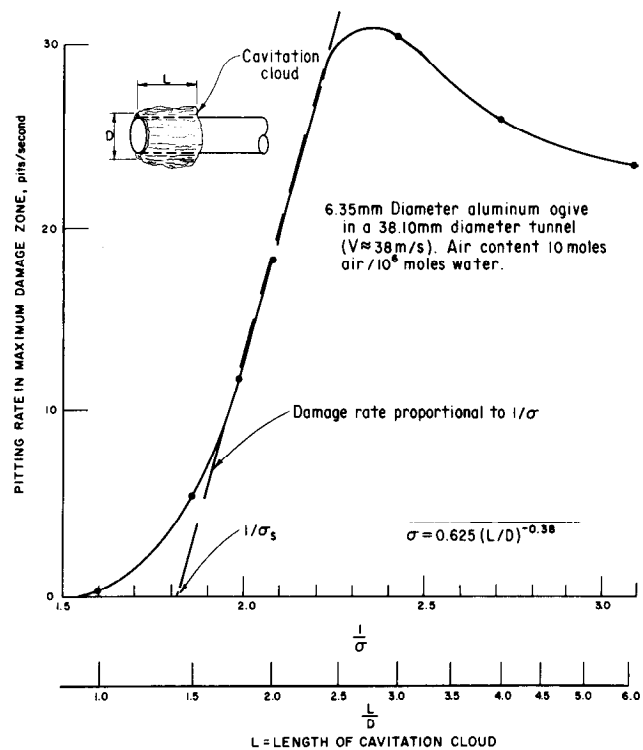


FIGURE 3-4.—Cavitation damage rate (Stinebring [2]).

discussed in detail in the Exposure Time Effect subparagraph.

Tests on aluminum plate show that the surface is being pitted during the incubation phase [2]. The average energy per pit increases as the 5th power and the number of pits increases as the 6th power

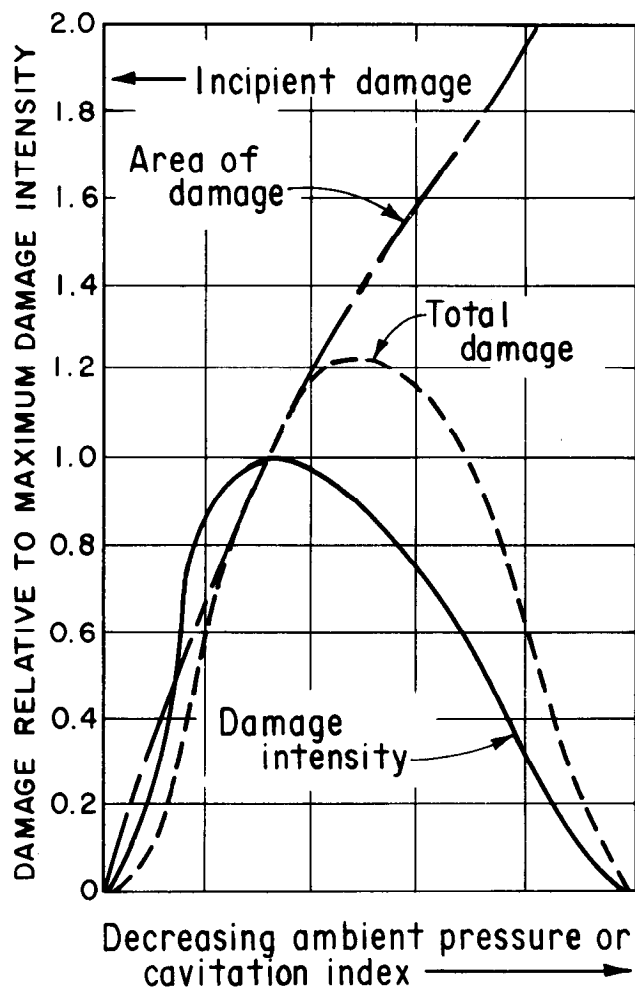


FIGURE 3-5.—Cavitation damage with respect to cavitation index (Colgate [3]).

of velocity. Therefore, the total energy of the collapsing bubbles increases as the 11th power of velocity.

Once material begins to be lost from the surface, the dependence of the rate of loss with respect to velocity becomes ambiguous. Some investigators claim the rate of loss varies with the 5th power of velocity, while others have found it varies with the 6th power. Undoubtedly, the variation is a function of the base material, the method of testing, and the damage phase.

Air Content Effect

For low values of air concentration, damage has been found to vary inversely with the air concentration [2]. The tests were conducted at air concentrations between 8×10^{-6} and 20×10^{-6} moles of air per mole of water. At high air concentrations, of around 0.07 moles of air per mole of water, damage was found to be completely eliminated over a 2-hour test period in a venturi-type test facility, Peterka [4].

In 1945, assumptions were that air injected under a water prism would “act as a cushion between the high-velocity water and the tunnel lining,” Bradley [5]. It was further reasoned that “the air would aid in relieving the subatmospheric pressures” [5]. Neither axiom is correct.

Currently, two theories explain the mitigating effects of aeration on cavitation damage. One theory is based upon the presence of noncondensable gases in the vapor pocket that cushion or retard the collapse process. The second theory is based upon the change in sonic velocity of the fluid surrounding the collapsing vapor bubble due to the presence of undissolved air (see fig. 1-13).

Of the two current theories, about the effect of undissolved air in water, the theory regarding the change in sonic velocity seems to be the most valid. Studies have shown that diffusion of undissolved gases into a vapor cavity proceeds at a very slow rate relative to the rate of vaporization.

Because the vapor cavity growth time is short, it seems unlikely for sufficient gas to be present (in the vapor cavity) to significantly affect the rate of collapse of the cavity or the pressures generated by the collapse.

Surface Resistance to Cavitation Damage

The resistance of a surface to damage depends upon several factors including the ultimate strength of the material, ductility, and homogeneity. It is not clear which strength characteristics of a material are significant when evaluating the surface resistance. With metals, surface deformation caused by the impact of collapsing bubbles produces tensile forces within the material. On concrete surfaces, tensile forces are also possibly the significant factor. Thus, tensile strength and not compressive nor shear strengths may be the more important parameter. The properties of strength and ductility can be combined into one parameter known as resilience, Rao et al. [6]. Resilience is defined as the area under the stress-strain curve of a material.

Presently, correlations have not been developed that quantify the amount of damage, of a given material, for a specified amount of cavitation. However, to express the resistance of a material relative to the resistance of other materials—for a given cavitation condition—is possible. For example, in a venturi testing device, cavitation produced a hole 13 mm deep in concrete after 3 hours at a flow velocity of 30 m/s. The same size hole was produced in polymer concrete after 125 hours and in stainless steel after about 6,000 hours [3]. Carbon steel was found to be damaged about 7 times faster than stainless steel; aluminum or copper is damaged about 25 times faster than stainless steel. Figure 3-6 shows a curve [3] of relative damage developed for this and other data on materials conventionally used

in construction of hydraulic structures. For the effect of velocity, an 11th power dependence on velocity was assumed.

Exposure Time Effect

The rate of erosion—of any surface—caused by cavitation is not constant with time. Observations have shown that several different rates actually occur. Each rate has been given a specific name, Heymann [7], as noted on figure 3-7.

At first, a period begins where loss of material does not occur. The period is known as the "incubation zone." In this zone, metal surfaces become pitted. Many investigators use data taken in the incubation zone as the most significant for damage correlations [1, 7].

Following the incubation zone, the damage rate increases rapidly during a period called the "accumulation zone." This rate reaches a peak. Depending upon the type of testing facility, the damage rate follows one of two trends. The damage rate either decreases into an "attenuation zone"—which is followed by a constant damage rate plateau called a "steady-state zone," or the damage rate reaches a steady-state plateau—which is then followed by an attenuation zone, as shown on figure 3-7. These damage rate characteristics have been explained using a statistical representation of the cavitation collapse mechanism [7].

In hydraulic structures, which have irregularities on the boundaries, the location where cavitation bubbles collapse does not change significantly during the damage process. This means that as damage increases, the distance between the collapsing bubble and the surface increases. Thus, it can

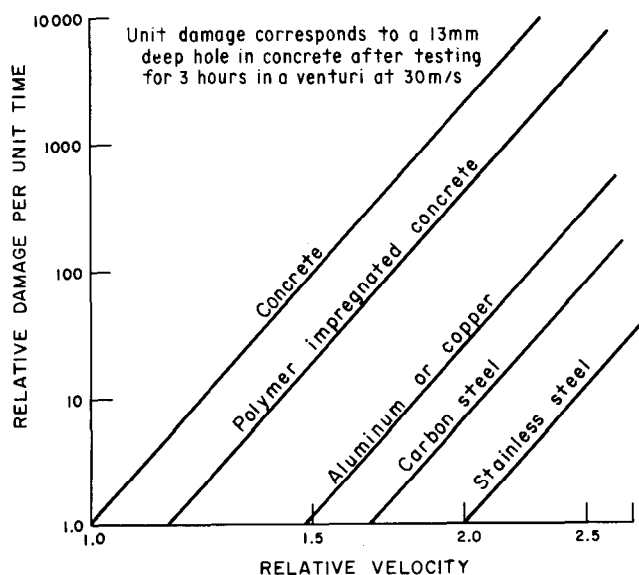


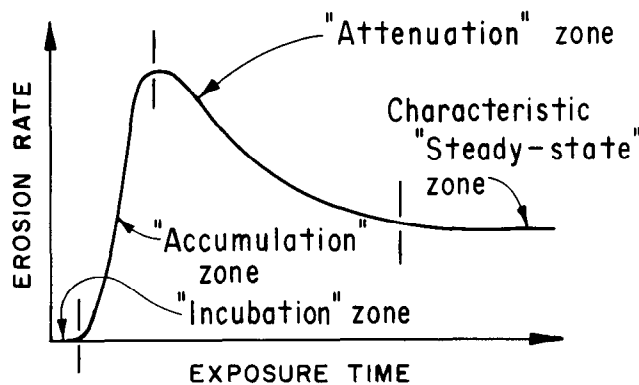
FIGURE 3-6.—Comparative cavitation resistance of various materials (Colgate [3]).

be expected that the damage rate will tend to vary inversely with time. With increasing time, for a constant flow rate, the depth of damage downstream from an irregularity will appear to reach a constant value. This hypothesis has been verified in field investigations, Wang and Chou [8].

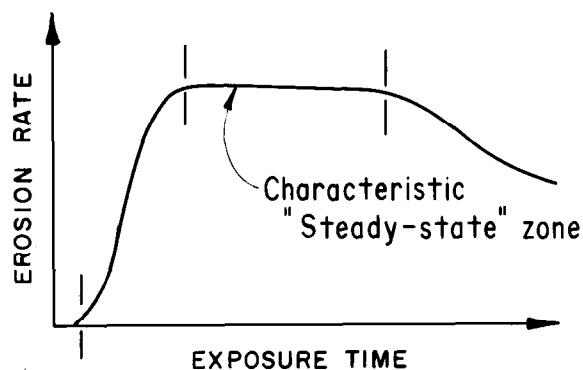
PARAMETERS FOR PREDICTING DAMAGE

Several attempts have been made to develop a parameter for quantitatively predicting cavitation damage. Generally, the attempts have recognized that the cavitation index, the flow velocity, the surface construction material, and the time of exposure are all important parameters. For example, an attempt to correlate the minimum cavitation index of the flow with time and the extent of the damage was made by Falvey [9] as shown on figure 3-8. Although the predictions were improved upon as a result of more data (Falvey [10]), the method did not include the effect of water velocity.

Another method for predicting the extent of cavitation damage was taken by Wang and Chou [8]. It was assumed cavitation damage would reach a



a. Characteristic rate-time curve according to Thiruvengadam



b. Characteristic rate-time curve according to Plesset and Devine

FIGURE 3-7.—Cavitation damage rate (Heyman [7]).

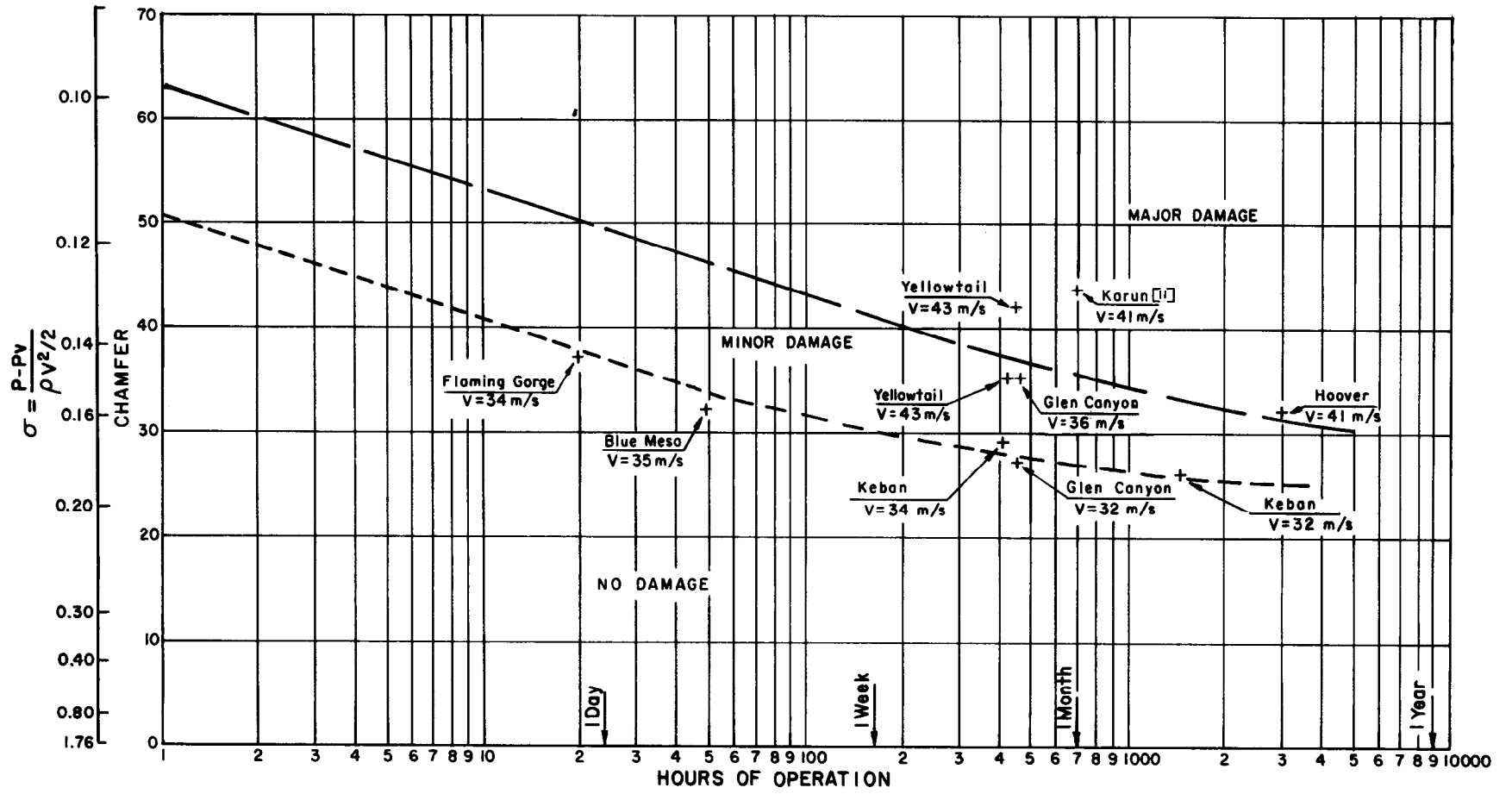


FIGURE 3-8.—Damage experience in spillways (Falvey [9]).

stabilized depth after a long period of operation. The time for stabilization was about 200 hours. The stabilized depth of damage, D_s , (in millimeters) is given by:

$$D_s = \left(\frac{V_h}{C_c} \right)^a \quad 3.2$$

where:

A = one-half amplitude of maximum negative pressure fluctuation

$$a = 7.7 I_c^{0.44}$$

C_c = stabilized damage depth factor = $9.61 I_c^{-0.32}$

D_o = flow depth upstream of offset

ΔH = negative pressure head pulsation at offset

$$\Delta H = \delta_o (V_m^2/2g)$$

g = gravitational constant (acceleration)

h = maximum time-average negative pressure head on the irregularity

I_c = cavitation damage intensity = $(\sigma_r - \sigma_{fh}) / \sigma_r$

P_a = atmospheric pressure

V_m = average flow velocity

V_h = velocity at height of offset

δ_o = pressure intensity coefficient = $A / (V_m^2/2g)$

ρ = density of water

σ_{fh} = cavitation index of flow based on conditions at height of offset, see equation 1.9

σ_r = cavitation index of the surface irregularity

$$\sigma_r = (D_o + \rho g P_a - h - \Delta H) / (V_h^2/2g)$$

In prototype measurements of the Feng Man Dam spillway reported by Wang and Chou, the pressure fluctuations in the flow were equal to 10.7 percent of the average velocity head. Therefore, the pressure intensity coefficient, δ_o , was equal to 0.05. The concrete strength of the Feng Man spillway was 20 to 25 megapascals. The total head was 72 meters while flow rates were as high as 760 m³/s.

Their method assumes the damaged area reaches a stable configuration if enough time is allowed to pass. However, the method does not allow for predicting how damage develops with time. Therefore, the following development presents a method to predict the potential for damage and to quantitatively measure the time-wise development of damage—based upon empirical evidence.

Presently, a quantitative method does not exist to predict the resistance of a surface to damage. Based upon the physical properties of the surface, the damage prediction method was developed in two stages. The first stage develops a parameter that indicates the aggressiveness of the cavitating flow; that is, its ability or potential to damage a surface. The second stage develops an index that indicates or describes the severity of the damage with time.

Damage Potential

In the subparagraph "Damage Location," total damage was shown to be related to the difference between the cavitation index of the surface

irregularity when damage begins, σ_r , and the cavitation index of the flow, σ . It was also shown on figure 3.4 that for part of the damage curve the damage rate is inversely proportional to the cavitation index of incipient damage. Based upon these two observations, a damage potential, D_p , can be formed in dimensionless terms as:

$$D_p \propto \left(\frac{\sigma_s}{\sigma_r} - 1 \right) \left(\frac{1}{\sigma_s} \right) \quad 3.3$$

where:

σ_s = cavitation index for the initiation of damage

σ_r = cavitation index of the flow

However, the aggressiveness of the cavitation is also a function of the relative velocity raised to a power. The reference velocity is obtained by solving equation 1.5 for velocity using the piezometric pressure at the location in question and a cavitation index corresponding to the cavitation index for the initiation of damage. Mathematically, the reference velocity for damage potential is:

$$V_r = \left[\frac{2(P_b - P_v)}{\rho \sigma_s} \right]^{1/2} \quad 3.4$$

where:

P_b = pressure in plane of irregularity

P_v = vapor pressure

V_r = reference velocity

Assuming a 6th power of velocity relationship for the damage potential gives:

$$D_p \propto \left(\frac{V}{V_r} \right)^6 \quad 3.5$$

where V equals flow velocity.

Combining equations 3.3 and 3.5:

$$D_p \propto \left(\frac{1}{\sigma_s} \right) \left(\frac{\sigma_s}{\sigma_r} - 1 \right) \left(\frac{V}{V_r} \right)^6 \quad 3.6$$

Damage Index

The damage rate, in hydraulic structures, is assumed to vary inversely with time. This can be expressed as:

$$\frac{dE_d}{dt} \propto \frac{1}{t} \quad 3.7$$

where:

E_d = depth of cavitation damage

t = time

Integrating equation 3.7 shows that the depth of cavitation damage should be proportional to the logarithm of time:

$$E_d \propto \ln(t - t_o) \quad 3.8$$

where t_0 equals integration constant.

Because the damage severity is proportional to both the aggressiveness of cavitation (damage potential) and the logarithm of time, a damage index, D_i , can be defined as:

$$D_i = D_p \ln(t - t_0) \quad 3.9$$

The integration constant, t_0 , is introduced into the equation to allow for the cumulative effect of flows at various discharges. The value of the integration constant is obtained from:

$$t_0 = t_c - e^{(D_i/D_p)} \quad 3.10$$

where:

- t_c = cumulative time of operation
- D_i = damage index, at end of previous discharge
- D_p = damage potential, for next discharge

At the start of operation of the structure; $D_i = 0$, $t_c = 0$, and $t_0 = -1$.

The damage index is a quasi-quantitative measure of the severity of the cavitation damage as a function of discharge and time as shown on figure 3-9. It can be used to differentiate between minor damage (which does not require repair) and major damage (which requires repair). The index does not appear to be a good predictor of catastrophic damage with one exception; catastrophic damage has never occurred if the index predicts minor damage. The means of evaluating damage severity (the damage index) are discussed in the following Design Values.

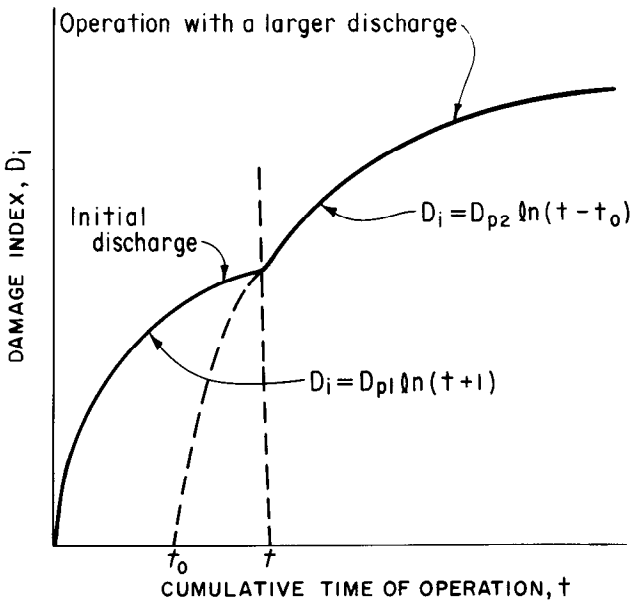


FIGURE 3-9.— Variation in damage index with discharge and time.

Two computer programs (included here) are on diskettes to assist in determining damage index for a specific structure. To use these programs, either the height and type of the surface irregularity must be known or assumed.

The first program determines the cavitation index and damage potential for six different types of offsets for a range of inputted discharges. The second program determines the damage index using historical flow records and the set of damage potential values from the first program.

Design Values

Difficulty is encountered in obtaining data points from which the damage index can be calibrated. Not only is obtaining the structure's operational record difficult, but the height of the "as built" irregularities and the depths of the damaged area are not routinely mapped in the field.

Calibration of the damage index is also difficult because some of the damage may be caused by factors other than flow surface irregularities. For example, evidence exists that indicates catastrophic damage may be caused by a longitudinal vortex structure in the flow. These longitudinal vortices can have a much higher cavitation intensity than that caused by boundary irregularities.

The Bureau's Glen Canyon Dam studies have some of the best available data for evaluating the damage index. The spillway structure operated for extended periods from 1980 through 1982. In 1981, an inspection revealed many areas of cavitation damage. After this inspection, a photographic survey was made and accurate locations of damaged areas were recorded. After significant damage occurred in 1983, several photographs were made of the same areas which had been identified in the 1981 photographs. Finally, following the 1983 flood, the severely damaged areas were surveyed to determine concrete repair quantities.

Damage indexes, computed from the historical flow rates at Glen Canyon Dam using equation 3.9, are shown in table 3-3.

Table 3-3.—Damage indexes for Glen Canyon Dam, left tunnel spillway

Date	Figure	Station m	Height of offset, mm	Damage index
Fall 1981	3.1a	760.7	7	4 040
Fall 1981	3.2a	739.4	5	3 000
Fall 1981	3.10a	729.3	30	4 420*
Jun 6, 1983	3.1b	760.7	7	5 360
Jun 6, 1983	3.2b	739.4	5	3 870
Post 1983 flood	3.10b	729.3	30	29 600

* Assumed popout occurred July 6, 1980.

The surface irregularity, at station 729.3, was a popout of an epoxy patch which had been used to repair the hole left by a grout pipe. The damage index for this station was calculated assuming the downstream edge of the hole functions as an into-the-flow offset. This assumption may be incorrect. The irregularities at other stations were into-the-flow offsets caused by the deposition of calcite on the flow surface. Calcite forms when water—flowing through temperature cracks in the wall—leaches lime from the concrete matrix.

The correlation between the damage index and the observed damage follows a predictable trend. If the damage index is less than 5000, damage is relatively minor. For indexes greater than 10 000, damage is severe and is extensive enough to require repair.

Catastrophic damage observed at Glen Canyon tunnel spillway does not appear to follow a predictable trend. The photographic survey did not record an offset or damage on the invert in the vicinity of station 760.70 during the fall of 1981. However, on June 6, 1983, major damage had developed at this location as shown on figure 3-11. The damage was initiated by a calcite deposit 6.5 mm high. Evidently, the deposit had grown between the survey in 1981 and the flood of 1983. The calculated damage index for 6.5-mm-high offset is roughly equivalent to the 7-mm offset observed just off the invert at the same station (see fig. 3-1a). Thus, equivalent size and shape offsets—at essentially the same location in the tunnel—produced completely different magnitudes of damage. The end of the damage zone from the deposit located on the side of the invert is visible on the right side of figure 3-11.

Another occurrence of catastrophic damage was noted at station 729.26 (during the 1983 flood) as shown on figure 3-10b. This damage was caused by the loss of an epoxy patch which was recorded in 1981 (fig. 3-10a). In this case, the catastrophic damage occurred for a calculated damage index of 30 000. Catastrophic damage also can be seen on the invert of figure 3.10b. The cause of this damage was not detected during the photographic survey in the fall of 1981.

In both examples, it appears that progressive growth of damage caused by surface irregularities was not the primary mechanism for the catastrophic damage to the surface. The impingement of the high velocity flow on the eroded surface may have been the most significant mechanism. Then too, vortices—formed by secondary flows in the elbow—may have accentuated the damage.

Evaluating the size and shape of the surface irregularities in these observations is somewhat subjective. All height or depth measurements were made with a surveyor's rod or were visually estimated. Molded casts of the surface, from which accurate profiles could have been measured, would have yielded much more consistent results.

Two methods are available to assess the possible damage to a chute or spillway. First, if it is assumed that the cumulative operation time for the structure will be long, say for 22,000 hours (more than 2½ years), then only the damage potential has to be checked. If the expected cumulative operation time of the structure is short, the damage index should be checked. To avoid damage, the damage potential or damage index should be less than the incipient values given in table 3-4. If the values are greater, then the extent of the damage can be assessed using the limits presented in table 3-4.

Table 3-4.—Design values of damage potential and damage index

Damage	Damage potential*	Damage index
Incipient	500	5 000
Major	1000	10 000
Catastrophic	2000	20 000

* The values of damage potential were calculated using equation 3.9, with $t_0 = 0$, $t = 22,000$ hours, and the given values of the damage index.

RECOGNITION OF CAVITATION DAMAGE

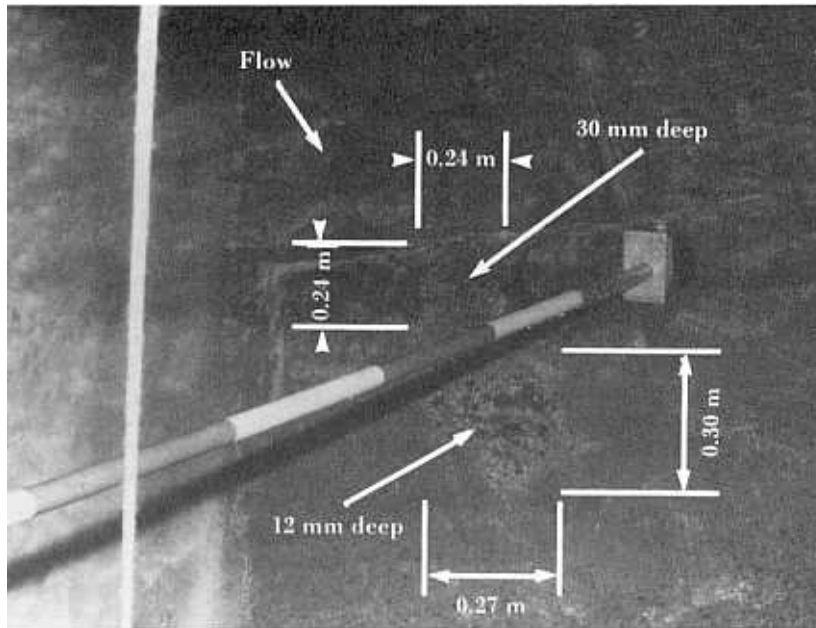
When damage has occurred in the field, it is important to know the cause of the damage so that appropriate remedial action can be initiated. The following discussion is general observations, which will provide guidelines, for the recognition of cavitation damage.

Texture

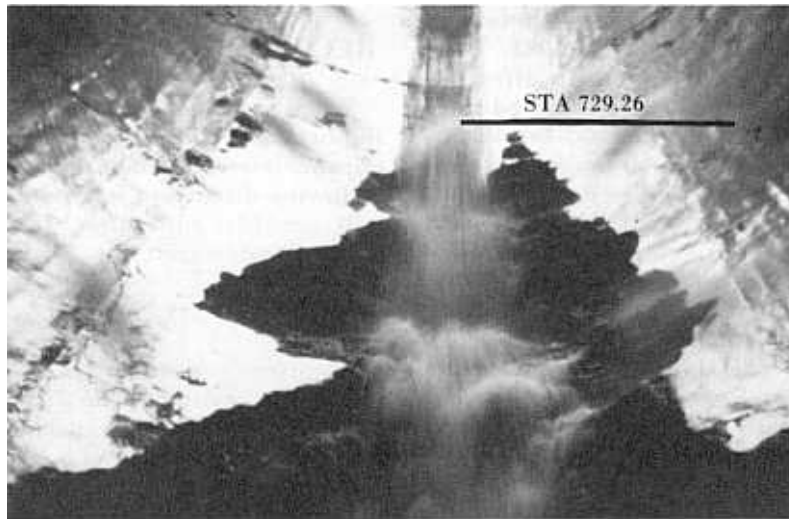
Chapter 1 noted that damage caused by a collapsing cavity is primarily caused by a pressure wave that travels at the speed of sound in the water. Since the speed of sound is between 10 and 40 times greater than the flow velocities, which are normally associated with damage, damage appears to be caused by a source perpendicular to the surface. This means the direction of flow cannot be determined by examining the damaged area. Also, this effect has an impact on the texture of the damage.

In steel, the effect of the collapse of the many minute cavitation bubbles perpendicular to the surface is to produce a grainy texture. The scale, of surface texture, depends upon the size of the cavitation bubbles which are produced. In a laboratory facility, the structure of the damage is fine grained as shown on figure 3-12a because the bubbles are small. Whereas, in the liner of an outlet conduit the surface texture is much coarser grained because the cavitation bubbles are larger as shown on figure 3-12b.

The effect of the collapse perpendicular to a concrete surface produces a surface in which the



Damage beginning at station 729.26 (m) [fall, 1981]



b. Major damage caused by loss of patch at station 729.26 (m) after 1983 flood

FIGURE 3-10.—Glen Canyon Dam, left tunnel spillway.

individual pieces of aggregate are cleaned of the cement which binds the concrete. Deep crevices and holes can be found in the matrix. It almost appears as though worms bored into the concrete. The difference in appearance of laboratory and field produced damage is not significant as shown on figure 3-13. None of the aggregate is broken.

The contrast between the texture of damage caused by cavitation and that caused by erosion, with sand-laden water, is easily recognized in steel and

noted on figure 3-14. With cavitation, direction cannot be detected and the surface has a grainy texture. With erosion by sand-laden water, flow direction is apparent and the surface is smooth and shiny.

Similarly, the difference between cavitation, freeze-thaw damage, and erosion by sand-laden water is apparent in concrete. With cavitation, individual, polished pieces of aggregate are exposed in the damaged zone as shown on figure 3-13a.

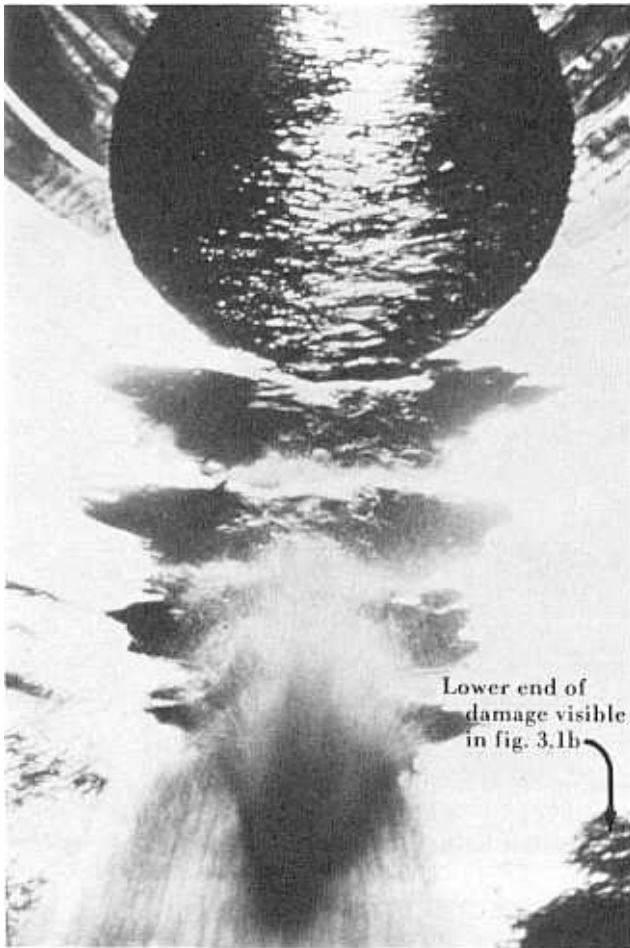


FIGURE 3-11.— *Glen Canyon Dam, left tunnel spillway*
— *damage at station 760.20, June 6, 1983.*

Whereas, in the freeze-thaw zone, individual pieces of aggregate are broken and the profile through the damaged area is relatively flat as shown on figure 3-15. With erosion by sand-laden water, individual pieces of aggregate are polished, as with cavitation, but the underlying surface is smooth and relatively even as shown on figure 6-1.

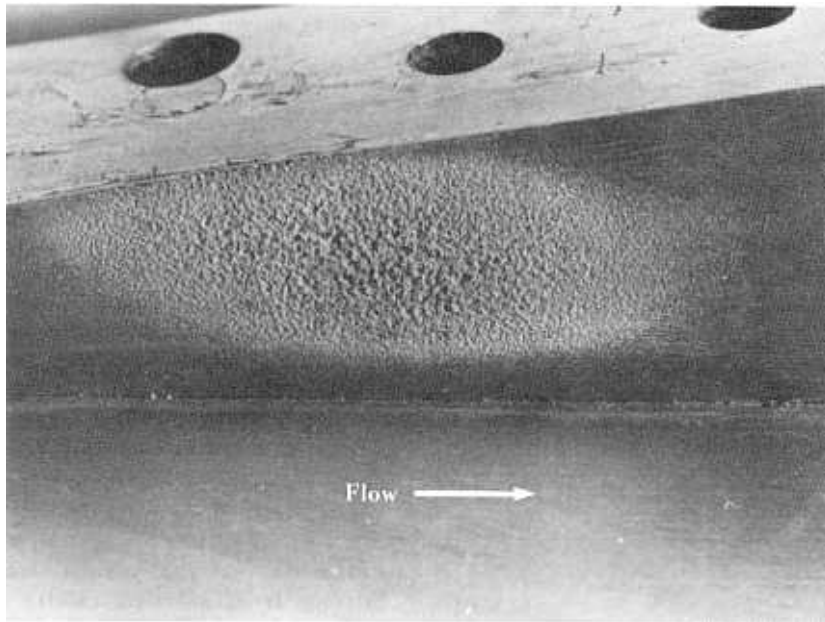
Symmetry

If cavitation damage occurs on a structure, it will occur in similar locations elsewhere on the structure. For instance, if cavitation damage is observed on the conduit wall downstream of a gate slot, it will occur downstream of the opposite gate slot as shown on figure 3-16.

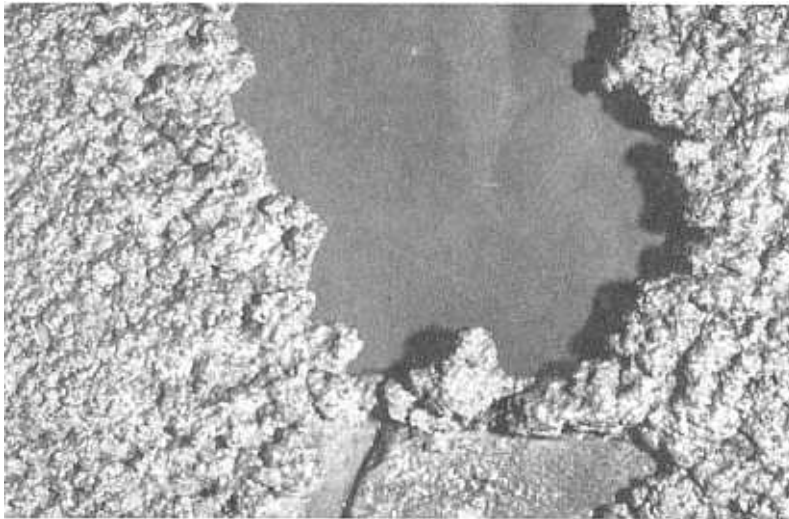
Origin

Cavitation damage always occurs downstream from its source. This has two important implications. First, there must be a source of the cavitation and secondly, the damage will not progress upstream of the source. Usually, the source is easily identified. Surface irregularities, calcite deposits, gate slots, and sudden changes in flow alignment are typical sources for damage.

Longitudinal vortices in the flow are known also to be sources of cavitation which have caused damage. Generally, the exact location of these sources cannot be accurately specified. A typical example of cavitation damage caused by longitudinal vortices in the flow through a slide gate is shown on figure 3-17.



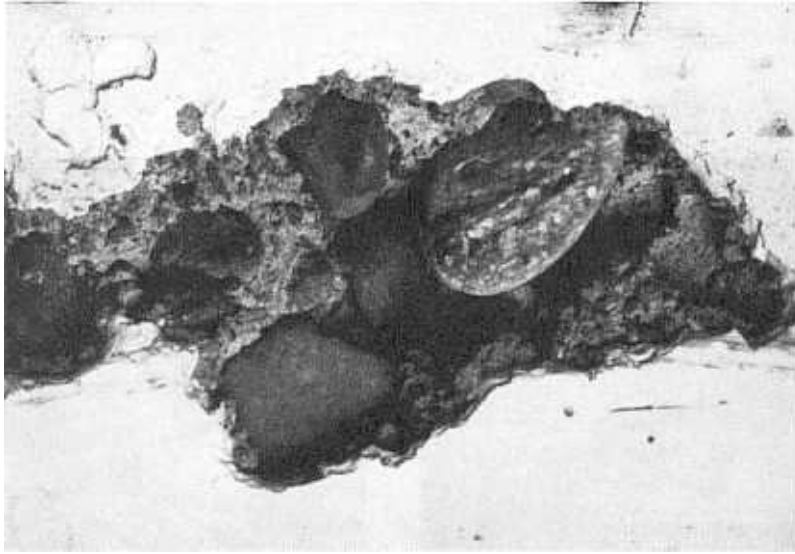
a. Venturi throat of cavitation test facility



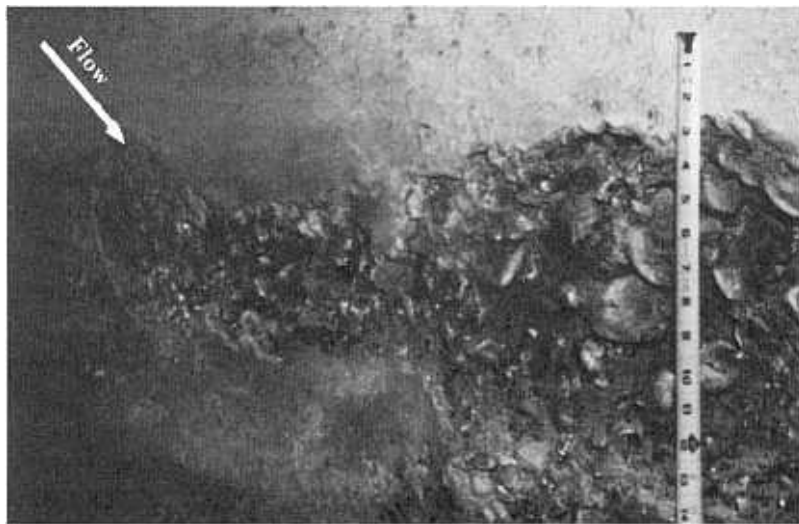
b. Ross Dam (Seattle, Washington) outlet works conduit

FIGURE 3-12.—*Texture of cavitation damage in steel.*

Flow



a. Cavitation damage produced in a venturi cavitation test facility



b. Hoover Dam, Nevada spillway tunnel — initiation of damage

FIGURE 3-13.—*Cavitation damage in concrete.*

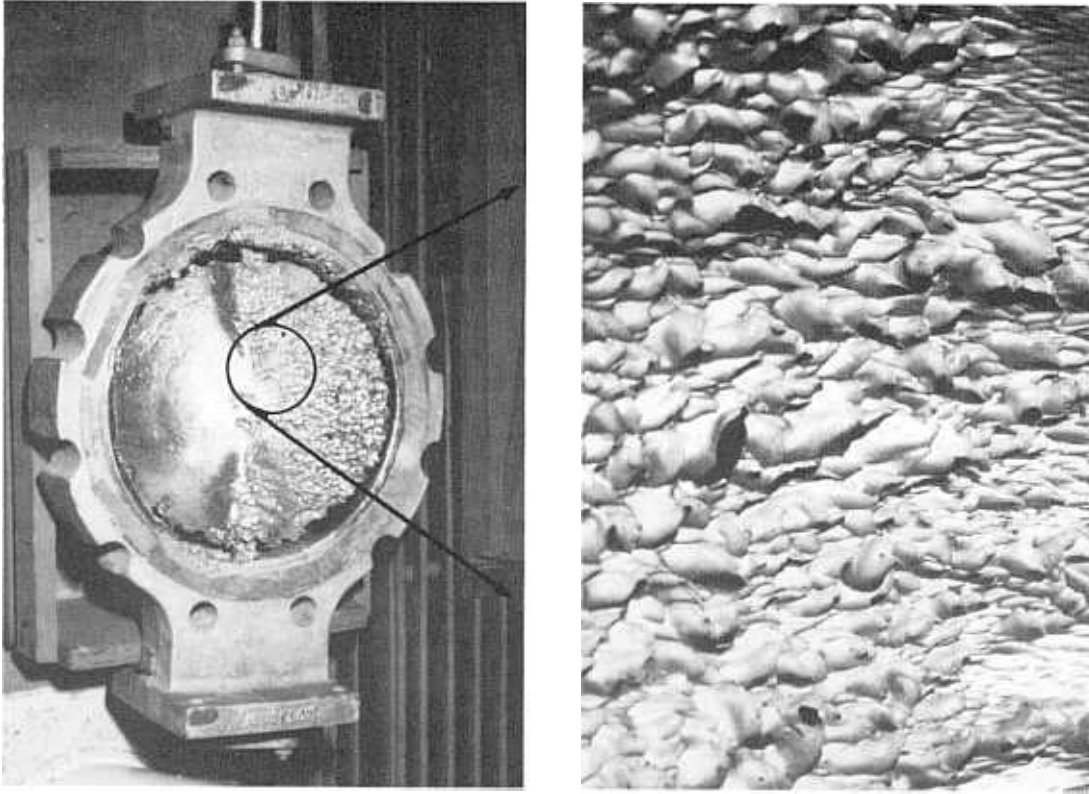


FIGURE 3-14.—*Bradbury Dam, California, damage produced in 254-mm-dia. butterfly valve by sediment-laden water.*

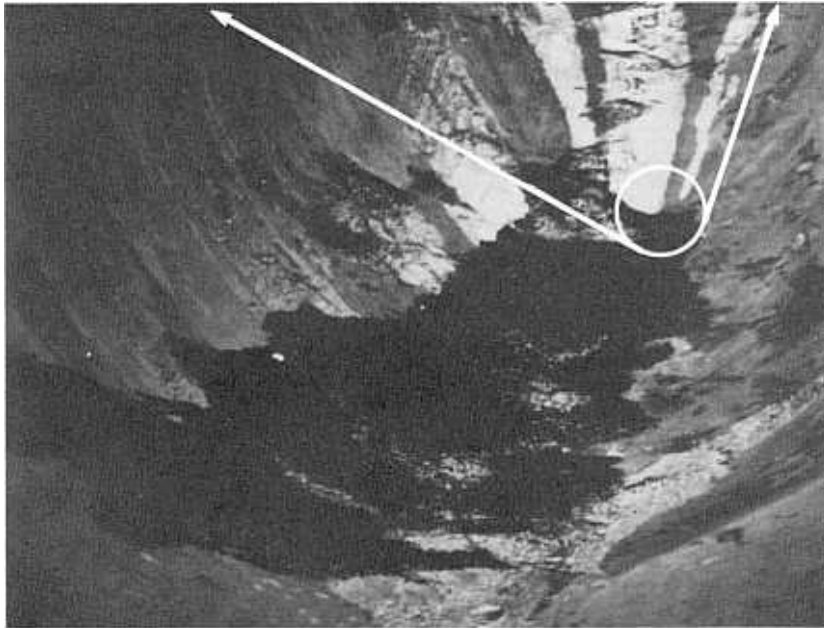
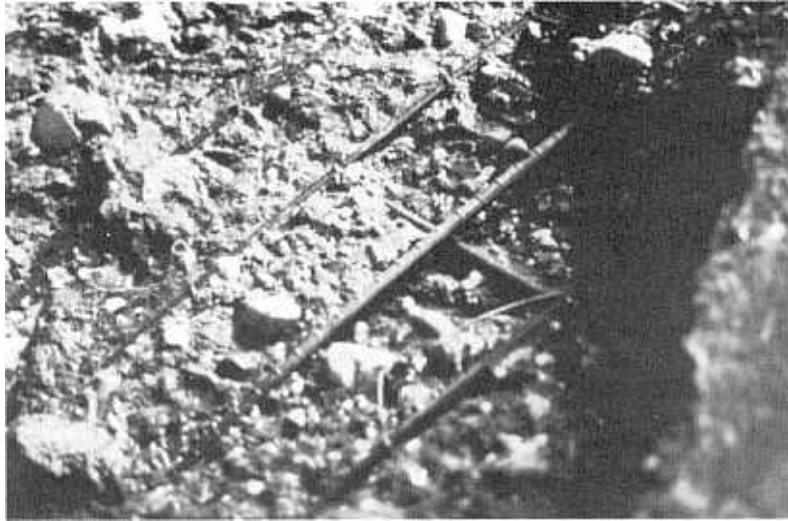
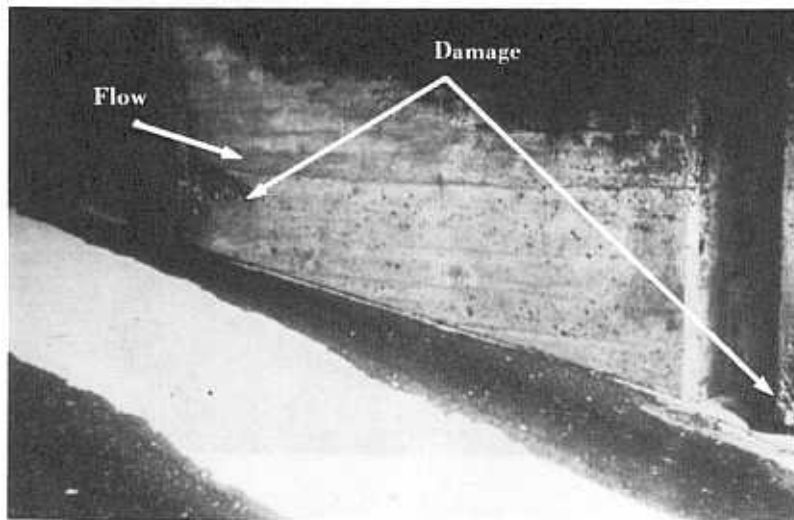
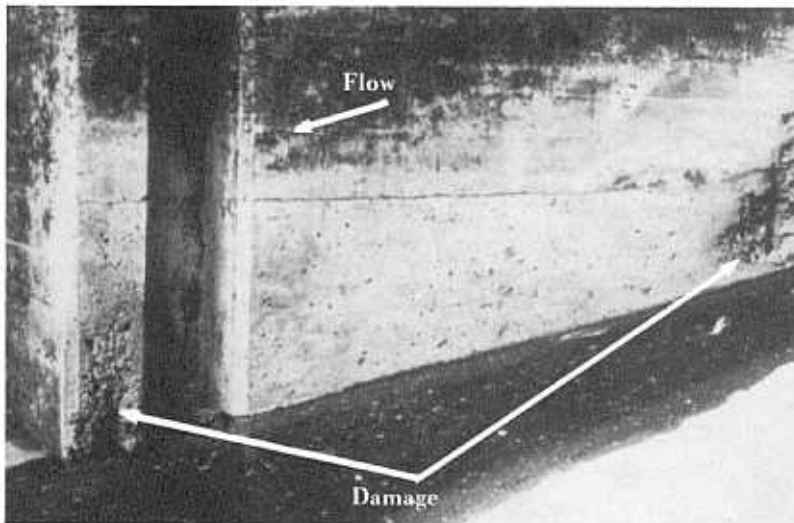


FIGURE 3-15.—Kortes Dam, Wyoming, freeze-thaw damage.



a. Left side of outlet



b. Right side outlet

FIGURE 3-16.—*Palisades Dam, symmetrical damage in outlet structure.*

Cavitation Damage



FIGURE 3-17.—*Palisades Dam, outlet works vortex caused damage downstream of slide gate.*

BIBLIOGRAPHY

- [1] Stinebring, D. R., Arndt, R.E.A., Holl, J. W., "Two Aspects of Cavitation Damage in the Incubation Zone: Scaling by Energy Considerations and Leading Edge Damage," *Journal of Fluids Engineering*, Transactions of the American Society of Mechanical Engineers, vol. 102, pp. 481-485, December 1980.
- [2] Stinebring, D. R., "Scaling of Cavitation Damage," masters thesis, Pennsylvania, State University, 160 pp., August 1976.
- [3] Colgate, D., "Cavitation Damage in Hydraulic Structures," International Conference on Wear of Materials, St. Louis, MO, pp. 433-438, April 25-28, 1977.
- [4] Peterka, A. J., "The Effect of Entrained Air on Cavitation Pitting," Proceedings of the Joint Meeting of the International Association for Hydraulic Research and the American Society of Civil Engineers, Minneapolis, MN, August 1953.
- [5] Bradley, J. N., "Study of Air Injection into the Flow in the Boulder Dam Spillway Tunnels — Boulder Canyon Project," Bureau of Reclamation Report No. HYD-186, October 1945.
- [6] Rao, P. V., Martin, C. S., Rao, B.C.S., Rao, N.S.L., "Estimation of Cavitation Eosion With Incubation Periods and Material Properties," *Journal of Testing and Evaluation*, American Society for Testing and Materials, pp. 189-197, 1981.
- [7] Heymann, F. J., "On the Time Dependence of the Rate of Erosion Due to Impingement or Cavitation," *Erosion by Cavitation or Impingement*, Special Technical Publication No. 408, American Society for Testing and Materials, pp. 70-110, 1967.
- [8] Wang, X., Chou, L., "The Method of Calculation of Controlling (or Treatment) Criteria for the Spillway Surface Irregularities," Proceedings of the Thirteenth International Congress of Large Dams, Q50, R56, pp. 977-1012, New Delhi, India, 1979.
- [9] Falvey, H. T., "Predicting Cavitation in Tunnel Spillways," *Water Power and Dam Construction*, vol. 34, pp. 13-15, August 1982.
- [10] ———, "Prevention of Cavitation on Chutes and Spillways," Proceedings of the Conference on Frontiers in Hydraulic Engineering, American Society of Civil Engineers, Cambridge, MA, pp. 432-437, August 1984.
- [11] Hopping, P. N., Mass, G. R., "Cavitation Damage on the Karun Dam," *Concrete International*, vol. 9, No. 3, pp. 41-48, March 1987.

Control of Cavitation Index by Geometry

Chapter 4

CONTROL METHODS

As water flows down a chute, its velocity increases and the flow depth decreases. This combined effect causes the cavitation index of the flow to decrease with the longitudinal distance along the chute. Eventually, a point is reached on the chute where normal surface irregularities will cause cavitation to begin.

Cavitation could be prevented from forming if it were possible to reduce the velocity or to increase the boundary pressure. For straight spillways, the pressure can be increased by increasing the flow depth through the use of convergent chute walls. For spillways—composed of vertical curves—the boundary pressure can be increased by changing the curvature of the flow boundary. The concept of varying both the width and invert curvature has been studied in the laboratory by Colgate [1].

Curvature on a spillway or chute can be manipulated to produce a profile having a constant cavitation index or it can be varied so as to control the pressure distribution in a prescribed manner. The first technique produces a *constant cavitation number spillway*. The second technique produces a *controlled pressure spillway*. Both techniques use the same fundamental equations discussed below in Equations of Motion.

Another method for reducing the flow velocity is to increase the boundary friction; that is, make the surface rougher. At first thought, this appears to be contrary to everything that has been published on the requirement of making boundaries smooth for high velocity flow. However, the real culprit in causing cavitation is not the roughness of the boundary, but the roughness of individual asperities. If making a surface uniformly rough is possible, then its cavitation characteristics will actually improve. This idea is demonstrated at the end section of this chapter.

EQUATIONS OF MOTION

Lin et al. [2] proposed a method in which the vertical radius of curvature is varied to produce a constant cavitation index value over the length of the vertical bend. The method is sufficiently general to include the effect of convergence of the sidewalls. The resulting profile produces a gradually increasing pressure distribution through the vertical curve. If the vertical curve terminates at a chute or in a tunnel, a large pressure gradient is produced at the point of tangency. The large gradient may have an adverse effect on the flow conditions at this point. However, if the vertical curve terminates in a flip bucket, the method produces an excellent spillway profile that has the minimum potential for cavitation damage. The invert profile produced by this method is known as a *constant cavitation number profile*.

To eliminate the generation of large pressure gradients at the end of the vertical curve, Ku and Jin [3] proposed an equation for the vertical curve which is tangent to the upstream and downstream slopes. In addition, the reciprocal of the radius of curvature varies uniformly from a value of zero, at the point of curvature, to a maximum value at the center of the curve and then back to zero at the end of the vertical curve. This method produces a triangular-shaped variation in the pressure distribution along the boundary. Although Ku and Jin used a linear variation for the radius of curvature, any shape of curve could be used. This method produces a *controlled pressure profile*.

The following development presents the equations that apply to both of the preceding methods. The development does not include the effect of boundary friction. Techniques to account for nonrectangular sections are included.

The most common way for developing the equations of motion is to use a rectilinear vector

notation. However, in many cases, problems can be solved easier by transforming the rectilinear notation into another orthogonal coordinate system. For instance,

- Displacements of a rectangular membrane are expressed in the Cartesian coordinate system.
- Heat flow in a sphere is expressed in a spherical coordinate system.
- Electrical fields around a wire are expressed in a cylindrical coordinate system.

For fluid flows, it is often convenient to express the equation of motion in terms of a coordinate system which is aligned with the motion. This system is called a natural or intrinsic system. The equations of motion for an intrinsic coordinate system have been defined by Milne-Thompson [4]. The equations are referred to the location b on a streamline C as shown on figure 4-1. The axis s is tangent and the axis n is normal to the streamline. The general momentum equations for two-dimensional flow in the s and n directions are given by:

$$U_s \frac{\partial U_s}{\partial s} + U_n \frac{\partial U_s}{\partial n} - U_s U_n K_s - U_n^2 K_n = - \frac{1}{\rho} \frac{\partial P}{\partial s} - \frac{\partial \Omega}{\partial s} \quad 4.1$$

and

$$U_s \frac{\partial U_n}{\partial s} + U_n \frac{\partial U_n}{\partial n} + U_s U_n K_n + U_s^2 K_s = - \frac{1}{\rho} \frac{\partial P}{\partial n} - \frac{\partial \Omega}{\partial n} \quad 4.2$$

where:

K_s = curvature of streamline

$$K_s = \frac{d^2 n}{ds^2} \left[1 + \left(\frac{dn}{ds} \right)^2 \right]^{-3/2}$$

K_n = curvature of curve normal to streamline

$$K_n = \frac{d^2 s}{dn^2} \left[1 + \left(\frac{ds}{dn} \right)^2 \right]^{-3/2}$$

P = pressure intensity

U_s = velocity tangent to streamline

U_n = velocity normal to streamline

ρ = density of water

Ω = potential of external force

n = coordinate distance normal to streamline

s = coordinate distance tangent to streamline

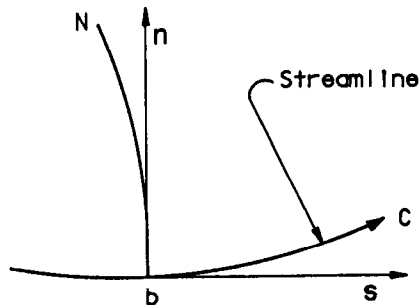


FIGURE 4-1.—Definition sketch of intrinsic coordinate system.

However, by definition, flow does not cross a streamline. Thus, $U_n = 0$ along the streamline. The potential of the external force, Ω , which in this case is gravity, is given by:

$$\Omega = gZ \quad 4.3$$

where:

g = gravitational constant (acceleration)

Z = elevation

With these considerations, the equation of motion becomes:

$$U_s \frac{\partial U_s}{\partial s} + \frac{1}{\rho} \frac{\partial P}{\partial s} + g \frac{\partial Z}{\partial s} = 0 \quad 4.4$$

and

$$U_s^2 K_s + \frac{1}{\rho} \frac{\partial P}{\partial n} + g \frac{\partial Z}{\partial n} = 0 \quad 4.5$$

Equations 4.4 and 4.5 can be written as:

$$\frac{\partial}{\partial s} \left(\frac{U_s^2}{2} + \frac{P}{\rho} + gZ \right) = 0 \quad 4.6$$

and

$$\frac{\partial}{\partial n} \left(\frac{U_s^2}{2} + \frac{P}{\rho} + gZ \right) + U_s \left(U_s K_s - \frac{\partial U_s}{\partial n} \right) = 0 \quad 4.7$$

or

$$\frac{\partial}{\partial n} \left(\frac{U_s^2}{2} + \frac{P}{\rho} + gZ \right) + U_s \zeta = 0 \quad 4.8$$

where ζ equals vorticity. These last three equations are significant because they show:

1. The Bernoulli equation is constant along a streamline (equation 4.6), and
2. The constant changes from streamline to streamline as the vorticity changes (equation 4.8).

In rotational flow, vorticity, ζ , is equal to twice the angular velocity, ω , or

$$\zeta = 2\omega \quad 4.9$$

In irrotational flow, the vorticity, ζ , is equal to zero; i.e.,

$$\zeta = 0 \quad 4.10$$

Each of these vorticity conditions will lead to different spillway profiles. Both can be investigated using the computer program in appendix C.

VELOCITY AND PRESSURE AT FLOW BOUNDARY

Integrating equation 4.6 along the free water surface between the reservoir and point a , as shown on figure 4-2, results in:

$$\frac{U_a^2}{2g} + Z_a - Z_r = 0 \quad 4.11$$

where:

U_a = velocity at point a

Z_a = elevation at point a

Z_r = elevation of reservoir

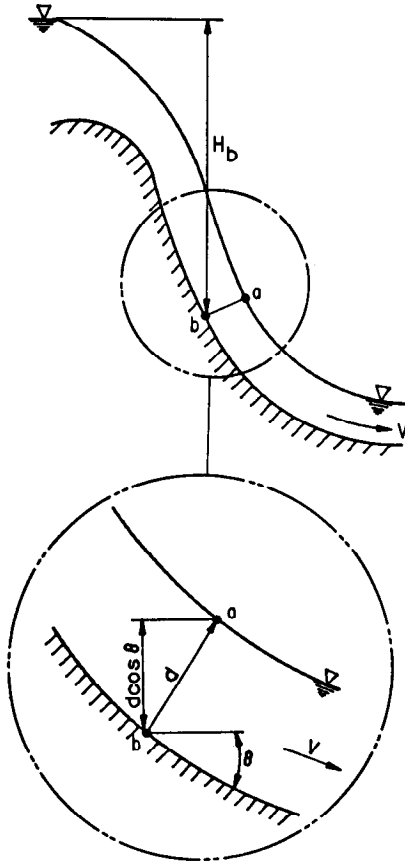


FIGURE 4-2.—Definition sketch for integration along a streamline.

However, the relationship between the free water surface and the point a is also given by:

$$Z_a - Z_r = -H_b + d \cos \theta \quad 4.12$$

where:

H_b = reservoir elevation minus elevation at point b

d = flow depth normal to invert

θ = angle between tangent to invert and horizontal

thus,

$$U_a = [2g(H_b - d \cos \theta)]^{1/2} \quad 4.13$$

The velocity and pressure at the flow boundary can be determined by integrating equation 4.7. This process can be simplified by making assumptions concerning the flow vorticity.

With the *rotational flow assumption*, velocity in the streamline direction is given by:

$$\frac{dq}{dn} = U_s = \omega(R - n) \quad 4.14$$

where:

q = unit discharge of water

R = radius of curvature of reference streamline

n = coordinate distance normal to streamline
 U_s = velocity tangent to streamline
 ω = angular velocity

Unit discharge is obtained by integrating equation 4.14 between points b and a . Thus, unit discharge:

$$q = \frac{d(1 - d/2R_b)}{(1 - d/R_b)} [2g(H_b - d \cos \theta)]^{1/2} \quad 4.15$$

where R_b equals radius of curvature at the boundary. Therefore, at any flow depth d :

$$U_s = \omega(R_b - d) \frac{(R_b - n)}{(R_b - d)} = U_a \frac{(1 - n/R_b)}{(1 - d/R_b)} \quad 4.16$$

At the flow boundary $n = 0$, results in:

$$U_b = \frac{U_a}{(1 - d/R_b)} = \frac{[2g(H_b - d \cos \theta)]^{1/2}}{(1 - d/R_b)} \quad 4.17$$

where U_b equals velocity at the boundary.

Having a relationship for the velocity at the flow boundary allows equation 4.8 also to be integrated between points b and a which results in:

$$\frac{P_b}{\rho g} = d \cos \theta + \frac{U_b}{g} \left(\frac{d}{R_b} \right) \left(1 - \frac{d}{2R_b} \right) \quad 4.18$$

or

$$\frac{P_b}{\rho g} = d \cos \theta + \frac{2(H_b - d \cos \theta) (d/R_b) (1 - d/2R_b)}{(1 - d/R_b)^2} \quad 4.19$$

With the *irrotational flow assumption*, vorticity is equal to zero. From equation 4.7:

$$\frac{dU_s}{dn} = U_s K_s = \frac{U_s}{R_s} \quad 4.20$$

Integrating between point a and any depth results in:

$$\frac{dq}{dn} = U_s = \frac{(1 - d/R_b)}{(1 - n/R_b)} U_a \quad 4.21$$

At the flow boundary $n = 0$, equation 4.21 becomes:

$$U_b = (1 - d/R_b) [2g(H_b - d \cos \theta)]^{1/2} \quad 4.22$$

Unit discharge, obtained by integrating equation 4.21 between points b and a , results in:

$$q = -R_b(1 - d/R_b) [\ln(1 - d/R_b)] [2g(H_b - d \cos \theta)]^{1/2} \quad 4.23$$

If $d/R_b < 0.05$, equation 4.23 can be approximated:

$$q = d(1 - d/R_b) [2g(H_b - d \cos \theta)]^{1/2} \quad 4.24$$

Pressure at the boundary is determined from equation 4.8 when $Z = 0$, or

$$\frac{P_b}{\rho g} = H_b - \frac{U_b^2}{2g} \quad 4.25$$

or

$$\frac{P_b}{\rho g} = H_b - [(1 - d/R_b)^2 (H_b - d \cos \theta)] \quad 4.26$$

GEOMETRIC RELATIONSHIPS

To apply the preceding equations to spillway chute design, the intrinsic coordinates need to be defined in terms of the Cartesian coordinate system as noted on figure 4-3.

The slope of the tangent to the invert is given by:

$$\frac{dH_b}{dx} = \tan \theta = \frac{(1 - \cos^2 \theta)^{1/2}}{\cos \theta} \quad 4.27$$

A relationship between θ , H_b , and the radius of curvature of the invert, R_b , can be obtained by realizing that

$$\frac{d \cos \theta}{dH_b} = -\sin \theta \frac{d\theta}{dH_b} \quad 4.28$$

However, $dH_b = \sin \theta ds$, thus

$$-\frac{d \cos \theta}{dH_b} = \frac{d\theta}{ds} = \frac{1}{R_b} \quad 4.29$$

CAVITATION PARAMETER

The cavitation index is defined as:

$$\sigma = \frac{P_a + P_b - P_v}{\rho U_b^2 / 2} \quad 4.30$$

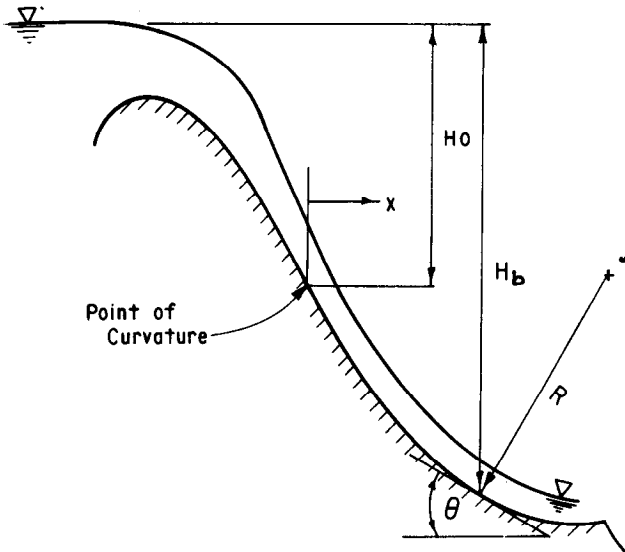


FIGURE 4-3.—Definition sketch for geometry.

This equation is identical to equation 1.5 where the reference pressure is equal to the local pressure on the boundary—measured in gauge pressure.

CONSTANT CAVITATION NUMBER SPILLWAY

The five equations which are needed to solve for the equal cavitation number spillway are 4.15, 4.19, 4.27, 4.29, and 4.30 for the rotational flow assumption; and 4.24, 4.26, 4.27, 4.29 and 4.30 for the irrotational flow assumption. The equations are interrelated and can be condensed to four equations for each assumption. Then, the four equations can be simplified by expressing them in dimensionless parameters. The parameters are chosen so that their values vary between 0 and 1. The dimensionless parameters are defined as follows:

$$\eta = \frac{H}{H_i} \quad \xi = \frac{x}{H_i} \quad A_n = \frac{P_a - P_v}{\rho g H_i} \quad F = \cos \theta$$

$$q_n = \frac{q}{(2g H_i^2)^{1/2}} \quad d_n = \frac{d}{H_i} \quad R_n = \frac{R}{H_i}$$

where:

- A_n = dimensionless pressure ratio
- d_n = dimensionless flow depth
- F = cosine of invert slope
- g = gravitational constant (acceleration)
- H_i = initial head at beginning of constant cavitation number profile
- R_n = dimensionless radius of curvature
- q_n = dimensionless unit discharge
- η = dimensionless head
- ξ = dimensionless distance horizontal
- ρ = density of water

The four dimensionless equations for rotational flow are:

$$d_n = \frac{q_n (1 - d_n/R_n)}{(1 - d_n/2R_n) (\eta - d_n F)^{1/2}} \quad 4.31$$

$$\frac{1}{R_n} = \frac{\sigma(\eta - d_n F) - (d_n F + A_n) (1 - d_n/R_n)^2}{2d_n [1 - d_n/(2R_n)] (\eta - d_n F)} \quad 4.32$$

$$\frac{dF}{d\eta} = \frac{1}{R_n} \quad 4.33$$

$$\frac{d\eta}{d\xi} = \frac{(1 - F^2)^{1/2}}{F} \quad 4.34$$

The four dimensionless equations for irrotational flow are:

$$d_n = \frac{q_n (d_n/R_n)}{(d_n/R_n - 1) [\ln (1 - d_n/R_n)] (\eta - d_n F)^{1/2}} \quad 4.35$$

$$\frac{1}{R_n} = \frac{[(\sigma + 1) (\eta - d_n F)]^{1/2} - (\eta + A_n)^{1/2}}{d_n [(\sigma + 1) (\eta - d_n F)]^{1/2}} \quad 4.36$$

$$\frac{dF}{d\eta} = \frac{1}{R_n} \quad 4.37$$

$$\frac{d\eta}{d\xi} = \frac{(1 - F^2)^{1/2}}{F} \quad 4.38$$

Differential equations 4.33 and 4.34 or 4.37 and 4.38 can be solved by a Runge-Kutta method subject to the following initial conditions:

$$\eta_i = 1 \quad \xi_i = 0 \quad F_i = \cos \xi_i \quad 1/R_i = 0$$

$$q_i = \frac{q}{(2gH_i^2)^{1/2}} \quad d_i = \frac{q_i}{(1 - d_i F_i)^{1/2}}$$

where the subscript i refers to initial conditions.

This method assumes a rectangular section. To use the method with flow in circular sections flowing part full, the unit discharge of water, q , is calculated from:

$$q = d_c [2g(H_b - d_c \cos \theta)]^{1/2} \quad 4.39$$

where d_c equals flow depth at beginning of constant cavitation number profile as determined from the output of the program HFWS in appendix A.

With circular conduits, the velocities given in the output of the constant cavitation number profile program are too large when based on the unit discharge computed from equation 4.39. These false values of velocities also influence the accuracy of the computed cavitation index. The equivalence between the cavitation indexes, as given by the constant sigma spillway computations, and the true values for the circular conduit are given by:

$$\sigma_c = \frac{\sigma_e}{V_c^2} \left(\frac{q}{d_e} \right)^2 \quad 4.40$$

where:

d_e = flow depth from constant cavitation number profile

V_c = flow velocity in circular conduit

σ_c = cavitation index in circular conduit

σ_e = cavitation index from constant cavitation number spillway

The effect of convergent sidewalls can be included in the analysis by redefining only the dimensionless discharge, q_n , at each computational point. With a linear convergence of the sidewalls over a distance L , the discharge is given by:

$$q_n = \frac{q_i}{1 - \mu \xi} \quad 4.41$$

where:

μ = dimensionless convergence ratio

$$\mu = \left(\frac{B_u - B_l}{L} \right) \left(\frac{H_l}{B_u} \right)$$

B_l = width at lower end of spillway

B_u = width at upper end of spillway
 L = difference in stationing between upper and lower ends of spillway

Subscripts u and l refer to the upper and lower ends of the spillway, respectively. Subscript i refers to initial conditions at the start of the constant cavitation number spillway.

The computer program in appendix C can be used to solve the constant cavitation number spillway equations. Either the rotational or the irrotational assumption can be selected. From a practical viewpoint, both assumptions give essentially the same result when the flow depth is less than 5 percent of the radius of curvature.

CONTROLLED PRESSURE SPILLWAY PROFILE

The controlled pressure spillway uses only equation 4.29 in the form:

$$\frac{d\theta_d}{dS_b} = \frac{1}{R_b} = f(s) \quad 4.42$$

where:

R_b = radius of curvature at the boundary

$f(s)$ = a specified function

S_b = coordinate distance on invert curve

θ_d = deflection angle of curve, radians

The function is chosen so that the radius of curvature is infinite at each end of the controlled pressure spillway profile and it has a minimum at the midpoint of the controlled pressure spillway profile.

Ku and Jin [3] used a function that has a triangular distribution over the length of the controlled pressure spillway profile:

$$f(s) = k_r s \quad \text{for } s \leq s_m/2 \quad 4.43$$

and

$$f(s) = k_r (s_m - s) \quad \text{for } s > s_m/2 \quad 4.44$$

where:

k_r = constant to control the radius of curvature

s_m = maximum length of invert curve

With this function, the length of the invert curve is given by:

$$s_m = 2 \left(\frac{\theta_d}{k_r} \right)^{1/2} \quad 4.45$$

In this formulation, the minimum value of the radius of curvature can be controlled by the appropriate selection of the constant k_r . For a given

minimum radius of curvature and deflection angle, the constant, k_r , is given by:

$$k_r = \frac{1}{4 R^2 \theta_d} \quad 4.46$$

The function used by Ku and Jin is not unique to this type of problem. A smoother variation in the pressure distribution can be obtained by using a cosine function defined as:

$$f(s) = k_r [1 - \cos(2\pi s / s_m)] \quad 4.47$$

In this case, the length of the invert curve, s_m , is given by:

$$s_m = \left(\frac{2 \theta_d}{k_r} \right)^{1/2} \quad 4.48$$

The value of the constant, k_r , for a given minimum radius of curvature is determined from:

$$k_r = \frac{1}{2 \theta_d R^2} \quad 4.49$$

The rectilinear coordinates are determined from:

$$\frac{dx}{ds} = \cos \theta \quad 4.50$$

and

$$\frac{dy}{ds} = \sin \theta \quad 4.51$$

After substituting the appropriate functional relationships (equations 4.43 and 4.44 or equation 4.47), equations 4.42, 4.50, and 4.51 can be integrated. Two programs using Simpson's Rule are provided in appendix C to solve these equations numerically.

CHANGING INVERT CURVATURE—EXAMPLE

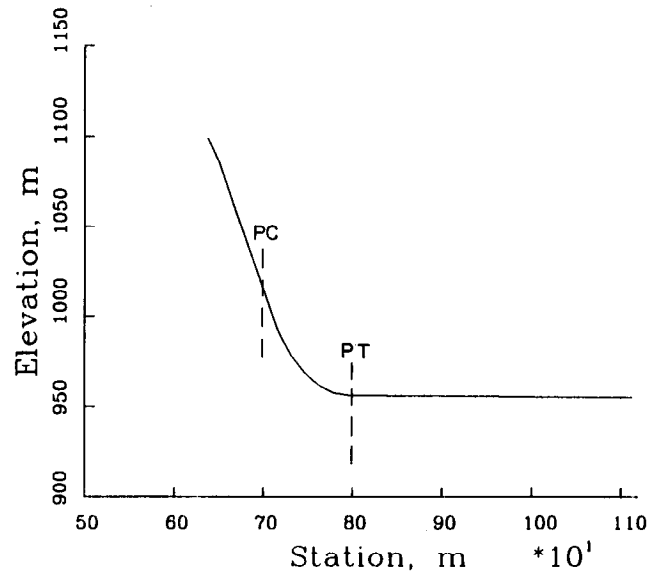
The techniques of designing with a constant cavitation number and a controlled pressure profile were applied to the Bureau's Glen Canyon Dam configuration to illustrate the methods and the potential benefits. The benefits are increased values of the cavitation index of the flow. Increasing the cavitation index reduces the potential for damage by cavitation. This implies that during construction surface tolerances might be relaxed. In addition, potentially dangerous conditions caused by growth of calcite deposits after construction will not develop.

An analysis of the cavitation potential, of Glen Canyon Dam tunnel spillway, using the program HFWS in appendix A, showed the lowest values of the cavitation index occurred upstream of the point of curvature and downstream of the point of

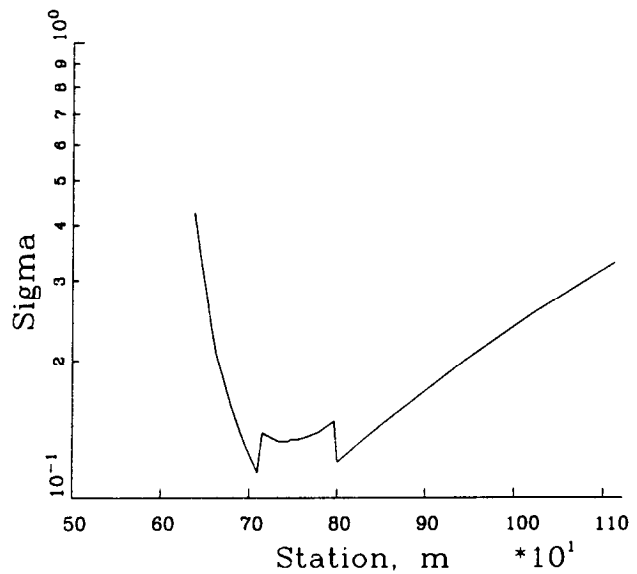
tangency of the vertical bend (see fig. 4-4). The lowest values of the cavitation index for flow through the elbow occurred for a discharge of about 475 m³/s.

Constant Cavitation Number Profile

With a constant cavitation number profile it is not possible to control the cavitation index downstream of the point of tangency. However, all of the spillway from the end of the crest profile to the point of tangency can be controlled.



a. Invert profile



b. Cavitation index

FIGURE 4-4.—Glen Canyon Dam, left spillway tunnel — cavitation index for flow of $Q = 475$ m³/s.

The problem is to determine a constant cavitation number profile that is tangent to the spillway crest profile and that terminates at an elevation equal to the elevation of the point of tangency. To perform these computations, the following procedure was followed:

1. Variation in flow depth and velocity is determined along the spillway crest profile using the computer program HFWS.
2. A point is arbitrarily selected along the crest profile as the starting location for the constant sigma profile. This point should have a value of the cavitation index greater than or equal to 0.2. In some cases, this is not possible if the vertical drop to the lower tangent point is too great.
3. Initial conditions are calculated using equation 4.39 for the definition of the unit discharge in a circular section and using the flow depth and invert slope at the selected starting location.
4. Constant cavitation number profile program is run.
5. If the final elevation of the constant cavitation profile does not match the desired elevation of the point of tangency, increase the value of the unit discharge and repeat steps 3 and 4. If the unit discharge gets so large that the radius of curvature becomes negative—somewhere on the profile—select, for the initial station, a location that has a lower elevation.
6. Flow conditions with the resulting profile are recalculated with program HFWS to investigate the effect of boundary friction.

The results of the analysis show that the cavitation index could have been increased from a minimum value of $\sigma = 0.104$ (shown on fig. 4-4) to a minimum value of $\sigma = 0.115$ (shown on fig. 4-5) for the portion of the tunnel between the spillway crest and the point of tangency at the end of the vertical curve. This increase in the flow cavitation index would not have prevented the damage which occurred in the Glen Canyon spillways during the 1983 flood. However, the time of operation before damage occurred would have been extended.

The cavitation index of figure 4-5 is not constant because the equal cavitation number profile was developed using rectangular sections. The conversion of the cavitation index from the rectangular to the circular section is given by equation 4.40. Also, the index is not constant because boundary friction is neglected in the development of the equal cavitation number profile, but is considered in the water surface profile program HFWS.

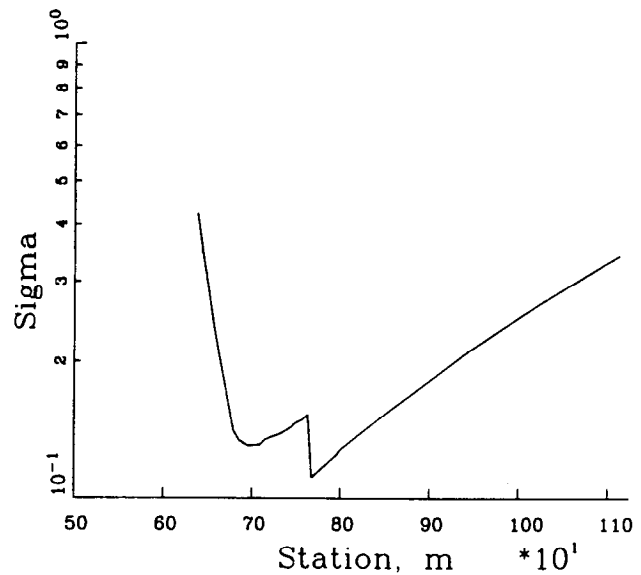


FIGURE 4-5.—Glen Canyon Dam, equal cavitation number spillway profile — cavitation index for flow of $Q = 475 \text{ m}^3/\text{s}$.

Two problems exist with the constant cavitation number profile: a large pressure gradient exists at the point of tangency, and the curve is too short. The gradient will not induce cavitation, but it may cause rapid variations in the water level depth. The second problem is the most severe. Because the curve is too short, the cavitation index at the end of the curve is still very low—being about equal to 0.101.

Controlled Pressure Profile

With the controlled pressure profile, the radius of curvature at both the point of curvature and at the point of tangency are infinite. Therefore, large pressure gradients do not exist with these profiles. A great difference between the cavitation indexes, with either the linear or the sinusoidal variation in pressure along the vertical curve, is not evident as noted on figure 4-6. Because both curves are longer than the equal cavitation number profile, improvements in the cavitation index have been made at the point of tangency.

For Glen Canyon Dam, the controlled pressure profile resulted in the most favorable cavitation characteristics in the vertical bend. At station 720 the cavitation index reached a value of 0.20 as compared to a value of 0.14 in the existing design.

All of the controlled pressure profiles began at station 678.86 which is the location where the crest profile matches the equal cavitation number profile.

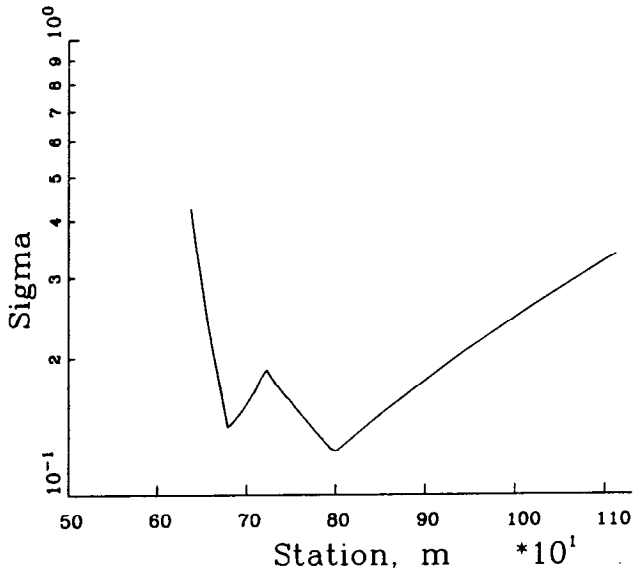
CHANGING SURFACE ROUGHNESS—EXAMPLE

The beneficial effect of increasing the surface roughness on the cavitation index can be seen by

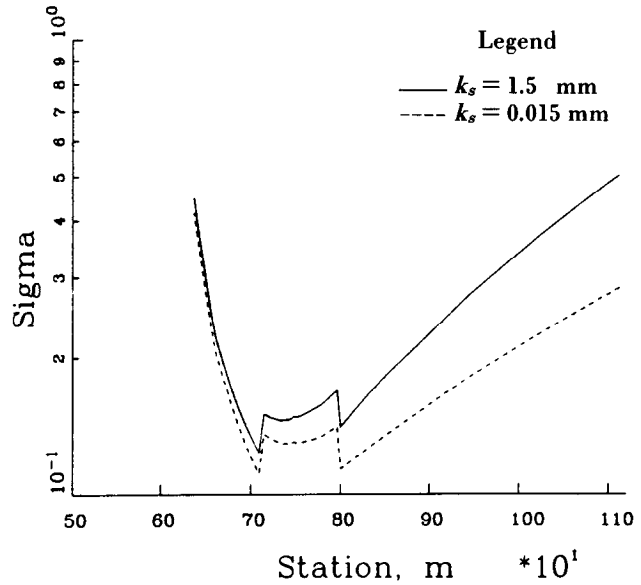
examining the cavitation index of the flow for the Glen Canyon tunnel spillways having rugosities of 0.015 and 1.5 millimeters. The smaller value of the rugosity corresponds to new, unusually smooth, concrete placed against steel forms having excellent workmanship. With this surface, construction joints are well aligned. The larger value of rugosity corresponds to an unusually rough surface placed against rough wood forms, where erosion at poor concrete and poor alignment of joints occurred. These values represent the extremes of what actually will be achieved in the field.

As shown on figure 4-7, increasing the rugosity results in an increase in the cavitation index from 0.091 to 0.118 at station 80—the site of the most severe damage during the 1983 spill. The damage potential also experienced significant decreases. For the larger rugosity value, the damage potential was 3.2 times smaller than for the smaller rugosity as shown on figure 4-7.

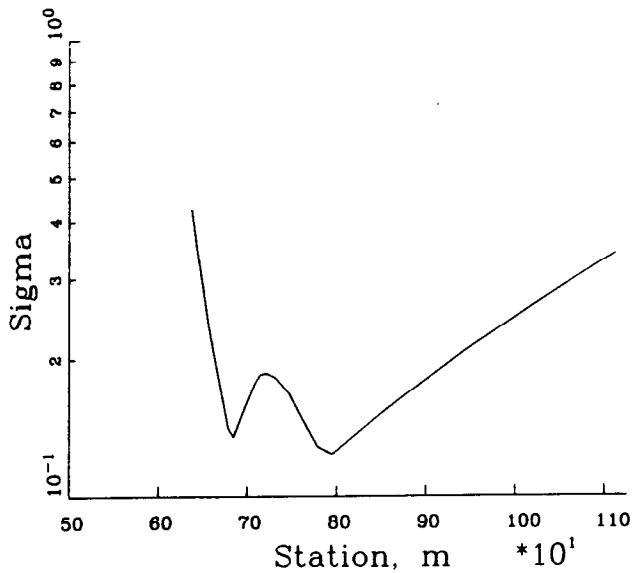
These examples show that, on Glen Canyon Dam tunnel spillways, the effect of increasing the surface roughness is greater than the effect of changing the invert curvature.



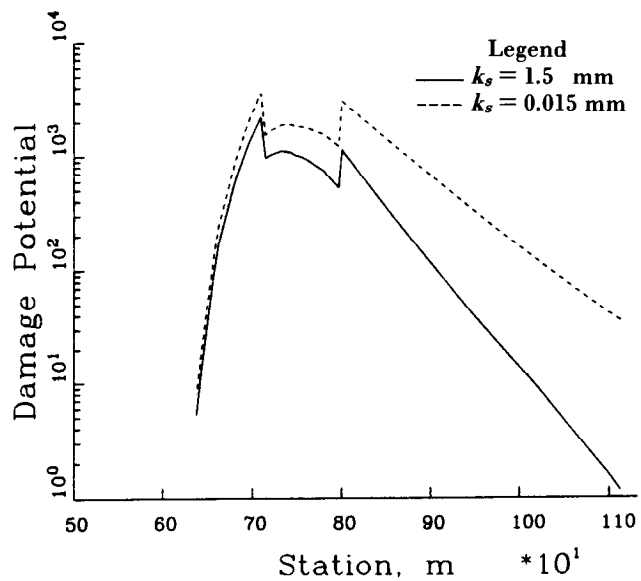
a. Triangular distribution of pressure



a. Cavitation index



b. Cosine distribution of pressure



b. Damage potential

FIGURE 4-6.—Glen Canyon Dam, controlled pressure spillway profiles — cavitation index for flow of $Q = 475 \text{ m}^3/\text{s}$.

FIGURE 4-7.—Effect of rugosity on cavitation characteristics.

The effect of increased surface roughness has not been conclusively tested in the field. However, at Glen Canyon Dam, the left tunnel spillway invert was not repaired downstream of station 850. This area had suffered severe erosion during diversion; irregularities varied between 25 and 76 millimeters deep, Tyler [5]. During the 1984 tests, cavitation damage did not occur in this area. The air content

in the water (from the aerator) probably had the greatest impact on this result. Similarly, the "rocky road" or "cobble stone" appearing surface of the invert (downstream of the vertical bend at the Nevada spillway of Hoover Dam) was not repaired when the aerator was installed. Nevertheless, all isolated irregularities on the otherwise smooth walls above the invert were removed.

BIBLIOGRAPHY

- [1] Colgate, D., "Hydraulic Model Studies of Amaluza Dam Spillway," Bureau of Reclamation Report No. GR-25-76, 65 pp., December 1976.
- [2] Lin, B., Gong, Z., Pan, D., "A Rational Profile for Flip Buckets of High Head Dams," *Scientia Sinica*, series A, vol. 25, No. 12, pp. 1343-1352, China, December 1982.
- [3] Ku, C. H., Jin, Z., "The Investigation of a More Rational Configuration of the Invert Curve of a Spillway," Joint American Society of Mechanical and American Society of Civil Engineers Symposium, Albuquerque, NM, pp. 143-148, June 1985.
- [4] Milne-Thompson, L. M., *Theoretical Hydrodynamics*, MacMillan Co., 2d ed, 1950.
- [5] Tyler, J. L., "Final Construction Report on Repair Spillway Tunnels, Glen Canyon Dam, Colorado River Storage Project, Page, Arizona," Contract NO.3-CC-40-0110, Bureau of Reclamation, December 1984.

Aerator Design

Chapter 5

JUSTIFICATION FOR AERATORS

Damage experience, for flows in spillway tunnels and chutes, indicates that damage becomes significant when water velocities exceed 30 meters per second (see fig. 3.8). This velocity corresponds to a head of about 45 meters. From a cavitation damage viewpoint, this velocity or head can be considered as the borderline for high velocity or high head flows. Past practice recommended that surfaces exposed to high velocity flows be protected by strict attention to the surface tolerances, Ball [1]. For new construction, this procedure may be acceptable. However, weathering of the concrete surface or the deposition of calcite through minute cracks in the boundary (after construction) can soon create a surface which is not within the specified or constructed tolerances. Therefore, other means of protecting the surface need to be considered.

It is known that extremely small quantities of air, dispersed through a water prism, will significantly reduce the tendency for cavitation to damage a surface. Peterka [2] found that about 7.5-percent air was needed to stop damage in concrete having a 28-day compressive strength of about 17 megapascals. Semenov and Lentiaev [3] found that the quantity of air needed to protect a surface increased as the strength of the surface decreased. They found an air concentration of 3 percent was needed for 40-megapascal strength concrete and an air concentration of almost 10 percent is needed to protect 10-megapascal strength concrete. These values compare favorably with the experiments of Peterka.

Apparently, the first successful application of aerators in a hydraulic structure—to prevent cavitation damage—was at Grand Coulee Dam, Colgate and Elder [4]. In this case, excessive damage had occurred at the intersection of the river outlet tubes with the downstream face of the spillway. Previous attempts to protect the surface with epoxy coatings had been unsuccessful. After installing the aerators, reports of damage have stopped.

The first known installation of aerators in a spillway was at the Bureau's Yellowtail Dam following large discharges in June 1967, Borden et al. [5]. The installation included not only the construction of an aerator, but careful attention was given to flow surface irregularities downstream of the aerator. For the first 7-meters downstream from the vertical bend, all into-the-flow misalignments were removed by grinding to a 1:100 chamfer. For the next 15 meters, a 1:50 chamfer was used. After all holes were patched and all misalignments were removed by grinding, the entire surface below the springline was painted with a two-coat epoxy phenolic paint to provide a smooth surface and to cement particles of the epoxy mortar or concrete to each other. This work was one of the most difficult repairs undertaken by the Bureau. However, subsequent tests indicated that the repairs were completely successful.

Following the success at Yellowtail Dam spillway, aerators have been installed on spillways worldwide. Although much theory has been developed, aerator design is still somewhat of an art. The following sections summarize the present theory and design methods that can be used to size aerators. However, the results should be regarded as preliminary—subject to verification by model testing.

The interrelationship between the design studies and model investigations should be understood. Generally, model studies will not indicate where damage or cavitation will occur on a structure. The location of the damage site is a function of the cavitation index of the flow and of the surface roughness or misalignments. These parameters can be best determined by a union of the analytic techniques outlined in chapter 3 and a knowledge of construction techniques. Having located the potential damage site—if one exists—the equations in this chapter can be used to obtain a trial design for the aerator. After this has been done, model studies should be performed to verify the aerator performance.

The purpose of model studies is to ensure:

- Jet trajectory is satisfactory for all discharges.
- Filling of the air groove will not cause problems with aeration.
- Undesirable flow conditions will not develop where the jet impacts on the downstream slope.

Usually, the model cannot be used to predict air flow rates because it is almost impossible to construct a large enough model of a spillway to adequately simulate the jet turbulence. An exception to this is on chute spillways for which large sectional models of the spillway can be constructed.

TYPES OF AERATORS

The principal types of aerators shown on figure 5-1 consist of deflectors, grooves, offsets, and combinations of these, Vischer et al. [6]. The purpose of the deflector is to lift the flow from the boundary so that air can be entrained underneath the flow surface. In this manner, air enters the flow without using mechanical methods like air pumps—which require energy. Aeration grooves, slots, or air ducts are used to distribute air across the entire width of the aerator. Various air supply methods are discussed later. Finally, an offset is used on flat

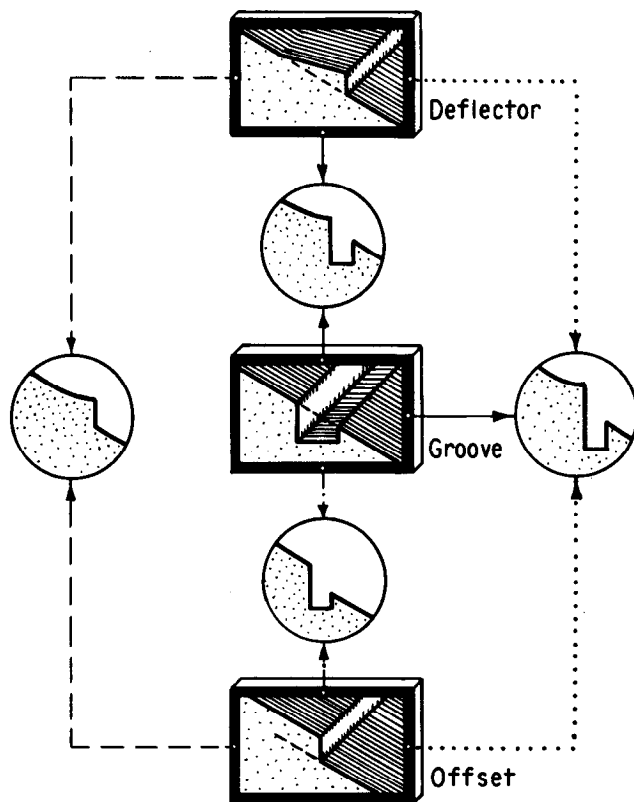


FIGURE 5-1.—Types of aerators.

slopes to prevent the aerator from being submerged by a portion of the flow from the jet as it strikes the downstream boundary.

The design of an aerator consists of:

- Locating the aerator
- Proportioning the ramp or deflector
- Sizing the air supply duct and air groove
- Dimensioning the downstream offset

The goals of the aerator design are to construct a device that will protect the flow surface and not self-destruct if the aerator happens to fill with water.

LOCATION OF AERATOR

Significant damage on spillways has been observed to occur when the cavitation index of the flow is less than 0.20 (see fig. 3-8). Minor damage can occur for indexes greater than 0.20, but the extent of the damage generally has not required repair. Therefore, from a design viewpoint, flow boundaries exposed to flows that have cavitation indexes greater than 0.20 will be essentially safe from damage. Obviously, the strength of the concrete and the surface tolerances will influence this assumption.

In actual practice, this criterion is difficult to achieve. Placement of an aerator high enough on a chute or spillway to keep the cavitation index greater than 0.20 may require the use of excessively large ramp heights. The large ramps can cause the jet to touch the crown of a tunnel spillway or to overtop the walls of chute spillways. Placement of the aerator in areas where the cavitation index is less than 0.20 requires careful consideration of the flow tolerances upstream of the aerator.

The maximum discharge is not necessarily the flow rate that produces the lowest values of the cavitation index of the flow. This can be rationalized in the following manner.

- For low flow rates, friction dominates. Although flow depths are small, velocities are also small. Therefore, the cavitation index of the flow can be large.
- As the flow rate increases, the relative effect of the boundary friction decreases and the flow velocity increases. This causes the cavitation index of the flow to decrease.
- Finally, at much higher flow rates, the increase in flow velocity is small. Hence, flow depths are increasing and the cavitation index of the flow increases.

The cavitation index at the aerators and the critical discharge (as a percent of the design discharge) for a variety of tunnel spillways—constructed by the Bureau—are given in table 5-1. With respect to the cavitation index, Yellowtail and

Glen Canyon spillways have the lowest values. However, at both of these spillways, special care was given to the tolerances of the flow surface upstream of the aerator. For other spillways, the required construction tolerances were relaxed due to the higher values of the cavitation index of the flow.

Table 5-1. - Location of aerator and critical discharge

Spillway	Cavitation index at aerator	Critical discharge (percent of maximum)
Blue Mesa	0.22	30
Flaming Gorge	.19	52
Glen Canyon	.14	14
Hoover	.18	19
McPhee	.19	100
Yellowtail	.13	16

With exception of McPhee, all spillways shown in table 5-1 are tunnel spillways having vertical bends that are concave upward. McPhee is a chute spillway having vertical bends that are concave downward.

In addition to consideration of the cavitation index of the flow, curvature of the boundary should be considered. In particular, aerator installation in vertical bends which are concave upward should be avoided. Normally, the range of flow rates over which aerators in vertical bends will function satisfactorily is severely limited. For flows outside this range, grooves will fill with water or the underside of the jet will not remain aerated.

RAMP DESIGN

The purpose of the ramp is to lift the flow away from the lower boundary of the chute or spillway. By lifting the flow away from the boundary, it forms a free trajectory allowing the underside of the nappe to become aerated. When flow once again rejoins the boundary, it should have entrained enough air to protect the downstream flow surface from cavitation damage.

The water trajectory is a function of the:

- Height of the ramp
- Depth of flow at the ramp
- Slope of the ramp
- Length of the ramp
- Pressure underneath the nappe
- Average velocity at the ramp
- Transverse turbulent velocity component at the ramp

Several methods are available to determine the jet trajectory. Wei and DeFazio [7] used a finite element method to solve the Laplace equation for

flow over the ramp. This method produces excellent results for both ramps and free overfalls. In addition to solving for the jet trajectory, the pressure distribution around the ramp is determined. Knowledge of the pressure distribution is valuable for design of chute training walls in the vicinity of the ramp.

Pan et al. [8] ignored the reduced pressure under the jet and developed the trajectory equation referenced to the jet centerline. Then, the resulting equation was modified by: (1) coefficients to account for the relative height of the ramp, (2) the energy loss, and (3) a distance correction coefficient to account for the difference between the location of the point of impact of the center of the jet and of the lower edge, $(L_c - L_i)$, as shown on figure 5-2.

The trajectory angle needs to be corrected when the ramp height is less than one-tenth of the flow depth or when the angle between the ramp and the invert is greater than 2° . Since Pan et al. ignored the reduced pressure under the nappe; some of their experimentally determined coefficients undoubtedly contained energy loss effects.

Glazov [9] ignored the effect of the relative height of the ramp to the flow depth, but included the effect of the reduced pressure and the offset height in his equations.

Based upon the studies of Glazov and Pan, an accurate method for determining the jet trajectory—without needing a finite difference program—is to use a combination of their studies. The parametric equations [9] of the nappe are:

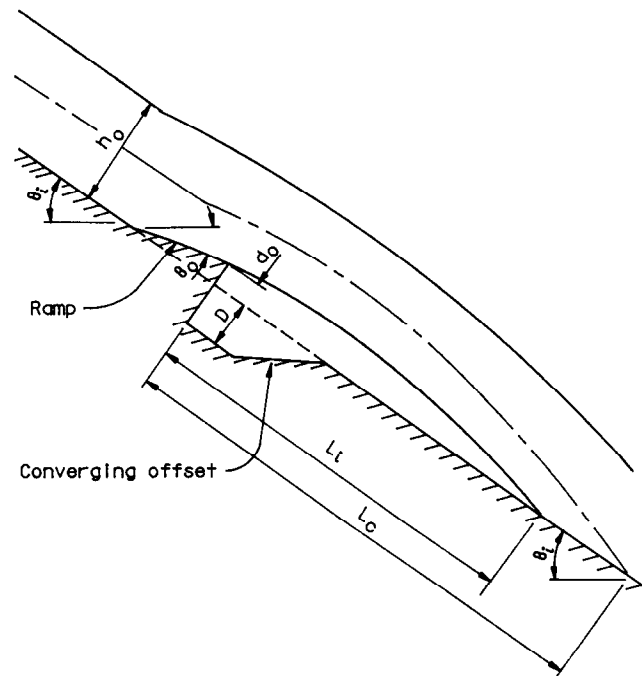


FIGURE 5-2.—Length of jet trajectory.

$$\frac{d^2x}{dt^2} + C_n^2 x = -C_n (g t + U_o \sin \theta_e) \quad 5.1$$

and

$$\frac{d^2y}{dt^2} + C_n^2 y = C_n U_o \cos \theta_e + g \quad 5.2$$

where:

- C_n = pressure factor = $(P_a - P_j) / \rho q$
- g = gravitational constant (acceleration)
- P_a = atmospheric pressure
- P_j = pressure under the jet
- q = unit discharge of water
- U_o = mean flow velocity at ramp
- θ_e = angle between the tangent to nappe at ramp and horizontal
- ρ = density of water

The angle, θ_e , is determined by using the factor A_r given on figure 5-3. This angle, in terms of the invert and ramp angle, is given by:

$$\theta_e = \theta_i (1 - A_r) + A_r \theta_o \quad 5.3$$

where:

- A_r = jet trajectory coefficient, from figure 5-3
- θ_i = angle between invert and horizontal
- θ_o = angle between ramp and horizontal

Through the proper choice of ramp angle and height, it is possible to cause the trajectory to impact the downstream chute at any desired location. Generally, the trajectory should impact downstream of the area that has the smallest value of the cavitation index of the flow. In some cases, this is impossible because the smallest values occur downstream of the vertical bend of a tunnel spillway. The trajectory should be chosen so it does not impact within the vertical bend because this usually causes the formation of fins which lead to poor downstream flow conditions. An impact location in an area having an extremely small cavitation index is acceptable because the surface downstream of the impact area will be adequately aerated.

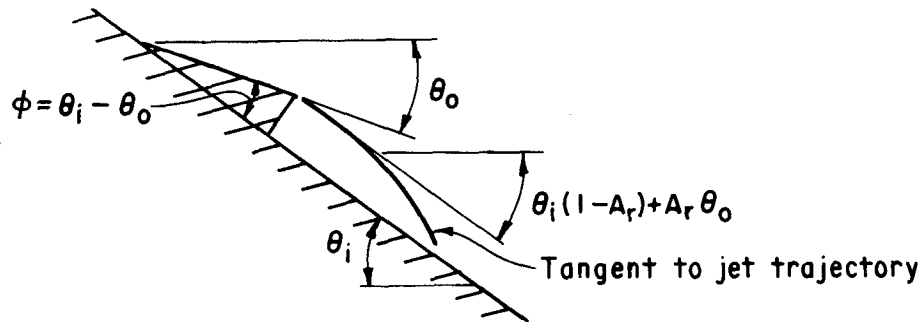
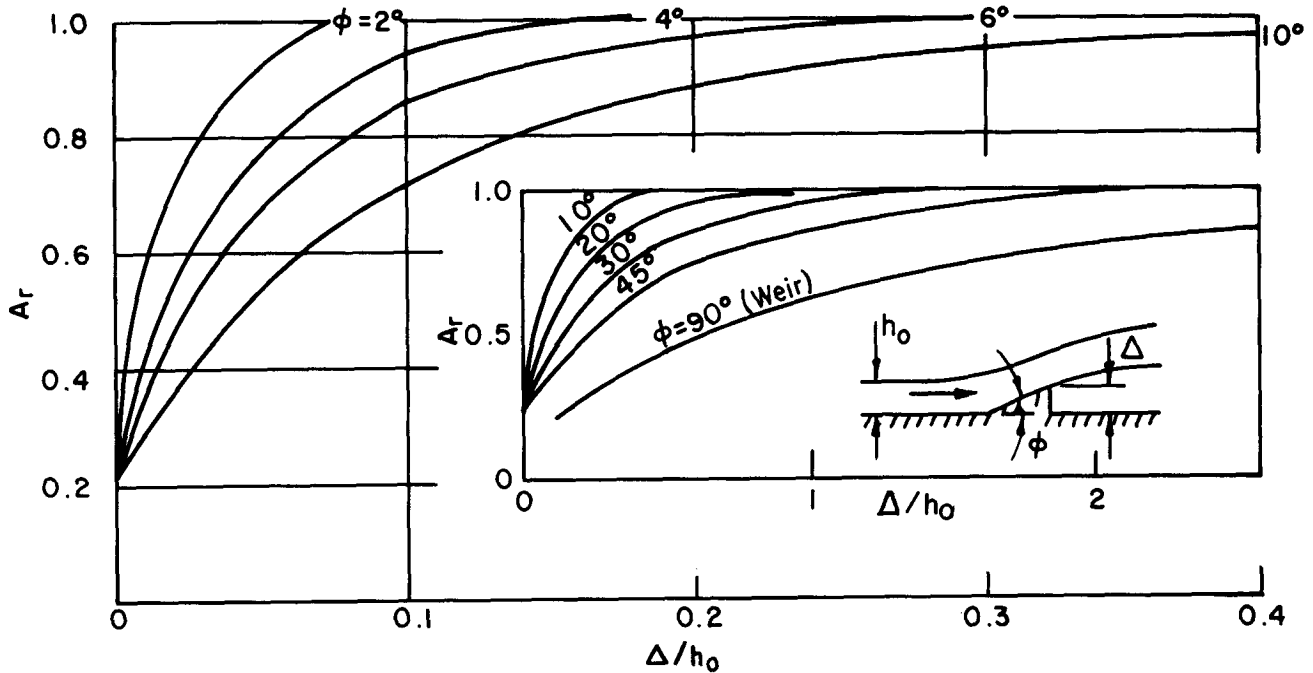


FIGURE 5-3.—Jet trajectory coefficients.

For a first rough approximation of the jet trajectory, use the following equation:

$$\cos^2 \theta_o (\tan \theta_i - \tan \theta_o) = \frac{gX_i}{2U_o^2} \quad 5.4$$

where:

- X_i = horizontal distance from end of ramp to jet impact point
 θ_i = angle between downstream chute and horizontal

Equation 5.4 neglects both the reduced pressure under the nappe and the relative ramp height effect.

In circular tunnels, the ramp height must be tapered around the circumference from a maximum value at the invert to zero at or above the point where the free water surface, at maximum discharge, intersects the tunnel wall. This is done to prevent a fin from forming where the jet impinges on the tunnel wall. Without the taper, the fin size increases as the discharge increases. At large enough flow rates, the fin can fold over and choke the tunnel. With a tapering ramp, the upper portion of the jet is subjected to less contraction than the lower portion of the jet. Because of this, the angle where the jet impinges on the tunnel wall decreases as the flow rate is increased. A disadvantage of tapering is that the jet impinges closer to the ramp at the water surface than at the invert. Model studies are usually required with aerators in circular tunnels to verify proper design of the downstream offset for all discharges.

AIR VENT DESIGN

Air Vent Configurations

Several methods have been devised to vent air from the atmosphere to the underside of the nappe as shown on figure 5-4. These include the following:

- Ramps or deflectors on sidewalls
- Offset sidewalls
- Piers in the flow
- Slots and ducts in sidewalls
- Duct system underneath the ramp
- Duct system downstream of ramp

Ramps or deflectors, offset sidewalls, and piers in the flow are frequently used to supply aeration downstream of control gates. Normally, these air vent types are not used on wide chutes because the required offsets are impractical from a construction or structural point of view.

Slots in walls are used in control gate structures. This solution lends itself to cases where installation in an existing structure is required. The downstream end of the slot may be offset in conjunction with deflectors to keep water from entering the slot. If

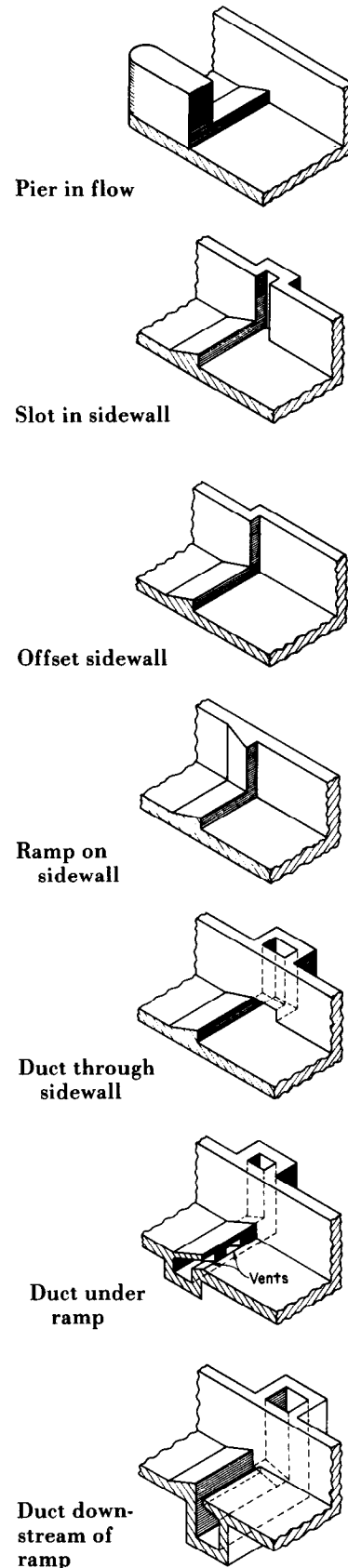


FIGURE 5-4.—Air supply to aerators.

the cross-sectional area of the slot is too small, water and spray will be pulled into the high velocity airstream flowing in the slot. The result will be insufficient air to protect the flow surface on the chute floor.

Ducts through the sidewall are used on wide chutes when the required slot size or sidewall offsets are excessive. A duct is a closed conduit which may have a rectangular or circular cross section. In areas where freezing is a problem, ducts are routed through an embankment. This prevents the formation of ice plugs in the duct during times when water may be standing in the chute area.

A duct, under the ramp, is used on wide chutes or in installations where a hydraulic jump may cover the ramp. In both cases, the system of ducts and vents ensures adequate aeration of the jet undernappe.

A duct—downstream of the ramp or offset—is used when the ramp height is too small to allow adequate venting. This scheme also simplifies construction. However, a drain for the duct must be provided to keep the duct free of water. Leakage and extremely low flow would tend to fill the duct on flat chutes if drainage is not provided. When operating the chute or spillway, air will enter the aerator not only through the duct but also through the drainage gallery.

In circular conduits on steep slopes, filling of the duct is not normally a problem because only a small portion of the duct can contain water. The air duct for circular conduits is commonly called an aeration groove or air slot.

In some cases, an air duct design having a direct connection to the atmosphere is not feasible. This is true especially with tunnel spillways and control gates located in outlet-works tunnels. For these structure types, ventilation is supplied to the duct above the flowing water. If space above the free water surface is too small, pressures under the nappe may begin to fluctuate. Criteria for the air space above the flowing water have not been established. Presently, physical model studies must be used to investigate ventilation adequacy.

Airflow Relationships in Ducts

The air duct cross-sectional area must be large enough to distribute the entrained air and not decrease the pressure under the nappe appreciably. The pressure drop between the atmosphere and the lower side of the nappe, ΔP , can be estimated from:

$$\Delta P = \frac{\rho_a (1 + C_l) Q_a^2}{2A_v^2} \quad 5.5$$

where:

- A_v = cross-sectional area of air duct
- C_l = summation of loss coefficients through the air duct

Q_a = air discharge in duct

ρ_a = density of air

If the drop in pressure becomes too large, sonic velocity will occur in the duct. When this occurs, the flow is said to be choked because the discharge will not increase as the pressure is decreased further. The pressure ratio at which choking occurs is a function of friction losses in the duct leading to the aerator and the inlet configuration of the duct as shown on figure 5-5.

Current practice is to size a duct by dividing the airflow rate by a design velocity. This procedure appears valid; however, the value to use for a design velocity is not a constant. A better procedure is to limit the pressure drop to some percent of the critical pressure ratio. For example, if the pressure drop is limited to one-tenth of the critical pressure ratio, excessive noise in the duct and instabilities in the airflows can generally be avoided. With this criterion, the maximum allowable velocity in the duct and the pressure drop across the duct is a function of the losses in the duct as noted in table 5-2.

Table 5-2.—Maximum pressure drop and air duct velocity

Friction loss factor fL/D_e	Total loss	Critical pressure ratio P_i/P_a	Pressure drop kPa	Maximum velocity m/s
0.01	0.51	0.68	6.88	87
0.1	0.6	.66	6.67	83
1.0	1.5	.57	5.76	62
10.0	10.5	.36	3.64	23
100.0	100.5	.13	1.31	4.6

Table 5-2 values are based upon the following conditions:

- Inlet loss coefficient = 0.5
- Atmospheric pressure, $P_a = 101.3$ kPa
- Pressure drop = 0.1 critical pressure ratio $\times P_a$
- Air density = 1.23 kg/m^3

If noncircular sections are used for the air duct, the diameter—in the friction term—should be replaced by four times the hydraulic radius.

Estimation of Air Entrainment Capacity of the Jet

Many empirical expressions have been proposed for the air entraining capacity below the nappe. Two prominent equations are:

$$q_a = C_1 d_o U_o \quad 5.6$$

and

$$q_a = C_2 L_j U_o \quad 5.7$$

where:

- C_1 & C_2 = constants
- d_o = ramp height or offset height

- L_j = slope distance from aerator to impact point of jet
- q_a = unit discharge of air
- U_o = mean flow velocity at ramp lip

The experimental values of C_1 range between 0.1 and 0.64 (Glazov [9] and Bruschin [10]). Values given for C_2 range between 0.012 [9] and 0.033, Pinto et al. [11].

The one who first proposed these correlations is unknown. They can be found in the literature as early as 1975, Pinto [12] and as late as 1985 [10]. Neither equation results in accurate predictions of air flow rates since the range of values, of the constants, varies by as much as a factor of 5. Two influences account for poor predictions; the equations (1) ignore the effect of the turbulence in the flow, and (2) neglect the depression of the jet caused by reduced pressures under the nappe.

The method for determining the air entrainment rate, as outlined by Glazov [9], appears to be the most accurate procedure available. First, one calculates the shape of the nappe—including the effects of the reduced pressure. Then it is assumed that turbulence displaces a volume of water below the bottom of the nappe. Similarly, as a result of turbulence, an equal volume of air penetrates into the body of the nappe as shown on figure 5-6. The unit discharge of air, q_a , is given by:

$$q_a = U_i \left\{ [(X_i - X_n)^2 + (Y_i - Y_n)^2]^{1/2} - \frac{q}{2U_i} \right\} \quad 5.8$$

where:

- q = unit discharge of water
- U_i = mean velocity of jet at impact point
- X_i = horizontal distance from end of ramp to jet impact location

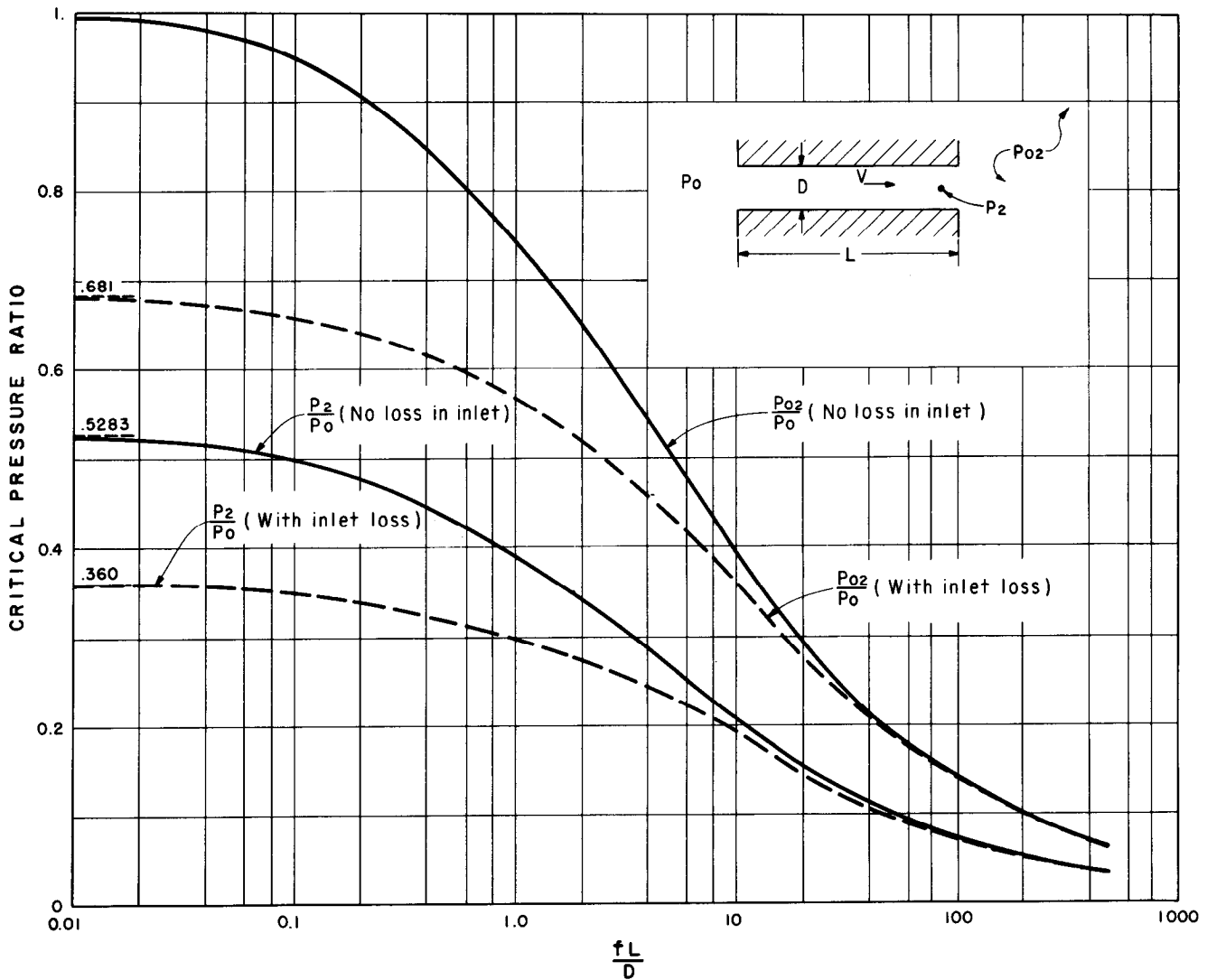


FIGURE 5-5.—Air vent critical pressure ratio.

X_n = horizontal distance from end of ramp to centerline of jet at impact point
 Y_i = elevation at impact point
 Y_n = elevation of centerline of jet at impact point

Mean velocity, U_i , of jet at impact point is:

$$U_i = U_o^2 + 2g[Y_o - Y_n + 0.5(h_o \cos \theta_o)] \quad 5.9$$

where:

h_o = flow depth at end of ramp
 Y_o = elevation of ramp lip

X_i and Y_i values are determined by solving equations 5.1 and 5.2 using a modified definition of the tangent to the jet trajectory bottom slope θ'_o . The tangent to the jet trajectory is defined as:

$$\theta'_o = \theta_o + \tan^{-1}\left(\frac{v'}{U_o}\right) \quad 5.10$$

where v' equals root mean square value of the transverse turbulent velocity component.

The transverse turbulent velocity component, v' , is about one-half of the longitudinal turbulent velocity component. This is expressed as:

$$v' = 0.5 u' \quad 5.11$$

The longitudinal turbulent velocity component, u' , is given approximately by:

$$u' = 0.5 U_o f^{1/2} \quad 5.12$$

where f equals Darcy-Weisbach friction factor.

This relationship is identical with that used by Arndt et al., in chapter 2, to predict the onset of cavitation over uniformly distributed roughnesses.

The computer program in appendix D can be used to integrate equations 5.1 and 5.2 to determine the

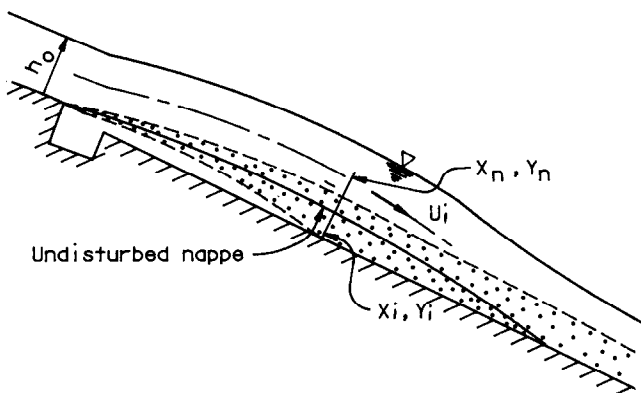


FIGURE 5-6.—Air entrainment under nappe.

values of X_i , X_n , Y_i , and Y_n as well as the quantity of air entrained.

OFFSET DESIGN

When a jet impacts on a sloping surface, a portion of the jet is directed upstream as noted on figure 5-7. The portion which returns upstream forms a pool. If the pool is too deep and too near the aerator, it can prevent proper aeration of the jet. By providing an offset, the pool can be prevented from interfering with the proper functioning of the aerator.

From momentum considerations, the pool level is given (approximately) by:

$$\frac{h_p^2}{h_o^2} = \frac{2F_o^2}{h_i/h_o} [1 - (h_i/h_o)^2] + \cos \theta_i [(h_i/h_o)^2 - 1] \quad 5.13$$

where:

F_o = Froude number of flow at ramp
 $F_o = U_o / [g(h_o \cos \theta_j)]^{1/2}$
 h_o = flow depth at end of ramp
 h_p = pool depth
 h_i = flow depth downstream of impact point
 θ_i = angle between downstream chute invert and horizontal

The relationship between the flow depth at the ramp and the flow depth downstream of the impact point can be derived using rather gross assumptions given by White [13]. The equation is:

$$h_i/h_o = \frac{2}{(U_i/U_o)(1 + \cos \theta_j)} \quad 5.14$$

where:

U_i = mean velocity of jet at impact point, given by equation 5.9

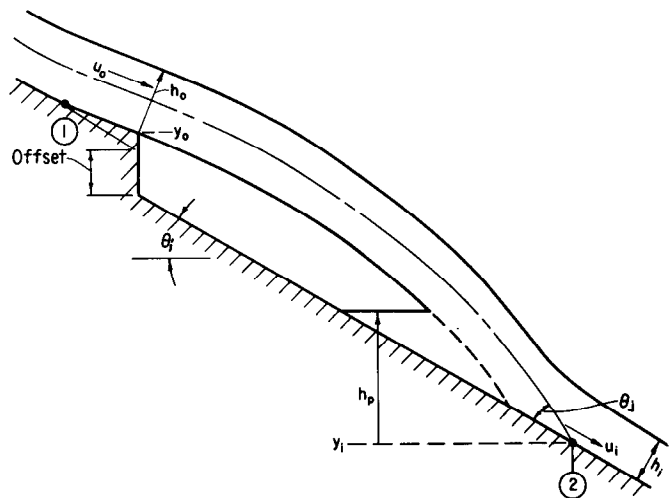


FIGURE 5-7.—Pool depth under nappe.

U_o = mean velocity at ramp lip
 θ_j = angle between centerline of jet at impact point and invert of chute

An offset is needed if:

$$h_p > (Y_o - Y_i) \quad 5.15$$

These design criteria have not been verified through model investigations for flows on steep chutes and spillways.

Beichley [14] studied design criteria for offsets when the downstream invert was horizontal and found that the offset should be one-sixth of the flow passage width. He concluded the flow was barely aerated for Froude numbers less than 3.3.

A converging offset is used downstream of aerators that use a duct downstream of a ramp as shown on figure 5.8. The purpose of the offset is to prevent the duct from causing cavitation if it fills with water. To be effective, the offset should be equal to or greater than $0.15 D$, where D is the depth of the air duct or air slot. For a free draining duct, the offset should be equal to the depth of the duct. The convergence may be accomplished with either a straight line or with an arc.

AERATOR SPACING

Aerators produce an air-water mixture at the flow boundary. If the concentration of the mixture is large enough, cavitation damage will be prevented. As flow progresses downstream from an aerator, the air concentration decreases because of buoyancy of the air bubbles. However, the bubbles' tendency to rise is opposed by diffusive effects of turbulence which is generated at the boundary. If the concentration at the boundary becomes too small, another

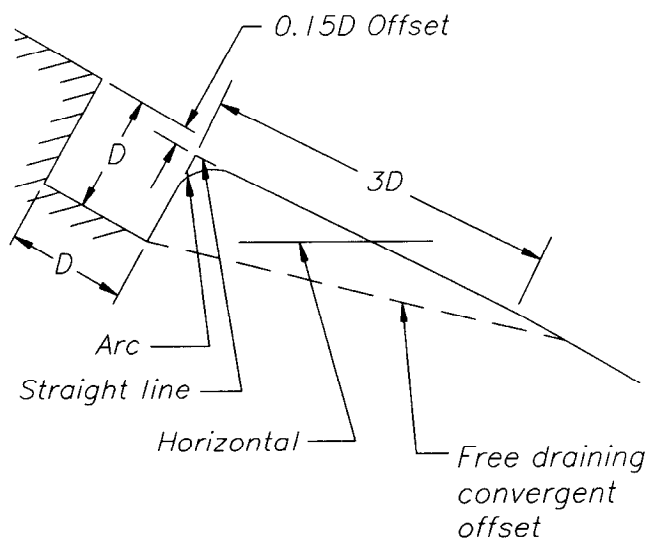


FIGURE 5-8.—Converging offset downstream of aerator.

aerator would be needed. Therefore, a means of predicting the air concentration near the boundary, as a function of distance, is needed.

Spillway tests (Kudriashov [15] and Prusza [16]) have shown air concentration decreases in the following manner:

straight section	0.15 to 0.20% per meter
concave section50 to .60% per meter
convex section15 to .20% per meter

Instead of a linear decrease in air concentration, it has been proposed that the air concentration decreases in proportion to its local value, May [17]. For this assumption, air concentration is given by:

$$\frac{C_x}{C_o} = e^{-0.017(L_x - L_i)} \quad 5.16$$

where:

C_x = mean air concentration at distance X
 C_o = mean air concentration at beginning of aeration

L_x = slope distance downstream from aerator

L_i = slope distance downstream from aerator to beginning of aeration

0.017 = dimensional constant per meter, 0.017 m^{-1}

None of these methods considers the process of self-aeration of flow in a chute or spillway. The development of self-aerated flow consists of three zones as shown on figure 5-9:

- A developing, partially aerated flow
- A developing, fully aerated flow
- A fully developed, aerated flow (equilibrium state)

A well designed aerator will produce, locally, higher air concentrations than those associated with the equilibrium state of aeration. Therefore, downstream of the aerator, the air concentration will decrease to that of the equilibrium state and not to zero as predicted by equation 5.16.

Air concentration in the equilibrium state is governed by:

- surface roughness
- surface tension effects
- flow velocity
- turbulent energy at the air-water interface
- gravity

Therefore, correlations of air concentration should include terms that contain a friction factor, a Boussinesq number, and an Eötvös number. Yevjevich and Levin [18] proposed a correlation of the form:

$$\frac{C_a}{1 - C_a} = \beta = 0.062 B^2 \alpha_o f^{1/2} \quad 5.17$$

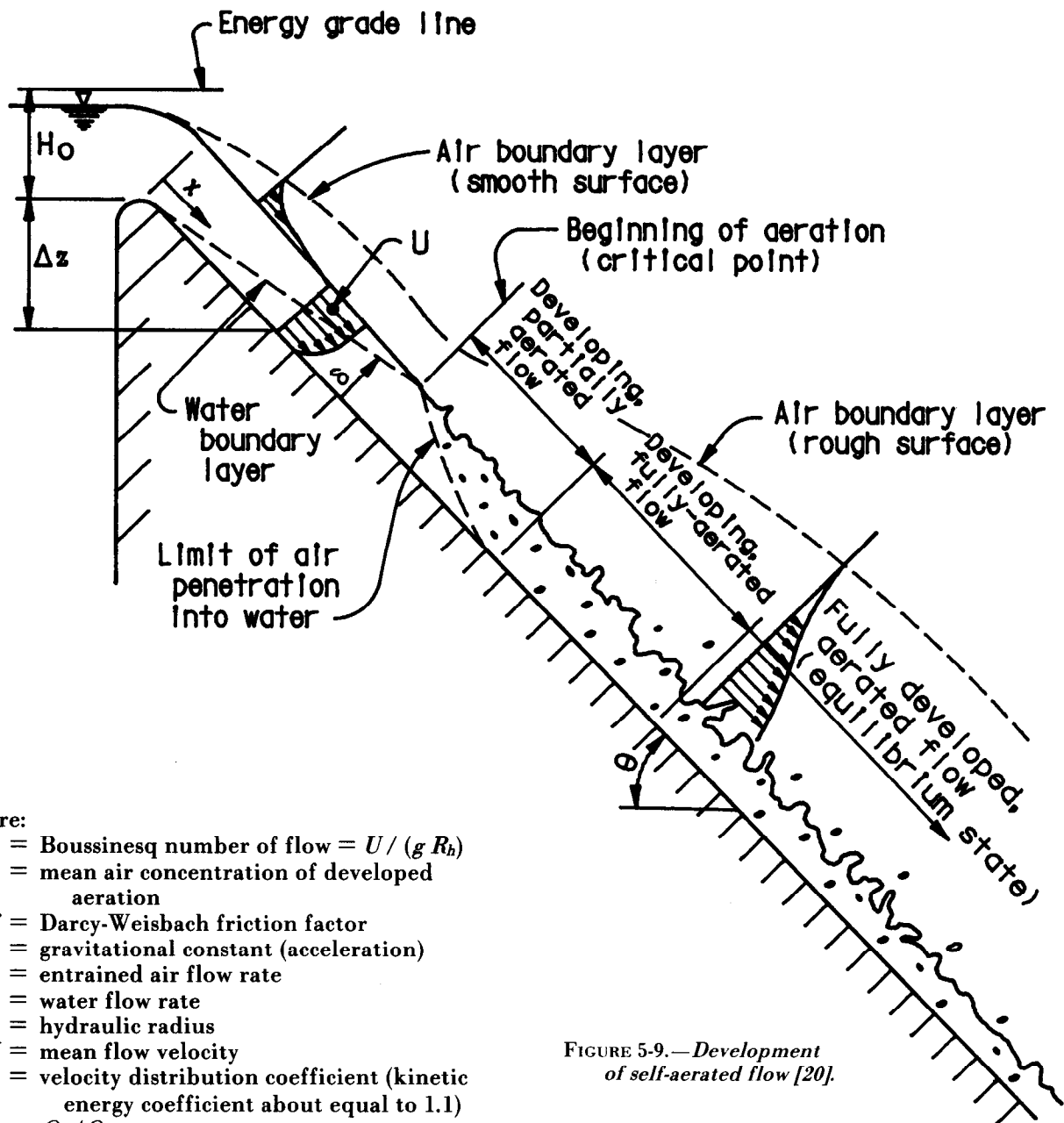


FIGURE 5-9.—Development of self-aerated flow [20].

where:

B = Boussinesq number of flow = $U / (g R_h)$

C_a = mean air concentration of developed aeration

f = Darcy-Weisbach friction factor

g = gravitational constant (acceleration)

Q_e = entrained air flow rate

Q_w = water flow rate

R_h = hydraulic radius

U = mean flow velocity

α_o = velocity distribution coefficient (kinetic energy coefficient about equal to 1.1)

$\beta = Q_e / Q_w$

Volkart [19] proposed a similar equation that ignored the boundary friction.

$$C_a = \frac{\beta}{1 + \beta} = 1 - \frac{1}{0.02 (B - 6.0)^{1.5} + 1} \quad 5.18$$

Finally, Falvey [20] proposed an equation accounting for surface tension.

$$C_a = \frac{\beta}{1 + \beta} = 0.05 B - \frac{(E \sin \theta)^{0.5}}{63} \quad 5.19$$

where:

E = Eötvös number = $(g R_h^2) / (\rho \epsilon)$

ϵ = interfacial surface tension

Obviously, none of these equations consider all the pertinent parameters. However, equations 5.18 and 5.19 tend to predict the same air concentration values; whereas, equation 5.17 is somewhat high for high velocity flows.

Using the concept of self-aerated flow, change in mean air concentration, C_x , as a function of distance can be written (using the form of equation 5.16) as:

$$C_x = (C_o - C_a) e^{-0.017 (L_x - L_i)} \quad 5.20$$

where:

L_i = slope distance downstream from aerator to beginning of aeration

L_x = slope distance downstream from aerator

For cavitation damage on a flow surface, the air concentration at the wall—and not the mean air concentration—is the important factor. For the wall air concentration, C_w , Rao, and Gangadharaiah [21] derived the following expression, in terms of the mean air concentration, C_a :

5.21

$$C_w = 1.17 C_a^{3.3} + \frac{(1 - 1.11 C_a^{2.18})^3 (4.2 \times 10^{-4} - 0.1 C_a^{6.5})}{C_a^{6.5}}$$

The mean air concentrations in equation 5.21 are determined from any of equations 5.17 through 5.19.

Equation 5.21 predicts a higher air concentration at the wall than the mean air concentration if the mean air concentration is less than about 0.3 as shown on figure 5-10. For fully developed aerated flow, the minimum air concentration at the wall (fig. 5-10) is 7 percent. This relationship needs

further study as it indicates that only one aerator would be needed on a chute of infinite length.

DESIGN PROCEDURE

An aerator can be designed using the following procedure:

1. Determine the cavitation indexes of the flow for the entire length of the structure using at least 20-percent increments of discharge which encompass the design capacity of the spillway. The computer program in appendix A can be used to calculate the cavitation indexes for each flow increment.
2. Locate the aerator and the desired point of impact of the jet from the aerator using the values of the cavitation indexes found in step 1.

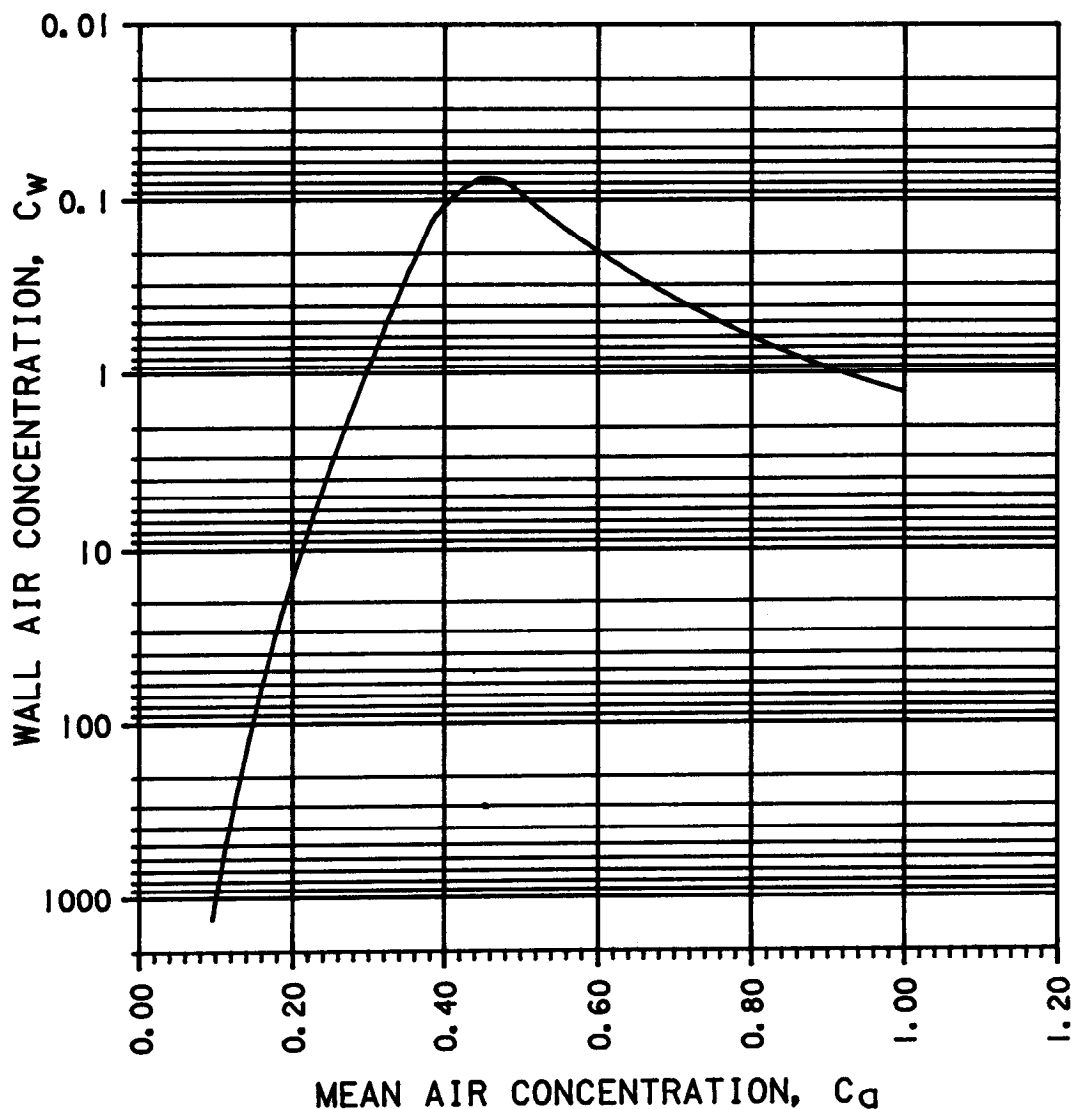


FIGURE 5-10.—Air concentration at wall.

3. Estimate the ramp angle, θ_o , using equation 5.4. In the case of stepped chutes which do not use ramps, proceed directly to step 5.

4. Estimate the ramp height, d_o . As a first rough estimate, the ramp height should be chosen so that the relative ramp height factor, on figure 5-3, is not less than 0.7 for the ramp angle found in step 3.

5. Tentatively size the air duct so that the pressure drop is less than or equal to one-tenth of the critical pressure ratio (fig. 5-5).

6. The airflow quantity is determined from equation 5.5 by solving for Q_a using the pressure drop determined in step 5.

7. Determine the type of air supply to the aerator.

- If sidewall deflectors or offsets are used to supply the aerator, the offset or ramp should be equal to or greater than one-twelfth the width of the flow passage, but not less than 100 millimeters [10].
- If piers are used to supply the aerator, the pier width should be at least one-sixth of the width of the flow passage on either side of the pier.
- If vents are used, in the ramp of an aerator, the total cross-sectional area of the vents in a duct under a ramp should be less than the cross-sectional area of the supply duct.

However, the vent velocities should be less than 100 meters per second. To minimize head losses, streamlining of the vent intake should be considered.

8. Determine the size of the offset—if one is required—using equations 5.13 through equation 5.15.

9. Verify the aerator design using equations 5.1 and 5.2 in conjunction with figure 5-3 for the discharges chosen in step 1. The computer program in appendix D can be used in this step to calculate the trajectory, the air entrained by the jet, and the pressure under the nappe.

10. Calculate the equilibrium air concentration using either equations 5.17, 5.18, or 5.19.

11. Estimate the air concentration downstream of the aerator using equation 5.20.

12. Calculate the wall air concentration downstream of the aerator using equation 5.21. If the wall air concentration is greater than 0.10, another aerator is not needed. If wall air concentration is less than 0.08, proceed to step 13.

13. Using equation 5.20, determine the value of distance, L_x , which will produce a wall air concentration value of 0.10. This is the location of the next aerator.

14. Repeat steps 3 through 11 until all aerators are located and designed.

BIBLIOGRAPHY

- [1] Ball, J. W., "Construction Finishes and High Velocity Flow," *Journal of the Construction Division*, Transactions of the American Society of Civil Engineers, CO2, No. 3646, September 1963.
- [2] Peterka, A. J., "The Effect of Entrained Air on Cavitation Pitting," Proceedings of the Joint Meeting of the International Association for Hydraulic Research, American Society of Civil Engineers, Minneapolis, MN, August 1953.
- [3] Semenkov, V. M., Lentiaev, L. D., "Spillway with Nappe Aeration," *Gidrotekhnicheskoe Stroitel'stvo*, U.S.S.R., No. 5, pp. 16-20, May 1973.
- [4] Colgate, D., Elder, R., "Design Considerations Regarding Cavitation in Hydraulic Structures," Tenth Hydraulics Division Conference, American Society of Civil Engineers, Urbana, IL, August 16-18, 1961.
- [5] Borden, R.C., Colgate, D., Legas, J., Selander, C.E., "Documentation of Operation, Damage, Repair, and Testing of Yellowtail Dam Spillway," Bureau of Reclamation Report REC-ERC-71-23, 76 pp., May 1971.
- [6] Vischer, D., Volkart, P., Siegenthaler, A., "Hydraulic Modelling of Air Slots in Open Chute Spillways," International Conference on the Hydraulic Modelling of Civil Engineering Structures, BHRA Fluid Engineering, Coventry, England, pp. 239-252, September 1982.
- [7] Wei, C. Y., DeFazio, F. G., "Simulation of Free Jet Trajectories for the Design of Aeration Devices on Hydraulic Structures," 4th International Symposium of Finite Elements on Hydraulic Structures, Hannover, Germany, pp. 1-11, June 1982.
- [8] Pan, S., Shao, Y., Shi, Q., Dong, X., "Self-Aeration Capacity of a Water Jet Over an Aeration Ramp," *Shuili Xuebao*, No. 5, pp. 13-22, 1980, Beijing, China. (Bureau of Reclamation translation 1868, book No. 12,455, paper No. 2)
- [9] Glazov, A. I., "Calculation of the Air-Capturing Ability of a Flow Behind an Aerator Ledge," *Hydrotechnical Construction*, vol. 18, No. 11, pp. 554-558, Plenum Publishing Corp., 1985.
- [10] Bruschin, J., "Hydraulic Modelling at the Piedra del Aguila Dam," *Water Power and Dam Construction*, pp. 24-28, January 1985.
- [11] Pinto, N. L. de S., Neidert, S. H., Ota, J. J., "Aeration at High Velocity Flows — Part One," *Water Power and Dam Construction*, pp. 34-48, February 1982, and "Aeration at High Velocity Flows — Part Two," *Water Power and Dam Construction*, pp. 42-44, March 1982.
- [12] _____, "Recommendations on Consideration of Cavitation When Designing Hydraulic Spillway Structures," VNIIG, Energiia, Leningrad, pp. 38-75, 1975.
- [13] White, M.P., Discussion by W. L. Moore, "Energy Loss at the Base of a Free Overfall," (Transactions of the American Society of Civil Engineers, vol. 108, pp. 1343-1360, 1943), Transactions of the American Society of Civil Engineers, vol. 108, pp. 1361-1364, 1943.
- [14] Beichley, G. L., "Hydraulic Model Studies of Chute Offsets, Air Slots, and Deflectors for High-Velocity Jets," Bureau of Reclamation Report No. REC-ERC-73-5, 35 pp., March 1973.
- [15] Kudriashov, G. V., "Cavitation and Cavitation Erosion of Members of Water Outlet Structures," International Association for Hydraulic Research, Proceedings of the XXth Congress, Moscow, vol. 3, pp. 453-461, 1983.
- [16] Prusza, V., "Remedial Measures Against Spillway Cavitation," International Association for Hydraulic Research, Proceedings of the XXth Congress, Moscow, vol. 3, pp. 468-476, 1983.
- [17] May, R.W.P., "Cavitation in Hydraulic Structures: Occurrence and Prevention," Hydraulics Research Report No. SR 79 Wallingford, England, March 1987.
- [18] Yevdjevich, V., Levin, L., "Entrainment of Air in Flowing Water and Technical Problems Connected With It," International Association for Hydraulic Research, Proceedings of the Vth Congress, Minneapolis, MN, pp. 439-454, 1953.
- [19] Volkart, P., "Transition From Aerated Supercritical to Subcritical Flow and Associated Bubble De-Aeration," International Association for Hydraulic Research, Proceedings of the XXIst Congress, Melbourne, Australia, August 19-23, 1985.
- [20] Falvey, H. T., "Air-Water Flow in Hydraulic Structures," Bureau of Reclamation Engineering Monograph No. 41, 143 pp., December 1980.
- [21] Rao, N. S., Gangadharaiah, T., "Self-Aerated Flow Characteristics in Wall Region," *Journal of the Hydraulics Division*, American Society of Civil Engineers, vol. 97, No. 9, September 1971.

Chapter 6

Design Recommendations

BACKGROUND

The first known major cavitation damage in a tunnel spillway occurred at the Bureau's Hoover Dam. After investigation and research, it was concluded the damage was initiated by a misalignment in the spillway invert. This resulted in an intensive period of investigations of surface irregularities and flow alignments. The tendency was to specify more stringent design tolerances in hydraulic structures, Ball [1]. The only way to achieve rigorous tolerances was by careful attention to the methods used in finishing concrete. As a result, the concept of surface tolerance and surface finish became intertwined. As late as 1981, surface finishes to be used with high velocity flow had separate requirements [2].

In 1981, the *Concrete Manual* specified that a stoned finish should be provided for all spillways having flow velocities greater than about 23 meters per second. The technique needed to produce the surface is quite intricate [2]:

The surface to receive the special finish should be thoroughly cleaned with high-velocity water jets to remove loose particles and foreign material and then brought to a surface-dry condition, as indicated by the absence of glistening-free water, by clean air jet. A plastic mortar consisting of 1 part of cement and 1 to 1-1/2 parts of sand, by weight, that will pass a No. 16 screen should be rubbed over the surface and handstoned with a No. 60 grit carborundum stone, using additional mortar until the surface is evenly filled. Stoning should be continued until the new material has become rather hard. After moist curing for 7 days, the surface should be made smooth and even by use of a No. 50 or No. 60 grit carborundum stone or grinding wheel. A flexible disk power sander may produce an acceptable surface. After final stoning, curing is continued for the remainder of the 14-day curing period.

After the surface was finished, it was inspected to determine adherence to specified tolerances. If an into-the-flow offset greater than 3 millimeters high was found, it was to be eliminated using bevels given in table 6-1.

Table 6-1.-Grinding tolerances
for high velocity flow [2]

Velocity range m/s	Grinding bevel, height to length
12 to 27	1 to 20
27 to 36	1 to 50
over 36	1 to 100

The tolerances were in perfect agreement with the current theory and reflected the best efforts of concrete specialists to accomplish the exacting requirements. However, from a practical aspect, these specifications were too exacting. Even if a structure was constructed according to rigid specifications, deposits left by moderate seepage could create local irregularities which would be out of the specified tolerances—within a short period. For instance, at Glen Canyon Dam, within one month following the reconstruction and installation of the spillway aerators, calcite deposits—up to 10 millimeters high—had formed on the invert. Therefore, to maintain the exacting tolerances for preventing cavitation damage, an extensive maintenance program would have to be initiated before each expected spill.

In 1961, the concept for providing aeration to prevent damage from cavitation was demonstrated in the river outlets of Grand Coulee Dam, Colgate and Elder [3]. The first installation of aerators on spillways was at Yellowtail Dam in 1967. However, complete reliance was not placed on the aerator.

All irregularities immediately downstream of the vertical bend were ground to a 1:100 chamfer and the entire tunnel was covered with a two-coat epoxy phenolic paint. Reliance upon aeration alone began in 1983, with the Glen Canyon Dam experience, and surface tolerance specifications began to be relaxed. The maximum chamfer specified in 1983 for the tunnel at Glen Canyon Dam was 1:20. This chamfer was only required for gouges in the tunnel liner which were greater than 13 mm deep. A large area of eroded concrete in the vicinity of the elbow was not repaired. The trend has continued; in 1987, a decision was made to leave the eroded surface, on the invert of the Hoover spillway tunnels, unrepaired. This surface has a cobble stone type surface as shown on figure 6-1. The height of the 90-percentile size irregularity was equal to 9 mm.

In realizing the difficulties encountered to obtain and maintain strict surface tolerances, a team at the Bureau's Denver Office was appointed (in 1987) to review the tolerance specifications and to make recommendations. The team consisted of a designer, a research engineer, a construction engineer, and a concrete specialist. They recognized the problem that had been created by combining the tolerance requirements and the surface finish specifications into one parameter. Therefore, the team recommended that the standard surface finish descriptions be retained. Standard finishes are described in the *Concrete Manual* [2]. However, a new concept was introduced for a tolerance specifications.

From a design viewpoint, flow surface tolerances are needed to specify how accurately certain parts of a hydraulic structure need to be constructed. During the design process it may become evident that the required surface tolerances are unachievable. In this case, design needs to be revised.

From a construction standpoint, flow surface tolerances are needed to determine if the structure has been constructed as intended. If the surface is not within the specified tolerance, the construction engineer and inspectors need to know what is required to fulfill the specified tolerances.

SPECIFICATIONS OF SURFACE TOLERANCES

Tolerance is defined as the range of variation allowed in a constructed dimension from the design dimension. A tolerance can refer to either a structural feature or to a flow surface feature. Structural tolerances include specifications of line, grade, length, width, and plumb. Although these specifications are important, they do not have a significant effect on the cavitation characteristics of a hydraulic structure.

The following three basic types of flow surface variations are present in hydraulic structures.

Offset

Offset tolerances refer to variations caused by isolated abrupt surface irregularities where the dimension of the irregularity perpendicular to the flow is large relative to its dimension parallel with the flow. Normally, offset tolerances are the most critical. A smooth surface containing an offset is the most susceptible surface to being damaged by cavitation.

Slope

Slope tolerances refer to variations caused by surface irregularities where the dimension parallel with the flow is large relative to the variation perpendicular to the flow. The specifications of the slope tolerances ensures that variations will be gradual enough to prevent the irregularity from causing cavitation damage.

Uniformly Distributed Roughness

Uniformly distributed roughnesses refer to variations that occur over a relatively wide area. This type of irregularity is caused by erosion of a concrete surface by sand or gravel in the water passing over the surface. Another example is the rough surface left by poorly consolidated concrete which has been placed against a form. In most cases, the absolute height of uniformly distributed roughnesses can be much larger than offsets on a smooth surface without initiating cavitation damage. The critical element is the uniformity of the surface roughness.

Flow Surface Tolerance: Definition and Specifications

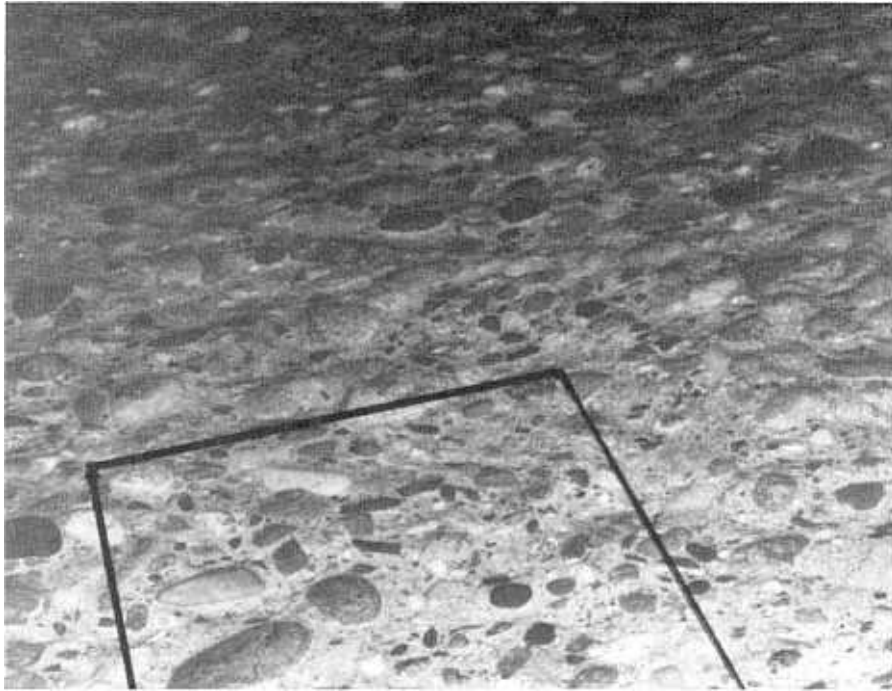
Flow surface tolerances for offset and slope variances, as shown in table 6-2, have been quantified.

Table 6-2.-Flow surface tolerances

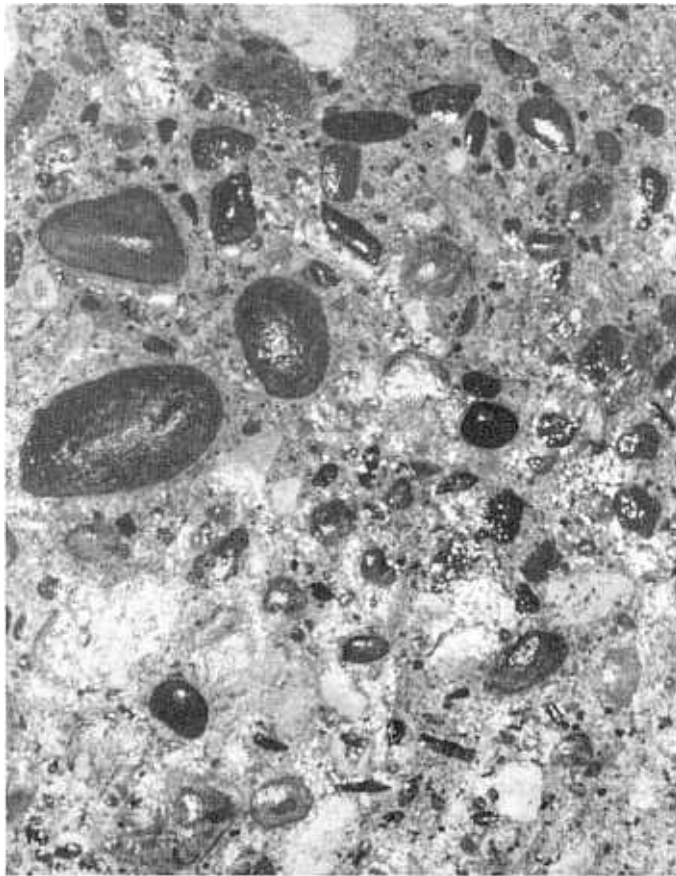
Tolerance, T	Offset, mm	Slope
T1	25	1:4
T2	12	1:8
T3	6	1:16

The tolerances (see table 6-2) can be associated with the cavitation index of the flow. The effect of aerated flow is included in the specifications of the required tolerance as shown in table 6-3.

Flow surface tolerances for uniformly distributed roughnesses have not been developed. Generally, cavitation characteristics of a uniformly rough surface are much better than for an isolated surface roughness element on a smooth surface. This was noted in chapter 4. If uniformly rough surfaces could



a. View of invert



b. Invert closeup

FIGURE 6-1.—*Hoover Dam, Nevada, spillway — concrete surface near station 994.00.*

Table 6-3.—Specification of flow surface tolerance

Cavitation index of the flow	Tolerance without aeration	Tolerance with aeration
> 0.60	T1	T1
0.40 to 0.60	T2	T1
0.20 to 0.40	T3	T1
0.10 to 0.20	revise the design	T2
< 0.10	revise the design	revise the design

be created in the field, they would perform much better than the very smooth surfaces with isolated irregularities. However, a uniformly rough surface is difficult to construct. Research studies in this area will have to concentrate on the areal statistical properties of the roughness. One useful parameter might be the ratio of the standard deviation of the surface roughness to the 90-percent size of the roughness elements. When this parameter is developed, table 6-2 will require another column to show the allowable variation of a rough surface for each of the tolerance specifications.

GEOMETRIC CONSIDERATIONS

Few structures have been designed in which the cavitation characteristics were the overriding consideration; one exception was the Aldeadavila Dam in Spain, Galindez et al. [4]. Over 800 hydraulic tests on models of the spillway were performed to develop the spillway shape. After a few years of operation with large flows, some cavitation damage appeared at the end of the chutes caused by irregularities in the surface. The irregularities were repaired and damage stopped. Lin, et al. [5], showed that this spillway conformed closely to the constant cavitation number spillway described in chapter 4.

The *constant cavitation number* and the *controlled pressure* spillways use centrifugal force effects to improve the cavitation characteristics. The constant cavitation number spillway should be used for structures that terminate with a flip bucket. The controlled pressure spillways produce profiles that are more applicable for structures that terminate in a tunnel or on chute. Neither of these profiles should present any construction problems even though the vertical bend is not a curve of constant radius. Generally, the deviation from a constant radius curve is relatively small.

As water flows down a chute or through a tunnel spillway, flow velocity increases; hence, the flow depth decreases. Both effects lead to low cavitation indexes and potential cavitation damage. If the structure does not have a vertical curve, which can be used to control the cavitation index, then the flow depth can be controlled by decreasing the width of the chute or diameter of the tunnel. The change in cross section must be done carefully so that the

chute walls are not overtopped or the tunnel does not fill with water. The decrease in the cavitation index through rougher surfaces is accomplished primarily as the result of increased flow depth.

Control of pressures in the chute downstream of the spillway crest can be accomplished through variations in both the invert curvature and chute width. For example, a crest having both invert curvature and converging sidewalls was designed by G. Lombardi of Locarno, Switzerland, as shown on figure 6-2, Colgate [6]. This spillway profile consists of a conventional spillway crest, a transition section having a constant slope invert, and a flip bucket. The invert profile of the bucket obeys a power law. In plan, the sidewalls converge uniformly at an included angle of approximately 3.3° . Both of these variations in geometry (invert curvature and convergent sidewalls) were not sufficient to prevent the cavitation index of the flow from being less than a value of 0.2. Therefore, as was shown in chapter 3,

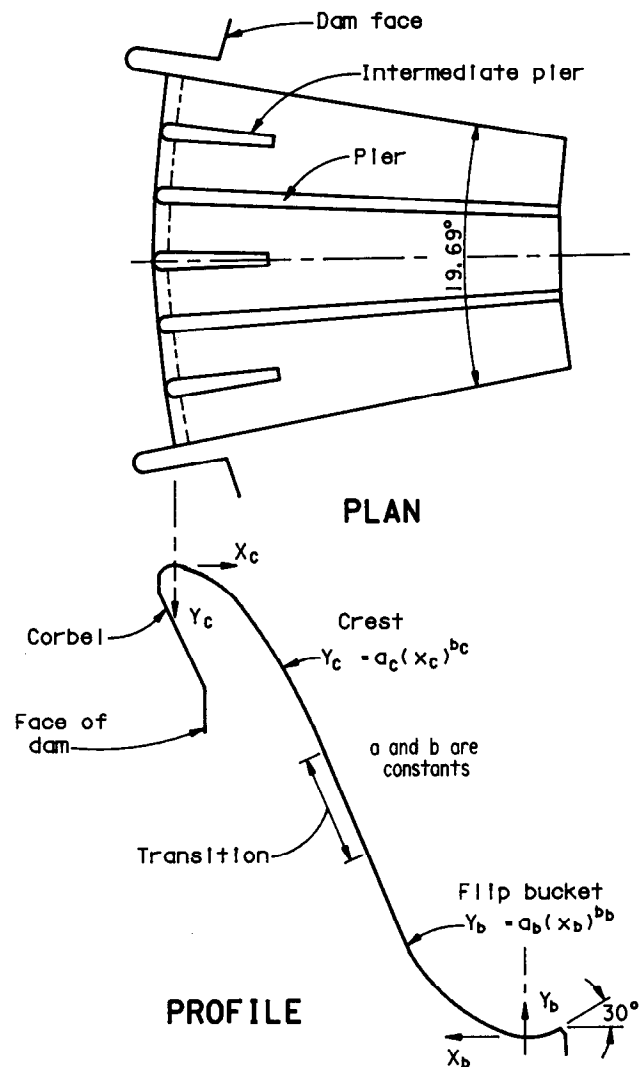


FIGURE 6-2.—Lombardi crest.

damage probably would be expected to occur with the profile if the flow is not aerated.

The cavitation characteristics of the crest profile could be improved by eliminating the transition section and by using a constant cavitation number crest. With these modifications, the flip bucket lip would have terminated at a higher elevation than the elevation shown on figure 6-2. However, this would not have caused any problems since the jet from the spillway was planned to terminate in a plunge pool. Instead of redesigning the spillway profile, a decision was made to aerate the flow, Rutschmann [7, 8].

The preceding example illustrates a somewhat circular design process that must be performed if a structure is to be protected against cavitation caused damage. The concept was to use invert curvature and convergent sidewalls to control the cavitation index. However, the invert curvature was begun at too low an elevation to be effective. The convergence of the sidewalls could not be increased because it would have caused the jet to be too compact at the impingement point in the plunge pool. The alternatives would be to install an aerator or to use a constant cavitation number profile. The constant cavitation number profile would result in the lip of the flip bucket being located at a higher elevation. To ensure proper entry of the jet into the plunge pool, physical model studies are needed.

DESIGN PROCEDURE

The following steps are recommended in the design of a structure where cavitation is one of the overriding considerations:

1. Decide upon a preliminary design configuration of the structure. Include the alignment and

profile, the capacity of the structure required to pass the maximum flows, and the location of ancillary structures such as diversion tunnels, plunge pools, energy dissipaters, etc.

2. Study the cavitation characteristics of the structure through the use of the computer program given in appendix A. At least five increments of discharge encompassing the range of flows anticipated to pass through the structure should be simulated. This will ensure that the most critical flow condition is considered.

3. Determine the required surface tolerances as a function of the minimum value of the cavitation index using table 6-2. Table 6-2 will indicate if aeration is desirable or required.

4. If the flow cavitation index is less than 0.2, investigate the effect of changes to the spillway geometry on the cavitation index. The computer programs in appendix C can be used to develop the optimum curvature in the case of vertical bends. If the invert profile is linear, then changes in the width or diameter of the structure can be investigated using the computer program in appendix A.

5. If low values of the cavitation indices cannot be ameliorated by changes in geometry, then an aeration device can be designed using the computer program in appendix D.

6. For very small values of the cavitation indices, ($\sigma < 0.10$), changes to the design concept should be considered. For instance, replacing a tunnel spillway with a free jet that impinges into a plunge pool may be possible.

BIBLIOGRAPHY

- [1] Ball, J. W., "Why Close Tolerances Are Necessary Under High-Velocity Flow," Bureau of Reclamation Report No. HYD-473, October 1960.
- [2] *Concrete Manual*, 8th ed., Bureau of Reclamation, U.S. Government Printing Office, stock No. 024-003-00092-2, Washington, D.C., 1981.
- [3] Colgate, D., and Elder, R., "Design Considerations Regarding Cavitation in Hydraulic Structures," Tenth Hydraulics Division Conference, American Society of Civil Engineers, Urbana, Ill, August 16-18, 1961
- [4] Galindez, A., Guinea, P. M., Lucas, P., and Aspuru, J. J., "Spillways in a Peak Flow River," Transactions of the 9th International Congress of Large Dams, vol. 2, Q33, R22, pp. 365-389, Istanbul, Turkey, September 1967.
- [5] Lin, B., Gong, Z., and Pan, D., "A Rational Profile for Flip Buckets of High Dams," *Scientia Sinica*, series A, vol. 25, No. 12, pp. 1343-1352, China, December 1982.
- [6] Colgate, D., "Hydraulic Model Studies of Amaluza Dam Spillway," Bureau of Reclamation Report No. GR-25-76, 65 pp., December 1976.
- [7] Rutschmann, P., "Beluftungseinbauten in Schussrinnen, Wirkungsweise, Formgebung und Berechnung von Schussrinnenbeluftern," Mitteilungen der Versuchsanstalt fur Wasserbau, *Hydrologie und Glaziologie*, Report No. 97, Zurich, 1988.
- [8] _____, "Calculation and Optimum Shape of Spillway Chute Aerators," International Association for Hydraulic Research, Proceedings of the International Symposium on Model-Prototype Correlation of Hydraulic Structure, American Society of Civil Engineers, Colorado Springs, CO, pp. 118-127, August 1988.

Chapter 7

Spillways — Field Experience

CASE STUDIES

The proof of the usefulness of this monograph is in the successful application of the concepts to hydraulic structures. The following case studies were selected to illustrate many of the concepts discussed earlier.

- The geometry of each case study is described in enough detail to provide a concept of the pertinent parameters.
- This is followed by a description of damage, if any occurred, and an analysis of its cause. The analysis is based upon studies using the computer programs in the appendix.
- Finally—when applicable—remedial measures, which were taken to reduce the likelihood of damage in the future, are presented. All examples are from Bureau of Reclamation experience.

The operating histories of these structures are on the diskette “Source Codes and Data” under the file name HYDROL. The geometries of the spillways can be found under the file name SPWY.

The usefulness of the case studies is limited in many instances by the lack of essential data. This was caused by oversight, by a lack of awareness of what data were pertinent at the time it could have been obtained, and by a lack of time to do significant data acquisition during emergency spills.

Blue Mesa Dam is a part of the Bureau’s Wayne N. Aspinall (formerly the Curecanti) Storage Unit, Gunnison Division of the Colorado River Storage Project. The dam is located in mountainous country on the Gunnison River 40 km west of Gunnison, Colorado. The primary purpose of the unit is to develop the water storage and hydroelectric power generating potential along a 64-km section of the Gunnison River above the Black Canyon of the Gunnison National Monument. Other purposes of the unit are irrigation, recreation, and flood control.

The dam is a zoned earthfill structure 240 m long at the crest and 104 m high above the riverbed. The reservoir is 30-km long having a storage capacity of 1.2×10^9 m³. A 60-MW powerplant is located at the toe of the dam.

Figure 7-1 shows the spillway on the right abutment [1]; its capacity is about 963 m³/s at the maximum reservoir water surface elevation of 2292 m. Water discharges through: a gate section, a tunnel transition section, a tapering inclined tunnel, a vertical bend, a nearly horizontal tunnel, and a flip bucket. Two 7620- by 10 210-mm radial gates control the flow. The flip bucket directs flow into the river channel about 150 m downstream of the powerplant.

During construction, the nearly horizontal section of the tunnel and the flip bucket were used to pass diversion flows around the construction site.

The spillway operated several days in June and July 1970. On 2 days, the discharge reached 99 m³/s. Upon inspection, an area of cavitation damage was discovered. At station 4+54.15, cavitation damage

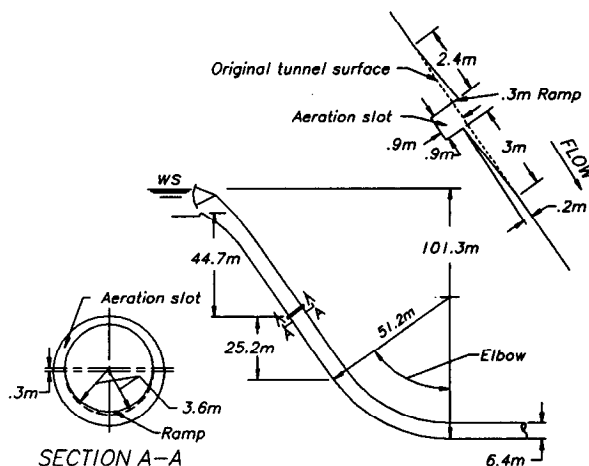


FIGURE 7-1.—Blue Mesa Dam, tunnel spillway — aeration slot.

had begun downstream from a hole which was formed when a piece of wood popped out of the concrete liner. The popout was 150 mm wide, 127 mm long and 25 mm deep. Cavitation damage began 63 mm downstream of the popout. The damage—nearly circular—with a diameter of 76 mm was 13 mm deep. The cavitation index at this location is 0.19 at 10 percent of the design discharge. The spillway operating history is not known; therefore, the damage index could not be calculated. Other popouts and spalls had occurred throughout the tunnel. However, cavitation was not discovered at any of the other sites.

The analysis reveals that the lowest cavitation index occurs at the point of tangency of the vertical curve with the nearly horizontal tunnel (STA 4+73.88). The second lowest value occurs at the point of curvature of the vertical bend (STA 4+33.66). Cavitation indexes at these locations are 0.159 and 0.188 respectively, for a flow of 99 m³/s. The maximum values of the damage potential also occur at these locations.

The analysis indicated extensive damage could be expected if the spillway were to operate for periods of 1 week or more. The most susceptible location for damage to occur was immediately downstream of the vertical bend. Because of this potential for damage, an aerator was designed and constructed in the spillway tunnel.

The aerator was placed at station 4+16.05. At this location, the cavitation index is greater than a value of 0.218 for all discharges. Therefore, damage upstream of the aerator is extremely unlikely. At this location, the aerator is 54.3 m below the maximum reservoir elevation.

The aerator consisted of a ramp, a downstream aeration groove, and a concentric conical offset located downstream of the aeration groove as noted on figure 7-1. The ramp feathered from its maximum height of 254 mm at the invert to zero height 254 mm above the springline¹ of the tunnel. At the maximum discharge, the tunnel flows 65-percent full at the aerator location. Therefore, for this tunnel, the ramp probably should have feathered out to zero at the 65-percent depth. Since this was not done, a conical offset was provided downstream of the aerator to keep the aeration groove from filling with water. The offset was recessed 203 mm back from the original tunnel alignment. It was 3050 mm long. The aeration groove encircled the tunnel and had a 914- by 914-mm cross section. At maximum flow rate, air could enter the aeration groove above the water surface.

The aerator was completed in 1985. Following its completion, the spillway passed flows up to 56.63 m³/s. These flows occurred in the late summer of

1986 and lasted for several days. There have been no reports of damage to the tunnel.

Flaming Gorge Dam is part of the Flaming Gorge Unit, Green River Division of the Colorado River Storage Project. The dam is located on the Green River in northwestern Utah, 64 km north of Vernal, Utah. The dam is a concrete, thin arch type structure 150 m high having a crest length of 360 m. The principal features of the dam are: a tunnel spillway, a river outlet, and a 36-MW-capacity powerplant. The river outlet can discharge up to 113 m³/s through two 1676-mm hollow jet valves. The spillway has a maximum capacity of 815 m³/s. Flow into the spillway is controlled by two 5105-mm-wide by 9450-mm-high fixed-wheel gates [2].

In July 1975, the spillway was operated to determine the potential for cavitation damage. Each test period required 5 hours to start up and shut down the flow. On July 6, the spillway was operated at 140 m³/s for a little more than 1 hour. On July 7 and 8, the spillway was again operated at 140 m³/s for 19 hours. Cavitation damage was not observed in the nearly horizontal portion of the spillway. A spalled area around station 3+25.0, which was about 255 mm square and 13 mm deep, did not change its extent during the spill. However, adjacent, previously smooth areas at the spall were pockmarked. Cavitation did not seem to be the cause of the pockmarks.

An analysis, of the cavitation potential of the tunnel, shows cavitation danger is greatest downstream of station 5+18.30 for the 140-m³/s flow. However, at this rate, the flow is aerated naturally from the water surface. The natural aeration is probably the reason that damage was not observed during the July 1975 operation. Aeration from the large gate slots also may have contributed to the lack of damage during the tests.

A tunnel inspection showed the concrete was poor between stations 1+74.00 and 2+66.00. It was decided to replace the poor concrete and to install an aerator in the tunnel at station 2+56.00. The aerator consists of a ramp, an aeration groove, and an offset downstream section as shown on figure 7-2. The ramp is 100 mm high and 914 mm long. It feathers from a maximum height at the invert to zero height at the springline. The aeration groove has a square cross section 610 mm on a side. The groove extends about three-fourths of the distance around the tunnel. At maximum discharge, the entrance to the groove is partially submerged. The downstream offset is recessed 100 mm back from the original flow surface. The length of the offset is 2413 mm. The minimum cavitation index at the aerator is 0.181.

A model study was not made of the aerator. Subsequent experience has shown the design is probably inadequate for flows greater than 566 m³/s. The maximum design flow is 821 m³/s.

¹ The springline is the generatrix for the tunnel roof arch.

In 1983, the aerator had been constructed and the concrete repair was underway downstream of the aerator when operation became necessary to pass $113 \text{ m}^3/\text{s}$ for 30 days through the spillway. For several hours, during this spill, the discharge was $141 \text{ m}^3/\text{s}$. Cavitation damage was not observed in the exceedingly rough construction area where the jet from the aerator had impinged. A number of bolts which held the contractor's stairways in place had not been removed prior to operating the spillway. Cavitation damage was not apparent around these bolts.

Glen Canyon Dam is part of the Glen Canyon Unit, Middle River Division of the Colorado River Storage Project. The dam is located on the Colorado River in northeast Arizona 25 km upstream of Lee's Ferry. The project furnishes longtime regulatory storage needed to permit States in the upper basin of the Colorado to meet their flow obligations at Lee's Ferry and still use their apportioned water.

The structure is a 216-m-high concrete arch dam having a crest length of 475 m. The reservoir has a storage capacity of $3.3 \times 10^9 \text{ m}^3$. A 950-MW powerplant is located at the toe of the dam. An outlet works, with four hollow jet valves, having a total capacity of $425 \text{ m}^3/\text{s}$ is located on the left abutment of the dam.

The dam has an open-channel flow tunnel spillway on each abutment as shown on figure 7-3. Each spillway is 12 500 mm in diameter and has a maximum capacity of $2900 \text{ m}^3/\text{s}$. Flow to each spillway passes through: two 12 192- by 16 000-mm radial gates, a 55° inclined tunnel, a vertical bend (elbow), and 305 m of horizontal tunnel to a flip bucket.

Both spillways were operated for extended periods in 1980 [3]. In 1981, an inspection revealed that deposits from cracks in the lining had initiated cavitation damage at several locations in the left spillway. Little damage had occurred in the right spillway. This was probably due to the shorter operating time. Following this inspection, a

photographic survey of the tunnels was performed to document the damage.

Following the inspection, a study was made to identify the scope of work required to repair the damage and to prevent future occurrence. It was recommended the damage be repaired and aerators be installed near station 6+86.0. These modifications were planned to begin in 1984. Unfortunately, high flows in the Colorado River occurring in the spring of 1983 had to be passed through the spillways.

The first indication that damage was occurring to the left tunnel spillway (during the 1983 flood) came on June 6, when loud rumblings were heard from the tunnel [4]. Several large holes were found in the invert during an inspection in the afternoon of June 6 (see fig. 3-11). Flows were resumed through both tunnels. At the end of the flood, extensive damage had taken place in both tunnels as shown on figure 7-4. Even though damage was extensive, it only excavated a hole whose depth was about equal to the spillway diameter. At this point, the eroded cavity was evidently large enough to dissipate the energy of the high velocity water. In the elbow portion of the tunnels, the depth of the damage as noted on figure 7-5 was on the same order as the depth of the flow.

Even while the spillway flows were continuing, an emergency program was initiated to design, model test, and construct aerators in the inclined portions of the spillways [5]. These aerators consisted of: a ramp, a groove or slot, a downstream offset, and a transition back to the original tunnel diameter as shown on figure 7-3. The ramp is 1295 mm long and 180 mm high at the centerline of the invert. The ramp feathers out to zero height at the springline. The groove is 1200 by 1200 mm. The downstream edge of the slot is offset 305 mm

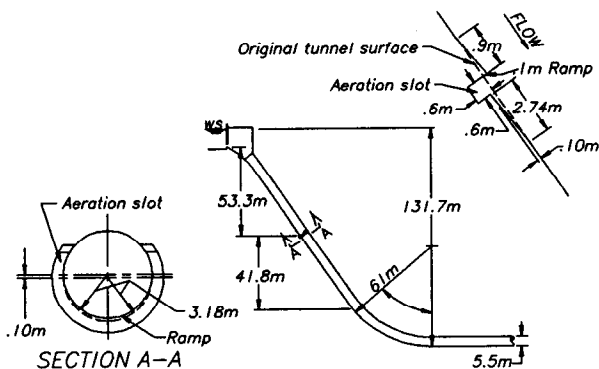


FIGURE 7-2.—Flaming Gorge Dam, tunnel spillway — aeration slot.

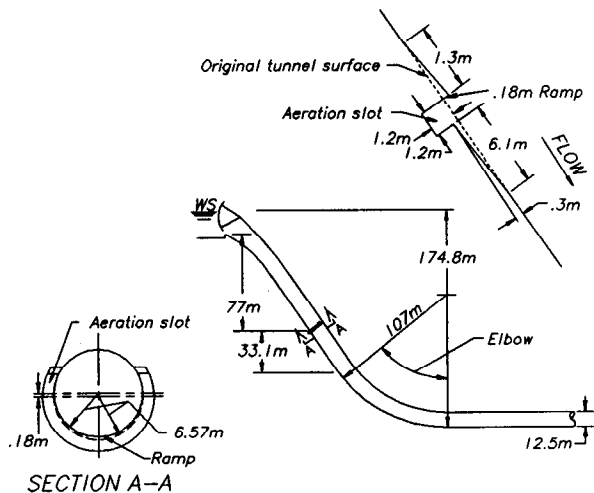
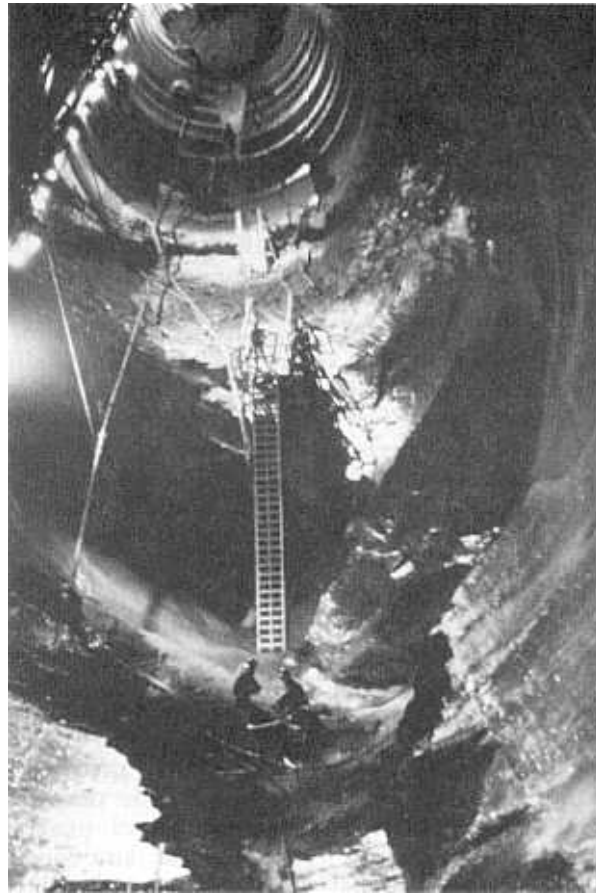


FIGURE 7-3.—Glen Canyon Dam, tunnel spillways — aeration slots.



a. Left tunnel



b. Right tunnel

FIGURE 7-4. *Glen Canyon Dam, tunnel spillways major damage.*

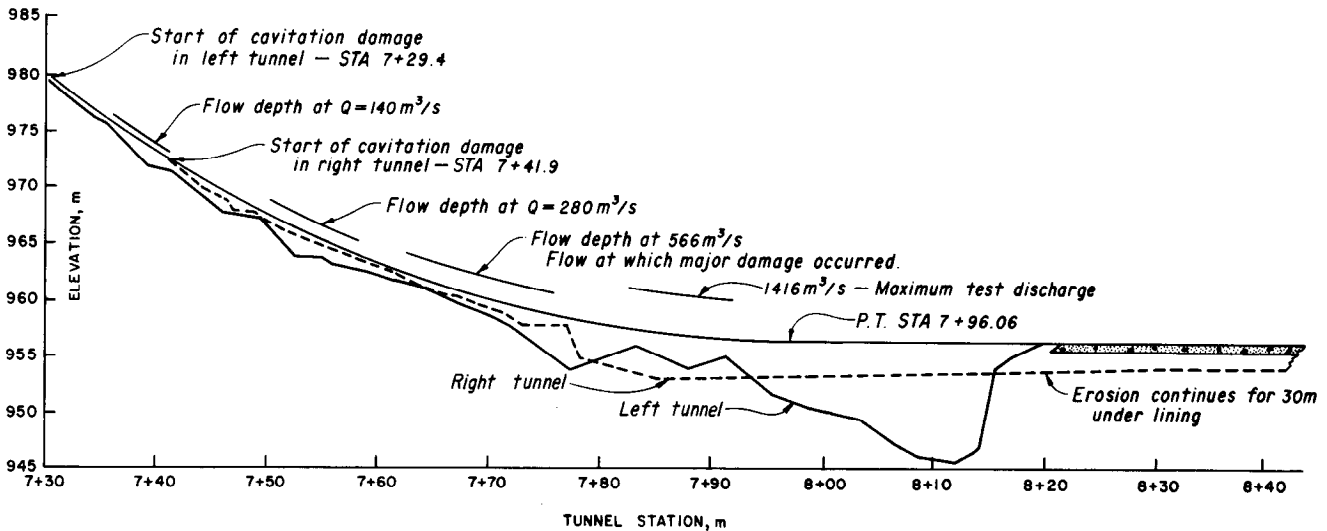


FIGURE 7-5.—Glen Canyon Dam, tunnel spillways — damage profiles.

from the original tunnel diameter. The length of the transition to the original tunnel diameter is 6096 mm. The end of the ramp is at station 6+85.80 which is 96.2 m below the maximum reservoir elevation.

The tunnels were ready for service after finishing construction on October 10, 1984.

In August 1984, the left tunnel was tested to verify the operation of the aerator. Pressure measurements were taken in the invert to compare with model studies and air velocities were measured in the air groove to estimate the airflow quantities [6]. Flow rates up to 1416 m³/s were passed through the spillway. This discharge was 40 percent greater than had previously passed through the spillways. In addition, a discharge of 566 m³/s was maintained for 48 hours. This flow rate and duration had caused damage to the spillway during the 1980-81 flows.

Evidence of damage could not be found following the tests even though some eroded areas, at the end of the elbow, had been left unrepaired. These tests justified the relaxation in the repair criteria from that used during the Yellowtail Dam spillway repairs.

At Glen Canyon Dam, in the section downstream of the elbow, only damaged sections deeper than 19 mm were repaired. Depending upon the extent of the damage one of two methods of repair was used. For small areas, the damaged surface was ground to a 1:20 (vertical to horizontal) slope in the direction of flow and to a 1:5 slope perpendicular to the direction of flow. For extensively damaged areas, the concrete was removed down to the first mat of reinforcing steel and then replaced with a concrete patch. Bolts and expansion anchors, which could not be removed, were cut off above the surface and ground down to be flush with the surface. Cutting off the bolts below the surface and plugging the hole, with hydrated cement or "Burke Water

Plug" compound,² was limited to bolts or anchors in which the concrete around them had spalled.

Hoover Dam is a part of the Boulder Canyon Project. It is located on the Colorado River about 58 km from Las Vegas, Nevada. The purpose of the project is to: provide river regulation, flood control, storage for irrigation, and power generation.

The dam is a concrete gravity-arch structure 221 m high having a crest length of 373 m. The original reservoir had a storage capacity of 40 × 10⁹ m³. A survey in 1963-64 showed that the original capacity had been reduced by 12 percent since its dedication in 1935. The powerplant has 14 hydroturbines with a combined capacity of 1344.8 MW. The combined output of the river outlet works is 1269 m³/s.

The dam has an open-channel type tunnel spillway on each abutment of the dam as shown on figure 7-6. Water enters each spillway by first passing

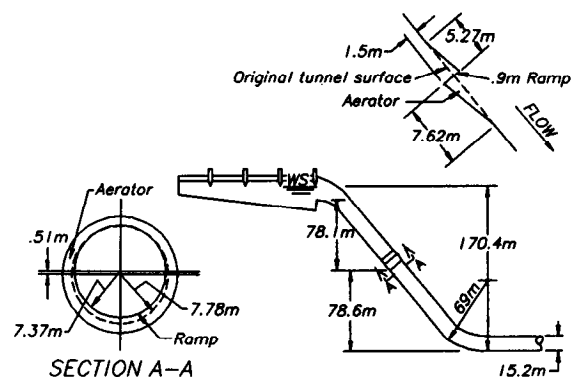


FIGURE 7-6.—Hoover Dam, tunnel spillways—aeration slots.

² Burke Company, The; Burke Concrete Accessories, Inc., 2655-T Campus Dr., San Mateo, CA 94402.

through a gated, side-channel overflow weir. Then it flows over an ogee crest into an inclined tunnel. A vertical bend connects the end of the inclined tunnel to an almost horizontal tunnel. The horizontal tunnel terminates in a flip bucket. The combined capacity of the tunnels is about 11 300 m³/s.

The spillway tunnels operated for the first time in the winter of 1941. The Arizona spillway operated for 116.5 days at an average flow of 366 m³/s with a maximum flow of 1076 m³/s. The Nevada spillway operated for only 19.5 hours at an average flow of 227 m³/s and a maximum flow of 407 m³/s [7]. At the conclusion of the spill, the Arizona spillway had suffered severe damage, but the Nevada spillway was essentially undamaged. Figure 7-7 shows the damage to the Arizona spillway consisting of a hole 35 m long, 9 m wide and 13.7 m deep. Evidently, the damage was caused by a misalignment in the tunnel invert [8]. The misalignment is shown on figure 7-8. Undoubtedly, the depth of the hole was influenced by the presence of a fault that passed obliquely across the tunnel. Hot water (32 °C) flowed from the fault under a pressure of 895 kPa [9].

The Arizona tunnel was repaired by backfilling and compacting river rock and then covering with a thick layer of concrete. Finishing was done by bushing and wet sandblasting, followed by stoning, and finally, by grinding with a terrazzo machine. This produced an exceptionally smooth and durable surface.

In 1983, both tunnels operated for several hundred hours at discharges of about 283 m³/s. This time only minor damage occurred in the Arizona tunnel. However, in the Nevada tunnel the damage was on the verge of becoming severe (see fig. 3-3). The cause of this damage was a relatively insignificant popout (see also fig. 3-13b). The damage index, at the station where the damage began, is 6900 for a 10-mm sudden offset. This value compares favorably with the recommended range of design values for the description of damage (see table 3-4).

Since damage occurred in both tunnels—even with exceptionally smooth surfaces—aeration devices were designed for each spillway [10] as shown on figure 7-6. Each aerator consisted of a ramp and a downstream offset. The ramp is 900 mm high on the invert and feathers to zero height at 35° on each side of the tunnel crown. The offset is concentric with the original tunnel diameter. The 1500-mm offset transitions back to the original diameter in 7620 mm. Each aerator is located about 78 m below the inlet to the tunnel. The installation of both aerators was completed in June 1987.

Kortes Dam was the first unit initiated under the Missouri River Basin Project. The dam is located on the North Platte River 96 km southwest of Casper, Wyoming. The purpose of the dam is to provide power generation for distribution by: municipalities, rural electric associations, and private utilities.

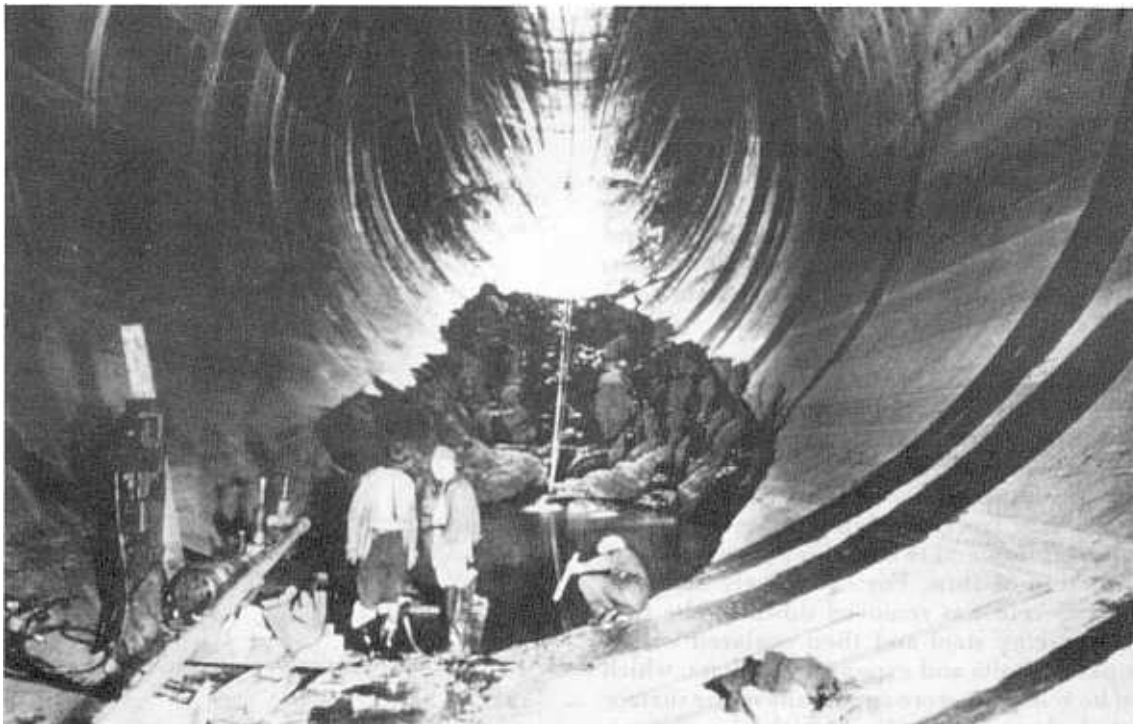


FIGURE 7-7.—Hoover Dam, Arizona tunnel spillway — major damage (1942).



FIGURE 7-8.—Hoover Dam, Arizona tunnel spillway — misalignment that caused major damage.

The dam is a concrete gravity structure 61 m high having a crest length of 59 m. The storage capacity of the reservoir is $5.7 \times 10^6 \text{ m}^3$. The powerplant has three units with a combined nameplate capacity of 36.0 MW. The structure does not have a river outlet works.

The dam has one open-channel tunnel spillway having a maximum capacity of about $1400 \text{ m}^3/\text{s}$. Spillway flows pass: over an ogee crest, through an inclined tunnel, in a vertical bend, and into an almost horizontal 9100-mm-diameter tunnel before reentering the river (fig. 7-9). There is no flip bucket on the end of the horizontal tunnel.

The spillway at Kortes was inspected in the summer of 1983 as a result of the high water which had been experienced at almost all Bureau dams during that season. A severely damaged area was discovered in the invert of the elbow (see fig. 3-15). At first it was thought that the damage was caused by cavitation. However, the cavitation index in the area was greater than 0.31 for all flows which had been passed. Additionally, the surface texture was not characteristic of cavitation damage. Finally,

there was no source for the damage if it was initiated by cavitation. Therefore, this damage must have been due to erosion by a high velocity jet, even though the pattern is the typical “Christmas tree” shape.

Downstream of the elbow the cavitation index of the flow drops to 0.21. Freeze-thaw popouts up to 32 mm deep in this area caused minor damage to the surface immediately downstream of the popout as shown on figure 7-10. Note the difference in the concrete texture in the freeze-thaw popout and that in the area damaged by cavitation. The cavitation damage was formed with a damage index of 4820, which agrees favorably with the recommended values for minor damage (see table 3-4).

Cavitation damage also was noted above the springline on the wall of the tunnel as noted on figure 7-11a. This damage was caused by a thin sheet of water which rises up on the wall downstream of the bend [11] as shown on figure 7-11b. The computer program of appendix A would not give reliable predictions for this damage since the program assumes a level water surface at this station.

The damage potential indicates that major damage caused by cavitation will not occur at Kortes Dam. Therefore, aerators were not designed for this spillway. The major problem at this structure is freeze-thaw damage which will require periodic maintenance and repair. Any cavitation damage caused by the freeze-thaw popouts will be minor and can be repaired during periodic maintenance.

Yellowtail Dam is located 66 km southeast of Billings, Montana, on the Bighorn River. It is a part of the Pick-Sloan Missouri Basin Program. The purpose of the project is to: provide irrigation water, flood control, and power generation.

The dam is a concrete thin arch structure having a height of 151 m and a crest length of 451 m. The reservoir capacity is $0.32 \times 10^9 \text{ m}^3$. The powerplant contains four units with a combined nameplate capacity of 250 MW.

The spillway consists of: an approach channel, a radial gate controlled intake structure, a concrete lined tunnel, and a combination stilling basin-flip bucket [12] (fig. 7-12). The maximum capacity of the spillway is $2605 \text{ m}^3/\text{s}$.

Because of high inflows to the reservoir, the spillway began discharging for the first time on June 26, 1967 [13]. On July 4, the flows were high enough to flip the water out of the bucket at the end of the spillway. The flows continued at a discharge of about $425 \text{ m}^3/\text{s}$ until July 14 when the flip suddenly stopped. The cessation of the flip indicated that energy dissipation was occurring within the spillway tunnel. The cause of the energy dissipation was discovered to be a large cavitation caused hole 2.1 m deep, 14.0 m long, and 5.9 m wide as shown on figure 7-13. Downstream of this large hole, several smaller holes had developed. The large

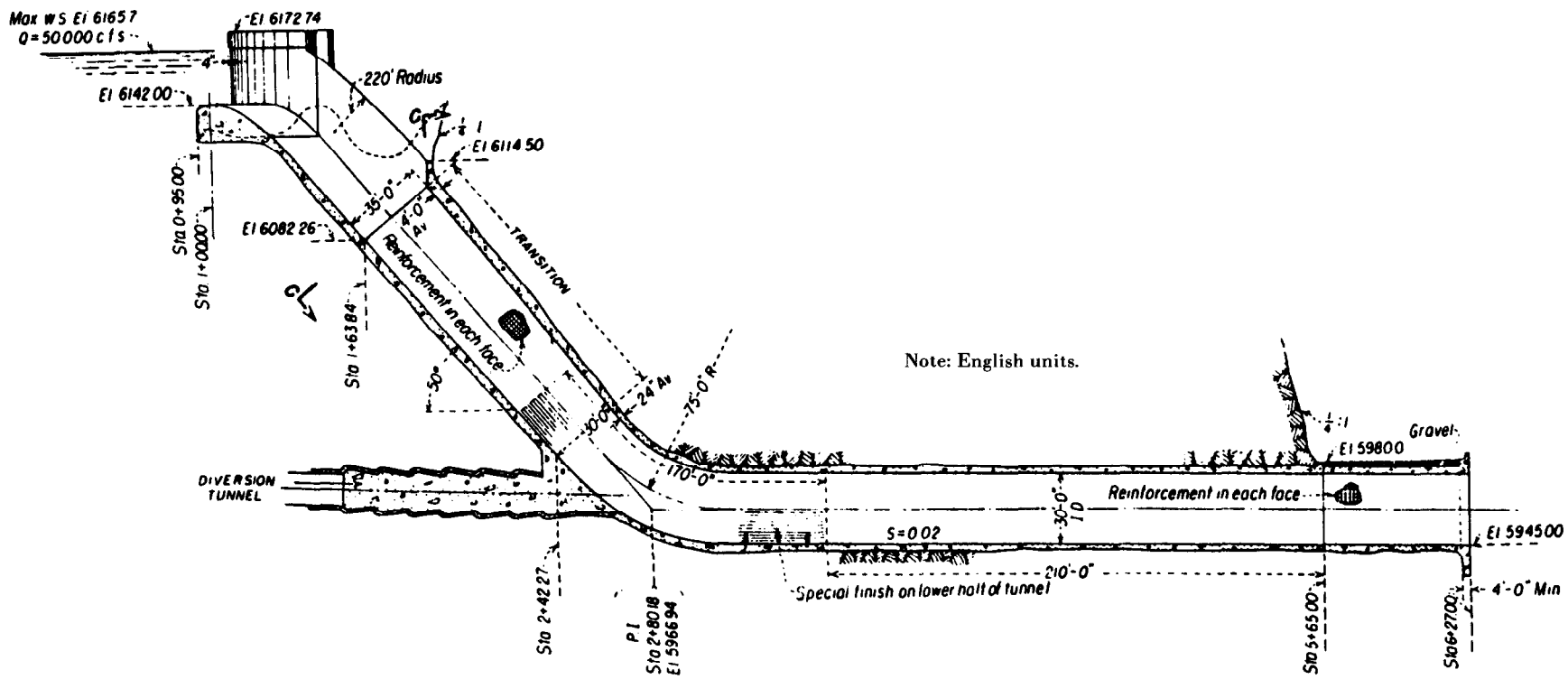


FIGURE 7.9.—Kortes Dam, tunnel spillway — profile.

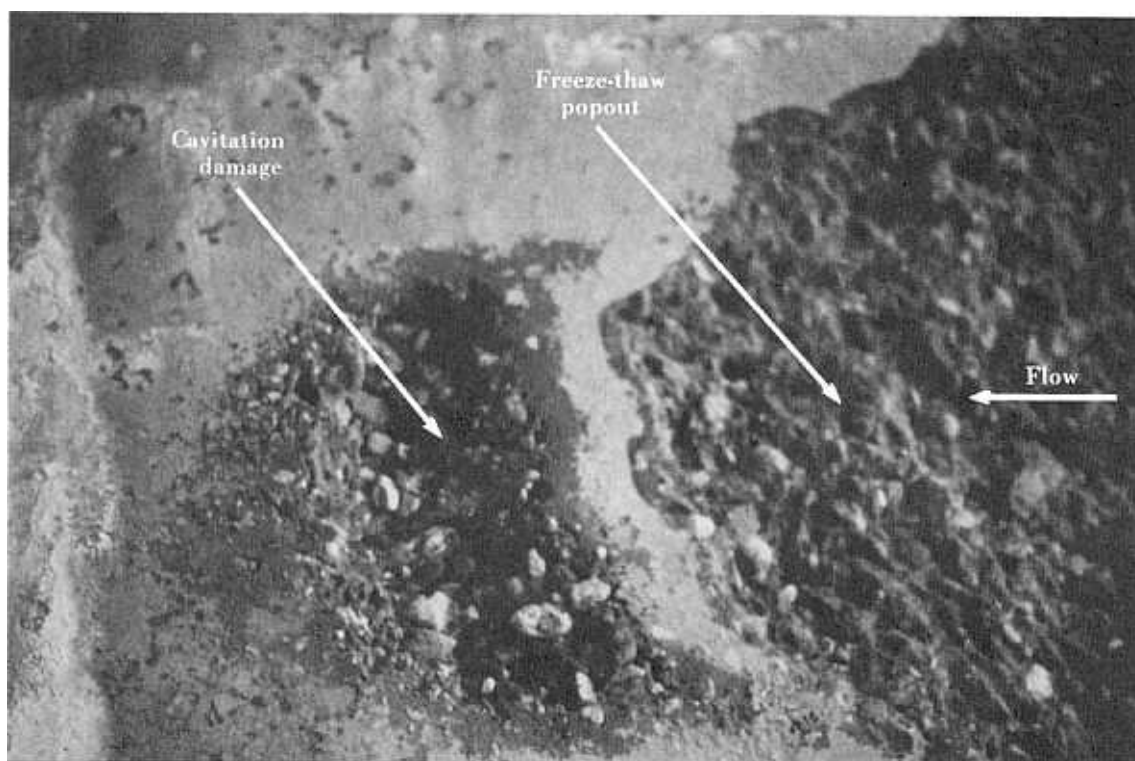


FIGURE 7-10.—Kortes Dam, tunnel spillway—invert cavitation damage (left side) caused by freeze-thaw popout (right).

hole was caused by the failure of an epoxy mortar patch 6 mm deep, 152 mm wide, and 254 mm long at station 3+16. The damage index for this hole is 9600. The minimum cavitation index at station 3+16 is 0.15.

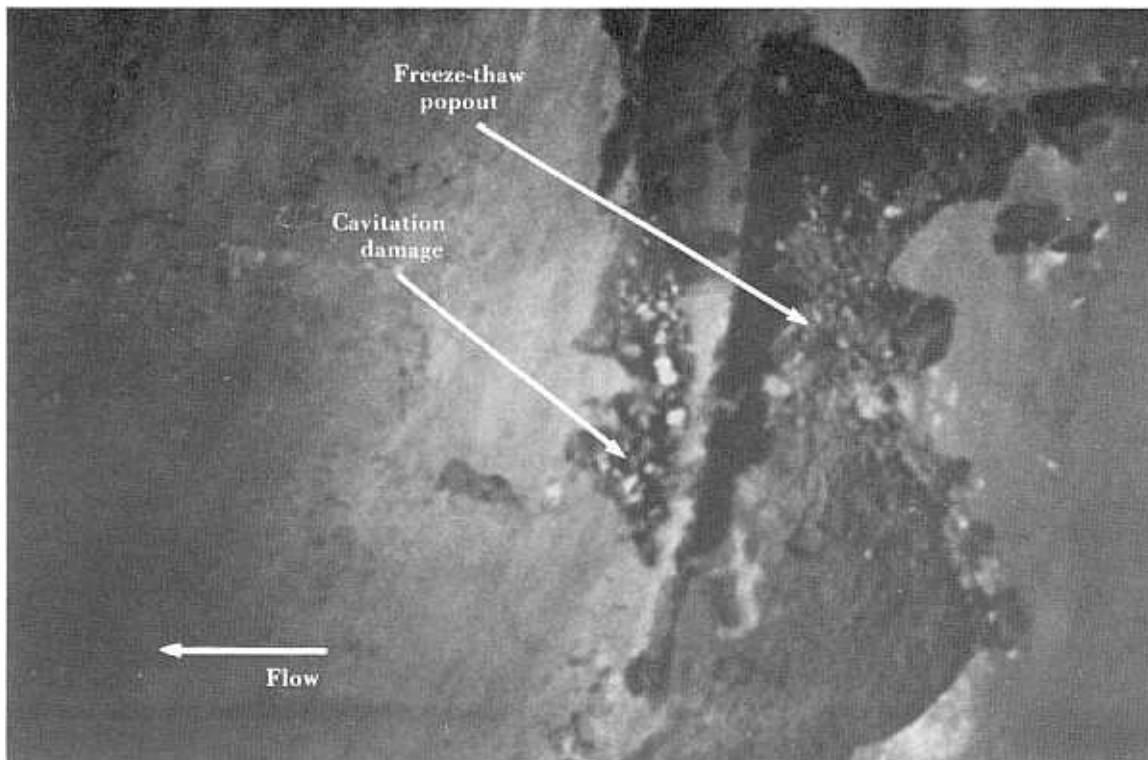
Higher up in the elbow of the tunnel, another damaged area was found at station 2+88 which was 9 m long and centered about 1 m to the right of the tunnel centerline as shown on figure 7-14. This damage was initiated by the failure of an epoxy-mortar patch located within a 457-mm square dry-patch. This damage formed five distinct teardrop shaped holes. The most upstream hole was 305 mm wide and 152 mm deep. The next downstream hole was 610 mm wide, followed by a hole 910 mm wide. The fourth hole was 1829 mm wide and the last about 1520 mm wide. The damage index for this damaged area is 3520. The minimum cavitation index at station 2+88 is 0.15.

Following this damage, one of the most ambitious repair procedures ever undertaken by the Bureau was begun. [13] An aerator was designed for the tunnel, which was located 103 m below the maximum reservoir elevation [14], as shown on figure 7-15. The aerator consisted of a ramp 685.8 mm long and 76.2 mm high at the invert. The ramp feathered out to zero height at the springline of the tunnel. Immediately downstream of the ramp, a 914-mm square aeration groove was located. The downstream

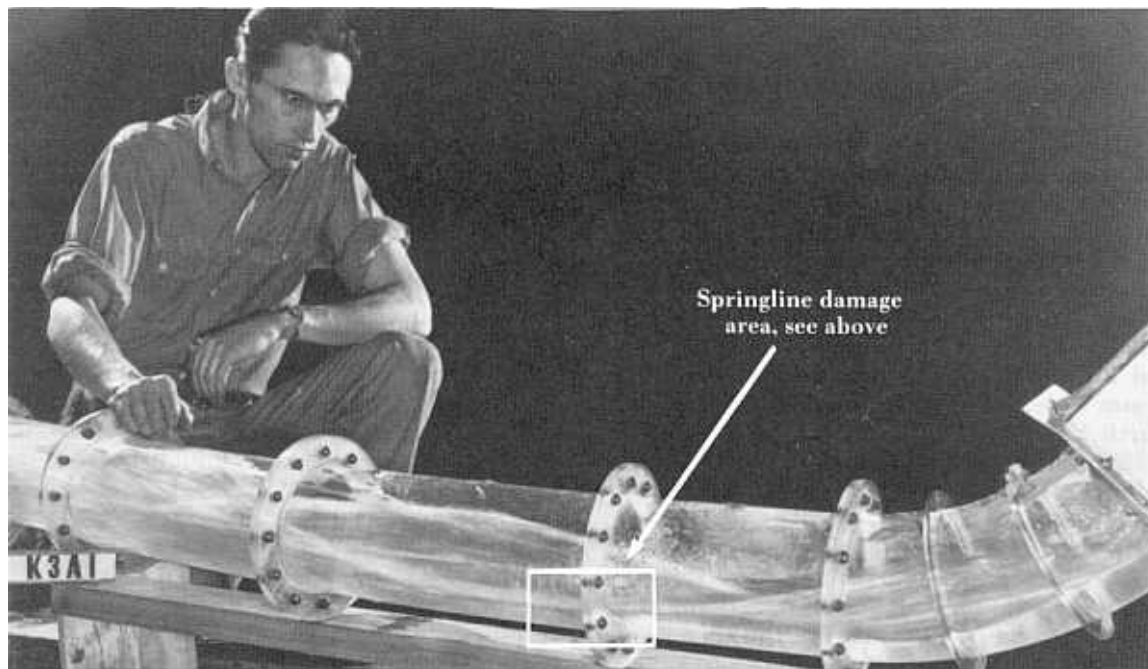
edge of the groove was connected to a 152-mm offset which transitioned back to the original diameter of the tunnel in 2635 mm. The transition had a 22.86-m radius of curvature in the flow direction.

In addition to the aerator installation, large damaged areas were repaired with epoxy bonded concrete [13]. Shallower damaged areas were repaired with epoxy-bonded concrete and epoxy-bonded epoxy mortar. Irregularities in the epoxy-bonded concrete were removed by grinding them to a 1:100 slope. Finally, the tunnel surface below the springline was painted with an epoxy-phenolic paint.

Following the 1969 repair, the spillway was operated at a discharge of 141 m³/s for 118 hours and at a discharge of 425 m³/s for 24 hours. In 1970, another spillway test was conducted. The test began with a flow of 141 m³/s for 11.5 hours; then the flow was increased to a discharge of 396 m³/s and held there for 95.2 hours. This was followed by a release of 113 m³/s for about 18 hours. Following the test, an inspection of the tunnel revealed absolutely no damage. The damage index for the station at which the maximum damage occurred was 7690. Without an aerator or the extremely smooth surface treatment, moderate damage would have been predicted for a damage index this large. Therefore, the tests at sufficiently high discharges and durations proved the effectiveness of the repair.



a. Damage caused by freeze-thaw popout at springlin



b. Model investigation of flow conditions in tunnel

FIGURE 7-11.—Kortes Dam, tunnel spillway — springline damage.

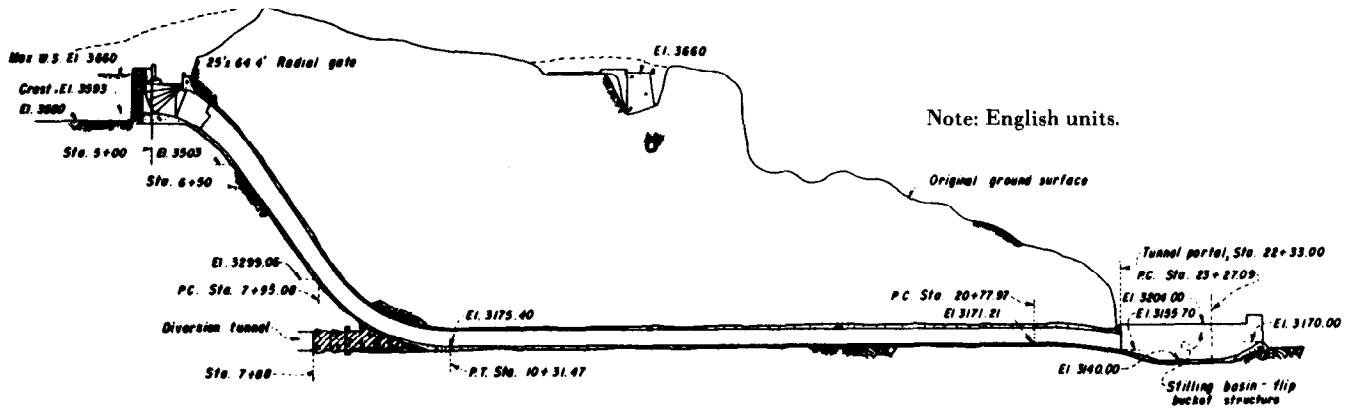


FIGURE 7-12.— Yellowtail Dam, tunnel spillway — profile.



FIGURE 7-13.— Yellowtail Dam, tunnel spillway — major damage downstream of elbow.

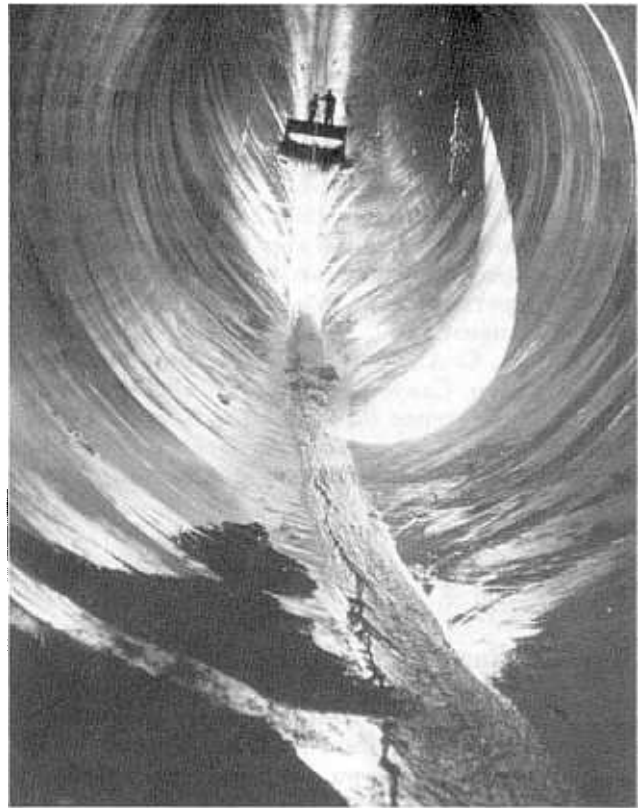


FIGURE 7-14.— Yellowtail Dam, tunnel spillway — damage in elbow.

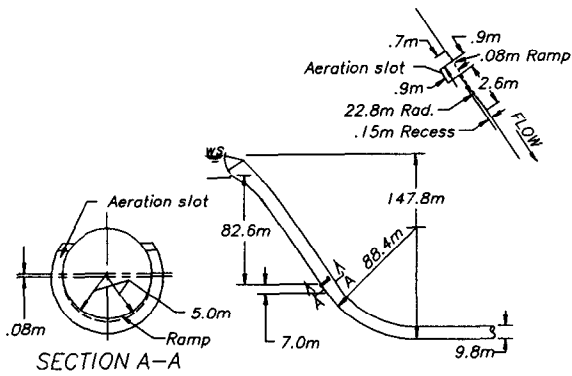


FIGURE 7-15.— Yellowtail Dam, tunnel spillway — aeration slot.

BIBLIOGRAPHY

Blue Mesa Dam

- [1] Beichley, G. L., "Hydraulic Model Studies of the Blue Mesa Dam Spillway," Bureau of Reclamation Report No. HYD-515, July 1964.

Flaming Gorge Dam

- [2] Rhone, T. J., "Hydraulic Model Studies of Flaming Gorge Dam Spillway and Outlet Works," Bureau of Reclamation Report No. HYD-531, 1964.

Glen Canyon Dam

- [3] Burgi, P. H., Eckley, M. S., "Repairs at Glen Canyon Dam," *Concrete International*, pp. 24-31, March 1987.
- [4] Burgi, P. H., Moyes, B. M., Gamble, T. W., "Operation of Glen Canyon Dam Spillways—Summer 1983," Proceedings of the Conference on Water for Resource Development, American Society of Civil Engineers, pp. 260-265, Coeur d'Alene, Idaho, August 14-17, 1984.
- [5] Pugh, C. A., "Modeling Aeration Devices for Glen Canyon Dam," Proceedings of the Conference on Water for Resource Development, American Society of Civil Engineers, Coeur d'Alene, Idaho, pp. 412-416, August 14-17, 1984.
- [6] Frizell, W. K., "Spillway Tests at Glen Canyon Dam," Bureau of Reclamation, 52 pp., July 1985.

Hoover Dam

- [7] Keener, K. B., "Erosion Causes Invert Break in Boulder Dam Spillway Tunnel," *Engineering News Record*, pp. 763-766, November 1943.

- [8] Warnock, J. E., "Experiences of the Bureau of Reclamation," Proceedings of the American Society of Civil Engineers, vol. 71, No. 7, pp. 1041-1056, 1945.

- [9] Walter, D. S., "Rehabilitation and Modification of Spillway and Outlet Tunnels and River Channel Improvements at Hoover Dam," thesis for civil engineer degree, University of Colorado, 1957.

- [10] Houston, K. L., Quint, R. J., Rhone, T. J., "An Overview of Hoover Dam Tunnel Spillway Damage," *Waterpower 85*, Proceedings of an International Conference on Hydro-power, American Society of Civil Engineers, pp. 1421-1430, Las Vegas, Nevada, September 1985.

Kortes Dam

- [11] Adkins, C. V., "Model Studies of the Kortes Dam Spillway and the River Channel Downstream — Kendrick Unit, Wyoming-Missouri Basin Project," Bureau of Reclamation Report No. HYD 206, August 1946.

Yellowtail Dam

- [12] Beichley, G. L., "Hydraulic Model Studies of Yellowtail Dam Spillway — Missouri River Basin Project, Montana," Bureau of Reclamation Report No. HYD-483, August 1964.

- [13] Borden, R. C., Colgate, D., Legas, J., Selander, C. E., "Documentation of Operation, Damage, Repair, and Testing of Yellowtail Dam Spillway," Bureau of Reclamation Report No. REC-ERC-71-23, 76 pp., May 1971.

- [14] Colgate, D., "Hydraulic Model Studies of Aeration Devices for Yellowtail Dam Spillway Tunnel, Pick-Sloan Missouri Basin Program, Montana," Bureau of Reclamation Report No. REC-ERC-71-47, 13 pp., December 1971.

Cavitation Characteristics for Open Channel Flow Program

PROGRAM DESCRIPTION

For many years, pressures measured on models have been used to predict the occurrence of cavitation with free water surface flows. If the pressures are positive or if pressure fluctuations never drop below atmospheric pressure (scaled to model dimensions), hypothetically, cavitation damage will not occur on the surface. This supposition ignores the fact that local surface irregularities can cause low pressures within the body of the flow. Consequently, cavitation can occur even though the boundary pressures are always positive. A striking proof of this is the extensive damage produced in the elbows of tunnel spillways which exhibit large positive pressures.

The prediction of cavitation occurring at a boundary can best be accomplished by calculating the flow's cavitation index at the boundary and comparing this to the cavitation indices of surface irregularities which may be anticipated. To calculate the flow's cavitation index, the velocity and pressure conditions in the vicinity of the irregularities must be known.

The computer program described in this appendix was developed to calculate the hydraulic and cavitation properties of free water surface flows.

The program is based upon the determination of the water surface profile using the standard step method [1]. This method assumes gradually varied flow in a uniform channel. Simple algorithms are used to account for changes in shape and curvilinear flow. Although the simplifications are somewhat crude, the algorithms produce results having sufficient accuracy for engineering analysis purposes. The use of these algorithms keeps the computational time within reasonable limits.

The program output includes all the flow parameters as well as the cavitation characteristics of the structure. If air entrainment will occur due to aeration through the water surface, the air concentration is also output.

The computer program is written and compiled in Microsoft-Fortran.¹

ALGORITHMS USED IN PROGRAM

Since all the algorithms used in the program are not found in any single reference, a detailed description of the more pertinent algorithms follows.

Friction Factor

The standard step method requires the friction loss be determined for each computational increment. Many programs use the Manning equation to determine the loss [1]. However, studies have shown that Manning's "n" is not constant with respect to canal size [2]. Therefore, the program uses the concept of the Darcy-Weisbach friction factor to determine the losses. The Darcy-Weisbach friction factor is defined as:

$$S_f = \frac{f}{4R_h} \left(\frac{V^2}{2g} \right) \quad \text{A.1}$$

where:

- f = Darcy-Weisbach friction factor
- g = gravitational constant (acceleration)
- H_f = head loss due to friction, over length L_s
- L_s = distance over which friction loss occurs
- R_h = hydraulic radius
- S_f = friction slope = H_f/L_s
- V = flow velocity

The friction factor value is determined from the Colebrook-White equation for open channel flow given by:

$$F_r = -2 \log \left(\frac{k_s}{12 R_h} + \frac{2.5 F_r}{R_e} \right) \quad \text{A.2}$$

where:

- $F_r = 1/f^{1/2}$
- k_s = sand grain roughness or rugosity [3]
- R_e = Reynolds number = $4 R_h V / \nu$
- ν = kinematic viscosity

¹ A registered trademark of Microsoft Corporation, 16011 NE 36th Way, Box 97017, Redmond, WA 98073-9717.

The method's advantage is the boundary roughness is described by a number that does not vary with flow depth or flow rate. This number, known as the sand grain roughness or rugosity, has been carefully investigated for flow in pipes [3]. A further advantage is the great wealth of data obtained, for flow in closed conduits, can be used directly with open channel flow.

If the rugosity to flow depth ratio is greater than 0.10, vertical acceleration in the flow becomes significant. This ratio corresponds to a Darcy-Weisbach friction factor of 0.115. When vertical accelerations are significant, the gradually varied steady flow equations do not apply and the program will stop and output an appropriate warning.

Curvilinear Flow

The standard step method assumes a constant slope between computational points. If the streamlines have a substantial curvature in the vertical plane, the piezometric pressure at the boundary must be corrected by an appropriate factor. This factor is equal to the force produced per unit area of a mass of water undergoing centrifugal acceleration. For the channel invert, the factor is determined from the relationship:

$$C_g = \frac{d V^2}{g R_b} \tag{A.3}$$

where:

- C_g = centrifugal acceleration factor
- d = flow depth
- g = gravitational constant (acceleration)
- R_b = radius of curvature at the boundary
- V = flow velocity

If the flow tends to move into the boundary (concave curvature), the factor is positive. For flows moving away from the boundary (convex curvature), the factor is negative as shown on figure A-1.

The radius of curvature is given by:

$$R_b = \frac{\left[1 + \left(\frac{dy}{dx} \right)^2 \right]^{3/2}}{\frac{d^2y}{dx^2}} \tag{A.4}$$

For circular curves, the radius of curvature is constant and is equal to the radius of the curve.

For vertical curves, as used in highway construction, the radius of curvature is given by:

$$R_b = \frac{\left[1 + \left(S_1 + \frac{(S_2 - S_1) X}{L_v} \right)^2 \right]^{3/2}}{\frac{S_2 - S_1}{L_v}} \tag{A.5}$$

where:

- L_v = length of vertical curve
- S_1 = upstream slope
- S_2 = downstream slope
- X = horizontal distance from beginning of vertical curve

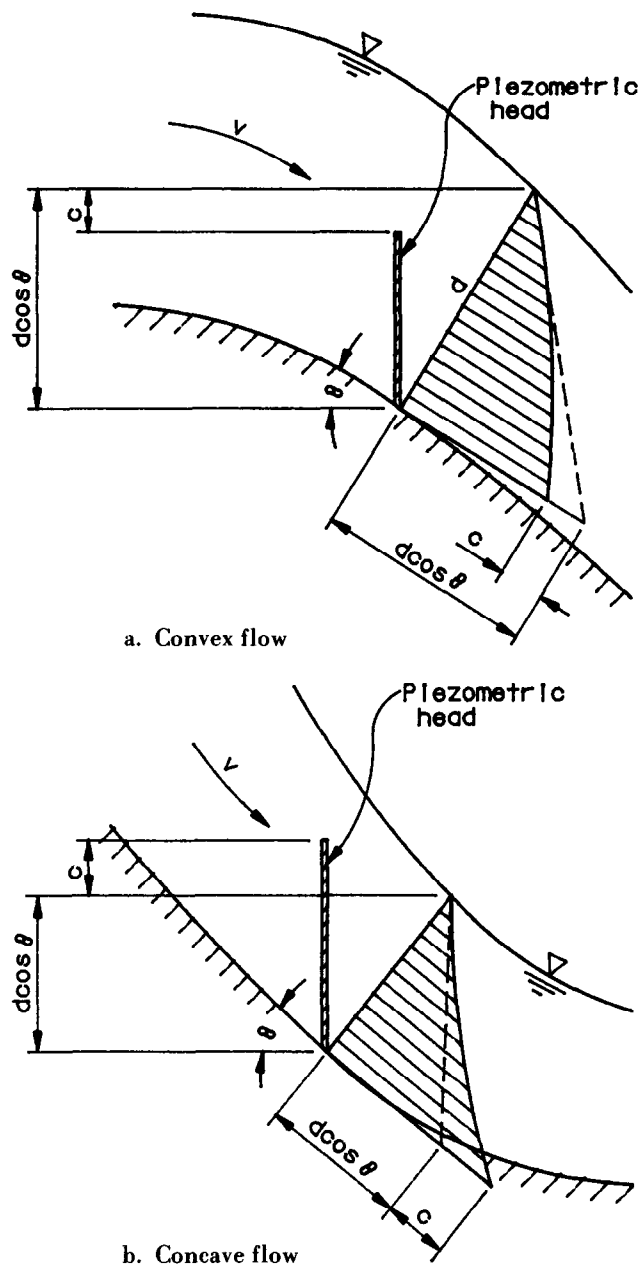


FIGURE A-1.—Piezometric pressure with curvilinear flow.

In computations, maintaining standard sign convention for the slopes in the equation is of utmost importance. That is, downward slopes are negative and upward slopes are positive.

Actually, the radius of curvature corresponds to the curvature of the flow streamlines—not to the radius of curvature of the boundary. At locations where the radius of curvature of the boundary is discontinuous, a value for the radius of curvature must be selected that most nearly simulates the streamline curvature. For instance, at locations where a constant boundary slope joins a finite radius of curvature, the radius of curvature should be infinite. In the program, an infinite radius of

curvature is input by setting the appropriate parameter equal to zero. For locations where a finite radius of curvature joins a constant boundary slope, the finite radius of curvature should be used in the program.

Pressure Distribution on Steep Slopes

A hydrostatic pressure distribution is a good assumption for flow on mild slopes. However, as slope increases, the pressure distribution no longer remains hydrostatic (see fig. A-2). Therefore, a pressure distribution correction must be made on steep slopes to obtain an accurate energy balance in the standard step method. The wall pressure head on steep slopes is given by:

$$h_w = d \cos \theta_i \tag{A.6}$$

where:

- d = flow depth measured normal to channel slope
- h_w = wall pressure head
- θ_i = angle of downstream chute invert relative to horizontal

It has been shown [1] that, with this correction, the Froude number on a steep slope should also be corrected. The appropriate expression for the Froude number is:

$$F = \frac{V}{\left(\frac{gd \cos \theta_i}{\alpha_o}\right)^{1/2}} \tag{A.7}$$

where:

- d = flow depth measured normal to channel slope

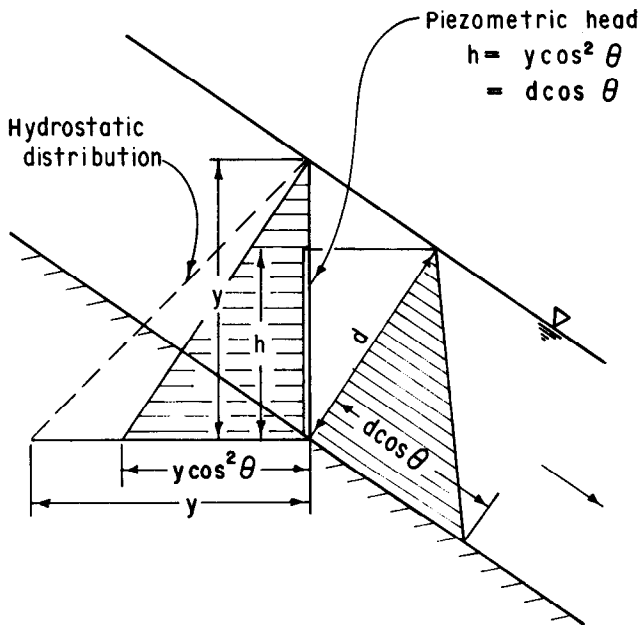


FIGURE A-2.—Pressure distribution on a steep slope.

- F = Froude number
- g = gravitational constant (acceleration)
- V = flow velocity
- α_o = kinetic energy correction factor

Kinetic Energy Correction Factor

The kinetic energy of the flow, at a station, is equal to the sum of the kinetic energies at each depth in the cross section. Common practice is to reference kinetic energy to the mean flow velocity. With a nonuniform distribution, the true kinetic energy will be greater than the kinetic energy referenced to mean flow velocity. This difference is accounted for by using a kinetic energy correction factor, α_o , defined by:

$$\alpha_o = \frac{1}{V^3 A_t} \int_0^A v^3 dA_i \tag{A.8}$$

where:

- dA_i = incremental area of cross section
- A_t = total area of cross section
- v = point velocity at any flow depth
- V = flow velocity in cross section

For rectangular shaped sections, the average kinetic energy correction factor is 1.15 with fully developed flow [1]. For uniform flow—that is, no boundary layer—the factor is 1.0.

In the program, the kinetic energy correction factor, α_o , is assumed to vary parabolically with the relative boundary layer thickness. That is,

$$\alpha = 1.15 \left(\frac{\delta}{d}\right)^2 \tag{A.9}$$

where:

- d = flow depth normal to invert
- δ = boundary layer thickness

Critical Depth

Critical depth is strictly defined as the depth that corresponds to the minimum energy in the cross section. On mild slopes, without curvilinear flow, and without a kinetic energy correction factor, critical depth is:

$$d_k = \left(\frac{q^2}{g}\right)^{1/3} \tag{A.10}$$

where q equals unit discharge of water.

However, the energy equation which is used in the program accounts for steep slopes, curvilinear flow, and the kinetic energy correction factor. Therefore, in the program subroutine which determines the critical depth, a Newton iteration method is used to determine the depth that minimizes the total energy of the flow.

Cavitation Computations

Using the velocity and the piezometric pressures from the program, a cavitation index for the flow is calculated using equation 1.5. The damage index is determined for three circular arcs and for three triangular into-the-flow offsets using equation 2.10. For the flow and cavitation computations the boundary layer thickness, δ , is estimated from:

$$\delta = \frac{0.38 X_b}{R_x^{0.2}} \quad \text{A.11}$$

where:

- R_x = distance Reynolds number = VX_b / ν
- V = flow velocity
- X_b = distance from start of boundary layer
- ν = kinematic viscosity

The difference between atmospheric pressure and vapor pressure is approximated for various elevations (at a temperature of 10 °C) based upon an approximation of the characteristics of a standard atmosphere. The equation used in inch-pound units and SI units, respectively, is:

in-lb:

$$P_a = 33.9 [1 - (Z_i/145,400)]^{5.255} - 0.39 \quad \text{A.12}$$

SI:

$$P_a = 10.33 [1 - (Z_i/44\,303)]^{5.255} - 0.12 \quad \text{A.13}$$

where:

- Z_i = invert elevation of the first station
- P_a = atmospheric pressure

This equation is almost identical to that recommended by Eskinazi [4], who developed an equation based upon a reference temperature of 15.56 °C.

Air Entrainment

Air entrainment quantities are calculated using empirical correlations [5]. The relationship is:

$$C_a = 0.05 F - \frac{(E \sin \theta_i)^{1/2}}{63} \quad \text{A.14}$$

where:

- C_a = air concentration
- E = Eötvös number = $(g\rho d^2)/\epsilon$
- F = Froude number, see equation A.7
- g = gravitational constant (acceleration)
- d = flow depth normal to invert
- ϵ = interfacial surface tension
- θ_i = angle between chute invert and horizontal
- ρ = density of water

If the air concentration (in equation A.14) is less than zero, the air concentration is set equal to zero.

An estimate of the point at which air entrainment can begin is obtained by observing the station in the program output at which the boundary layer thickness equals the flow depth.

PROFILE TYPES

The significant characteristics which define the type of water surface profile are normal and critical depths as shown on figure A-3. Normal and critical depths, computed by the program, include the effects of curvilinear flow, steep slopes, and the kinetic energy correction factor. Therefore, the values determined by the program may not agree with simplified equations commonly found in text books that ignore these effects.

COMPUTATIONAL PROBLEMS

In specifying the initial conditions for the program, the most significant problem is the determination of depth and station for the starting point of the computations.

Starting Station

Sometimes the program will not run if a first station is chosen too near to a spillway crest. The curvilinear flow at the crest is the cause of this problem. At the crest, every streamline has a different radius of curvature which is not accounted for in the program. It is better to begin the program at a station where streamlines are nearly parallel with the invert. If this is done, the location of the boundary layer origin should still be given as the crest station or the control gate station.

Starting Depth

In some cases the starting depth, for the program, can be obtained from model investigations. If flow is over a spillway, the following procedure can be used to set the energy gradeline at the beginning of the boundary layer equal to the reservoir elevation. This procedure assumes that losses between the reservoir and the spillway crest are negligible.

1. Set the station, at which the boundary layer starts to grow, equal to the crest station.
2. Assume a starting depth less than critical depth.
3. Run the program.
4. If the energy gradeline at the crest does not equal the reservoir elevation, then calculate G and dG/dd from:

$$G = Z_r - Z_g \quad \text{A.15}$$

where:

- Z_r = reservoir elevation
- Z_g = energy gradeline elevation
- G = iteration function

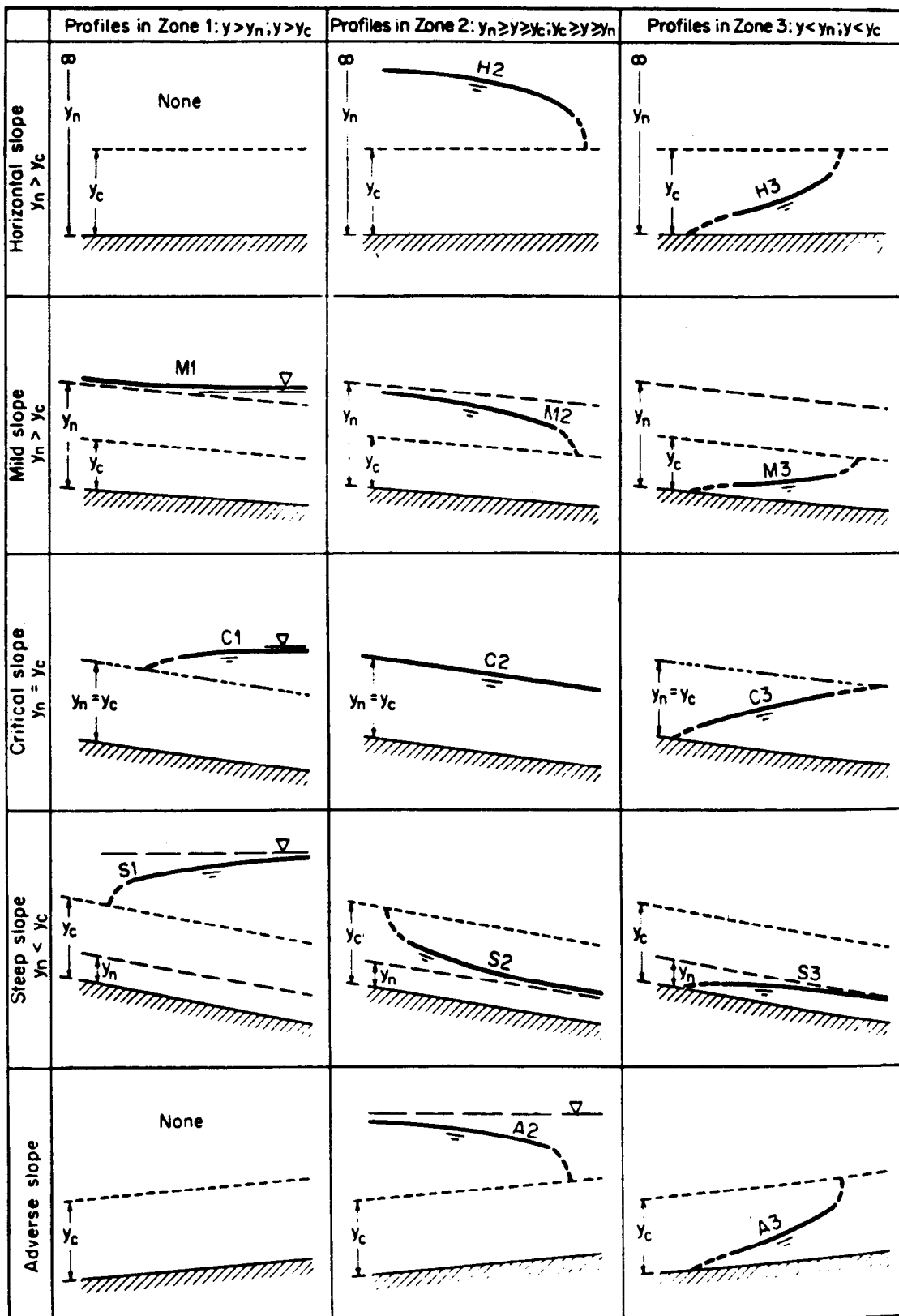


FIGURE A-3.—Profiles of gradually varied flow — classification [1]. [From: Chow, Open Channel Hydraulics, McGraw Hill, Inc., 1959, reproduced by permission of McGraw-Hill, Inc.]

and

$$\frac{dG}{dd} = \frac{Q^2 T}{g A_t^3} + \frac{2 h_l}{d_f} + \frac{4}{3} \left(\frac{h_l}{R} \right) \frac{dR_h}{dd} - 1 \quad \text{A.16}$$

where:

- A_t = area of cross section
- h_l = head loss from crest to first station equals energy gradeline crest minus energy gradeline at first station
- g = gravitational constant (acceleration)
- Q = discharge
- R_h = hydraulic radius at first station
- T = top width of water surface at first station
- d_f = effective flow depth at first station = A/T

5. Calculate a new starting depth from:

$$d = d - \frac{G}{dG/dd} \quad \text{A.17}$$

where d on the left side of equation A.17 is the new starting depth; d on the right side is the previous starting depth.

6. Repeat steps 3 through 5 until the function G is reasonably close to zero.

These steps are performed by the program if the reservoir elevation is specified.

Impossible Flow Conditions

If the program detects an impossible flow condition, it will stop and output an appropriate message.

The practical problems in analyzing flow profiles have been discussed by others [1, 5]. If problems are experienced in discovering what caused the program to abort, these references should be reviewed.

CROSS SECTION SHAPES

The program includes six shapes to define the cross section of the chute prism. They are:

- rectangular or trapezoidal
- circular
- egg shape
- horseshoe
- composite
- circular-arc (user defined)

By properly specifying the dimensions in these shapes, almost any prismatic cross section can be defined. The geometries are discussed below. The symbols on the figures are compatible with variables in the computer program.

Trapezoidal

The trapezoidal section is defined by a width, W , and a side slope, SS , as shown on figure A-4.

Rectangular sections are defined by setting the side slope value equal to zero.

Circular

The circular shape is defined by a radius, R , as shown in figure A-5. The circular shape also can be defined by the composite section described below. If the composite section is used, five parameters must be defined.

Egg Shape

The egg shape is constructed with three arcs as shown on figure A.6. With the egg shape definition, the user need define only the width, D , of the section. This section also may be described by the user defined arcs section described below. If the user defined arcs section is used, five parameters must be specified.

Horseshoe

Two types of horseshoe shapes exist—the conventional horseshoe and a modified horseshoe. The conventional horseshoe is constructed with three arcs as shown on figure A-7. The modified horseshoe has a horizontal invert as shown on figure A-9. For a conventional horseshoe, the user need define only the width, D , of the section. The conventional horseshoe shape also can be described as a user defined arcs section.

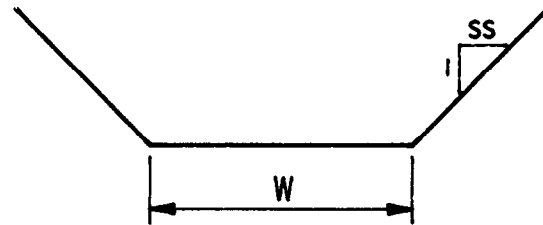


FIGURE A-4.—Trapezoidal and rectangular cross sections.

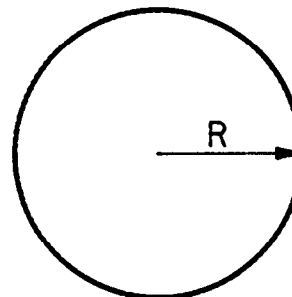


FIGURE A-5.—Circular cross section.

The definition of the modified horseshoe is described under the composite section.

Composite

The composite section is typical of sections which connect two rectangular gates to a rectangular or circular cross section. The composite section consists of a rectangular shape having a center wall. The intersection of the sidewalls and the floor, as well as the roof, are connected with fillets as shown on figure A-8. The user needs to define:

- width of the section, W
- radius of the upper fillet, R
- distance from the invert to the centerline of the upper fillet, $RADCL$
- radius of lower fillet, $R1$
- thickness of the center wall, T

If the structure does not have a roof, the distance from the invert to the upper fillet centerline should be set equal to minus 1.

Modified Horseshoe

The modified horseshoe is defined by setting:

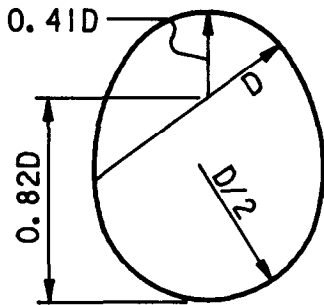


FIGURE A-6.—Egg-shape cross section.

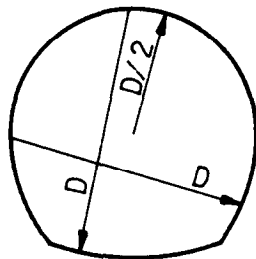


FIGURE A-7.—Horseshoe cross section.

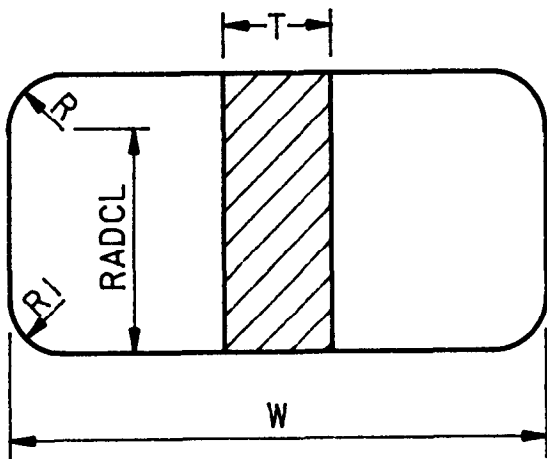


FIGURE A-8.—Composite cross section.

- wall thickness, T , to zero
- top fillet radius equal to one-half the bottom width, $R = W/2$
- bottom fillet radius equal to zero, $R1 = 0$
- the distance from the invert to the upper fillet centerline, $RADCL$, equal to the height of the sidewall of the modified horseshoe as shown on figure A-9

User Defined Circular-Arc Cross Section

As previously shown, the egg shape and the conventional horseshoe shape cross sections are constructed of four circular arcs. The only difference between the shapes are the radii lengths and the center points location of the radii. Therefore, a user defined circular-arc section is capable of providing flexibility in defining other sections that are formed from four circular arcs. The definition is limited only by the fact that the centers of the two vertically oriented arcs must lie on the opposite arcs as shown on figure A.10. The user need only define:

- length of three radii, $R1$, $R2$, and $R3$
- distance from the invert to the upper radius, $C3$
- two side radii, $C2$

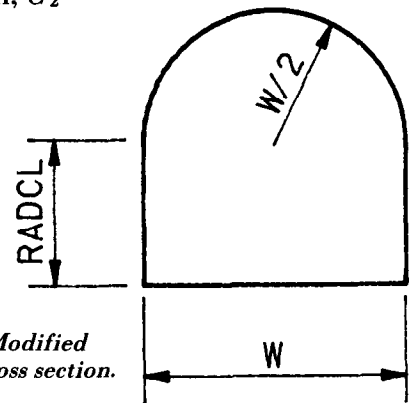


FIGURE A-9.—Modified horseshoe cross section.

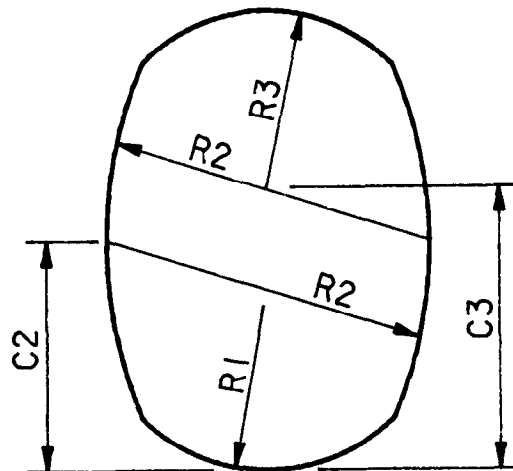


FIGURE A-10.—User defined circular-arc cross section.

INPUT FILE

A. PROGRAM DESCRIPTION

The program computes hydraulic and cavitation properties of open channel flow for prismatic cross sections. The hydraulic properties include flow depth, velocity, piezometric pressure, energy grade line, entrained air content, profile type, critical and normal flow depths, and boundary layer thickness. The cavitation properties include the cavitation index of the flow, the surface cavitation index, the chamfer required to prevent cavitation, damage potentials for six types of surface irregularities, and the turbulent intensity. The prismatic sections include trapezoidal, circular, egg, horse shoe, and composite shapes.

The program calculates either draw down and backwater curves using the standard step method.

The input data can be either created and read in from a file or created interactively as the program is run. Two executable files are available on the Source Disk to assist the user in converting or checking an existing file. CKDATA checks an existing data file for errors. If errors are present, the program points to the location of the error. During checking, the file can be put into a standard format if the user desires. CONVT converts a file from metric to English units or vice versa. The converted file must be given another name than the original file name. The program determines the units in the original file and asks the user if the conversion should take place.

The output consists of a formatted geometry file, a plot file. The hydraulic and cavitation properties can be sent either to a file or to the printer.

The program is dimensioned for up to 40 stations and 15 different discharges. If different discharges are used, the number of stations cannot be variable.

B. INPUT DATA

The required order for the input is as follows:

**** FIRST LINE ****

Discharge, initial depth, starting rugosity, direction of computation, units, initial bottom slope (distance vertical to distance horizontal), station of beginning of boundary layer, reservoir elevation.

TYPICAL RUGOSITIES

concrete	0.03-0.5 mm
steel	0.05 mm
tubing	0.0015 mm

DIRECTION OF COMPUTATION

upstream 0 downstream 1

DIMENSIONAL UNITS
metric 0 English 1

**** SECOND LINE ****

The title (up to 60 characters)

**** THIRD LINE ****

The number of stations

**** THE NEXT LINES ARE INPUT IN PAIRS ****

Two description lines are required for each station. These consist of the following;

First station description line

Shape of cross section

- 1 rectangular or trapezoidal
- 2 circular
- 3 egg
- 4 horse shoe
- 5 composite
- 6 user defined circular arc section

Slope of cross section at station

- 1 section vertical
- 2 section normal to floor)

Second station description line (one of the following sets)

a) Rectangular or trapezoidal section

Station, invert elevation, bottom width, channel side slope (distance horizontal to unity vertical), the vertical radius of curvature, rugosity.

b) circular section

Station, invert elevation, radius of circular section, the vertical radius of curvature, rugosity.

c) egg and horse shoe sections

Station, invert elevation, radius of maximum arc length, the vertical radius of curvature, rugosity.

The invert, side walls, and crown are all formed from circular arcs. The difference between the egg and the horse shoe is the

length of the radius and the location of the center of each arc. Only the largest radius is needed to describe each shape. The program defines the radii and center points using USBR standards. Other similar shapes can be defined by the user by changing the constants in either the egg or horse shoe statements. The subroutines used for the egg and horse shoe computations are general and can solve for any radius and center combination, see e) used defined circular arc section.

d) composite section

Station, invert elevation, width of section, radius of upper fillets, distance between invert and centerline of upper radius point (if not closed conduit flow, set this value to -1.0), radius of lower fillets, thickness of support wall, the vertical radius of curvature, rugosity.

The composite section is a square with circular fillets in the four corners and a center support wall. This section is useful in defining the transition from a rectangular section to a circular section. This transition frequently occurs where a tainter gate discharges into a circular tunnel or where a circular tunnel transitions into a flip bucket.

e) user defined circular arc section

Station, invert elevation, invert radius, crown radius, side wall radius, vertical distance from invert to center point of crown radius, vertical distance from invert to center point of side wall radius, the vertical radius of curvature, rugosity.

The user defined circular section is made up of four arcs. One forms the invert, another forms the crown, and the other two form the side walls. The side wall radii are equal. The radii and the vertical distance from the invert to the center points of the radii must be specified. Since the side wall radii are equal, they only have to be specified once. In addition, since the vertical distance of the invert centerline from the invert is equal to the invert radius it does not have to be specified

C. DETAILED NOTES

Aeration - For free surface aeration, the mean air content of the flow is computed from

$$C = 0.05 * F - \text{SQRT}(\text{SINE}(\text{ALPHA}) * E) / 63$$

where $F = V / \text{SQRT}(G * YE)$

$E = (\text{RHO} * G * YE * YE) / \text{SURFT}$

SURFT= interfacial tension

RHO= density of water

G= acceleration of gravity

YE= effective depth

= area/top width of water prism.

The air ratio is defined as $BETA = Q_{air}/Q_{water} = C/(1 - C)$

If a hydraulic jump forms in a circular, arc, or composite section, the air content of the water is computed from the Kalinski and Robertson equation

$$BETA = 0.0066 * ((F - 1)**1.4).$$

The computations do not continue once a hydraulic jump seals the conduit.

Bistable Flow - A condition can exist with closed conduit flow in which the discharge with open channel flow in the conduit equals or exceeds the closed conduit discharge. If this occurs, the program outputs a warning that "bistable flow" is possible. This condition should be avoided in design because it can lead to very explosive discharge of air pockets at the downstream end of the conduit.

Initial Depth - If the computations are based on an initial depth, set the reservoir elevation in the first line equal to -1. If the computations are based on reservoir elevation, guess an initial depth. The program will then compute the initial depth which should give you the proscribed reservoir elevation. The process involves the extrapolation of the energy grade line back to the location of the starting of the boundary layer (assumed reservoir location). This process may require several iterations before the extrapolated energy grade line is within 0.1 percent of the reservoir elevation. If more than one discharge is used in the input file, the reservoir elevation will be computed for each data set. If the estimated initial depth is accurate, you will not receive a new initial depth. To change the initial depth, you must exit the program and edit the input file. Sorry, I'll try to fix that on the next version.

The initial depth must be at least 0.5 percent larger or smaller than the critical depth to start the computations. The flow depth must also be less than 5 percent of the absolute value of the vertical radius of curvature. This restriction is imposed because of errors introduced by non uniform flow distributions with curvilinear flow. If the computations reach a point where the depth exceeds the 5 percent criterion, the computations will stop.

Input Format - The input is read with a free format. This means that the data for each set of items must be on a single line and separated by one or more blanks, or by a comma or a slash, either of which may be preceded or followed by any number of blanks. Blanks are not allowed as substitutes for zero. A decimal point omitted from a real constant is assumed to occur to the right of the right most digit of the mantissa.

Kinetic Energy Correction Factor - A kinetic energy correction factor is applied to every station. The value varies parabolically from 1.0 for no boundary layer to 1.1 for a fully developed boundary layer.

Rugosity - The rugosity can be changed at each station. If the rugosity is not changed at a particular station, input a 0.0 for the value of the rugosity at that station. The program will use the last non zero value of rugosity for the computations. The starting rugosity cannot be equal to zero.

Transition Losses - A transition loss factor can be applied if the cross sectional area changes rapidly. In this case enter a coefficient (usually 0.1) for the variable TLF in the section called initialization of data. The transition loss is equal to the transition loss factor times the difference in the upstream and downstream velocity heads. A factor of 0.1 is the default parameter if the section width changes by more than 0.1 Percent.

Vertical Radius of Curvature - If the invert moves away from the flow, the sign of the vertical radius of curvature is negative. If the section between stations is straight, set the vertical radius of curvature equal to 0. With the interactive data input option, the vertical radius of curvature must be input for the first two stations. After that, the vertical radius of curvature can either be input for each station or it will be computed from the station and invert elevation data.

* * * * *

GLEN CANYON LEFT SPILLWAY TUNNEL—INPUT

283.168	.7437	.30480000	1	0	.785000	609.600	1127.760		
GLEN CANYON LEFT SPILLWAY TUNNEL									
27									
5 2									
637.468	1099.481	22.372	12.65530	2.944368	2.081784	1.83	-75.2	.000000	
5 2									
643.524	1093.488	20.038	10.52779	5.017008	3.563112	.00	-100.5	.000000	
5 2									
649.821	1086.021	17.648	8.91540	6.547104	5.382768	.00	-135.3	.000000	
5 2									
656.253	1077.145	15.639	7.82422	7.278624	6.982968	.00	-181.3	.000000	
2 2									
662.071	1068.836	7.355	-233.3	.000000					
2 2									
678.863	1044.857	6.800	.0	.000000					
2 2									
685.800	1034.946	6.800	.0	.000000					
2 2									
695.651	1020.876	6.248	.0	.000000					
2 2									
709.038	1001.759	6.248	.0	.000000					
2 2									
714.756	994.312	6.248	106.7	.000000					
2 2									
720.852	987.653	6.248	106.7	.000000					
2 2									
732.620	977.451	6.248	106.7	.000000					
2 2									
743.712	970.200	6.248	106.7	.000000					
2 2									
746.760	968.536	6.248	106.7	.000000					
2 2									
754.380	964.902	6.248	106.7	.000000					
2 2									
762.634	961.763	6.248	106.7	.000000					
2 2									
778.764	957.740	6.248	106.7	.000000					
2 2									
796.052	956.270	6.248	106.7	.000000					
2 2									
800.100	956.255	6.248	.0	.000000					
2 2									
801.014	956.252	6.248	.0	.000000					
2 2									
807.720	956.228	6.248	.0	.000000					
2 2									
822.960	956.175	6.248	.0	.000000					
2 2									
853.440	956.069	6.248	.0	.000000					
2 2									
944.880	955.749	6.248	.0	.000000					
2 2									
1021.080	955.481	6.248	.0	.000000					
2 2									
1097.280	955.215	6.248	.0	.000000					
2 2									
1112.520	955.164	6.248	.0	.000000					

* * * * *

TYPICAL OUTPUT

The program output consists of a table of hydraulic properties and a table of cavitation properties. The user also is asked to supply the name of a file to which the geometric properties are to be written. This geometric file is useful in reports where a formatted description of the geometry is needed. Also, the user is asked to supply the name of a plot file. This file is used by the plotting program described in appendix B.

The following pages present an example of the output for the Bureau of Reclamation's Glen Canyon Dam Left Tunnel Spillway. The example includes:

- The hydraulic properties
- The cavitation properties
- The formatted geometry file
- The plot file

HYDRAULIC PROPERTIES OF GLEN CANYON LEFT TUNNEL SPILLWAY—OUTPUT

GLEN CANYON LEFT SPILLWAY TUNNEL

Q = 283.168 CMS INITIAL DEPTH = .744 M RUGOSITY = .30 MM N = .0136

STATION M	INVERT ELEV M	SLOPE	DEPTH M	VELOCITY M/SEC	PIEZ M	ENERGY GRADE LINE M	Q AIR/Q WATER	PROFILE	DEPTH		THICKNESS
									NORMAL M	CRITICAL M	BOUNDARY LAYER M
637.5	1099.48	.7850	.744	20.477	.585	1119.757	.000	S2	.430	3.038	.198
643.5	1093.49	.9896	.787	22.554	.150	1119.757	.000	S2	.456	3.301	.273
649.8	1086.02	1.1858	1.020	24.846	.177	1118.052	.000	S2	.590	4.090	.346
656.3	1077.15	1.3800	1.399	27.401	.223	1116.087	.000	S2	.846	5.092	.418
662.1	1068.84	1.4281	1.552	29.592	.291	1114.171	.000	S2	.999	5.527	.481
678.9	1044.86	1.4280	1.434	34.665	.822	1107.532	.000	S2	1.019	5.705	.637
685.8	1034.95	1.4287	1.389	36.296	.797	1104.237	.000	S2	1.019	5.720	.699
695.7	1020.88	1.4283	1.377	38.485	.790	1099.089	.000	S2	1.043	5.877	.783
709.0	1001.76	1.4280	1.318	41.048	.756	1091.196	.000	S2	1.043	5.887	.890
714.8	994.31	1.3024	1.313	41.241	3.032	1088.013	.000	S2	1.051	5.918	.933
720.9	987.65	1.0924	1.300	41.877	3.166	1084.738	.000	S2	1.070	5.765	.973
732.6	977.45	.8669	1.283	42.705	3.329	1078.968	.000	S2	1.101	5.603	1.041
743.7	970.20	.6537	1.277	42.977	3.471	1074.040	.000	S2	1.151	5.467	1.097
746.8	968.54	.5459	1.279	42.887	3.536	1072.766	.000	S2	1.189	5.408	1.112
754.4	964.90	.4769	1.277	42.962	3.576	1069.697	.000	S2	1.221	5.371	1.147
762.6	961.76	.3803	1.280	42.845	3.622	1066.538	.000	S3	1.280	5.328	1.184
778.8	957.74	.2494	1.290	42.321	3.650	1060.526	.000	S3	1.407	5.282	1.253
796.1	956.27	.0850	1.316	41.137	3.639	1054.316	.000	S3	1.826	5.256	1.316
800.1	956.26	.0037	1.313	41.236	1.313	1052.931	.614	S3	4.102	5.178	1.313
801.0	956.25	.0033	1.315	41.166	1.315	1052.607	.660	S3	4.245	5.178	1.315
807.7	956.23	.0036	1.326	40.661	1.326	1050.277	.587	S3	4.143	5.178	1.326
823.0	956.17	.0035	1.351	39.553	1.351	1045.263	.523	S3	4.174	5.178	1.351
853.4	956.07	.0035	1.402	37.488	1.402	1036.285	.399	S3	4.175	5.178	1.402
944.9	955.75	.0035	1.554	32.241	1.554	1015.599	.000	S3	4.168	5.178	1.554
1021.1	955.48	.0035	1.679	28.817	1.679	1003.732	.000	S3	4.162	5.178	1.679
1097.3	955.22	.0035	1.802	26.001	1.802	994.932	.000	S3	4.171	5.178	1.802
1112.5	955.16	.0033	1.826	25.501	1.826	993.459	.000	S3	4.219	5.178	1.826

ENERGY GRADE LINE AT BEGINNING OF BOUNDARY LAYER
1127.665

* * * * *

CAVITATION PROPERTIES OF GLEN CANYON LEFT TUNNEL SPILLWAY—OUTPUT

GLEN CANYON LEFT SPILLWAY TUNNEL

Q = 283.168 CMS INITIAL DEPTH = .744 M RUGOSITY = .30 MM N = .0136

CAVITATION CHARACTERISTICS

STATION	FLOW SIGMA	SIGMA OF UNIFORM ROUGHNESS	REQUIRED CHAMFER TO STOP CAVITATION	DAMAGE POTENTIAL						TURBULENCE INTENSITY
				CIRCULAR ARC			90-DEGREE OFFSET			
				1/4-IN 5-MM	1/2-IN 10-MM	1-IN 25-MM	1/4-IN 5-MM	1/2-IN 10-MM	1-IN 25-MM	
637.47	.425	.052	1 TO 8	.244E+01	.720E+01	.243E+02	.578E+01	.157E+02	.517E+02	.0321
643.52	.350	.051	1 TO 11	.727E+01	.188E+02	.588E+02	.135E+02	.343E+02	.108E+03	.0310
649.82	.290	.049	1 TO 14	.195E+02	.470E+02	.139E+03	.310E+02	.755E+02	.230E+03	.0303
656.25	.240	.048	1 TO 18	.497E+02	.114E+03	.328E+03	.708E+02	.167E+03	.496E+03	.0297
662.07	.207	.048	1 TO 23	.994E+02	.224E+03	.628E+03	.132E+03	.305E+03	.893E+03	.0292
678.86	.160	.048	1 TO 32	.331E+03	.722E+03	.198E+04	.385E+03	.870E+03	.249E+04	.0284
685.80	.146	.049	1 TO 37	.503E+03	.109E+04	.296E+04	.563E+03	.126E+04	.360E+04	.0282
695.65	.130	.049	1 TO 43	.844E+03	.181E+04	.490E+04	.902E+03	.201E+04	.569E+04	.0279
709.04	.114	.049	1 TO 52	.150E+04	.319E+04	.857E+04	.152E+04	.336E+04	.946E+04	.0275
714.76	.139	.049	1 TO 39	.636E+03	.137E+04	.372E+04	.636E+03	.143E+04	.406E+04	.0274
720.85	.137	.049	1 TO 40	.692E+03	.149E+04	.404E+04	.681E+03	.153E+04	.433E+04	.0273
732.62	.133	.049	1 TO 42	.769E+03	.166E+04	.448E+04	.740E+03	.165E+04	.470E+04	.0271
743.71	.133	.049	1 TO 42	.766E+03	.165E+04	.446E+04	.724E+03	.162E+04	.460E+04	.0270
746.76	.134	.049	1 TO 41	.731E+03	.158E+04	.426E+04	.689E+03	.154E+04	.439E+04	.0270
754.38	.134	.049	1 TO 41	.727E+03	.157E+04	.424E+04	.679E+03	.152E+04	.432E+04	.0269
762.63	.136	.049	1 TO 41	.691E+03	.149E+04	.404E+04	.640E+03	.143E+04	.408E+04	.0268
778.76	.139	.049	1 TO 39	.601E+03	.130E+04	.352E+04	.548E+03	.123E+04	.352E+04	.0267
796.05	.147	.049	1 TO 36	.455E+03	.989E+03	.269E+04	.412E+03	.932E+03	.267E+04	.0265
800.10	.120	.049	1 TO 49	.110E+04	.236E+04	.635E+04	.998E+03	.222E+04	.629E+04	.0265
801.01	.120	.049	1 TO 48	.108E+04	.232E+04	.624E+04	.982E+03	.219E+04	.619E+04	.0265
807.72	.123	.049	1 TO 47	.958E+03	.206E+04	.555E+04	.870E+03	.194E+04	.550E+04	.0265
822.96	.131	.049	1 TO 43	.729E+03	.157E+04	.425E+04	.662E+03	.148E+04	.422E+04	.0265
853.44	.146	.049	1 TO 37	.427E+03	.928E+03	.253E+04	.388E+03	.878E+03	.252E+04	.0264
944.88	.201	.048	1 TO 24	.905E+02	.205E+03	.578E+03	.822E+02	.194E+03	.577E+03	.0261
1021.08	.254	.047	1 TO 17	.267E+02	.635E+02	.187E+03	.242E+02	.604E+02	.187E+03	.0260
1097.28	.316	.046	1 TO 13	.792E+01	.206E+02	.643E+02	.710E+01	.195E+02	.647E+02	.0258
1112.52	.329	.046	1 TO 12	.618E+01	.165E+02	.523E+02	.553E+01	.156E+02	.527E+02	.0258

* * * * *

FORMATTED GEOMETRY FILE OF GLEN CANYON LEFT TUNNEL SPILLWAY—OUTPUT

STATION GEOMETRY FOR WATER SURFACE PROFILE PROGRAM GLEN CANYON LEFT SPILLWAY TUNNEL

STA	INVERT ELEV	WIDTH OR R2	SIDE SLOPE	RADIUS	UPPER RADIUS	CL HEIGHT	LOWER RADIUS	WALL OR C2	RAD CURV	RUGOSITY
637.47	1099.48	22.37			12.66	2.94	2.08	1.83	-75.2	.0003
643.52	1093.49	20.04			10.53	5.02	3.56	.00	-100.5	.0003
649.82	1086.02	17.65			8.92	6.55	5.38	.00	-135.3	.0003
656.25	1077.15	15.64			7.82	7.28	6.98	.00	-181.3	.0003
662.07	1068.84			7.36					-233.3	.0003
678.86	1044.86			6.80					.0	.0003
685.80	1034.95			6.80					.0	.0003
695.65	1020.88			6.25					.0	.0003
709.04	1001.76			6.25					.0	.0003
714.76	994.31			6.25					106.7	.0003
720.85	987.65			6.25					106.7	.0003
732.62	977.45			6.25					106.7	.0003
743.71	970.20			6.25					106.7	.0003
746.76	968.54			6.25					106.7	.0003
754.38	964.90			6.25					106.7	.0003
762.63	961.76			6.25					106.7	.0003
778.76	957.74			6.25					106.7	.0003
796.05	956.27			6.25					106.7	.0003
800.10	956.26			6.25					.0	.0003
801.01	956.25			6.25					.0	.0003
807.72	956.23			6.25					.0	.0003
822.96	956.17			6.25					.0	.0003
853.44	956.07			6.25					.0	.0003
944.88	955.75			6.25					.0	.0003
1021.08	955.48			6.25					.0	.0003
1097.28	955.22			6.25					.0	.0003
1112.52	955.16			6.25					.0	.0003

* * * * *

PLOT FILE OF GLEN CANYON LEFT TUNNEL SPILLWAY—OUTPUT

GLEN CANYON LEFT SPILLWAY TUNNEL							
NO OF PLOTS	1	NO STA	27				
DISCHARGE							
283.168							
STATION							
637.468	643.524	649.821	656.253	662.071	678.863	685.800	695.651
709.038	714.756	720.852	732.620	743.712	746.760	754.380	762.634
778.764	796.052	800.100	801.014	807.720	822.960	853.440	944.880
1021.080	1097.280	1112.520					
ELEVATION							
1099.481	1093.488	1086.021	1077.145	1068.836	1044.857	1034.946	1020.876
1001.759	994.312	987.653	977.451	970.200	968.536	964.902	961.763
957.740	956.270	956.255	956.252	956.228	956.175	956.069	955.749
955.481	955.215	955.164					
FLOW DEPTH							
.744	.787	1.020	1.399	1.552	1.434	1.389	1.377
1.318	1.313	1.300	1.283	1.277	1.279	1.277	1.280
1.290	1.316	1.313	1.315	1.326	1.351	1.402	1.554
1.679	1.802	1.826					
PIEZOMETRIC PRESSURE							
.159	.150	.177	.223	.291	.822	.797	.790
.756	3.032	3.166	3.329	3.471	3.536	3.576	3.622
3.650	3.639	1.313	1.315	1.326	1.351	1.402	1.554
1.679	1.802	1.826					
SIGMA							
.4248	.3501	.2896	.2396	.2071	.1600	.1458	.1298
.1139	.1392	.1366	.1332	.1331	.1344	.1344	.1357
.1394	.1474	.1199	.1203	.1235	.1308	.1463	.2007
.2541	.3158	.3290					
DAMAGE POTENTIAL							
.720E+01	.188E+02	.470E+02	.114E+03	.224E+03	.722E+03	.109E+04	.181E+04
.319E+04	.137E+04	.149E+04	.166E+04	.165E+04	.158E+04	.157E+04	.149E+04
.130E+04	.989E+03	.236E+04	.232E+04	.206E+04	.157E+04	.928E+03	.205E+03
.635E+02	.206E+02	.165E+02					
BOUNDARY LAYER THICKNESS							
.20	.27	.35	.42	.48	.64	.70	.78
.89	.93	.97	1.04	1.10	1.11	1.15	1.18
1.25	1.32	1.31	1.31	1.33	1.35	1.40	1.55
1.68	1.80	1.83					

* * * * *

BIBLIOGRAPHY

- [1] Chow, V. T., *Open Channel Hydraulics*, McGraw Hill, 1959.
- [2] Tilp, P. M., Scrivner, M. W., "Analysis and Description of Capacity Tests in Large Concrete-Lined Canals," Bureau of Reclamation Technical Memorandum 661, 1964.
- [3] Bradley, J. N., Thompson, L. R., "Friction Factors for Large Conduits Flowing Full," Bureau of Reclamation Engineering Monograph No. 4, 1951, out of print.
- [4] Eskinazi, S., *Principles of Fluid Mechanics*, Allyn and Bacon, Inc., Boston, 2d ed., 1968.
- [5] Posey, C. M., "Gradually Varied Channel Flow," *Engineering Hydraulics*, edited by H. Rouse, John Wiley and Sons, 1949.

Cavitation and Flow Characteristics Plotting Program

PROGRAM DESCRIPTION

The program is written in PLOT88¹ which is compatible with Microsoft-Fortran.² As input, it uses the plot file created with the appendix A program. The user can select the type of plot desired. Two types of plots are available—water surface profile information and cavitation information.

A wide variety of communications ports and output devices are supported. The user is requested to supply a number to identify the interface type for the output port and a number to identify the model of the device to be used for plotting the output. A complete list of communication ports (output interface) and output devices (model of plotter or printer), with their respective identification numbers, is given below.³ Communication port and output device numbers are also given to send the plots to the computer console screen.³

Communications Ports

Output No.	Interface type	Baud	Parity	Data bits
0	PRN: (Equivalent to LPT1:)			
1	LPT1:			
2	LPT2:			
3	LPT3:			
10	Disk file output for deferred printing			
300	COM1:	300	none	8
301	COM1:	300	even	7
302	COM1:	300	odd	7
1200	COM1:	1200	none	8
1201	COM1:	1200	even	7
1202	COM1:	1200	odd	7

		Baud	Parity	Data bits
2400	COM1:	2400	none	8
2401	COM1:	2400	even	7
2402	COM1:	2400	odd	7
9600	COM1:	9600	none	8
9601	COM1:	9600	even	7
9602	COM1:	9600	odd	7

All COM devices have 1 stop bits. If COM2: devices are used, add 50 to the identification number of the COM1 devices listed above.

Model of Output Device

Device No.	Device identification
0	Epson FX-80 printer, single density
1	Epson FX-80 printer, double density
2	Epson FX-80 printer, double speed, dual density
3	Epson FX-80 printer, quad density
4	Epson FX-80 printer, CRT graphics I
5	Epson FX-80 printer, plotter graphics
6	Epson FX-80 printer, CRT graphics II
10	Epson FX-100 printer, single density
11	Epson FX-100 printer, double density
12	Epson FX-100 printer, double speed, dual density
13	Epson FX-100 printer, quad density
14	Epson FX-100 printer, CRT graphics I
15	Epson FX-100 printer, plotter graphics
16	Epson FX-100 printer, CRT graphics II
20	HP 7470A graphics plotter
30	HP 7475A graphics plotter
40	Epson LQ-1500 printer, single density
41	Epson LQ-1500 printer, double density
42	Epson LQ-1500 printer, double speed, dual density
43	Epson LQ-1500 printer, quad density,
51	Houston Instrument DMP-51 MP, DMP-52 MP, DMP-56, 0.001 inch step size
52	Houston Instrument DMP-51 MP, DMP-52 MP, DMP-56, 0.002 inch step size
56	Houston Instrument DMP-56, 0.001 inch step size, E size paper

¹ Registered trademark of Plotworks, Inc., PO Box 12385, La Jolla, CA, 92037-0635.
² Registered trademark of Microsoft Corp., 16011 NE 36th Way, Box 97017, Redmond, WA, 98073-9717.
³ Reproduced from PLOT88 Software Library Reference Manual with permission of Plotworks, Inc.

<i>Device No.</i>	<i>Device identification</i>	<i>Device No.</i>	<i>Device identification</i>
60	HP LaserJet Printer, A size paper, 75 dots per inch	70	HP ThinkJet (2225A) Printer, low density
61	HP LaserJet Printer, B5 size paper, 75 dots per inch	71	HP ThinkJet (2225A) Printer, high density
62	HP LaserJet Printer, A size paper, 150 dots per inch	72	HP ThinkJet (2228A) Printer, single density
63	HP LaserJet Printer, B5 size paper, 150 dots per inch	73	HP ThinkJet (2228A) Printer, double density
64	HP LaserJet Printer, A size paper, 300 dots per inch	74	HP ThinkJet (2228A) Printer, quad density
65	HP LaserJet Printer, B5 size paper, 300 dots per inch	75	HP QuietJet Plus (2227A) Printer, single density
		76	HP QuietJet Plus (2227A) Printer, double density
		77	HP QuietJet Plus (2227A) Printer, quad density
		80	HP 7580B, HP 7585B, HP 7586B, HP 7595A or HP 7596A Drafting Plotter
		85	HP 7585B, HP7586B, HP 7595A, or HP 7596A Drafting Plotter
		90	Tektronix 4025

<i>Display adapter</i>	<i>Display</i>	<i>No. of colors</i>	<i>Resolution, (x by y)</i>	<i>Output No.</i>	<i>Device No.</i>
Hercules	Monochrome	2	720 × 348	93	93
CGA	Color graphics	2	640 × 200	99	99
CGA	Composite Monochrome	2	640 × 200	99	99
EGA (64K)	Color graphics	16	320 × 200	94	94
EGA (64K)	Color graphics	16	640 × 200	95	95
EGA (64K)	Color graphics	2	640 × 200	99	99
EGA (64K)	Enhanced graphics	2	640 × 200	99	99
EGA (64K)	Enhanced graphics	16	320 × 200	94	94
EGA (64K)	Enhanced graphics	16	640 × 200	95	95
EGA (128K)	Monochrome	2	640 × 200	96	96
EGA (128K)	Enhanced graphics	16	640 × 350	97	97

PROGRAM OUTPUT

The output can be placed on six types of plots as shown on figure B-1 (from bottom to top):

1. Invert profile
2. Cavitation index
3. Damage potential
4. Water surface profile
5. Piezometric pressure
6. Boundary layer thickness

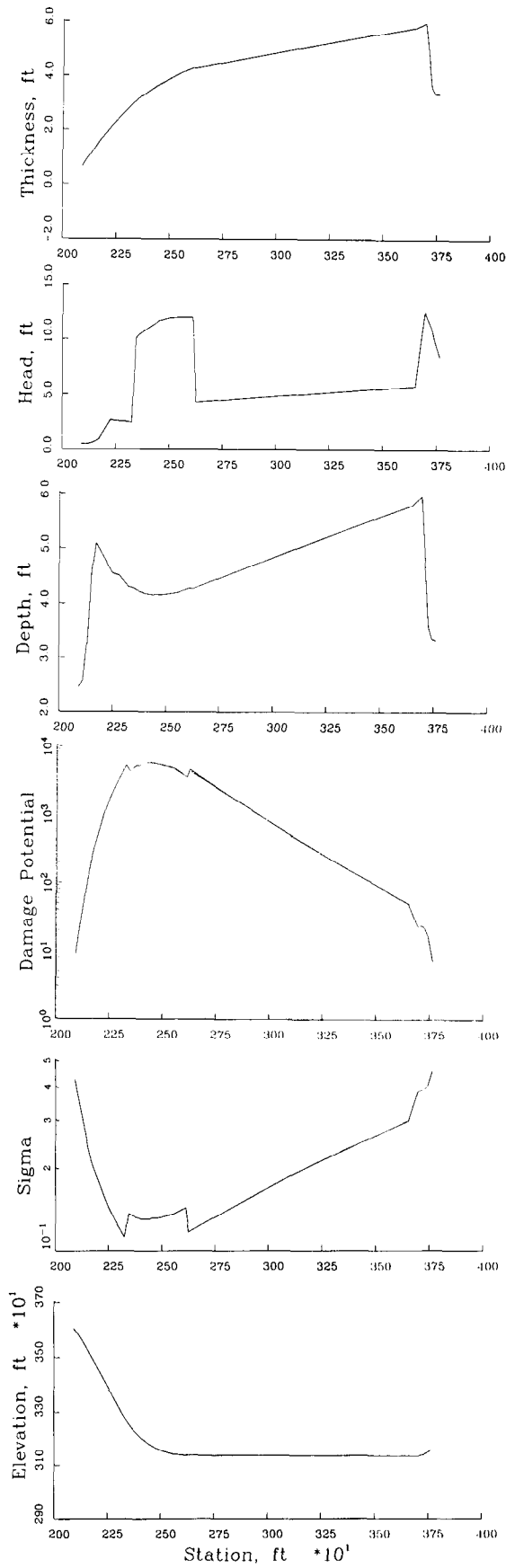


FIGURE B-1.—Glen Canyon Dam, left spillway tunnel — comparisons of outputs.

Geometry Programs

PROGRAM DESCRIPTION

This appendix contains three programs useful in determining boundary geometries for spillways and chutes having vertical curves. The first program can be used to determine a constant cavitation number profile. This shape has application for hydraulic structures that terminate in a flip bucket. The second and third programs can be used to determine profiles where the pressure through a vertical bend is to be controlled. The radius of curvature, at both ends of the vertical curve, is infinite with these latter two programs. The first of the controlled pressure programs produces a triangular variation in the pressure distribution through the vertical curve; the second produces a sinusoidal variation.

The programs have been documented internally. Basic mathematical algorithms are explained in chapter 4. The constant cavitation number program requires an external data file for the input of the geometric parameters. The two controlled pressure programs are short enough that the geometry can be easily input interactively during program execution. All three programs are written in Microsoft-Fortran.¹

CONSTANT CAVITATION NUMBER SPILLWAY

The constant cavitation number program solves a variation of the dimensionless form of the differential equations given in chapter 4. The equations are made dimensionless so that the dependent variables vary approximately between 0 and 1. The dimensionless variables are defined as:

$$\eta = \frac{H_b}{H_i} \quad \xi = \frac{X}{H_i} \quad A_n = \frac{P_a - P_v}{\rho g H_i} \quad F = \cos \theta$$

$$q_n = \frac{q}{(2g H_i^2)^{1/2}} \quad d_n = \frac{d}{H_i} \quad R_n = \frac{R}{H_i}$$

$$\mu = \frac{B_u - B_l}{L} \left(\frac{H_i}{B_u} \right)$$

where:

A_n = dimensionless pressure ratio

$A_n = (P_a - P_v)/(\rho g H_i)$

B_u = width at upstream end of constant cavitation profile

B_l = width at downstream end of constant cavitation profile

d = flow depth normal to invert

d_n = dimensionless flow depth

F = cosine of invert slope

g = gravitational constant (acceleration)

H_b = reservoir elevation minus elevation at point b

H_i = initial head at beginning of constant cavitation number spillway

L = difference in stationing between upper and lower ends of spillway

P_a = atmospheric pressure

P_v = vapor pressure of water

q = unit discharge of water

q_n = dimensionless unit discharge

R = radius of curvature of reference streamline

R_n = dimensionless radius of curvature

X = horizontal distance from beginning of vertical curve

ξ = dimensionless distance horizontal

η = dimensionless head

μ = dimensionless convergence ratio

ρ = density of water

The dimensionless equations are:

$$\frac{dF}{d\eta} = \frac{1}{R_n} \quad \text{C.1}$$

$$\frac{d\xi}{d\eta} = \frac{F}{(1 - F^2)^{1/2}} \quad \text{C.2}$$

For rotational flow, the dimensionless flow depth and radius of curvature are defined as:

$$d_n = \frac{q_n (1 - d_n/R_n)}{[1 - d_n/(2R_n)] (\eta - d_n F)^{1/2}} \quad \text{C.3}$$

and

$$\frac{1}{R_n} = \frac{\sigma (\eta - d_n F) - (d_n F + A_n) (1 - d_n/R_n)^2}{2 d_n [1 - d_n/(2R_n)] (\eta - d_n F)} \quad \text{C.4}$$

¹ A registered trademark of Microsoft Corporation, 16011 NE, 36th Way, Box 97017, Redman, WA, 98073-9717

For irrotational flow, the dimensionless flow depth and radius of curvature are defined as:

$$d_n = \frac{q_n (d_n/R_n)}{(d_n/R_n - 1) [\ln(1 - d_n/R_n)] (\eta - d_n F)^{1/2}} \quad \text{C.5}$$

and

$$\frac{1}{R_n} = \frac{[(\sigma + 1)(\eta - d_n F)]^{1/2} - (\eta + A_n)^{1/2}}{d_n [(\sigma + 1)(\eta - d_n F)]^{1/2}} \quad \text{C.6}$$

The differential equations are solved simultaneously using the Runge-Kutta method.² The equations are subject to the following initial conditions:

$$\begin{aligned} \eta_i &= 1 & \xi_i &= 0 & F_i &= \cos \xi_i \\ q_i &= \frac{q}{(2g H_i^2)^{1/2}} & d_i &= \frac{q_i}{(1 - d_i F_i)^{1/2}} \end{aligned}$$

where the subscript, i , refers to conditions at the start of the constant cavitation number spillway.

The initial depth, d_i , requires an iterative procedure for its solution.

CONTROLLED PRESSURE SPILLWAY

The controlled pressure spillway program solves the equations given in chapter 4. The integration is accomplished using Simpson's rule:

$$\int_a^b f(X) dX = \frac{h}{3} (f_0 + 4 f_1 + f_2) \quad \text{C.7}$$

where:

- $f_0, f_1, \& f_2$ = function value at points 0, 1, and 2
- $f(X)$ = a function in terms of distance X
- h = interval between points 0, 1, and 2
- X = distance

The functions solved in equation C.7 are:

$$\frac{dx}{ds} = \cos \theta \quad \text{C.8}$$

and

$$\frac{dy}{ds} = \sin \theta \quad \text{C.9}$$

Angle, θ , is given by the following relationships. Triangular distribution by:

$$0 \leq s \leq s_m/2, \quad \theta = k s^2/2 + \theta_o \quad \text{C.10}$$

$$s_m \leq s \leq s_m, \quad \theta = k (s_m s - s_m^2/4 - s^2/2) + \theta_o \quad \text{C.11}$$

Sinusoidal distribution by:

$$\begin{aligned} \theta &= \frac{s_m^2}{2} - \left(\frac{s_m}{2\pi}\right)^2 \cos [2\pi (s/s_m)] \\ &\quad - \left(\frac{s_m}{2\pi}\right) \sin [2\pi (s/s_m)] + \left(\frac{s_m}{2\pi}\right)^2 + \theta_o \end{aligned} \quad \text{C.12}$$

where:

- k = constant to control the length of the curve or the minimum radius of curvature
- s = distance along invert
- s_m = maximum invert distance
- θ = angle between tangent to invert and horizontal
- θ_o = angle at beginning of curve

The maximum length of the curve is given as follows. Triangular distribution by:

$$s_m = \left(\frac{4 \theta_d}{k}\right)^{1/2} \quad \text{C.13}$$

Sinusoidal distribution by:

$$s_m = \left(\frac{2 \theta_d}{k}\right)^{1/2} \quad \text{C.14}$$

where:

- θ_d = deflection angle = $\theta_o - \theta_t$
- θ_t = angle at end of curve

The minimum radius of curvature, R_m , of the controlled pressure invert (with either the triangular or the sinusoidal distribution) is given by:

$$R_m = \frac{1}{k s_m} \quad \text{C.15}$$

The program is written so that the value of the constant, k , can be chosen to be approximately equal to unity. The result is a curve that is similar to the desired curve; but a curve which will not pass through the given elevations at the two ends of the curve. To obtain the desired curve, a scaling factor is applied to the computed curve obtained by assuming $k = 1.0$. This method eliminates the need to seek the proper value of k by trial and error. The curvature of the invert curve can be modified by setting the value of k either larger or smaller than 1.0. Increasing k results in a smaller value of the minimum radius of curvature. To flatten out the curve (a larger value of the minimum radius of curvature), the value of k must be chosen to be less than 1.0.

² Wylie, C.R., Barrett, L.C., *Advanced Engineering Mathematics*, McGraw-Hill Book Co., 1982.

CONSTANT CAVITATION NUMBER INPUT

The input file for the constant cavitation number profile program consists of three lines.

The first line consists of the title of the project consisting of not more than 60 characters.

The second line consists of selecting the type of velocity distribution in the vertical elbow.

- If rotational flow is selected, respond with "Y."
- If irrotational flow is selected, respond with "N."

The third line consists of nine items that describe the pertinent geometries and initial conditions (point of curvature). They are:

- Cosine of slope at point of curvature
- Station at point of curvature
- Head from reservoir to point of curvature
- Unit discharge
- Convergence of sidewalls
- Atmospheric pressure minus water vapor pressure
- Gravitational constant (acceleration)
- Integration interval, in delta head
- Reservoir elevation

For example, the input to calculate the constant cavitation number for the Glen Canyon Dam spillway is as follows:

Equal Cavitation Number Input

THE FIRST LINE

THE TITLE (UP TO 60 CHARACTERS)

THE SECOND LINE

TWO ASSUMPTIONS ARE POSSIBLE FOR THE VELOCITY
DISTRIBUTION IN THE VERTICAL BEND;

A ROTATIONAL ASSUMPTION
IN THIS CASE SET THE LINE = Y.

AN IRRATIONAL ASSUMPTION
IN THIS CASE SET THE LINE = N.

THE THIRD LINE

COSINE OF SLOPE AT POINT OF CURVATURE
STATION AT POINT OF CURVATURE
HEAD FROM RESERVOIR TO POINT OF CURVATURE
UNIT DISCHARGE
CONVERGENCE OF SIDEWALLS
ATMOSPHERIC PRESSURE MINUS VAPOR PRESSURE OF WATER
GRAVITATIONAL CONSTANT
INTEGRATION INTERVAL IN DELTA HEAD
RESERVOIR ELEVATION

GLEN CANYON DAM LEFT TUNNEL SPILLWAY

N
0.4112 678.863 92.627 172.500 0.0 10.0 9.8076 1.0 1127.760

* * * * *

CONSTANT CAVITATION NUMBER OUTPUT—SOLID BODY ROTATION ASSUMPTION

The output for the constant cavitation number consists of geometrical properties, flow depths, and piezometric pressures. The controlling factor on the change in elevation was the integration interval given in the input. For the Glen Canyon Spillway, 1 meter was chosen as the interval. The 1-meter interval stays constant until station 7+56.88. At that point, the interval is decreased (by the program) to provide more data points near the terminal end of the curve.

EQUAL CAVITATION NUMBER PROFILE GLEN CANYON DAM LEFT TUNNEL SPILLWAY

SOLID BODY ROTATION ASSUMPTION
UNIT DISCHARGE - 172.50 SIGMA - .128

STA	ELEV	RADIUS	SLOPE DEGREES	DEPTH	PIEZ
678.86	1035.13	.100E+11	65.7	4.084	1.679
679.31	1034.13	.495E+04	65.7	4.075	1.828
679.77	1033.13	.233E+04	65.7	4.029	1.980
680.22	1032.13	.153E+04	65.7	3.983	2.133
680.67	1031.13	.114E+04	65.6	3.939	2.284
681.12	1030.13	.914E+03	65.6	3.896	2.436
681.58	1029.13	.763E+03	65.5	3.854	2.587
682.04	1028.13	.656E+03	65.4	3.812	2.738
682.50	1027.13	.576E+03	65.3	3.772	2.888
682.96	1026.13	.513E+03	65.2	3.733	3.038
683.42	1025.13	.464E+03	65.0	3.694	3.188
683.89	1024.13	.423E+03	64.9	3.656	3.338
684.36	1023.13	.389E+03	64.7	3.619	3.487
684.83	1022.13	.361E+03	64.6	3.583	3.636
685.31	1021.13	.337E+03	64.4	3.548	3.785
685.79	1020.13	.315E+03	64.2	3.513	3.934
686.28	1019.13	.297E+03	64.0	3.479	4.082
686.77	1018.13	.280E+03	63.8	3.446	4.230
687.26	1017.13	.266E+03	63.5	3.413	4.378
687.76	1016.13	.253E+03	63.3	3.382	4.526
688.27	1015.13	.241E+03	63.0	3.350	4.673
688.78	1014.13	.230E+03	62.8	3.319	4.821
689.30	1013.13	.221E+03	62.5	3.289	4.968
689.82	1012.13	.212E+03	62.2	3.260	5.115
690.35	1011.13	.204E+03	61.9	3.231	5.261
690.89	1010.13	.196E+03	61.5	3.202	5.408
691.44	1009.13	.189E+03	61.2	3.174	5.554
691.99	1008.13	.183E+03	60.8	3.147	5.701
692.55	1007.13	.177E+03	60.5	3.120	5.847
693.13	1006.13	.172E+03	60.1	3.093	5.993
693.70	1005.13	.166E+03	59.7	3.067	6.139
694.29	1004.13	.161E+03	59.3	3.042	6.284
694.89	1003.13	.157E+03	58.9	3.016	6.430
695.50	1002.13	.153E+03	58.5	2.992	6.575
696.12	1001.13	.149E+03	58.0	2.967	6.720
696.75	1000.13	.145E+03	57.5	2.943	6.866
697.39	999.13	.141E+03	57.1	2.920	7.011
698.05	998.13	.138E+03	56.6	2.897	7.156
698.71	997.13	.135E+03	56.1	2.874	7.293

EQUAL CAVITATION NUMBER PROFILE
GLEN CANYON DAM LEFT TUNNEL SPILLWAY

STA	ELEV	RADIUS	SLOPE DEGREES	DEPTH	PIEZ
699.39	996.13	.131E+03	55.6	2.852	7.445
700.08	995.13	.128E+03	55.0	2.830	7.590
700.79	994.13	.126E+03	54.5	2.808	7.734
701.51	993.13	.123E+03	53.9	2.786	7.879
702.25	992.13	.120E+03	53.3	2.765	8.023
703.00	991.13	.118E+03	52.7	2.745	8.167
703.77	990.13	.116E+03	52.1	2.724	8.311
704.56	989.13	.113E+03	51.5	2.704	8.455
705.37	988.13	.111E+03	50.8	2.685	8.599
706.19	987.13	.109E+03	50.1	2.665	8.743
707.04	986.13	.107E+03	49.4	2.646	8.887
707.90	985.13	.105E+03	48.7	2.627	9.031
708.79	984.13	.104E+03	48.0	2.608	9.174
709.71	983.13	.102E+03	47.2	2.590	9.318
710.64	982.13	.100E+03	46.5	2.572	9.461
711.61	981.13	.984E+02	45.7	2.554	9.604
712.60	980.13	.969E+02	44.8	2.536	9.748
713.62	979.13	.953E+02	44.0	2.519	9.891
714.67	978.13	.938E+02	43.1	2.502	10.034
715.76	977.13	.924E+02	42.2	2.485	10.177
716.88	976.13	.910E+02	41.3	2.468	10.320
718.04	975.13	.897E+02	40.3	2.452	10.463
719.24	974.13	.884E+02	39.3	2.436	10.606
720.49	973.13	.871E+02	38.2	2.420	10.749
721.78	972.13	.859E+02	37.1	2.404	10.892
723.13	971.13	.847E+02	36.0	2.389	11.035
724.53	970.13	.836E+02	34.8	2.373	11.177
726.00	969.13	.825E+02	33.6	2.358	11.320
727.54	968.13	.814E+02	32.3	2.343	11.463
729.17	967.13	.803E+02	31.0	2.328	11.605
730.88	966.13	.793E+02	29.6	2.314	11.748
732.70	965.13	.783E+02	28.1	2.299	11.890
734.64	964.13	.774E+02	26.5	2.285	12.032
736.72	963.13	.764E+02	24.7	2.271	12.175
738.99	962.13	.755E+02	22.9	2.257	12.317
741.49	961.13	.746E+02	20.8	2.244	12.459
744.29	960.13	.737E+02	18.5	2.230	12.602
747.52	959.13	.729E+02	15.9	2.217	12.744
751.45	958.13	.720E+02	12.7	2.203	12.886
756.88	957.13	.712E+02	8.2	2.190	13.028
757.59	957.03	.711E+02	7.7	2.189	13.042
758.37	956.93	.711E+02	7.0	2.188	13.056
759.22	956.83	.710E+02	6.3	2.187	13.071
760.18	956.73	.709E+02	5.6	2.185	13.085
761.29	956.63	.708E+02	4.7	2.184	13.099
762.69	956.53	.707E+02	3.5	2.183	13.113
764.87	956.43	.707E+02	1.8	2.181	13.127
765.22	956.42	.707E+02	1.5	2.181	13.129
765.65	956.41	.707E+02	1.1	2.181	13.130
766.31	956.40	.706E+02	.6	2.181	13.132
767.06	956.40	.706E+02	.0	2.181	13.132

* * * * *

CONSTANT CAVITATION NUMBER OUTPUT—IRROTATIONAL FLOW ASSUMPTION

The output for the irrotational flow assumption is similar to the solid body rotation assumption, except that the curve is about 32 meters longer.

EQUAL CAVITATION NUMBER PROFILE GLEN CANYON DAM LEFT TUNNEL SPILLWAY

POTENTIAL FLOW ASSUMPTION
UNIT DISCHARGE = 172.50 SIGMA = .128

STA	ELEV	RADIUS	SLOPE DEGREES	DEPTH	PIEZ
678.86	1035.13	.100E+11	65.7	4.084	1.679
679.31	1034.13	.612E+04	65.7	4.063	1.793
679.77	1033.13	.308E+04	65.7	4.042	1.907
680.22	1032.13	.207E+04	65.7	4.022	2.021
680.67	1031.13	.157E+04	65.6	4.002	2.135
681.12	1030.13	.127E+04	65.6	3.982	2.248
681.58	1029.13	.106E+04	65.5	3.962	2.362
682.03	1028.13	.919E+03	65.5	3.943	2.476
682.49	1027.13	.810E+03	65.4	3.924	2.590
682.95	1026.13	.726E+03	65.3	3.905	2.704
683.41	1025.13	.659E+03	65.2	3.887	2.817
683.87	1024.13	.603E+03	65.1	3.869	2.931
684.34	1023.13	.557E+03	65.0	3.851	3.045
684.80	1022.13	.518E+03	64.9	3.833	3.159
685.27	1021.13	.485E+03	64.8	3.816	3.273
685.75	1020.13	.456E+03	64.6	3.799	3.386
686.22	1019.13	.430E+03	64.5	3.782	3.500
686.70	1018.13	.408E+03	64.3	3.765	3.614
687.18	1017.13	.388E+03	64.2	3.749	3.728
687.67	1016.13	.370E+03	64.0	3.733	3.842
688.16	1015.13	.354E+03	63.8	3.717	3.955
688.65	1014.13	.340E+03	63.7	3.701	4.069
689.15	1013.13	.326E+03	63.5	3.685	4.183
689.65	1012.13	.314E+03	63.3	3.670	4.297
690.15	1011.13	.303E+03	63.1	3.655	4.411
690.67	1010.13	.293E+03	62.8	3.639	4.524
691.18	1009.13	.284E+03	62.6	3.625	4.638
691.70	1008.13	.275E+03	62.4	3.610	4.752
692.23	1007.13	.267E+03	62.1	3.596	4.866
692.76	1006.13	.259E+03	61.9	3.581	4.980
693.29	1005.13	.252E+03	61.6	3.567	5.093
693.84	1004.13	.245E+03	61.4	3.553	5.207
694.39	1003.13	.239E+03	61.1	3.539	5.321
694.94	1002.13	.233E+03	60.8	3.526	5.435
695.50	1001.13	.228E+03	60.6	3.512	5.549
696.07	1000.13	.223E+03	60.3	3.499	5.662
696.65	999.13	.218E+03	60.0	3.486	5.776
697.23	998.13	.213E+03	59.6	3.473	5.890
697.82	997.13	.209E+03	59.3	3.460	6.004

**EQUAL CAVITATION NUMBER PROFILE
GLEN CANYON DAM LEFT TUNNEL SPILLWAY**

STA	ELEV	RADIUS	SLOPE DEGREES	DEPTH	PIEZ
698.41	996.13	.204E+03	59.0	3.447	6.118
699.02	995.13	.200E+03	58.7	3.435	6.232
699.63	994.13	.197E+03	58.3	3.422	6.345
700.25	993.13	.193E+03	58.0	3.410	6.459
700.88	992.13	.190E+03	57.6	3.398	6.573
701.52	991.13	.186E+03	57.3	3.386	6.687
702.17	990.13	.183E+03	56.9	3.374	6.801
702.82	989.13	.180E+03	56.5	3.362	6.914
703.49	988.13	.177E+03	56.1	3.350	7.028
704.16	987.13	.174E+03	55.8	3.339	7.142
704.85	986.13	.172E+03	55.4	3.327	7.256
705.55	985.13	.169E+03	54.9	3.316	7.370
706.25	984.13	.167E+03	54.5	3.305	7.483
706.97	983.13	.164E+03	54.1	3.294	7.597
707.70	982.13	.162E+03	53.7	3.283	7.711
708.44	981.13	.160E+03	53.2	3.272	7.825
709.20	980.13	.158E+03	52.8	3.261	7.939
709.96	979.13	.156E+03	52.3	3.251	8.052
710.74	978.13	.154E+03	51.8	3.240	8.166
711.53	977.13	.152E+03	51.4	3.230	8.280
712.34	976.13	.150E+03	50.9	3.219	8.394
713.16	975.13	.148E+03	50.4	3.209	8.508
714.00	974.13	.146E+03	49.9	3.199	8.621
714.85	973.13	.145E+03	49.3	3.189	8.735
715.72	972.13	.143E+03	48.8	3.179	8.849
716.60	971.13	.141E+03	48.3	3.169	8.963
717.50	970.13	.140E+03	47.7	3.159	9.077
718.42	969.13	.138E+03	47.2	3.150	9.190
719.35	968.13	.137E+03	46.6	3.140	9.304
720.31	967.13	.135E+03	46.0	3.131	9.418
721.28	966.13	.134E+03	45.4	3.121	9.532
722.28	965.13	.133E+03	44.8	3.112	9.646
723.30	964.13	.131E+03	44.2	3.103	9.759
724.34	963.13	.130E+03	43.6	3.094	9.873
725.40	962.13	.129E+03	42.9	3.084	9.987
726.49	961.13	.128E+03	42.3	3.075	10.101
727.60	960.13	.126E+03	41.6	3.067	10.215
728.74	959.13	.125E+03	40.9	3.058	10.328
729.91	958.13	.124E+03	40.2	3.049	10.442
731.11	957.13	.123E+03	39.5	3.040	10.556
732.34	956.13	.122E+03	38.7	3.032	10.670
733.61	955.13	.121E+03	38.0	3.023	10.784
734.90	954.13	.120E+03	37.2	3.015	10.897
736.24	953.13	.119E+03	36.4	3.006	11.011
737.62	952.13	.118E+03	35.6	2.998	11.125
739.04	951.13	.117E+03	34.7	2.990	11.239
740.51	950.13	.116E+03	33.8	2.982	11.353
742.03	949.13	.115E+03	32.9	2.973	11.466

**EQUAL CAVITATION NUMBER PROFILE
GLEN CANYON DAM LEFT TUNNEL SPILLWAY**

STA	ELEV	RADIUS	SLOPE DEGREES	DEPTH	PIEZ
743.60	948.13	.114E+03	32.0	2.965	11.580
745.23	947.13	.113E+03	31.0	2.957	11.694
746.92	946.13	.113E+03	30.1	2.950	11.808
748.69	945.13	.112E+03	29.0	2.942	11.922
750.53	944.13	.111E+03	27.9	2.934	12.035
752.46	943.13	.110E+03	26.8	2.926	12.149
754.49	942.13	.109E+03	25.6	2.918	12.263
756.64	941.13	.109E+03	24.4	2.911	12.377
758.91	940.13	.108E+03	23.1	2.903	12.491
761.34	939.13	.107E+03	21.7	2.896	12.605
763.96	938.13	.106E+03	20.2	2.888	12.718
766.80	937.13	.106E+03	18.5	2.881	12.832
769.95	936.13	.105E+03	16.7	2.874	12.946
773.50	935.13	.104E+03	14.7	2.866	13.060
777.65	934.13	.104E+03	12.4	2.859	13.174
782.83	933.13	.103E+03	9.4	2.852	13.287
783.45	933.03	.103E+03	9.1	2.851	13.299
784.08	932.93	.103E+03	8.7	2.851	13.310
784.75	932.83	.103E+03	8.4	2.850	13.322
785.45	932.73	.103E+03	8.0	2.849	13.333
786.18	932.63	.103E+03	7.6	2.849	13.344
786.96	932.53	.103E+03	7.1	2.848	13.356
787.78	932.43	.103E+03	6.7	2.847	13.367
788.67	932.33	.102E+03	6.2	2.846	13.378
789.64	932.23	.102E+03	5.6	2.846	13.390
790.72	932.13	.102E+03	5.0	2.845	13.401
791.95	932.03	.102E+03	4.3	2.844	13.413
793.41	931.93	.102E+03	3.5	2.844	13.424
795.35	931.83	.102E+03	2.4	2.843	13.435
799.64	931.74	.102E+03	.0	2.842	13.446

* * * * *

CONTROLLED PRESSURE PROFILE—INPUT

The input for the controlled pressure profiles is interactive. That is, the computer will ask a series of questions that require answers from the user. Two examples, one for the triangular distribution of pressure and the other for the sinusoidal distribution of pressure, are given below.

Controlled Pressure Profile Input

```

TITLE GLEN CANYON TUNNEL SPILLWAY
UPSTREAM SLOPE (DEGREES, DOWNWARD SLOPE IS NEGATIVE)
YOUR SELECTION -65.7
UPSTREAM STATION 678.86
ELEVATION AT UPSTREAM STATION 1035.13
DOWNSTREAM SLOPE (DEGREES) -0.2
ELEVATION AT DOWNSTREAM END OF CURVE 956.268
PRESSURE DISTRIBUTION IN BEND
(T) - TRIANGULAR
(S) - SINUSIODAL
YOUR SELECTION T
RADIUS FACTOR
> 1.0 INCREASE RADIUS OF CURVATURE
< 1.0 DECREASE RADIUS OF CURVATURE
YOUR SELECTION 1.0

```

```

TITLE GLEN CANYON TUNNEL SPILLWAY
UPSTREAM SLOPE (DEGREES, DOWNWARD SLOPE IS NEGATIVE)
YOUR SELECTION -65.7
UPSTREAM STATION 678.86
ELEVATION AT UPSTREAM STATION 1035.13
DOWNSTREAM SLOPE (DEGREES) -0.2
ELEVATION AT DOWNSTREAM END OF CURVE 956.268
PRESSURE DISTRIBUTION IN BEND
(T) - TRIANGULAR
(S) - SINUSIODAL
YOUR SELECTION S
RADIUS FACTOR
> 1.0 INCREASE RADIUS OF CURVATURE
< 1.0 DECREASE RADIUS OF CURVATURE
YOUR SELECTION 1.0

```

* * * * *

CONTROLLED PRESSURE PROFILE—OUTPUT

The output for the triangular and the sinusoidal pressure distributions is given below. Both curves have identical terminal elevations. The effect of the subtle differences in radii of curvature between them can only be detected by comparing plots of the pressure distributions given on figure 4-6.

SPILLWAY PROFILE TRIANGULAR DISTRIBUTION OF PRESSURE

GLEN CANYON - TRIANGULAR PRESSURE
THETA = -65.70 DEFLECTION ANGLE = -65.50

X COORDINATE	Y COORDINATE	RADIUS OF CURVATURE	ARC DISTANCE
678.86	1035.13	.371E+12	.0000
679.68	1033.32	.371E+12	.0535
681.31	1029.72	.347E+03	.1069
682.97	1026.11	.231E+03	.1604
684.65	1022.52	.173E+03	.2138
686.36	1018.95	.139E+03	.2673
688.12	1015.40	.116E+03	.3208
689.94	1011.88	.991E+02	.3742
691.82	1008.39	.867E+02	.4277
693.78	1004.94	.770E+02	.4811
695.81	1001.54	.693E+02	.5346
697.94	998.20	.630E+02	.5881
700.17	994.93	.578E+02	.6415
702.51	991.72	.533E+02	.6950
704.96	988.61	.495E+02	.7484
707.53	985.59	.462E+02	.8019
710.22	982.68	.433E+02	.8554
713.03	979.89	.408E+02	.9088
715.97	977.24	.385E+02	.9623
719.05	974.74	.365E+02	1.0157
722.25	972.41	.347E+02	1.0692
725.57	970.25	.365E+02	1.1227
729.01	968.28	.385E+02	1.1761
732.55	966.50	.408E+02	1.2296
736.17	964.90	.433E+02	1.2830
739.86	963.46	.462E+02	1.3365
743.62	962.20	.495E+02	1.3899
747.42	961.09	.533E+02	1.4434
751.27	960.12	.578E+02	1.4969
755.14	959.30	.630E+02	1.5503
759.04	958.60	.693E+02	1.6038
762.96	958.02	.770E+02	1.6572
766.90	957.55	.867E+02	1.7107
770.84	957.17	.991E+02	1.7642
774.79	956.88	.116E+03	1.8176
778.75	956.66	.139E+03	1.8711
782.71	956.50	.173E+03	1.9245
786.67	956.39	.231E+03	1.9780
790.64	956.33	.347E+03	2.0315
794.60	956.29	.693E+03	2.0849
798.56	956.27	.371E+12	2.1384

**SPILLWAY PROFILE
SINUSOIDAL DISTRIBUTION OF PRESSURE**

GLEN CANYON - SINUSOIDAL PRESSURE
THETA = -65.70 DEFLECTION ANGLE = -65.50

X COORDINATE	Y COORDINATE	RADIUS OF CURVATURE	ARC DISTANCE
678.86	1035.13	.474E+12	.0000
679.60	1033.50	.474E+12	.0378
681.07	1030.23	.128E+05	.0756
682.55	1026.96	.384E+04	.1134
684.02	1023.70	.164E+04	.1512
685.50	1020.43	.856E+03	.1890
686.99	1017.17	.507E+03	.2268
688.48	1013.91	.328E+03	.2646
689.99	1010.66	.227E+03	.3024
691.52	1007.42	.165E+03	.3402
693.08	1004.19	.125E+03	.3780
694.68	1000.98	.986E+02	.4158
696.34	997.80	.798E+02	.4536
698.05	994.66	.664E+02	.4914
699.85	991.56	.564E+02	.5292
701.73	988.51	.490E+02	.5670
703.72	985.53	.433E+02	.6048
705.83	982.62	.390E+02	.6426
708.05	979.82	.357E+02	.6804
710.41	977.12	.332E+02	.7182
712.91	974.55	.314E+02	.7560
715.54	972.12	.300E+02	.7938
718.31	969.85	.292E+02	.8316
721.22	967.75	.288E+02	.8694
724.24	965.84	.289E+02	.9072
727.38	964.11	.294E+02	.9450
730.62	962.59	.304E+02	.9828
733.95	961.25	.319E+02	1.0206
737.35	960.12	.342E+02	1.0584
740.80	959.16	.374E+02	1.0962
744.30	958.38	.418E+02	1.1340
747.83	957.77	.480E+02	1.1719
751.38	957.29	.567E+02	1.2097
754.95	956.93	.696E+02	1.2475
758.52	956.68	.895E+02	1.2853
762.10	956.51	.122E+03	1.3231
765.68	956.40	.182E+03	1.3609
769.27	956.34	.311E+03	1.3987
772.85	956.30	.674E+03	1.4365
776.44	956.28	.261E+04	1.4743
780.02	956.27	.474E+12	1.5121

* * * * *

Aerator Trajectory Program

PROGRAM DESCRIPTION

This program solves simultaneously the equation for the airflow through an air duct and the equation for air entrainment into the jet produced by an aerator.

The method uses the equation of incompressible flow of air through the vent. The estimate of airflow into the jet is based upon equations 5.1 and 5.2 Glazov. (See ch. 5, ref. [9].) These equations assume that the subatmospheric pressure beneath the nappe is constant. For large vents or for trajectories that are large relative to ramp width, this assumption is valid. However, for short trajectories relative to ramp width, this is a poor assumption.

In the program, pressure under the jet is estimated by assuming Bernoulli's equation applies (without losses) between the end of the air duct and a cross section equal to the total width of the jet from the aerator.

Glazov's equations are solved using a Runge-Kutte numerical integration method. The solution procedure follows.

- Estimate the pressure under the nappe. (For the initial step, the pressure under the nappe is set equal to atmospheric pressure.)
- Calculate the nappe trajectory.
- Determine the pressure drop across the vent which gives a new pressure under the nappe.
- Repeat the nappe and the pressure drop calculations until there is no significant difference in the pressure under the nappe.

Because the amount of data required for this program is small and the user will probably be using the program for design, the input is interactive. After one geometry has been analyzed, the program loops back and prompts if changes to the data are required. If changes are required, the program will ask the user to input the changes into one or more of five major groups of data:

- the spillway geometry,
- the ramp geometry,
- the air vent geometry,
- the discharge, and
- the flow characteristics.

If a major group has no changes from the previous simulation, the program skips to the next group without requesting data for the skipped group.

Three trajectories are output, two for the lower nappe and one for the upper nappe. The two lower nappe trajectories correspond to the maximum air penetration into the jet and the maximum dispersion of water caused by turbulence. The upper jet trajectory corresponds to the maximum dispersion of water above the jet. Values, for the dispersion of the jet, will assist in estimating where the jet first strikes the invert and in determining the required height of the chute training walls to contain the jet.

A plotting program has not been written for the jet trajectory.

PROGRAM INPUT

The user will be prompted to input the ramp geometry, the duct geometry, the discharge, and flow properties at the end of the ramp. These are arranged into four groups of input as shown below. After completion of the run, the user is prompted to input an entirely new structure or to change one of the four groups of data previously inputted. An example is given to illustrate inputting only new air duct geometry.

After the credits, you will be asked to enter data concerning the properties of the air vent and ramp, if any. The program will allow any flow geometry downstream from the aerator. You must enter the name of the file which contains the input geometry. The following is an example of a session in which an aerator is designed and the effect of air vent inlet losses is considered. The symbol `< >`, denotes input from user. Do not type the `< >` symbol as a part of your input.

GEOMETRY FILE NAME ? `< B:GLENIN >`

The next line is the title as it is read from the file. If this is not the correct structure, press CTRL C and start over with the correct file.

GLEN CANYON LEFT SPILLWAY TUNNEL

STATION OF RAMP LIP = `< 685.8 >`
 ELEVATION OF RAMP LIP = `< 1035.112 >`
 ANGLE (DEG) BETWEEN RAMP AND HORIZONTAL = `< 53.975 >`

CROSS SECTIONAL AREA OF AIR VENT = `< 1.486 >`
 WIDTH OF VENT OPENING = `< 1.219 >`
 LOSS COEFFICIENT THROUGH AIR VENT = `< 1.2 >`
 NUMBER OF VENTS = `< 2 >`

DISCHARGE = `< 283.17 >`

TURBULENCE INTENSITY = `< 0.028 >`
 FLOW DEPTH AT RAMP = `< 1.385 >`
 VELOCITY AT RAMP = `< 36.463 >`

You can now investigate the effect of changes to the parameters given above. The changes specified by groups so that you do not have to go through every parameter to get at one which may be near the end of the list. The following example illustrates changing only the loss coefficient in the air duct.

NEW STRUCTURE GEOMETRY ? (Y/N) `< N >`

NEW RAMP GEOMETRY ? (Y/N) `< N >`

NEW AIR DUCT GEOMETRY ? (Y/N) `< Y >`

CROSS SECTIONAL AREA OF AIR VENT = `< 1.486 >`
 WIDTH OF VENT OPENING = `< 1.219 >`
 LOSS COEFFICIENT THROUGH AIR VENT = `< 1.0 >`
 NUMBER OF VENTS = `< 2 >`

NEW DISCHARGE ? (Y/N) `< N >`

NEW WATER FLOW PROPERTIES ? (Y/N) `< N >`

* * * * *

PROGRAM OUTPUT

An example of two input files used to analyze the aerator for Glen Canyon Dam spillway is presented. The difference between the two runs is the value of the vent loss coefficient. The effect of the lower vent loss coefficient is to decrease the pressure drop across the vent. An effect on the jet trajectory is not apparent.

JET AND AIR FLOW RELATIONSHIPS

GLEN CANYON LEFT SPILLWAY TUNNEL

RAMP :	WIDTH	STATION	ELEVATION	ANGLE
	5.61	685.80	1035.112	53.97
AIR DUCT :	AREA	LOSS COEFF	VENT WIDTH	NO VENTS
	1.49	1.00	1.22	2
FLows :	WATER	AIR	PRESSURE DROP ACROSS VENT	
	283.17	27.50	.006	
	TURBULENCE INTENSITY	WATER DEPTH	MEAN VELOCITY	
	.028	1.385	36.46	

JET TRAJECTORY

LOWER NAPPE

TOP NAPPE

STATION	ELEV	STATION	ELEV	STATION	ELEV
685.80	1035.11	685.80	1035.11	686.92	1035.93
686.08	1034.70	686.10	1034.72	687.20	1035.56
686.36	1034.29	686.41	1034.32	687.50	1035.17
686.64	1033.88	686.71	1033.93	687.80	1034.77
686.92	1033.46	687.01	1033.53	688.11	1034.37
687.20	1033.05	687.31	1033.13	688.41	1033.97
687.48	1032.63	687.62	1032.72	688.71	1033.57
687.76	1032.21	687.92	1032.32	689.02	1033.17
688.04	1031.78	688.22	1031.91	689.32	1032.76
688.32	1031.36	688.52	1031.51	689.62	1032.35
688.44	1031.18	688.66	1031.33	689.81	1032.09

JET AND AIR FLOW RELATIONSHIPS

GLEN CANYON LEFT SPILLWAY TUNNEL

RAMP :	WIDTH	STATION	ELEVATION	ANGLE
	5.61	685.80	1035.112	53.97
AIR DUCT :	AREA	LOSS COEFF	VENT WIDTH	NO VENTS
	1.49	1.20	1.22	2
FLOWS :	WATER	AIR	PRESSURE DROP	
	283.17	27.50	ACROSS VENT	
			.007	
TURBULENCE INTENSITY		WATER DEPTH		MEAN VELOCITY
.028		1.385		36.46

JET TRAJECTORY

LOWER NAPPE

TOP NAPPE

-----				-----	
STATION	ELEV	STATION	ELEV	STATION	ELEV
685.80	1035.11	685.80	1035.11	686.92	1035.93
686.08	1034.70	686.10	1034.72	687.20	1035.56
686.36	1034.29	686.41	1034.32	687.50	1035.17
686.64	1033.88	686.71	1033.93	687.80	1034.77
686.92	1033.46	687.01	1033.53	688.11	1034.37
687.20	1033.05	687.31	1033.13	688.41	1033.97
687.48	1032.63	687.62	1032.72	688.71	1033.57
687.76	1032.21	687.92	1032.32	689.02	1033.17
688.04	1031.78	688.22	1031.91	689.32	1032.76
688.32	1031.36	688.52	1031.51	689.62	1032.35
688.44	1031.18	688.66	1031.33	689.81	1032.09

* * * * *

Damage Index From Historical Data Program

PROGRAM DESCRIPTION

This program determines the damage index from historical data at a specified station in the hydraulic structure. Before using this program it is necessary to run the program described in appendix A for at least three different discharges which bracket the range of flows contained in the historical record. The damage potential data, corresponding to a specific station and a specific height and type of flow surface irregularity, are input into the program for each discharge. Then, the following is input:

- the day when the flow occurred
- the duration of the flow (in hours)
- the flow rate (cubic meters per second)

The output echoes back the input and the calculated value of the damage index at each daily entry. With this information, the time when damage occurred can be correlated with the value of the damage index. Conversely, the time at which varying degrees of damage probably occurred can be estimated from the values of the damage index given in chapter 3.

Program input can be interactive or from a file. If input is interactive, the user has an option to save the input to a file or to discard it. Saving the input is a good method to create a file that can be edited to determine the damage potentials at different stations.

PROGRAM INPUT

The following is an example of program input used for the analysis of the Glen Canyon Dam left tunnel spillway. Six values of damage potential data were used to encompass the range of possible flows. The example summarizes the operational history of the spillway from 1980 through the 1983 flood.

GLEN CANYON LEFT SPILLWAY - STA 26+25

1	JUN 13 80	JUN 24 80
3.48,35	.07	13.62
3.30,25	N	N
2.81,20	5.956	31.934
2.73,15	JUN 13 80	JUN 24 80
2.03,10	1.5	16
9.97,5	N	N
0,0	10.492	2.164
JUN 13 80	JUN 13 80	JUN 25 80
.47	.13	10.
N	N	N
.836	9.424	2.598
JUN 13 80	JUN 13 80	JUN 25 80
.48	.07	7.
N	N	N
1.254	8.358	3.03
JUN 13 80	JUN 13 80	JUN 25 80
.30	.1	11.25
N	N	N
2.09	7.722	7.54
JUN 13 80	JUN 13 80	JUN 26 80
.07	22.3	21.5
N	N	N
8.358	7.3	8.662
JUN 13 80	JUN 22 80	JUL 02 80
.03	.17	22.75
N	N	N
8.996	1.08	3.334
JUN 13 80	JUN 22 80	JUL 03 80
.38	15.95	24.
N	N	N
10.492	1.08	1.732
JUN 13 80	JUN 22 80	JUL 07 80
.13	14.	48.
N	N	N
9.424	1.512	1.298
JUN 13 80	JUN 23 80	OCT 31 81
.07	2.52	.13
N	N	N
8.996	1.512	6.168
JUN 13 80	JUN 23 80	NOV 01 81
.1	.35	.3
N	N	N
8.57	10.872	10.772
JUN 13 80	JUN 23 80	APR 24 82
.1	1.13	.95
N	N	N
8.146	8.628	10.614
JUN 13 80	JUN 23 80	APR 24 82
.1	.53	.42
N	N	N
7.722	10.872	13.384
JUN 13 80	JUN 23 80	APR 24 82
.05	.38	.35
N	N	N
7.3	18.574	13.384
JUN 13 80	JUN 24 80	JUN 02 83
.03	.27	23.
N	N	N
6.644	25.058	10.064

JUN 03 83
 45.
 N
 15.078
 JUN 05 83
 24.
 N
 20.176
 JUN 06 83
 3
 N
 10.106
 JUN 06 83
 .15
 N
 7.894
 JUN 06 83
 2.05
 N
 3.998
 JUN 07 83
 73.
 N
 4.014
 JUN 13 83
 50.
 N
 2.162
 JUN 15 83
 64.
 N
 11.84
 JUN 19 83
 53.
 N
 17.176
 JUN 21 83
 45.
 N
 20.07

JUN 23 83
 102.
 N
 10.322
 JUN 27 83
 1.
 N
 25.016
 JUN 27 83
 12.
 N
 25.016
 JUN 28 83
 .75
 N
 32.000
 JUN 28 83
 29.25
 N
 20.182
 JUN 29 83
 46.55
 N
 15.044
 JUL 01 83
 .1
 N
 15.044
 JUL 01 83
 44.07
 N
 20.006
 JUL 03 83
 49.7
 N
 20.164
 JUL 05 83
 6.58
 N
 18.83

JUL 05 83
 40.
 N
 12.994
 JUL 07 83
 5.7
 N
 11.001
 JUL 08 83
 1
 N
 10.002
 JUL 08 83
 6.
 N
 10.002
 JUL 06 83
 45.
 N
 5.01
 JUL 11 83
 141.03
 N
 7.458
 JUL 17 83
 .08
 N
 4.972
 JUL 17 83
 21.92
 N
 4.972
 JUL 18 83
 119.92
 N
 2.916
 Z

* * * * *

PROGRAM OUTPUT

The program output contains a summary of the historical operation, the interpolated values of the damage potential, and the damage index. Negative values of the reference time are indicative of periods when the damage index is increasing slowly.

DAMAGE INDEX

GLEN CANYON LEFT SPILLWAY - STA 24+25

VALUES OF CAVITATION POTENTIAL AND DISCHARGE

3.48	35.00
3.30	25.00
2.81	20.00
2.73	15.00
2.03	10.00
9.97	5.00
.00	.00

DATE	TOTAL TIME	DISCHARGE 1000"S	DAMAGE POTENTIAL	DAMAGE INDEX	REFERENCE TIME
JUN 13 80	.5	.836	.291E+04	.112E+04	-.10E+01
JUN 13 80	.9	1.254	.418E+04	.243E+04	-.84E+00
JUN 13 80	1.3	2.090	.635E+04	.361E+04	-.52E+00
JUN 13 80	1.3	8.358	.661E+04	.387E+04	-.48E+00
JUN 13 80	1.4	8.996	.506E+04	.394E+04	-.83E+00
JUN 13 80	1.7	10.492	.172E+04	.401E+04	-.86E+01
JUN 13 80	1.9	9.424	.386E+04	.418E+04	-.11E+01
JUN 13 80	1.9	8.996	.506E+04	.433E+04	-.42E+00
JUN 13 80	2.0	8.570	.613E+04	.463E+04	-.98E-01
JUN 13 80	2.1	8.146	.706E+04	.499E+04	.10E+00
JUN 13 80	2.2	7.722	.787E+04	.539E+04	.25E+00
JUN 13 80	2.3	7.300	.854E+04	.562E+04	.35E+00
JUN 13 80	2.3	6.644	.934E+04	.577E+04	.45E+00
JUN 13 80	2.4	5.956	.984E+04	.615E+04	.51E+00
JUN 13 80	3.9	10.492	.172E+04	.622E+04	-.34E+02
JUN 13 80	4.0	9.424	.386E+04	.632E+04	-.11E+01
JUN 13 80	4.1	8.358	.661E+04	.649E+04	.14E+01
JUN 13 80	4.2	7.722	.787E+04	.683E+04	.18E+01
JUN 13 80	26.5	7.300	.854E+04	.273E+05	.20E+01
JUN 22 80	26.6	1.080	.367E+04	.273E+05	-.17E+04
JUN 22 80	42.6	1.080	.367E+04	.274E+05	-.17E+04
JUN 22 80	56.6	1.512	.490E+04	.276E+05	-.22E+03
JUN 23 80	59.1	1.512	.490E+04	.277E+05	-.22E+03
JUN 23 80	59.5	10.872	.153E+04	.277E+05	-.71E+08
JUN 23 80	60.6	8.628	.599E+04	.277E+05	-.42E+02
JUN 23 80	61.1	10.872	.153E+04	.277E+05	-.74E+08
JUN 23 80	61.5	18.574	.285E+04	.277E+05	-.17E+05
JUN 24 80	61.8	25.058	.330E+04	.277E+05	-.44E+04
JUN 24 80	75.4	31.934	.354E+04	.277E+05	-.25E+04
JUN 24 80	91.4	2.164	.651E+04	.291E+05	.46E+01
JUN 25 80	101.4	2.598	.742E+04	.304E+05	.41E+02
JUN 25 80	108.4	3.030	.818E+04	.317E+05	.60E+02
JUN 25 80	119.7	7.540	.817E+04	.334E+05	.60E+02
JUN 26 80	141.1	8.662	.591E+04	.338E+05	-.17E+03
JUL 02 80	163.9	3.334	.864E+04	.371E+05	.91E+02
JUL 03 80	187.9	1.732	.548E+04	.372E+05	-.70E+03
JUL 07 80	235.9	1.298	.431E+04	.373E+05	-.54E+04
OCT 31 81	236.0	6.168	.972E+04	.373E+05	.19E+03
NOV 01 81	236.3	10.772	.157E+04	.373E+05	-.19E+11
APR 24 82	237.3	10.614	.165E+04	.373E+05	-.64E+10
APR 24 82	237.7	13.384	.156E+04	.373E+05	-.24E+11
APR 24 82	238.1	13.384	.156E+04	.373E+05	-.24E+11
JUN 02 83	261.0	10.064	.198E+04	.373E+05	-.14E+09

DAMAGE INDEX

GLEN CANYON LEFT SPILLWAY - STA 24+25

DATE	TOTAL TIME	DISCHARGE 1000*S	DAMAGE POTENTIAL	DAMAGE INDEX	REFERENCE TIME
JUN 03 83	306.0	15.078	.274E+04	.373E+05	-.83E+06
JUN 05 83	330.0	20.176	.282E+04	.373E+05	-.55E+06
JUN 06 83	333.0	10.106	.196E+04	.373E+05	-.19E+09
JUN 06 83	333.2	7.894	.756E+04	.373E+05	.19E+03
JUN 06 83	335.2	3.998	.941E+04	.376E+05	.28E+03
JUN 07 83	408.2	4.014	.942E+04	.457E+05	.28E+03
JUN 13 83	458.2	2.162	.651E+04	.460E+05	-.71E+03
JUN 15 83	522.3	11.840	.128E+04	.460E+05	-.79E+14
JUN 19 83	575.3	17.176	.284E+04	.460E+05	-.11E+08
JUN 21 83	620.3	20.070	.281E+04	.460E+05	-.12E+08
JUN 23 83	722.3	10.322	.181E+04	.460E+05	-.99E+11
JUN 27 83	723.3	25.016	.330E+04	.460E+05	-.11E+07
JUN 27 83	735.3	25.016	.330E+04	.460E+05	-.11E+07
JUN 28 83	736.0	32.000	.354E+04	.460E+05	-.44E+06
JUN 28 83	765.3	20.182	.282E+04	.460E+05	-.12E+08
JUN 29 83	811.8	15.044	.273E+04	.460E+05	-.20E+08
JUL 01 83	811.9	15.044	.273E+04	.460E+05	-.20E+08
JUL 01 83	856.0	20.006	.281E+04	.460E+05	-.13E+08
JUL 03 83	905.7	20.164	.282E+04	.460E+05	-.12E+08
JUL 05 83	912.3	18.830	.285E+04	.460E+05	-.10E+08
JUL 05 83	952.3	12.994	.141E+04	.460E+05	-.79E+14
JUL 07 83	958.0	11.001	.148E+04	.460E+05	-.32E+14
JUL 08 83	959.0	10.002	.203E+04	.460E+05	-.69E+10
JUL 08 83	965.0	10.002	.203E+04	.460E+05	-.69E+10
JUL 06 83	1010.0	5.010	.997E+04	.496E+05	.86E+03
JUL 11 83	1151.0	7.458	.830E+04	.522E+05	.62E+03
JUL 17 83	1151.1	4.972	.996E+04	.522E+05	.96E+03
JUL 17 83	1173.0	4.972	.996E+04	.533E+05	.96E+03
JUL 18 83	1292.9	2.916	.799E+04	.544E+05	.39E+03

* * * * *

Cavitation References

The following publications were selected because they are either current or of a classical nature that contain valuable concepts or data. Key words have been included in the publications. Many of the foreign publications have been translated by the Bureau of Reclamation (USBR).

- ACI Committee 210, "Erosion of Concrete in Hydraulic Structures," *Concrete International*, vol. 9, No. 3, pp. 67-73, March, 1987. (damage, control, prevention, tolerances).
- _____, "Erosion of Concrete in Hydraulic Structures," *ACI Materials Journal*, pp. 136-156, March 1987 (damage, control, prevention, tolerances)
- Adkins, C. V., "Model Studies of the Kortess Dam Spillway and the River Channel Downstream — Kendrick Unit, Wyoming-Missouri, Basin Project," Bureau of Reclamation Report No. HYD-206, August 1946 (model, Kortess, spillway).
- Aksoy, S., Etembabaoglu, S., "Cavitation Damage at the Discharge Channels of Keban Dam," XIIIth International Congress on Large Dams, New Delhi, vol. III, Q50, R21, pp. 369-379, 1979 (damage, repair, prototype, isolated irregularity).
- Anastasi, G., "Besondere Aspekte der Gestaltung von Grundablassen in Stollen," *Die Wasserwirtschaft*, vol. 73, pp. 501-508, December 1983 (outlet works, aeration).
- Appel, D. W., "An Experimental Study of the Cavitation of Submerged Jets," Iowa Institute of Hydraulic Research, Progress Report for the Office of Naval Research, Iowa City, IA, Contract No. ONR-500 (03), 9 pp., June 1956 (incipient, noise, model, frequency).
- Arakeri, V. H., "Inception of Cavitation From a Backward Facing Step," American Society of Mechanical Engineers, International Symposium on Cavitation Inception, New York, pp. 101-109, December 1979 (inception, model studies, backward facing step).
- Arndt, R.E.A., Discussion of "Cavitation From Surface Irregularities in High Velocity Flow," Proceedings of the American Society of Civil Engineers, vol. 103, No. HY4, pp. 469-472, April 1977 (surface irregularities, turbulence, shear flows).
- _____, "Cavitation in Fluid Machinery and Hydraulic Structures," *Annual Review of Fluid Mechanics*, pp. 273-328, 1981 (theory, inception, hydraulic machinery).
- _____, Daily, J. W., "Cavitation in Turbulent Boundary Layers, Cavitation State of Knowledge," Fluids Engineering and Applied Mechanics Conference, American Society of Mechanical Engineers, Northwestern University, pp. 64-86, 1969 (cavitation inception, isolated roughnesses, rough boundaries).
- _____, Holl, J. W., Bohn, J. C., Bechtel, W. T., "Limited Cavitation on Surface Irregularities," International Association for Hydraulic Research, Hydraulic Machinery and Cavitation Symposium, Rome, Italy, 1972 (isolated roughnesses, theory, scale effects).
- _____, Holl, J. W., Bohn, J. C., Bechtel, W. T., "Influence of Surface Irregularities on Cavitation Performance," *Journal of Ship Research*, vol. 23, No. 3, pp. 157-169, September 1979 (inception, surface irregularities).
- _____, Taghavi, R., "Cavitation in Various Types of Shear Flow," Proceeding of the Conference, Water for Resource Development, American Society of Civil Engineers, Coeur d'Alene, ID, pp. 417-421, August 1984 (turbulence, scaling, nuclei).
- Backstrom, T. E., "Preliminary Study of Cavitation Prevention in Alloys," Bureau of Reclamation Report No. ChE-24, 5 pp., April 1965 (damage, alloys).
- Baikov, I. R., Berngardt, A. R., Kedrinskii, V. K., "Methods of Examining the Dynamics of Cavitation Clusters," *Journal of Applied Mechanics and Technical Physics*, vol. 25, No. 5, pp. 677-681, March 1985 (clusters, bubbles).
- Ball, J. W., "Cavitation Characteristics of Gate Valves and Globe Valves Used as Flow Regulators Under Heads up to About 125 ft.," Transactions of the American Society of Mechanical Engineers, vol. 79, No. 9, August 1957 (valves, model).
- _____, "Hydraulic Characteristics of Gate Slots," *Journal of the Hydraulics Division*, Proceedings of the American Society of Civil Engineers, vol. 85, No. HY10, pp. 81-114, October 1959 (gate slots, pressures, model).
- _____, "Why Close Tolerances Are Necessary Under High Velocity Flow," Bureau of Reclamation Report No. HYD-473, October 1960 (surface irregularities, high velocity flow, tolerances).
- _____, "Construction Finishes and High-Velocity Flow," *Journal of the Construction Division*, Transactions of the American Society of Civil Engineers, CO2, No. 3646, September 1963 (surface irregularities, high velocity flow, tolerances).

- _____, "Cavitation Characteristics of Gate Valves and Globe Valves," American Society of Mechanical Engineers, Paper 56 F10, fall meeting, Denver, CO, September 1966 (valves, model).
- _____, "Cavitation From Surface Irregularities in High Velocity Flow," *Journal of the Hydraulics Division*, Proceedings of the American Society of Civil Engineers, vol. 102, No. HY9, pp. 1283-1297, September 1976 (model, prototype, inception, surface irregularities).
- Beichley, G. L., "Hydraulic Model Studies of the Blue Mesa Dam Spillway," Bureau of Reclamation Report No. HYD-515, July 1964 (model, spillway, Blue Mesa Dam).
- _____, "Hydraulic Model Studies of Yellowtail Dam Spillway — Missouri River Basin Project, Montana," Bureau of Reclamation Report No. HYD-483, August 1964 (model, spillway, Yellowtail).
- _____, "Hydraulic Model Studies of Chute Offsets, Air Slots, and Deflectors for High-Velocity Jets," Bureau of Reclamation Report No. REC-ERC-73-5, 35 pp., March 1973 (aerators, air slots, offsets, deflectors, model).
- Berger, S. A., Talbot, L., Yao, L. S., "Flow in Curved Pipes," *Annual Review of Fluid Mechanics*, pp. 461-512, 1983 (secondary flow, theory, bends).
- Bernal, L. P., Roshko, A., "Streamwise Vortex Structure in Plane Mixing Layers," *Journal of Fluid Mechanics*, vol. 170, pp. 499-525, 1986 (vortices, measurements, model).
- Billet, M. L., "Scale Effects on Various Types of Limited Cavitation," International Symposium on Cavitation Inception, American Society of Mechanical Engineers, New York, pp. 11-23, December 1979 (scale effects, hydrofoils, desinent, models).
- _____, "Cavitation Nuclei Measurements With an Optical System," Transactions of the American Society of Mechanical Engineers, vol. 108, pp. 366-372, September 1986 (nuclei, measurements, optical).
- _____, "The Importance and Measurement of Cavitation Nuclei," Proceedings of the Specialty Conference, *Advancements in Aerodynamics, Fluid Mechanics and Hydraulics*, American Society of Civil Engineers, Minneapolis, MN, pp. 967-988, June 1986 (nuclei, measurement, models, laser).
- Blake, J. R., Taib, B. B., Doherty, G., "Transient Cavities Near Boundaries, Part 1. Rigid Boundary," *Journal of Fluid Mechanics*, vol. 170, pp. 479-497, 1986 (bubbles, collapse).
- _____, "Cavitation Bubbles Near Boundaries," *Annual Review of Fluid Mechanics*, vol. 19, pp. 99-123, 1987 (bubbles, collapse, boundary).
- Bohn, J. C., "The Influence of Surface Irregularities on Cavitation," M.S. thesis, Pennsylvania State University, December 1972 (isolated, distributed, inception).
- Borden, R. C., Colgate, D., Legas, J., Selander, C. E., "Documentation of Operation, Damage, Repair, and Testing of Yellowtail Dam Spillway," Bureau of Reclamation Report No. REC-ERC-71-23, 76 pp., May 1971 (prototype, spillway, Yellowtail Dam).
- Bradley, J. N., "Study of Air Injection Into the Flow in the Boulder Dam Spillway Tunnels — Boulder Canyon Project," Bureau of Reclamation Report No. HYD-186, October 1945.
- Bretschneider, H., "Der Beginn des Luftertrages bei Sohlennischen," *Die Wasserwirtschaft*, vol. 76, pp. 203-207, May 1986 (air entrainment, inception, aeration slots).
- Bruschin, J., "Aeration Off-Sets for Spillway Chutes and Bottom Outlets," Symposium on Modeling Scale Effects in Hydraulic Structures, International Association for Hydraulic Research, Esslingen, Germany, paper No. 4.3, pp. 1-4, September 1984 (aerators, models).
- _____, "Hydraulic Modelling at the Piedra del Aguila Dam," *Water Power and Dam Construction*, pp. 24-28, January 1985 (aeration, model, Piedra del Aguila).
- Burgi, P. H., Eckley, M. S., "Repairs at Glen Canyon Dam," *Concrete International*, pp. 24-31, March 1987 (erosion, repairs, spillways, tunnel linings, damage).
- _____, Moyes, B. M., Gamble, T. W., "Operation of Glen Canyon Dam Spillways — Summer 1983," Proceedings of the Conference Water for Resource Development, American Society of Civil Engineers, Coeur d'Alene, ID, pp. 260-265, August 1984 (Glen Canyon Dam, spillway, damage, prototype).
- Cai, W., "Acoustic Method for Measuring Cavitation and Impulse Counting of Its Noise," *Shuili Xuebao*, No. 3, pp. 49-54, China, 1983 (USBR translation No. 1889, book No. 12,481, paper No. 6) (noise, frequency domain, model).
- Calehuff, G. L., Wislicenus, G. F., "ORL Investigations of Scale Effects on Hydrofoil Cavitation," Ordnance Research Laboratory, Pennsylvania State University, TM 19.4212-03, 1956 (model, scale effects).
- Canavelis, P. R., "Analyse du Mechanism de L'Érosion de Cavitation," *La Houille Blanche*, No. 2-3, pp. 189-196, 1968 (damage, bubbles, model experiments).
- Cassidy, J. J., Elder, R. A., "Spillways of High Dams," *Developments in Hydraulic Engineering — 2*, Elsevier Applied Science Publishers, New York, ch. 4, pp. 159-182, 1983 (spillways, aeration, aerators, surface irregularities).
- Castillejo, N. R., Marcano, A., "Aeration at Guri Final Stage," Proceedings of the International

- Symposium on Model-Prototype Correlation of Hydraulic Structures, American Society of Civil Engineers, International Association for Hydraulic Research, pp. 102-109, August 1988 (aerator, prototype, model tests).
- Chahine, C. L., Sirian, C. R., "Collapse of a Simulated Multibubble System," Cavitation and Polyphase Flow Forum, American Society of Mechanical Engineers, Albuquerque, NM, pp. 78-81, 1985 (collapse, bubbles, swarms).
- _____, Bovis, A. G., "Pressure Field Generated by Nonspherical Bubble Collapse," Transactions of the American Society of Mechanical Engineers, vol. 105, pp. 356-363, September 1983 (bubble, collapse).
- _____, Cohen, D., Ducasse, P., Ligneul, P., "Influence d'un Revêtement Elastique sur le Collapse d'une Bulle de Cavitation," IV Rencontre International sur la Rupture de Veine, Cagliari, Italy, 19 pp., September 1979 (bubbles, elastic coatings, collapse).
- _____, Morine, A. K., "Collapse d'une Bulle de Cavitation Entre Deux Parois Solides," IV Rencontre Internationale sur la Rupture de Veine, Cagliari, Italy, 23 pp., September 1979 (collapse, bubbles, solid walls).
- _____, Shen, Y. T., "Bubble Dynamics and Cavitation Inception in Cavitation Susceptibility Meter," Transactions of the American Society of Mechanical Engineers, vol. 108, pp. 444-437, December 1986 (scale effects, models, inception, meter).
- Chanson, H., "A Study of Air Entrainment and Aeration Devices on a Spillway Model," University of Canterbury, Christchurch, New Zealand, Research Report 88-8, October 1988 (aerators, model, theory).
- Colgate, D., "Cavitation Damage of Roughened Concrete Surfaces," American Society of Civil Engineers, annual convention, Pittsburgh, PA, October 1956 (damage, uniform roughness, Grand Coulee Dam, spillway, Davis Dam).
- _____, "Hydraulic Model Studies of Aeration Devices for Yellowtail Dam Spillway Tunnel, Pick Sloan Missouri Basin Program, Montana," Bureau of Reclamation Report No. REC-ERC-71-47, 13 pp., December 1971 (model, spillway, Yellowtail).
- _____, "Hydraulic Model Studies of Amaluza Dam Spillway," Bureau of Reclamation Report No. GR-25-76, 65 pp., December 1976 (model, spillway, Amaluza).
- _____, "Cavitation Damage in Hydraulic Structures, International Conference on Wear of Materials," St. Louis, MO, pp. 433-438, April 25-28, 1977 (damage, materials, offsets).
- _____, Elder, R., "Design Considerations Regarding Cavitation in Hydraulic Structures," Tenth Hydraulics Division Conference, American Society of Civil Engineers, Urbana, IL, August 16-18, 1961 (tolerances, model, prototype).
- Daily, J. W., Johnson, V. E. Jr., "Turbulence and Boundary-Layer Effects on Cavitation Inception From Gas Nuclei," Transactions of the American Society of Mechanical Engineers, vol. 78, pp. 1695-1706, 1956 (bubbles, growth, inception, turbulence).
- _____, Lin, J. D., Broughton, R. S., "The Distribution of the Mean Static Pressure in Turbulent Boundary Layers in Relation to Inception of Cavitation," Hydrodynamics Technical Report No. 34, Massachusetts Institute of Technology, 54 pp., June 1959 (turbulence, inception, model).
- Darvas, L. A., Aust, M.E.I., "Cavitation in Closed Conduit Flow Control Systems," Civil Engineering Transactions, The Institution of Engineers, Australia, CE12, No. 2, pp. 213-219, October 1970 (valves, needle, hollow jet, gate, butterfly).
- DeFazio, F. G., Wei, C. Y., "Design of Aeration Devices on Hydraulic Structures," Hydraulics Division Specialty Conference, American Society of Civil Engineers, Cambridge, MA, August 1983 (aerators, spillways, prototype, Guri Dam, jets, computer model).
- Demiröz, E., Acatay, T., "Influence of Chamfers Away From Flow on Cavitation Inception," XXI Congress of the International Association for Hydraulic Research, Melbourne, Australia, seminar 2, 4 pp., 1985.
- Destenay, J., Bernard, J., "Quelques Exemples de Degradation des Betons par Cavitation dans des Ouvrages," *La Houille Blanche*, No. 2-3, pp. 167-176, 1968 (damage, prototype, velocity dependence, energy dissipation).
- Eccher, L., Siegenthaler, A., "Spillway Aeration of the San Roque Project," *Water Power and Dam Construction*, pp. 37-41, September 1982 (spillway, aerator, San Roque).
- Echavez, G., "Cavitacion en Vertedores," Instituto de Ingenieria, Universidad Nacional Autonoma de Mexico, No. 415, 80 pp., 1979 (spillways, aerators, surface irregularities).
- _____, Bourguett, V., "Optimum Design of Aeration Ramp Slots in Tunnel Spillways," Proceedings of the Specialty Conference, *Advancements in Aerodynamics, Fluid Mechanics and Hydraulics*, American Society of Civil Engineers, Minneapolis, MN, pp. 178-185, June 1986 (aerators, theory).
- Eisenhauer, N., "Location of Aerators in Spillways," *Concrete International*, vol. 9, No. 3, pp. 62-66, March 1987 (aerators, location, theory).
- Fairall, R., Task, H., Simms, T., Quinton, C., "Rebuilding the Hollow-Jet Outlet Valves at

- Monticello Dam," *Water Operation and Maintenance*, Bureau of Reclamation Bulletin No. 128, pp. 1-14, June 1984 (valves, hollow jet, prototype).
- Falvey, H. T., "Air-Water Flow in Hydraulic Structures," Bureau of Reclamation Engineering Monograph No. 41, 143 pp., December 1980 (aeration, summary, design).
- _____, "Predicting Cavitation in Tunnel Spillways," *Water Power and Dam Construction*, vol. 34, pp. 13-15, August 1982 (prototype, damage, inception).
- _____, "Prevention of Cavitation on Chutes and Spillways," Proceedings of the Conference on Frontiers in Hydraulic Engineering, American Society of Civil Engineers, Cambridge, MA, pp. 432-437, 1983 (prototype, damage, inception).
- _____, "Cavitation Studies in Tunnel Spillways," International Association for Hydraulic Research, Symposium on Scale Effects in Modeling Hydraulic Structures, Esslingen, Germany, paper 5.7, September 1984 (prototype, model, damage, inception).
- Flynn, H. G., "Growth of Gas Nuclei in Water Under Negative Pressure Pulses," Proceedings of the Third International Congress on Acoustics, Stuttgart, Germany, pp. 336-339, 1959 (nuclei, pulses).
- Franc, J. P., Michel, M. L., "Attached Cavitation and the Boundary Layer," *Journal of Fluid Mechanics*, vol. 154, pp. 63-90, 1985 (air foil, boundary layer, cavitation patterns).
- Franklin, R. E., "Jet Cavitation," International Symposium on Jets and Cavitation, American Society of Mechanical Engineers, Miami Beach, FL, winter meeting, 11 pp., November 1985 (noise, jets).
- Frizell, K. W., "Spillway Tests at Glen Canyon Dam," Bureau of Reclamation, 52 pp., July 1985 (prototype, Glen Canyon Dam, tests).
- _____, Pugh, C. A., "Chute Spillway Aerators — McPhee Dam Model/Prototype Comparison," International Association for Hydraulic Research, Proceedings of the International Symposium on Model-Prototype Correlation of Hydraulic Structures, American Society of Civil Engineers, pp. 128-137, August 1988 (aerator, prototype, model tests).
- Fujikawa, S., Akamatsu, T., "Effects of the Non-Equilibrium Condensation of Vapor on the Pressure Wave Produced by the Collapse of a Bubble in a Liquid," *Journal of Fluid Mechanics*, vol. 97, part 3, pp. 481-512, 1980 (bubble, collapse, vapor).
- _____, _____, "On the Mechanisms of Cavitation Bubble Collapse," International Association for Hydraulic Research, 10th Symposium of Section for Hydraulic Machinery, Equipment and Cavitation, Tokyo, Japan, pp. 91-102, 1980.
- Galindez, A., Guinea, P. M., Lucas, P., Aspuru, J. J., "Spillways in a Peak Flow River," Transactions of the 9th International Congress of Large Dams, Q33, R22, vol. 2, pp. 365-389, Istanbul, Turkey, September 1967 (Aldeadavila Dam, damage, prototype).
- Gal'perin, R. S., Oskolkov, A. G., Semenkov, V. M., Tsedrov, G. N., "Cavitation in Hydraulic Structures," *Energiia*, 10 Shliuzovaia Nabe-rezhnaia, Moscow M-114, 113114, Russia, 1977. (USBR translation 1450 of chs. 1, 2, 3, 4, 5, and 7) (theory, prototype, model studies, design data).
- Gimeniz, G., "Essai de Synthèse des Recherches sur la Cavitation," *La Houille Blanche*, No. 5, pp. 323-337, 1984 (summary, research).
- Glazov, A. I., "Calculation of the Air-Capturing Ability of a Flow Behind an Aerator Ledge," *Hydrotechnical Construction*, Plenum Publishing Corp., vol. 18, No. 11, pp. 554-558, 1985 (aerators, turbulence, boundary layer, air demand).
- Grant, M. M., Lush, P. A., "Liquid Impact on a Bilinear Elastic-Plastic Solid and Its Role in Cavitation," *Journal of Fluid Mechanics*, vol. 176, pp. 237-252, 1987 (microjets, model, theory, damage).
- Gulliver, J. S., Halverson, M. J., "Measurements of Large Streamwise Vortices in Open-Channel Flow," *Water Resources Research, American Geophysical Union*, vol. 23, No. 1, pp. 115-123, January 1987 (vorticity, open channel flow).
- Hamilton, W. S., "Preventing Cavitation Damage to Hydraulic Structures — Part One," *Water Power and Dam Construction*, pp. 40-43, November 1983 (theory, damage).
- _____, "Preventing Cavitation Damage to Hydraulic Structures — Part Two," *Water Power and Dam Construction*, pp. 46-52, December 1983 (baffle blocks, gates, aeration).
- _____, "Preventing Cavitation Damage to Hydraulic Structures — Part Three," *Water Power and Dam Construction*, pp. 42-45, January 1984 (aeration, Palisades Dam, Yellowtail Dam, Ust-Ilim Dam).
- _____, "Avoiding Cavitation Damage to Hydraulic Structures," Proceedings of the Conference on Water for Resource Development, American Society of Civil Engineers, Couer d'Alene, ID, pp. 407-411, August 1984 (surface irregularities, aeration, geometry).
- Hammitt, F.G., "Effects of Gas Content Upon Cavitation Inception, Performance, and Damage," Report for Working Group No. 1 of Section for Hydraulic Machinery and Cavitation, XIV Congress of the International Association for Hydraulic Research, Proceed-

- ings, Annex to vol. 6, 1971 (inception, damage, gas content).
- _____, "Cavitation Erosion: The State of the Art and Predicting Capability," *Applied Mechanics Reviews*, vol. 32, No. 6, pp. 665-675, June 1979 (cavitation erosion, prediction).
- Harrison, A.J.M., "Boundary-Layer Displacement Thickness on Flat Plates," *Journal of the Hydraulic Division*, American Society of Civil Engineers, vol. 93, No. HY4, pp. 79-91, July 1967 (boundary layer thickness, flat plate, friction factor).
- Hart, E. D., "Prototype Studies of Corps of Engineers Structures Experiencing Cavitation," Proceedings of the Conference, Water for Resource Development, American Society of Civil Engineers, Coeur d'Alene, ID, pp. 427-431, August 1984 (prototype, Libby Dam, Wilson Dam, Bull Shoals Dam).
- Haerter, A., "Theoretische und Experimentelle Untersuchungen über die Lüftungsanlagen von Strassentunneln," *Mitteilungen aus dem Institut für Aerodynamik*, Eidgenoessischen Technischen Hochschule Zürich, Switzerland, No. 29, 1961 (ducts, air flow rate).
- Hentschel, W., Lauterborn, W., "High Speed Holographic Movie Camera," *Optical Engineering*, vol. 24, No. 4, pp. 687-691, July 1985 (holography, bubble dynamics).
- Heyman, F. J., "On the Time Dependence of the Rate of Erosion Due to Impingement or Cavitation," *Erosion by Cavitation or Impingement*, Special Technical Publication No. 408, American Society for Testing and Materials, pp. 70-110, 1967.
- Hickling, R., Plessett, M. S., "Collapse and Rebound of a Spherical Bubble in Water," *Physics of Fluids*, vol. 7, pp. 7-14, 1964 (cavitation bubbles, theory).
- Holl, J. W., "An Effect of Air Content on the Occurrence of Cavitation," *Journal of Basic Engineering*, Transactions of the American Society of Mechanical Engineers, series D, vol. 82, pp. 941-946, December 1960 (air content, inception, gaseous cavitation, vaporous cavitation).
- _____, "The Inception of Cavitation on Isolated Surface Irregularities," *Journal of Basic Engineering*, Transactions of the American Society of Mechanical Engineers, pp. 169-183, March 1960 (inception, isolated irregularities, theory, model studies).
- _____, Arndt, R.E.A., Billet, M. L., "Limited Cavitation and the Related Scale Effects Problem," Second International Japanese Society of Mechanical Engineers Symposium on Fluid Machinery and Fluids, Tokyo, pp. 303-314, September 1972 (theory, turbulence, air content, surface irregularities).
- _____, Billet, M. L., Tada, M., Stinebring, D. R., "The Influence of Pressure Gradient on Desinent Cavitation From Isolated Surface Protrusions," *Journal of Fluids Engineering*, Transactions of the American Society of Mechanical Engineers, vol. 108, pp. 254-260, June 1986 (inception, surface irregularities, pressure gradient).
- _____, Wislicenus, G. F., "Scale Effects on Cavitation," *Journal of Basic Engineering*, Transactions of the American Society of Mechanical Engineers, pp. 385-398, September 1961 (inception, scale effects).
- Hopping, P. N., Mass, G. R., "Cavitation Damage on the Karun Dam," *Concrete International*, vol. 9, No. 3, pp. 41-48, March 1987 (prototype, Karun Dam, damage, repair).
- Horster, M., Rabben, S., Rouve, G., "Belüftung an Sohlprüngen von Grundablässen," *Die Wasserwirtschaft*, vol. 72, pp. 157-159, March 1982 (aerator, outlets).
- Houston, K.L., Quint, R.J., Rhone, T.J., "An Overview of Hoover Dam Tunnel Spillway Damage," *Waterpower 85*, Proceedings of an International Conference on Hydropower, American Society of Civil Engineers, Las Vegas, NV, pp. 1421-1430, September 1985 (prototype, Hoover Dam, tunnel spillway, damage).
- Hsa, W., Shen, M., Sun, T., Sun, C., Cha, C., "Measurement of Gas Bubble Frequency in Water," East China Hydraulic College (USBR translation 1891, book No. 12,481, paper No. 8) (bubbles, frequency, experiments).
- Hsun, K. C., Jin, A., "The Investigation of a More Rational Configuration of the Invert Curve of a Spillway," Joint Conference of the American Society of Civil and Mechanical Engineers, Albuquerque, NM, pp. 143-148, June 1985 (spillway, geometry).
- Hsu, H., "The Pressure Distribution Along Semi-Infinite Gate Piers in Two-Dimensional," *Scientia Sinica*, vol. 12, No. 9, pp. 1357-1364, China, 1963 (pressure distribution, piers, model, desinence).
- _____, "A Method for the Solution of Free Surface Gravity Flow by Finite Elements," Water Conservancy and Hydroelectric Power Research Institute, Beijing, China, 1979 (computer, finite element, free water surface).
- Huang, J., Li, S., Ni, H., "Effect of Air Entrainment on Collapsing Pressure of a Cavitation Bubble in a Liquid," *Shuili Xuebao*, No. 4, pp. 10-17, China (USBR translation 2018, book No. 12,562, April 1985) (air entrainment, collapse, bubble, theory).
- Hu, M., "Analysis on the Characteristics of Cavita-

- tion Downstream From the Reversion," *Shuili Xuebao*, No. 3, pp. 14-21, China (USBR translation 1885, book No. 12,481, paper No. 2, 1983) (vertical bend, pressure distribution, inception).
- Isbester, T. J., "Cavitation in Submerged Jet Flow Gates," National Convention, American Society of Civil Engineers, Denver, CO, November 1975 (jet flow gates, head loss, discharge coefficients).
- Jahnke, H., "Die Ermittlung der Kavitationserosion an Wasserbauwerken," *Wissenschaftliche Zeitschrift der Technischen Universitat Dresden*, 33. Heft 3, pp. 195-199, 1984 (damage, prediction).
- Jang, P. S., Benney, D. J., Gran, R. L., "On the Origin of Streamwise Vortices in a Turbulent Boundary Layer," *Journal of Fluid Mechanics*, Great B., vol. 169, pp. 109-123, 1986 (vortices, boundary layer).
- Jin, G., "Cavitation Characteristics of Baffle Blocks in the Downstream Part of a Hydraulic Structure," collected research papers, *Academia Sinica*, Ministry of Water Resources, Water Conservancy and Hydroelectric Power Research Institute, vol. 13, pp. 237-254, China (USBR translation 1935, book No. 12,529, paper No. 14, 1983) (baffle blocks, hydraulic jump, incipient, pressure distribution).
- _____, Liu, C., Liu, X., "Cavitation Inception of Gate Slots," collected research papers, *Academia Sinica*, Ministry of Water Resources, Water Conservancy and Hydroelectric Power Research Institute, vol. 13, pp. 57-78, China (USBR translation 1934, book No. 12,529, paper No. 3, 1983) (gate slots, inception, models).
- _____, _____, _____, "Cavitation Inception of Gate Slots," Department of Hydraulics, Water Conservancy and Hydroelectric Power, Scientific Research Institute, Beijing, China, 1980.
- Johnson, V. E., "Mechanics of Cavitation," *Journal of the Hydraulics Division*, Proceeding of the American Society of Civil Engineers, vol. 89, No. HY3, pp. 251-275, May 1963 (bubbles, inception, basics, damage).
- Karaki, S., Brisbane, T. E., Kazi, A. H., Chao, P. C., Luecker, A. R., "Performance of Air Slots in High Velocity Chutes at Tarbela Tunnel Outlet," Hydraulics Division Specialty Conference, American Society of Civil Engineering, Cambridge, MA, August 1983 (aerator, outlet works, Tarbela Dam, prototype).
- Karpoff, K. P., Harboe, E. M., Mitchell, L. J., "Design and Construction of New Cavitation Machine," Bureau of Reclamation Report No. C-1070, 7 pp., November 1963 (venturi, damage, test facility).
- Katz, J., "Cavitation Phenomena Within Regions of Flow Separation," *Journal of Fluid Mechanics*, vol. 140, pp. 397-436, 1984 (blunt bodies, separation, holograms).
- _____, O'Hern, T. J., "Cavitation in Large Scale Shear Flows," *Journal of Fluids Engineering*, Transactions of the American Society of Mechanical Engineers, vol. 108, pp. 373-376, September 1986 (shear flows).
- Keener, K. B., "Erosion Causes Invert Break in Boulder Dam Spillway Tunnel," *Engineering News Record*, pp. 763-766, November 1943 (prototype, damage, Boulder Dam, Hoover Dam).
- Kenn, M. J., Garrod, A. D., "Cavitation Damage and the Tarbela Tunnel Collapse of 1974," Proceedings of the Institution of Civil Engineers, Part 1, vol. 70, pp. 65-89, February 1981 (prototype, damage, Tarbela).
- _____, Garrod, A. D., Discussion of "Cavitation Damage and the Tarbela Tunnel Collapse of 1974," Proceedings of the Institution of Civil Engineers, part 1, vol. 70, pp. 779-810, November 1981 (prototype, damage, Tarbela).
- Kermeeen, R. W., McGraw, J. T., Parkin, B. R., "Mechanism of Cavitation Inception and the Related Scale-Effects Problem," Transactions of the American Society of Mechanical Engineers, pp. 533-511, 1955 (inception, scale effects).
- Knapp, R. T., "Accelerated Field Tests of Cavitation Intensity," Transactions of the American Society of Mechanical Engineers, pp. 91-102, January 1958 (damage, turbine, Parker Dam, prototype).
- _____, Daily, J. W., Hammitt, F. G., *Cavitation*, McGraw Hill, Inc., New York, 1970 (theory, prototype, model, basic text).
- Koschitzky, B., Westrich, B., Kobus, H., "Effects of Model Configuration, Flow Conditions and Scale in Modeling Spillway Aeration Grooves," Symposium on Modeling Scale Effects in Hydraulic Structures, International Association for Hydraulic Research, Esslingen, Germany, paper No. 4.4, pp. 1-6, September 1984 (aerators, model).
- Ku, C. H., Jin, Z., "The Investigation of a More Rational Configuration on the Invert Curve of a Spillway," Joint American Society of Mechanical and American Society of Civil Engineers Symposium, Albuquerque, NM, pp. 143-148, June 1985 (theory, pressure distribution, spillways, design).
- Kudriashov, G.V., "Cavitation and Cavitation Erosion of Members of Water Outlet Structures," International Association for Hydraulic Research, Proceedings of the XXth Congress, Moscow, vol. 3, pp. 453-461, 1983 (damage, prototype, model).

- Kuiper, G., "Reflections on Cavitation Inception," Cavitation and Polyphase Flow Forum, American Society of Mechanical Engineers, Albuquerque, NM, pp. 1-14, 1985 (nuclei, inception).
- Laali, A. R., Michel, J. M., "Air Entrainment in Ventilated Cavities: Case of the Fully Developed 'Half-Cavity'," *Journal of Fluids Engineering*, American Society of Mechanical Engineers, vol. 105, pp. 327-335, September 1984 (model studies, jet trajectory).
- Lauterborn, W., Bolle, H., "Experimental Investigations of Cavitation-Bubble Collapse in the Neighborhood of a Solid Boundary," *Journal of Fluid Mechanics*, vol. 72, part 2, pp. 391-399, 1975 (bubbles, boundary, microjet, experiments).
- _____, Vogel, A., "Modern Optical Techniques in Fluid Mechanics," *Annual Review of Fluid Mechanics*, pp. 223-244, 1984 (model, optical techniques, cavitation bubbles).
- Lecoffre, Y., Marcoz, J., "Essais en Cavitation a Bulles Separées, Méthodes de Contrôle — Venturi de Mesure de Germes," *La Houille Blanche*, No. 5, 1978 (Separate-Bubble Cavitation Tests, Control Methods, Nucleation Measurement by Venturi Tube, USBR translation 1649, book No. 12,216) (nuclei, measurement, venturi tube).
- Leducq, D., Wegner, M., "Méthodes d'approche du Bruit Engendré par la Cavitation," *La Houille Blanche*, pp. 697-707, July 1985 (noise).
- Lencastre, A., "Etat des Connaissances sur le Dimensionnements des Évacuateurs de Crue des Barrages," *La Houille Blanche*, No. 1, pp. 19-52, 1985 (surface irregularities, summary, spillways).
- Leslighter, E., "Cavitation in High-Head Gated Outlets — Prototype Measurements and Model Simulation," International Association for Hydraulic Research, 20th Congress, Moscow, vol. 3, sec. b., pp. 495-503, September 1983 (prototype, model, Dartmouth Dam, gates).
- Liang, Z., Wang, D., "On the Air Carrying Capacity in Turbulent Boundary Layer," *Shuili Xuebao*, No. 2, pp. 24-31, China (USBR translation 1876, book No. 12,469, 1982) (turbulence, air entrainment, boundary layer, theory).
- Lichtarowicz, A., Kay, P., "Erosion Testing With Cavitating Jets," Proceedings 6th International Conference on Erosion by Liquid and Solid Jets, paper No. 15, 6 pp., 1984 (erosion, jets).
- Lin, B., Gong, Z., Pan, D., "A Rational Profile for Flip Buckets of High Dams," *Scientia Sinica*, series A, vol. 25, No. 12, pp. 1343-1352, China, December 1982 (spillway, profile, flip bucket, Aldeadavila Dam).
- Liu, C., "A Study on Cavitation Inception of Isolated Surface Irregularities," collected research papers, *Academia Sinica*, Ministry of Water Resources, Water Conservancy and Hydroelectric Power Research Institute, vol. 13, China (USBR translation 1931, book No. 12,529, paper No. 2, 1983) (inception, irregularities, noise).
- Liu, Y., "Effects of Suspended Sediments on Cavitation Phenomena," *Shuili Xuebao*, No. 3, pp. 55-58, China (USBR translation 1890, book No. 12,481, paper No. 7, 1983) (sediments, inception).
- Li, Z., Huang, J., "Relation Between Cavitation Resistance of Metals and Their Ultimate Resilience," *Shuili Xuebao*, No. 4, pp. 60-66, China (USBR translation book No. 12,561, 1985) (resilience, damage, experiments).
- Lopardo, R. A., Lio, J. C., Vernet, G. F., "Physical Modeling on Cavitation Tendency for Microturbulence of Hydraulic Jump," International Conference on the Hydraulic Modeling of Civil Engineering Structures, BHRA Fluid Engineering, Coventry, England, pp. 109-121, September 1982 (stilling basin, hydraulic jump, models, pressure fluctuations).
- Lush, P. A., Angell, B., "Correlation of Cavitation Erosion and Sound Pressure Level," *Journal of Fluids Engineering*, Transactions of the American Society of Mechanical Engineers, vol. 106, pp. 347-351, September 1984 (erosion, noise, correlations).
- _____, Wood, R.J.K., Carpanini, L. J., "Pitting in Soft Aluminum by Spark-Induced Cavitation Bubbles," Proceedings 6th International Conference on Erosion by Liquid and Solid Impact, paper No. 5, 8 pp., 1984 (bubbles, pitting, aluminum).
- Lysenko, P. E., Chepaikin, G. A., Tumanov, S. A., "Prediction and Prevention of Cavitation-Erosion Damage on High-Head Spillways," *Gidrotekhnicheskoe Stroitel'stvo*, No. 11, pp. 11-13, 1983 (USBR translation 1916, book No. 12,512) (damage, prediction, materials, spillways).
- Marcano, A., Castillejo, N., "Model-Prototype Comparison of Aeration Devices of Guri Dam Spillway," Symposium on Modeling Scale Effects in Hydraulic Structures, International Association for Hydraulic Research, Esslingen, Germany, paper No. 4.6, pp. 1-5, September 1984 (aerators, model, prototype, Guri Dam).
- Matsumoto, Y., "Contribution of Homogeneous Condensation Inside Cavitation Nuclei to Cavitation Inception," *Journal of Fluids Engineering*, American Society of Mechanical Engineers, vol. 108, pp. 433-437, December 1986 (nuclei, inception, model, bubble dynamics).
- May, R.W.P., "Cavitation in Hydraulic Structures:

- Occurrence and Prevention," Hydraulics Research Report No. SR 79, Wallingford, England, March 1987 (summary, aerators, inception).
- McGee, R. G., "Prototype Evaluation of Libby Dam Sluiceway Aeration System," American Society of Civil Engineers, International Association for Hydraulic Research, Proceedings of the International Symposium on Model-Prototype Correlation of Hydraulic Structures, pp. 138-147, August 1988 (aerator, prototype).
- Mefford, B. W., Falvey H. T., "Cavitation Inception From Cylindrical Holes," Conference on Water for Resources Development, American Society of Civil Engineers, Coeur d'Alene, ID, pp. 422-426, August 1984 (inception, holes, model studies).
- _____, Muller, B. C., Jr., "Cavitation Damage and Repair of Stampede Dam," *Concrete International*, vol. 9, No. 3, pp. 49-54, March 1987 (prototype, Stampede Dam, damage, aerator, model).
- Michel, J. M., "Some Features of Water Flows With Ventilated Cavities," *Journal of Fluids Engineering*, American Society of Mechanical Engineers, vol. 106, pp. 319-326, September 1984 (model studies, cavity flow).
- Milne-Thompson, L. M., *Theoretical Hydrodynamics*, Macmillan Co., 2d ed, 1950.
- Mohammad, W. A., Hutton, S. P., "Improved Monitoring of Air in Water," *Water Power and Dam Construction*, pp. 48-52, September 1986 (monitoring, air, bubbles).
- Naude, C. F., Ellis, A. T., "On the Mechanism of Cavitation Damage by Nonhemispherical Cavities Collapsing in Contact With a Solid Boundary," *Journal of Basic Engineering*, Transactions of the American Society of Mechanical Engineers, pp. 648-656, December 1961 (damage, bubbles, jets).
- Oba, R., Ikohagi, T., Ito, Y., Miyakura, H., Sato, K., "Stochastic Behavior (Randomness) of Desinent Cavitation," Transactions of the American Society of Mechanical Engineers, vol. 108, pp. 438-443, December 1986 (model, desinence, air content, randomness).
- Ooi, K. K., "Scale Effects on Cavitation Inception in Submerged Water Jets," *Journal of Fluid Mechanics*, vol. 151, pp. 367-390, 1985 (jets, scale effect, inception).
- Oskolkov, A. G., Semenkov, V. M., "Opyt razrabotki metodov predotvrashcheniia kavitatsionnoi erozii vodosbrosnykh sooruzhenii (Experience in Developing Methods for Preventing Cavitation Erosion of Spillway Structures) Gidrotekhnicheskoe stroitel'stvo, No. 8, Energiia, Moscow, pp. 11-15, 1979 (USB translation, book No. 12,232) (prototype, inception criteria, aeration).
- Pan, S., Shao, Y., "Hydraulic Estimation of a U-Shaped Abrupt-Offset Aeration Device," *Shuili Xuebao*, No. 8, pp. 12-20, China (USB translation book No. 12,618, 1986) (aerator, gate, outlet works, downstream offset).
- _____, _____, "Scale Effects in Modeling Air Demand by a Ramp Slot," Symposium on Modeling Scale Effects in Hydraulic Structures, International Association for Hydraulic Research, Esslingen, Germany, paper No. 4.7, pp. 1-5, September 1984 (aerators, model, prototype, Fengjiashan Dam).
- _____, _____, Shi, Q., Dong, X., "Self-Aeration Capacity of a Water Jet Over an Aeration Ramp," *Shuili Xuebao*, No. 5, pp. 13-22, Beijing, China (USB translation 1868, book No. 12,455, paper No. 2, 1980) (aerator, air entrainment, trajectory, theory).
- Peterka, A. J., "The Effect of Entrained Air on Cavitation Pitting," Proceedings of the Joint Meeting of the International Association for Hydraulic Research, American Society of Civil Engineers, Minneapolis, MN, August 1953 (damage, air entrainment).
- Petrov, A. G., Sotina, N. B., "Universal Cavity-Shape Independent Relations for Cavitation Flow," *Journal of Applied Mechanics and Technical Physics*, vol. 25, No. 5, pp. 758-766, March 1985 (supercavitation).
- Pinto, N. L. de S., "Model Evaluation of Aerators in Shooting Flow," Symposium on Modeling Scale Effects in Hydraulic Structures, International Association for Hydraulic Research, Esslingen, Germany, paper No. 4.2, pp. 1-6, September 1984 (aerators, model, prototype, Foz do Areia Dam).
- _____, "Basic Hydraulics of Shooting Flow Over Aerators," Specialty Conference, *Advancements in Aerodynamics, Fluid Mechanics and Hydraulics*, American Society of Civil Engineers, Minneapolis, MN, pp. 1007-1017, June 1986 (aerators, model, prototype, theory).
- _____, "Recommendations on Consideration of Cavitation When Designing Hydraulic Spillway Structures," VNIIG, Energiia, Leningrad, pp. 38-75, 1975 (hydraulic structure).
- _____, Neidert, S. H., "Model Prototype Conformity in Aerated Spillway Flow," International Conference on Hydraulic Modeling of Civil Engineering Structures, BHRA Fluid Engineering, Coventry, England, paper No. E6, pp. 273-284, September 1982 (model, prototype, Foz do Areia Dam, scale effects).
- _____, _____, Ota, J. J., "Aeration at High Velocity Flows — Part One," *Water Power and Dam Construction*, pp. 34-38, February 1982 (aerators, Foz do Areia Dam, prototype).

- _____, _____, _____, "Aeration at High Velocity Flows — Part Two," *Water Power and Dam Construction*, pp. 42-44, March 1982 (aerators, model correlation).
- Plesset, M. S., "The Dynamics of Cavitation Bubbles," *Journal of Applied Mechanics*, American Society of Mechanical Engineers, vol. 16, pp. 277-282, 1949 (bubbles).
- _____, Chapman, R. B., "Collapse of an Initially Spherical Vapor Cavity in the Neighborhood of a Solid Boundary," *Journal of Fluid Mechanics*, vol. 47 part 2, pp. 283-290, 1971 (bubble, collapse, jet).
- Pode, L., "Diffusion of Air Into a Pulsating Cavitation Bubble," David Taylor Model Basin, Report No. 804, 17 pp., March 1955 (bubbles, diffusion, air, theory).
- Prusza, V., "Remedial Measures Against Spillway Cavitation," International Association for Hydraulic Research, Proceedings of the XXth Congress, Moscow, vol. 3, pp. 468-476, 1983 (spillway, aeration).
- Pugh, C. A., "Modeling Aeration Devices for Glen Canyon Dam," Proceedings of the Conference on Water for Resource Development, American Society of Civil Engineers, Coeur d'Alene, ID, pp. 412-416, August 1984 (models, aerators, spillway, Glen Canyon Dam).
- Pylkkanen, J. V., "Characteristics of Spherical Cloud Cavity," Proceedings of the Specialty Conference, *Advancements in Aerodynamics, Fluid Mechanics and Hydraulics*, American Society of Civil Engineers, Minneapolis, MN, pp. 96-103, June 1986 (bubbles, collapse, cloud, theory).
- Quintela, A. C., "Flow Aeration to Prevent Cavitation Erosion," *Water Power and Dam Construction*, pp. 17-22, January 1980 (damage, aeration, prototype, aerators).
- Rabben, S. L., Rouve, G., "Belüftung von Grundablassen," *Die Wasserwirtschaft*, Heft. 75, pp. 393-399, September 1985 (aeration, outlet works, spillways).
- Rahmeyer, W. J., "Cavitation Damage to Hydraulic Structures," *Journal of the American Water Works Association*, pp. 270-274, May 1981 (damage, irregularities).
- Rao, N.S.L., Gangadharaiah, T., "Self-Aerated Flow Characteristics in Wall Region," *Journal of Hydraulics Division*, American Society of Civil Engineers, vol. 97, No. 9, September 1971 (aeration, wall region).
- Rao, P. V., Martin, C. S., Rao, B.C.S., Rao, N.S.L., "Estimation of Cavitation Erosion With Incubation Periods and Material Properties," *Journal of Testing and Evaluation*, American Society for Testing Materials, pp. 189-197, 1981 (damage, material properties, prediction).
- _____, Rao, B.C.S., "Similarities in Different Experiments of Erosion Caused by Cavitation and Liquid Impingement," *Journal of Testing and Evaluation*, American Society for Testing and Materials, pp. 179-188, 1981 (damage, venturi, rotating disk, metals).
- Rhone, T. J., "Hydraulic Model Studies of Flaming Gorge Dam Spillway and Outlet Works," Bureau of Reclamation Report No. HYD-531, 1964 (tunnel spillways, high-velocity flow).
- Rouse, H., Jezdinsky, V., "Cavitation and Energy Dissipation in Conduit Expansions," Proceedings of the International Association for Hydraulic Research, 11th Congress, Leningrad, 1965 (expansions, energy dissipation, cavitation).
- Russell, S. O., Ball, J. W., "Sudden-Enlargement Energy Dissipater for Mica Dam," *Journal of the Hydraulics Division*, American Society of Civil Engineers, vol. 93, No. HY4, pp. 41-56, July 1967 (sudden enlargements, Mica Dam).
- Rutschmann, P., "Calculation and Optimum Shape of Spillway Chute Aerators," International Association for Hydraulic Research, Proceedings of the International Symposium on Model-Prototype Correlation of Hydraulic Structures, American Society of Civil Engineers, Colorado Springs, CO, pp. 118-127, August 1988 (aerator, model tests).
- _____, "Belüftungseinbauten in Schussrinnen, Wirkungsweise, Formgebung und Berechnung von Schussrinnenbelüftern," *Mitteilungen der Versuchsanstalt für Wasserbau, Hydrologie und Glaziologie*, Report No. 97, Zürich, 1988.
- _____, "Belüftungseinbauten in Schussrinnen Wirkungsweise, Formgebung und Berechnung von Schussrinnenbelüftern," *Mitteilungen der Versuchsanstalt für Wasserbau, Hydrologie und Glaziologie*, Eidgenössische Technische Hochschule Zürich, Switzerland, No. 97, 1988 (aerators, model tests, design).
- Schrader, E., Tatro, S., "Cavitation and Erosion Damage to Concrete in Dams," *Concrete International*, vol. 9, No. 3, pp. 15-23, March 1987 (prototype, Dworshak Dam).
- Schuster, J. C., "Hydraulic Model Studies of the Palisades Dam Outlet Works and Spillway, Palisades Project, Idaho," Bureau of Reclamation Report No. HYD-350, June 1956 (model, spillway, Palisades Dam) (chutes, high velocity flow).
- Selim, S.M.A., "A Theoretical Study on Cavitation Erosion Rate," Cavitation and Polyphase Forum, Fluid Engineering Division, American Society of Mechanical Engineers, Albuquerque, NM, vol. 23, pp. 41-51, 1985 (erosion, theory).
- Selander, C. E., "Resistance to Cavitation Damage

- Laboratory and Field Tests on Four Selected Coatings," Bureau of Reclamation Report No. ChE-25, 9 pp., June 1964 (damage, coatings).
- Semenkov, V. M., Lentiaev, L. D., "Spillway With Nappe Aeration," *Gidrotekhnicheskoe Stroitel'stvo*, U.S.S.R., No 5., pp. 16-20, May 1973 (aerators, prototypes, air content, damage).
- Seng, L. H., "Model Studies of Clyde Dam Spillway Aerators," Research Report, No. 86-6, Department of Civil Engineering, University of Canterbury, Christchurch, New Zealand, March 1986 (aerators, model).
- Shi, Q., Pan, S., Shao, Y., Yuan, X., "Experimental Investigation of Flow Aeration to Prevent Cavitation Erosion," *Shuili Xuebao*, No. 3, pp. 1-13, China (USBR translation 1884, book No. 12,481, paper No. 1, 1983) (aerator, model, air duct, design).
- Smith, P. M., Perkins, L. Z., "Dworshak Dam, North Fork Clearwater River, Idaho," Technical Report No. 116-1, U.S. Army Corps of Engineers, Walla Walla District, North Pacific Division, pp. 228, September 1984 (Dworshak Dam, prototype, damage, aeration).
- Smits, A. J., Wood, D. H., "The Response of Turbulent Boundary Layers to Sudden Perturbations," *Annual Review of Fluid Mechanics*, vol. 17, pp. 321-358, 1985 (turbulence, curved boundary, theory, experiment).
- Solov'yeva, A. G., Korkhova, N. P., "Opredelenie znachenii kriticheskogo koeffitsienta kavitatsii nerovnosti tipa volny," (Determination of the Critical Cavitation Coefficient Due to Wave Shaped Irregularities), *Izvestiia VNIIG*, vol. 112, pp. 83-89, 1976 (USBR translation, book No. 12,069, paper No. 13) (surface irregularities, model).
- Stein, U., "Zur Untersuchung der Stromungskavitation unter Berucksichtigung von Turbulenz, Wirbelbildung und Blasendynamik," (Investigation of Cavitation in Flows Taking Into Account Turbulence, Vorticity, and Bubble Dynamics), *Mitteilungen des Instituts für Wasserbau und Wasserwirtschaft*, Heft. 43, Aachen, Germany, 143 pp., October 1982 (USBR translation 1929, book 12,525) (turbulence, inception, vortices, bubbles, irregularities).
- Stinebring, D. R., "Scaling of Cavitation Damage," masters thesis, Pennsylvania State University, 160 pp., August 1976 (damage, aluminum, pits).
- _____, Arndt, R.E.A., Holl, J. W., "Scaling of Cavitation Damage," *Journal of Hydro-nautics*, vol. 11, No. 3, pp. 67-73, July 1977 (damage, scale effects, air content).
- _____, _____, _____, "Two Aspects of Cavitation Damage in the Incubation Zone: Scaling by Energy Considerations and Leading Edge damage," *Journal of Fluids Engineering*, Transactions of the American Society of Mechanical Engineers, vol. 102, pp. 481-485, December 1980 (damage, energy, leading edge).
- Stonemetz, R. E., "Liquid Cavitation Studies in Circular Pipe Bends," NASA Technical Memorandum TM-X-53278, George C. Marshall Space Flight Center, Huntsville, AL, 21 pp., June 1965 (bends, closed conduit flow, incipient).
- Taghavi, R., Arndt, R.E.A., "Cavitation in Various Types of Shear Flow," Cavitation and Poly-phase Flow Forum, Fluid Engineering Division, American Society of Mechanical Engineers, Albuquerque, NM, vol. 23, pp. 129-133, 1985 (shear flow).
- Tomita, Y., Shima, A., "Mechanism of Impulsive Pressure Generation and Damage Pit Formation by Bubble Collapse," *Journal of Fluid Mechanics*, vol. 169, pp. 535-564, 1986 (pits, bubbles, collapse, pressure).
- _____, _____, Takahashi, K., "The Collapse of a Gas Bubble Attached to a Solid Wall," *Transaction of the American Society of Mechanical Engineers*, vol. 105, pp. 341-363, September 1983 (collapse, bubble, wall, shock wave).
- Tyler, J. L., "Final Construction Report on Repair Spillway Tunnels, Glen Canyon Dam, Colorado River Storage Project, Page, Arizona," Contract No. 3-CC-40-0110, Bureau of Reclamation, December 1984 (prototype, repair, Glen Canyon Dam, spillway).
- Uppal, H. L., Gulati, T. D., Paul, T. C., "Cavitation in High-Head Outlet Conduits," *International Association for Hydraulic Research*, 11th Congress, Leningrad, 17 pp., 1965 (high-head outlets).
- Vakhitova, N. K., Shagapov, V. Sh., "Propagation of Small Disturbances in Vapor-and-Liquid Bubbling Media," *Journal of Applied Mechanics and Theoretical Physics*, vol. 25, No 5, March 1985 (bubbles, propagation, pressures).
- Vernet, G. F., Angelaccio, C. M., Chividini, M. F., "Model-Prototype Comparison in the Alicura Chute Spillway Air System," *International Association for Hydraulic Research*, Proceedings of the International Symposium on Model-Prototype Correlation of Hydraulic Structures, American Society of Civil Engineers, pp. 110-117, August 1988 (aerator, prototype, model tests).
- Vigander, S., "An Experimental Study of Wall-Pressure Fluctuations in a Cavitating Turbulent Shear Flow," *Studies in Engineering Mechanics*, Center for Research, Inc., University of Kansas, Lawrence, KS, Report No. 21, 116 pp., May 1965 (turbulence, pressure fluctuations, model).
- Vischer, D., Volkart, P., Siegenthaler, A., "Hydraulic

- Modelling of Air Slots in Open Chute Spillways," International Conference on the Hydraulic Modelling of Civil Engineering Structures, BHRA Fluid Engineering, Coventry, England, pp. 239-252, September 1982 (models, scale effects, air concentrations).
- Volkart, P., "Sohlenbelüftung gegen Kavitationserosion in Schussrinnen," *Dis Wasserwirtschaft*, Heft. 74, September 1984 (aeration, spillways).
- _____, "Transition from Aerated Supercritical to Subcritical Flow and Associated Bubble De-Aeration," International Association for Hydraulic Research, Proceedings of the XXIst Congress, Melbourne, Australia, August 19-23, 1985 (aeration, deaeration, bubbles).
- _____, Rutschmann, P., "Aerators on Spillway Chutes: Fundamentals and Applications," Proceedings of the Specialty Conference, *Advancements in Aerodynamics, Fluid Mechanics and Hydraulics*, American Society of Civil Engineers, Minneapolis, MN, pp. 163-177, June 1986 (aerators, theory).
- _____, "Rapid Flow in Spillway Chutes With and Without Deflectors," Symposium on Modeling Scale Effects in Hydraulic Structures, International Association for Hydraulic Research, Esslingen, Germany, paper No. 4.5, pp. 1-8, September 1984 (aerators, model).
- Vorob'ev, G. A., "Standard Cavitation Erosion Resistance of Building Materials," *Hydrotechnical Construction*, Plenum Publishing Corp., vol. 19, No. 6, pp. 280-284, 1985 (erosion, resistance).
- Walter, D. S., "Rehabilitation and Modification of Spillway and Outlet Tunnels and River Improvements at Hoover Dam," thesis for civil engineer degree, University of Colorado, 1926 (spillway, repair, Hoover Dam, spillway).
- Wang, X., Chou, L., "The Method of Calculation of Controlling (or Treatment) Criteria for the Spillway Surface," Proceedings of the Thirtieth International Congress of Large Dams, Q50, R56, pp. 977-1012, New Delhi, India, 1979 (prototype, damage, criteria).
- Ward, T. M., "Slot Cavitation," Cavitation and Polyphase Flow Forum, American Society of Mechanical Engineers, pp. 24-20, 1973 (inception, slots, vortices).
- Warnock, J. E., "Experiences of the Bureau of Reclamation," Proceedings of the American Society of Civil Engineers, vol. 71, No. 7, pp. 1041-1056, September 1945 (valves, gate slots, spillway, damage).
- Wei, C. Y., DeFazio, F. G., "Simulation of Free Jet Trajectories for the Design of Aeration Devices on Hydraulic Structures," 4th International Symposium of Finite Elements on Hydraulic Structures, Hannover, Germany, pp. 1-11, June 1982 (computational, finite elements, spillway, jet, trajectory).
- White, M. P., Discussion by W. L. Moore, "Energy Loss at the Base of a Free Overfall," (Transactions of the American Society of Civil Engineers, vol. 108, pp. 1343-1360, 1943), Transactions of the American Society of Civil Engineers, vol. 108, pp. 1361-1364, 1943 (overfalls, energy dissipation).
- Xu, X., Zhou, S., "Pressure Distribution and Incipient Cavitation Number for Circular Arc and Half-Arc Surface Irregularities," collected papers, Institute of Hydraulics, vol. 7, China (USBR translation 1905, book No. 12,497, 1981) (incipient, circular arc, half arc, experiments, theory).
- Yan, S., "Cavitation Damage in the Bottom Sluice at the Jiaokou Reservoir," *Shuili Xuebao*, No. 3, pp. 22-30, China (USBR translation 1886, book No. 12,481, 1983, paper No. 3) (damage, sluice, Jiaokou Dam, prototype, model).
- Yan, Z., "Similarity of Subatmospheric Hydraulic Model Test," *Shuili Xuebao*, No. 3, pp. 32-40, China (USBR translation 1887, book No. 12,481, 1983, paper No. 4) (similarity, model, prototype).
- Yevdjovich, V., Levin, L., "Entrainment of Air in Flowing Water and Technical Problems Connected With It," International Association for Hydraulic Research, Proceedings of the Vth Congress, Minneapolis, MN, pp. 439-454, 1953 (air entrainment, theory).
- Yu, F., Zhang, L., "Equipment for the Study of Cavitation — A Variable Pressure Tank," *Shuili Xuebao*, No. 3, pp. 41-48, China (USBR translation 1888, book No. 12,481, paper No. 5, 1983) (test facility, model, low ambient pressure).
- Yu, J., "Quo-Dhu Dam Number Three Lock Flow Entrance Section Subatmospheric Pressure," *Shuili Xuebao*, No. 3, pp. 64-69, China (USBR translation 1892, book No. 12,481, paper No. 9, 1983) (lock, damage, prototype, Quo-Dhu Dam, noise, model, aeration).
- Zagustin, K., Mantellini, T., Castillejo, N., "Some Experience on the Relationship Between a Model and Prototype for Flow," International Conference on Hydraulic Modeling of Civil Engineering Structures, BHRA Fluid Engineering, Coventry, England, paper No. E7, pp. 285-295, September 1982 (model, prototype, Guri, aerator, scaling).
- Zharov, N. E., "O melodike operedeleniia kriticheskikh chisel kavitatsii obtekanii nerovnostei" (Cavitation Parameters of Flows Near Surface Irregularities), *Izvestiia VNIIG im. B. E. Vedeneeva, Sb., nauchnykh trudov*, vol. 126, Leningrad, pp. 43-48, 1978 (USBR translation, book No. 12,245, paper No. 6).

